Thermochemical co-liquefaction of waste plastics and biomass for the production of fuels and further chemicals

Hongthong, Sukanya

Award date:
2021

Awarding institution:
University of Bath

Thermochemical co-liquefaction of waste plastics and biomass for the production of fuels and further chemicals

Sukanya Hongthong

A thesis submitted for the degree of Doctor of Philosophy

University of Bath

Department of Chemical Engineering

October 2020

Abstract

There is increasing concern over the levels of plastic waste that are entering the environment or being collected with no appreciable route to disposal. While recycling, as an alternative to disposal, offers one route, the need for uncontaminated sources and the lower quality of recycled plastics presents huge challenges. Alternatively, an increasing body of research has aimed to use plastic waste as a feedstock in a circular economy methodology to produce more valuable products such as fuels. Plastic waste could potentially be co-processed with biomass to create biofuels and chemicals, decreasing dependence on fossil fuels and remediating the plastic problem. The aim of this thesis is to explore the valorisation of plastic waste, through co-processing with biomass. To this end thermochemical co-liquefaction was explored.

Initially a novel type of liquid based pyrolysis was assessed on the lab and pilot scale. The technique is known as the pressure-less catalyst depolymerisation (KDV, in the original German), and has been claimed to depolymerise organic feedstocks to produce a hydrocarbon biofuel, in one step, without the need for hydrogen or chemical upgrading. However, despite a number of pilot plants in operation, no systematic mechanistic studies have been reported and it is unclear how this pyrolysis can be achieved. To determine these outstanding questions, pistachio hulls were liquefied using a KDV process in the lab and through collaboration with the Wonderful Company to assess the pilot scale mass balance and determine the suitability of the KDV approach. The process was carried out using an aluminosilicate 4Å zeolite catalyst at atmospheric pressure and temperatures at 300 °C. In this process the biomass and catalyst are suspended in a petroleum carrier oil and the fuel recovered though distillation from the reaction vessel. The process has a stated productivity of 32.8 L distillate oil/1,000 kg pistachio hull on pilot plant scale. However, the ^{14}C analysis demonstrated that most of the product came from the fossil carrier oil. The process was then mimicked on the lab scale, on both 1L and 5L scales and the optimal catalyst type was tested using aluminosilicate 4A zeolite, zeolite, aluminosilicate catalyst, and a calcium hydroxide neutraliser at atmospheric pressure and temperature at 300 °C. Despite the lab scale tests, the yield was not improved through using the more stable zeolite catalyst. The maximum distillate obtained when using a heavier carrier oil was relatively low (approximately 6.5v/w%) with less than half of the pistachio hull used.

The liquid product contained not only pyrolysis oil but also 30-50 wt.% water. The bio-content as determined through ^{14}C analysis was remarkably low for all reaction conditions, demonstrating that the majority of the product came from the carrier oil. The concerted efforts on lab and pilot plant scale demonstrated the unsuitability of this one step process for fuel production, and therefore was not used to co-process plastics.

Hydrothermal liquefaction is another promising, low-energy route for the bio-crude conversion of biomass which can be upgraded to advanced biofuels. The co-processing of common plastic waste (including; polyethylene, polypropylene, PET and nylon-6,) with pistachio hulls was therefore assessed to investigate the suitability of the HTL approach at 350 °C. High yields of up to 35% bio-crude were achieved. Synergistic effects between plastics and pistachio hulls conversion were stronger in the presence of nylon-6 and PET. Nylon-6 almost completely depolymerised under the optimal HTL conditions and generated the caprolactam monomer. PE and PP were less reactive; a limited degree of decomposition formed oxidised products, which distributed into the bio-crude phase. The HHV of the bio-crudes increased substantially in the presence of plastic blends.

The recalcitrant polyolefins also need to be converted before plastic waste can become an integral part of a biorefinery. In order to enhance the conversion of these plastics, a possible solution through the catalytic co-liquefaction of a model waste (pistachio hulls) and polypropylene (PP) was assessed. Pure PP did not break down under HTL conditions, and only small synergistic effects occurred when placed with biomass. In the presence of typical HTL catalysts including Fe, $FeSO_4$, $MgSO_4$, $ZnSO_4$, ZSM-5, aluminosilicate, Y-zeolite, and Na_2CO_3, the PP almost exclusively broke down into a solid phase product with no enhancement of the bio-crude fraction. However, the plastic conversion was enhanced up to 50% through the addition of the hydrogen donor formic acid. This reduced the amount of carbon going to the solid phase and the volatile organic produced was increased in the gas phase. The gaseous products were an array of short chain hydrocarbons, which could be repolymerised as a polyolefin or combined with the bio-crude for further processing.

Several broad classes of plastics have a high possibility of ending up in the ocean environment. Extensive fishing, recreational and maritime uses of the ocean increase the influx of plastic waste into the oceans. The concept of implementing HTL as a route to processing marine plastic and macroalgae was therefore investigated. Co-processing of marine macroalgae was undertaken with a range of different nylons (nylon-6, nylon6/6, nylon6/12, and nylon12) including an actual sample of marine macroalgae collected at sea, entangled with nylon fishing line. Due to the variation in macroalgae composition, synergetic effects between macroalgae and nylon conversion were observed, producing bio-crudes in higher yields and with better fuel properties. Co-processing of marine macroalgae and contaminant marine plastic therefore is a potentially useful method to solve the ocean environmental problem and create value for fuel production.

Based on the investigations, HTL has been demonstrated to be a highly promising route to convert the energy from biomass and plastic to valuable bio-crude, liquid products, gaseous and bio-char. The HTL could be achieved in both thermal and catalytic processes. However, catalytic processes provide higher plastic conversion with greater yield of gaseous products. With the potential HTL method, waste management can become more efficient, with reduced need of waste disposal, less pollution, and is seemingly cost effective.

Acknowledgement

I would like to express my deep and sincere gratitude first and foremost to my supervisor, Professor Chris Chuck for giving me the research opportunity and providing invaluable support and guidance throughout this project. Thank you for being so kind and understanding. It was a great privilege and honour to work under his guidance. Without his constant help, encouragement and support, this PhD would certainly not have been possible. I could not have imagined having a better supervisor for my PhD study. A huge thanks also goes to my second supervisor, Dr. Hannah Leese. I appreciate all the support I received and her help and advice throughout my PhD.

My sincere thanks also go to Dr. Joseph Donnelly, for his training at the early stages of my research on LPP. Special thanks must go to Dr. Sofia Raikova for not only training me to run HTL, but she was a lovely friend and always provided great support and wise guidance.

My PhD would have been exceptionally hard to complete without the assistance of a great number of technical staff. I would like to extend my thanks to all the technicians for their help. I would like to specifically mention Dr. Shaun Reeksing, who has been kindly helping me with analytical biofuel production.

My time in Bath would have been hard without my Thai friends and colleagues. I would like to especially mention Nurul, however there are many others that have made my time here in Bath very enjoyable. Thank you all for sharing good times, energy, understanding and help throughout my PhD. Special thanks also to everyone who helped with proof reading my work.

I had such a great time as part of Professor Chuck's group. I feel proud to have been part of such a talented, fun, supportive, and motivated group like a second family. Thank you for a wonderful time spent together in the lab and social setting.

I could not have done my PhD without the generous funding provided by the Royal Thai Government. Thank you for giving me the opportunity to gain more knowledge and experience.

A huge thanks need to go my parents and Sanparon for their love, support, and encouraging me through the good times and downright sad times. Thank you for always being there for me. My PhD would never have been possible without all their encouragement and support all through my studies.

Dissemination

Journal articles

Sukanya Hongthong, Sofia Raikova, Hannah S. Leese, and Christopher J. Chuck. 2019. *Co-processing of common plastics with pistachio hulls via hydrothermal liquefaction*. Waste management 102:351-361. doi:10.1016/j.wasman.2019.11.003. This publication is presented as Chapter 3.

Sukanya Hongthong, Hannah S. Leese, and Christopher J. Chuck. 2020. *Valorizing Plastic-Contaminated Waste Streams through the Catalytic Hydrothermal Processing of Polypropylene with Lignocellulose.* ACS Omega 2020, 5, 32, 20586–20598. doi:10.1021/acsomega.0c02854. This publication is presented as Chapter 4.

Draft manuscripts in Process

Sukanya Hongthong, Hannah S. Leese, and Christopher J. Chuck**. 2020.** Assessment of the impact of nylon contamination on the optimised macroalgal hydrothermal liquefaction process. This manuscript is presented as Chapter 5.

Abbreviations

AP	Aqueous phase
ASTM	American standards for testing and material
BHT	Butylated hydroxytoluene
CHN	Carbon, hydrogen and nitrogen
CPD	Catalytic pressure-less depolymerisation
daf	Dry, ash free
ER	Energy recovery
FA	Formic acid
FTIR	Fourier-transform infrared spectroscopy
GC-MS	Gas chromatography – mass spectrometry
HDO	Hydrodeoxygenation
HHV	Higher heating value
HTL	Hydrothermal liquefaction
ICP-OES	Inductively-coupled plasma optical emission spectrometry
KDV	Katalytische Drucklose Verölung
LCMS	Liquid chromatography – mass spectrometry
LPP	Liquid phase pyrolysis
NMR	Nuclear magnetic resonance
NY	Nylon
PE	Polyethylene
PET	Polyethylene terephthalate
PP	Polypropylene
TGA	Thermo-gravimetric analysis

Content

List of figures

List of tables

Chapter 1

Literature review

1.1 Introduction

The growth in demand for natural resources is predicted to increase continuously at an annual rate of 1.6% in the next two decades [1]. Petroleum fuel resources are a valuable supply for limited natural energy as the rate of petroleum fuel resources exhaustion is higher than the rate of regeneration. The enormous consumption of petroleum fuel resources results in increased emissions of harmful pollutants. Carbon dioxide, a key greenhouse gas released into the atmosphere through burning petroleum resources, resulting in environmental impacts and serious threats to human health [2]. Despite the environmental impacts associated with the use of petroleum fuel resources, petroleum-derived liquid hydrocarbons are still attractive and feasible forms of transportation fuel [3]. With increases in energy demands, petroleum resources are estimated to be exhausted worldwide after 2042 with the current rate of petroleum fuel consumption [4]. To control the pollutant emissions and moderate the energy predicament, the development of alternative resources to replace petroleum-derived chemicals and fuels has been explored. Several efforts are currently being developed to find alternative energy sources and develop technologies which are high efficiency and environmentally friendly. In this regard, most of the investigation has been contributed through research into biomass energy. Biomass has been considered as the most promising resource for the production of sustainable biofuels. Biomass is a major source of energy and is currently estimated to account for approximately 10–14% of the world's energy consumption [5]. Unlike petroleum sources, biomass has been treated as a carbon-neutral source, conducive to mitigating global warming effects [6].

Appropriate waste management strategy is another key aspect of sustainable development. The growing size of welfare states in modern society has led to a huge increase in the production of all kinds of commodities, which generate waste incidentally. Plastic has become the main material which has gained much popularity as being used in a wide range of applications due to its stability, light weight and low cost [7] Since it is resistant to degradation, substantial quantities of plastics waste have accumulated in the natural environment and landfills. It is estimated that global plastic waste generation in 2025 will increase to 9-13% of total municipal solid waste [8]. In the UK, approximately 55% of plastic wastes were found in landfill, 26% were recycled, and 18% were used for energy recovery [9]. This demonstrates that despite a large

effort around collection and recycling the majority of plastic waste ends up in landfill. Polyolefins are not biodegradable over acceptable timeframes and it has been estimated that it would take over 500 years for them to biodegrade [10]. As result of that plastics have become a potential health risk to aquatic and terrestrial animals [11], and impact on environmental pollution [12]. There are several methods for disposal of municipal and industrial plastic waste, however the traditional methods for the removal of plastic wastes such as landfilling and incineration do not constitute a certain solution from an environmental standpoint [13].

To address these issues, the problem of replacing energy resources related environmental pollution must be solved. This project will therefore aim to investigate the potential of plastic waste as co-feedstock with biomass in a circular economy methodology to produce more valuable products such as fuels and chemicals. The focus will be to understand the reaction mechanisms and the synergistic effects between biomass and waste plastics during thermochemical processes.

1.2 Feedstocks for energy production

Continued population growth and rapid industrialization across the world has led to increasing demand for energy. This has in turn led to an increasing number of energy related challenges that must be solved over the coming century. This includes the replacement of over-exploited fossil resources, and the reduction in the resulting environmental pollution from these sources. One promising alternative is therefore to combine waste management and energy production, creating suitable fuel and chemical precursors from the conversion of wastes currently underexploited including waste biomass such as agricultural residues and waste fossil plastics.

1.2.1 Biomass

Biomass is a major source of energy and is currently estimated to account for approximately 10–14% of the world's energy consumption [5, 14]. Biomass can generally be classified as organic matter produced via photosynthesis derived from available atmospheric carbon dioxide, water, and sunlight. The primary use of biomass does not directly result in the carbon accumulation in the atmosphere since the carbon released during combustion was taken by the growing plant. However, the overall carbon balance is not neutral when the biomass harvesting, collection and processing is powered through fossil fuels. In the simplest form, biomass can be burned directly to produce heat, fuel gases, steam, and biomass can be converted into electricity via steam turbines [15]. Biomass can also be upgraded into higher-grade fuels such as charcoal, liquid fuels, and gaseous fuels with promising a realistic choice of flexible production [16]. Therefore, the development and production of biomass derived fuels and chemicals has been heavily researched and developed since the 1970s [17-20].

The use of biomass in biofuels is classified into three main types of biomass categories as first, second and third generation fuels. It is generally agreed that first generation biofuels are produced from agricultural crops, in direct competition with food, which are mainly used for the production of bioethanol (i.e. sugar cane) or biodiesel (i.e. palm oil) production [21]. The use of these resources for energy production leads to competition with food crops, the competition for fresh water, and also has been demonstrated to impact on biodiversity, especially in the case of palm oil. Second generation biofuels tend to refer to the transformation of municipal waste, agricultural residues, or alternative lignocellulosic material which do not compete with food crops.

This has several advantages over bioenergy sourced from first generation sources such as better energy balances, lower greenhouse gas emissions, lower land requirements and less competition with food production [22]. As such the use of lignocellulosic biomass can be one of the most promising sources of biofuel as it provides a way to simplify the disposal process as well as providing energy rich useful products [15]. One promising example of lignocellulosic agricultural residues are pistachio hulls.

The pistachio nut is one of the most popular tree nuts of the world originally from central and western Asia which was spread throughout the Mediterranean countries [23]. According to the reports of the Food and Agriculture Organisation (FAO), approximately 30 million tonnes of pistachio nut waste is annually disposed to landfills by the pistachio nut processing industries, i.e. a huge number of pistachio hulls and shells are available. Currently, large quantities of pistachio biomass are disposed of as agricultural waste, resulting in the considerable issue of the need of waste disposal. Considering the chemical composition, pistachio hulls provide a rich source of natural phenolics and oxidants. Phenolics content of pistachio hull is found higher than the skin and nuts [24, 25]. Consequently, the pistachio hulls, particularly the phenolics derived have gained attention recently as an alternative renewable source. Phenol is an organic compound which is produced from petroleum derived feedstock. Processing of pistachio hull wastes to a renewable energy source is therefore a promising step towards reducing the environmental impacts of fuel production.

Some publications also include a third-generation biofuel feedstock which is typically a marine resource such as microalgae or macroalgae. For example, biomass from marine macroalgae is reported in the UK bioenergy strategy as “an important source of liquid biofuel” [26]. Macroalgae-derived fuels are receiving growing attention, with substantially high growth rates and photosynthetic efficiencies. The key benefit of macroalgae is the potential to cultivate and harvest in large equal environmental merits as they are grown in marine systems. In addition, macroalgae can be grown under worse water and nutrient conditions and thus do not require additional fertilizer or artificial illumination [27]. Also, macroalgae contains higher carbohydrate content which makes them suitable for bioconversion into fuel molecules [28]. After harvest, marine macroalgae go through several process units, including pre-treatment, saccharification and fermentation, and the thermochemical process to be converted to

biofuel [29-31]. Therefore, macroalgae is a promising raw material to provide environmentally and economically feasible alternatives for energy and environmental challenge.

1.2.2 Fossil derived plastic waste

Ever since the first commercial production of synthetic polymer took place in 1940s, the global production of plastic has been increasing substantially. The total plastic production is estimated to exceed 300 million tonnes and is still increasing by approximately 4 wt.% a year [32]. Plastic waste can be divided as municipal and industrial wastes [33]. Industrial plastics are generally homogeneous and have good physical characteristics, this make them useful for downcycling into lower-grade plastic products [34]. Municipal plastics tend to be heterogeneous in nature and have a number of different materials derived from various types of applications [34]. Municipal wastes, commonly known as municipal solid wastes as they are discarded and collected as household wastes [33]. In general, about 10-15 wt.% of municipal wastes consist of plastics [35, 36]. It is estimated that the global plastic waste generation in 2025 will increase to 9-13% of total municipal solid waste [8]. The plastics contained in municipal solid waste consist of 50-70% packaging material which derived from low-density polyethylene (LEPE), high-density polyethylene (HDPE), polypropylene (PP), polyethylene terephthalate (PET), polystyrene (PS) and polyvinyl chloride (PVC).

The largest volume of plastic produced by far is the polyolefins (PP and PE). HDPE can be found in bottles, storage boxes, pipes and cable insulations. LDPE can be utilized for packing like foils, tray, and film material. PP, PS and PE, have also been extensively found in the packaging industry [37, 38]. Poly(vinyl chloride) (PVC) is another commercial plastic commonly used in the fabrication of pipe, packing materials, and insulation [39]. Poly(ethylene terephthalate) (PET) use has increased with various applications such as food and drink containers, electronic components, and textile fibres [40].

Between 4.8 and 12.7 million tons of mismanaged land-based plastic was predicted to enter the ocean during 2010 [41]. 5.25 trillion plastic particles (weighing 268,940 tonnes) were estimated to be floating in the world's oceans in 2014 [42]. The actual number is difficult to calculate, due to the many different sources and environment

transport pathways, but this plastic debris has been accumulating in the marine environment and has been an environmental concern for decades. There has been evidence showing negative effects on organisms, ecosystems, and socioeconomic sectors[43].

High volume plastic packaging usage includes polyethylene, polypropylene, polystyrene, polyethylene terephthalate, and polyvinyl chloride are reflected in their production and consequently these have high possibility of ending up in the ocean environment. An estimated 60-80% of plastic found in the marine environment is from terrestrial sources [44], with the remaining number of marine plastic fragments found in the ocean environment has resulted from the fishing industry [45]. Currently, at least 640,000 tonnes of discarded fishing gear is estimated to flow into the sea every year, which amounts to 10% of total marine debris. These discarded fishing items are mainly nylon monofilament lines and netting[46].

Indeed, the management of plastic waste is a key challenge for many countries. The UK exported some of its plastics for recycling to China, however since the Chinese government banned the import of certain grades of solid waste, exports to Southeast Asian markets have been rapidly increasing. However, plastic scrap export presents a lost resource, investment and job opportunities as well as increasing the risk of materials being processed at overseas facilities[47]. The cost of transportation, labour and maintenance may also increase the cost of the recycling process. In the UK, approximately 55% of the plastic wastes were found in landfill, 26% were recycled, and 18% were used for energy recovery [9]. This demonstrates that despite a large effort around collection and recycling the majority of plastic waste ends up in landfill. Polyolefins are not biodegradable over acceptable timeframes and it has been estimated that it would take over 500 years for them to biodegrade [10]. Since the molecular bonds are made up of hydrocarbon chain polymer derived-petroleum refining, resulting in the strong bonds between hydrocarbon monomers. Thus it is hard to make the degradation process at ambient temperature [32]. The continuous disposal of plastic in landfill, therefore, has become a major environmental issue.

Recycling is widely applied to minimise plastic waste. The most common method for the recycling of plastic waste is mechanical recycling consisting of collection, sorting, resizing, wet separation, dry separation, and compounding. These techniques result in significant energy consumption. Also, recycling degrades the quality of the resource.

Recycled virgin plastic material can be reused 2-3 times only because the strength of plastic material is reduced after every recycling due to the thermal degradation.

As such, alternative routes to use plastic have been investigated, so called upcycling, where higher value products are produced (as opposed to the down-cycling to make lower quality plastic). One such route is to produce crude oils from the pyrolysis of used polyolefins, which can be upgraded into transport fuels. As there is little oxygen in the polymers, the fuel obtained from plastic wastes has a comparably high calorific value to petroleum fuels [48].

1.3 Liquid biofuel production

The conversion of renewable feedstocks into liquid fuels are generally classified into either biochemical [49, 50] or thermochemical pathways [51-53]. The most successful routes to date are mainly biochemical with both ethanol and butanol fuels readily available [54]. However, in the processing of plastics wastes and complex biomass sources, thermochemical processes have been shown to be more effective [55]. Thermochemical processing uses rapid heating to breakdown the feedstock, to produce a range of products including a bio-oil that can be further upgraded. The two major routes to liquid fuels are pyrolysis and hydrothermal liquefaction. However, there are significant differences between these two pathways: pyrolysis is typically defined as a thermochemical decomposition of biomass at a temperature between 375-700°C, which requires biomass drying, while hydrothermal liquefaction processes the biomass in subcritical water, under high pressure, using this as the reaction medium, avoiding the energy losses associated with drying the feedstock.

1.4 Pyrolysis processing

Pyrolysis is defined as the efficient thermal decomposition of complex macromolecules to smaller molecules occurring in the absence of the oxidizing agent. During the pyrolysis process, three products are always forming including organic vapours, which is known as ‘pyrolysis-oil’ when condensed, together with pyrolysis gas and biochar (**Fig. 1.4-1)**. Among the three major biomass components of cellulose, hemi-celluloses, and lignin, the decomposition of cellulose has been most widely analysed and best comprehended [56]. During the pyrolysis process, lignocellulose can be decomposed via several reactions which include dehydration, depolymerisation, isomerization, aromatization, decarboxylation, and charring. There are three main

stages that occur during the pyrolysis process: (i) initial evaporation of free moisture at the medium surface, (ii) primary decomposition, (iii) lignocellulose cracking and re-polymerisation [57, 58].

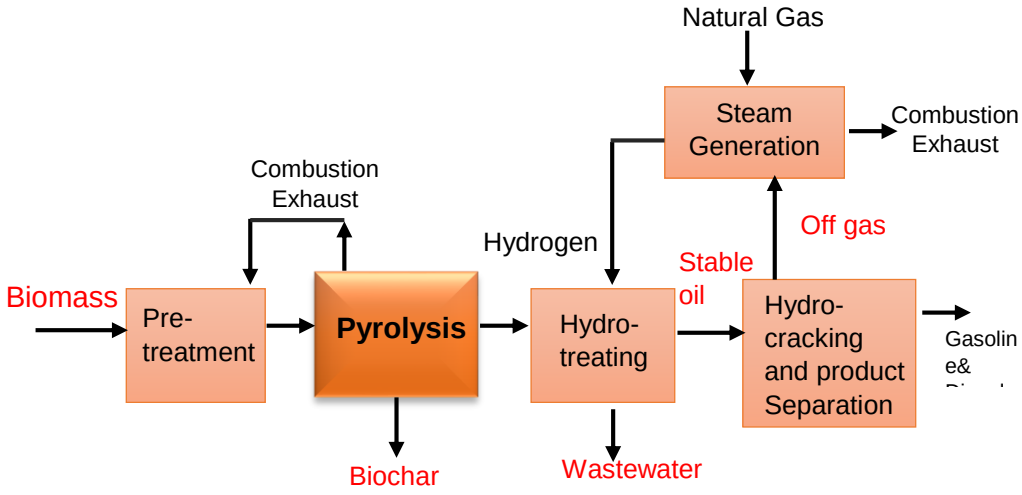

Figure 1.4- 1–Represent downstream processing of pyrolysis products [59]

The proportions of the products produced are dependent on the type of material feed and the use of pyrolysis operating conditions. Pyrolysis of lignocellulosic biomass generally starts at the temperature range between 300 and 650°C. Hemicellulose decomposes from 250 to 400 °C, cellulose decomposes between 310-430°C, some char formation is always observed with cellulose. Lignin begins to decompose at between 300-350°C though a large proportion of up to 55 wt.% of char is produced [60]. The liquid product from the biomass pyrolysis process is termed pyrolysis oil or bio-oil. During the storage process, the properties are changed considerably due to the inherent chemical instability. Bio-oil is a complex mixture of many organic compounds, comprising of acids, alcohols, aldehydes, esters, ketones, phenols, and lignin-derived oligomers.

According to the heating rate during pyrolysis, pyrolysis can be classified into three categories: conventional or slow pyrolysis, intermediate pyrolysis, and fast or flash pyrolysis. In slow pyrolysis, the process is carried out under very slow heating rates (0.1–1°C/s) [61]. The major production of slow pyrolysis has been conventionally applied to the production of charcoal which is also known as carbonisation [62] and the product also consists of up to 25% water content. At the intermedia (75°C/s)[63], pyrolysis consists of a fast heating rate, a residence time between 10 and 30 s at a higher temperature (300-700°C) [64]. Regarding the fast pyrolysis process, biomass

rapidly decomposes, with a heating rate between 10 and >1000°C /s. The process is quickly heated in the absence of air, vaporises and the process provides the liquid products via the short residence time (< 2 seconds).

Although pyrolysis offers an effective technology to convert the biomass, pyrolysis oil produced from biomass requires expensive and energy intensive postprocessing. For instance, pyrolysis fuels obtained from biomass are deoxygenated in the presence of hydrogen under high-pressure (∼10 MPa) catalytic reactors operated at temperatures of ∼350−400°C. The pre-drying process of biomass is necessary, particularly when processing with wet feedstock such as food waste and algal biomass. Pyrolysis also needs crushed biomass particles to improve heat transfer, heating rate and to quench the hot pyrolysis vapours. The fuel characteristic of pyrolysis oil before its treatment by deoxygenation shows high oxygen content of around 30-40%, which leads to undesirable properties such as low energy, instability, high density and corrosion [65].

1.4.1 Pyrolysis products

1.4.1.1 Pyrolysis oil

Pyrolysis oil is the multi-component mixture comprised of various molecules that are produced via depolymerisation and fragmentation of cellulose, hemicellulose, and lignin. Pyrolysis oil mainly composed of oxygenated compounds, which lead to high thermal instability, and low heating value, making it unusable as an engine fuel[66]. Pyrolysis oil generally contains a high-water content (15-30 wt.%) from the initial moisture of biomass and dehydration reaction that occurs during the pyrolysis process. The high amount of water results in phase separation between the liquid phase resulting in lowering the heating and flame temperature. In contrast, the high water content has some positive side effects; increasing the flow property (viscosity) which helps in improving the atomization and combustion in engine [67]. Pyrolysis oil is moderately acidic (2.5-3.0 pH), resulting in an extremely unstable product.

The viscosity of pyrolysis oil is another important specification of oil influencing the pumping condition. High viscosity can result in ineffective pumping and atomization. The reduction of the viscosity can be achieved by adding polar solvents. Different biomass feedstocks lead to different viscosity properties. The viscosities were also decreased in the presence of higher water content and less water insoluble components [68]. The kinetic viscosity of 70 –350 mPa s, 10 –70 mPa s and 5 –10

mPa s were observed for *Pterocarpus indicus, Fraxinus mandshurica,* and rice straw, respectively [69]. Basic data for pyrolysis oil and conventional petroleum fuels are compared in **Table** 1.4-1.

Table 1.4- 1–Composition and physicochemical properties of wood pyrolysis oil and heavy oil [70]

Physical property	Pyrolysis-oil	Heavy fuel oil
Moisture content (wt.%)	15-30	0.1
pH	2.5	-
Specific gravity	1.2	0.94
Elemental composition (wt.%)		
C	54-58	85
H	5.5-7.0	11
O	35-40	1.0
N	0-0.2	0.3
Ash	0-0.2	0.1
HHV (MJ/kg)	16-19	40
Viscosity (at 50°C) (cP)	40-100	180
Solids (wt.%)	0.2-1	1
Distillation residue (wt.%)	Up to 50	1

Due to the high oxygen content of pyrolysis oil, the pyrolysis oil is immiscible with non-polar liquid hydrocarbons, and it cannot be used or processed together in the same facilities. The high oxygen content leads to major drawbacks including the polarity, the acidity, the low relative heating value, the viscosity and the reactivity, and these parameters influence its overall phase stability.

In order to increase the stability and decrease the oxygen content of pyrolysis oil, a mild hydrotreating process has shown the advantage of stabilization through hydrodeoxygenation (HDO). Hydrotreating is a well-established refinery process for ensuring emission regulations and removing hazardous substances of fuels such as sulphur, and metal from petroleum fractions. The pyrolysis oil upgrading step takes place between 250-450 °C under high-pressure hydrogen (7.5-30MPa) in fixed bed reactors[71]. Since a first attempt at using a single-hydrotreating resulted in fouling of the catalyst bed after few hours on stream[72], a two-step process using a mild severity condition was therefore developed to overcome the reactivity of bio-oil. In this process,

the bio-oil was stabilised in a lower temperature reactor (150-280°C) before bio-oil was further processed in the second state hydrotreater at higher temperature reactor (350-400°C) where the main chemical reactions took place[73]. This product was then hydrocracked, and the second-stage product separated into product oil. Wastewater, and off gas streams were also produced as a by-product (**Figure 1.4-2**). Bio-oil can be further processed into gasoline and diesel stream or sent to refinery. The wastewater product contains dissolved organics which can be treated to reduce their proportion to less than 2% by anaerobic digestion. The gas stream contains light hydrocarbons, excess hydrogen, and carbon dioxide, and it can be sent to a Pressure Swing Adsorption (PSA) module to recover the hydrogen gas and send it back to the hydrotreater [59].

Hydrogen consumption was reduced but large amounts of CO_2 are generated [74]. The oxygen content of the final product was 0.5 to 2.3 wt.% and gasoline range aromatic hydrocarbon in the liquid product was reported to be 87 % (v/v)[75]. The hydrotreating process is usually carried out with a biofunctional catalyst containing hydrogenation promoters, for example, nickel and tungsten or molybdenum sulphide (MoS_2) on acid support, such as silica-alumina.

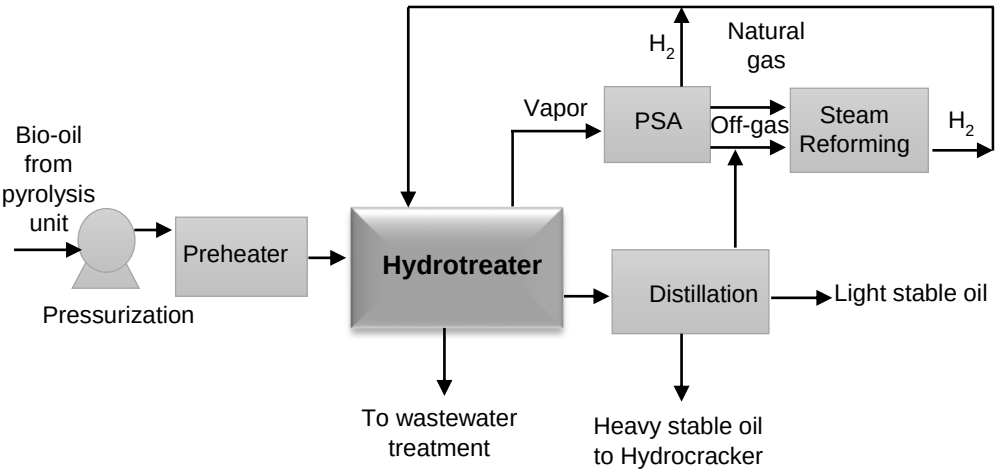

Figure 1.4- 2–Diagram of bio-oil upgrading by hydrotreating process[59]

1.4.1.2 Pyrolysis char

Pyrolysis char is a stable carbon-rich by-product obtained via the pyrolysis process of biomass. Pyrolysis char has different chemical and physical properties depending on

biomass composition and process conditions. Pyrolysis char contains a carbon content of 53-96 wt.%. The yield and heating value of bio-char varied in a range of 30-90 wt.% and 20-36 MJ/kg, respectively [76, 77]. Pyrolysis char can be burned to generate heat energy in most systems that are currently burning solid fuels [78]. The potential bio-char applications include carbon sequestration, soil fertility improvement, pollution remediation, and agricultural by-product/waste recycling [79]. Pyrolysis char is also used as catalyst, energy storage and environmental protection, and a sorbent for the removal of pollutants in flue gas, such as SO_2 and NO_x [76].

1.4.1.3 Pyrolysis gas

The pyrolysis of biomass forms a gas product consisting of carbon dioxide, carbon monoxide, hydrogen, methane, ethylene, propane, sulphur oxide, nitrogen oxide, and ammonia[80]. Carbon dioxide and carbon monoxide generally originate from decomposition and reforming of carboxyl and carbonyl groups [79]. Since the pyrolysis gases are the components of syngas (carbon monoxide, carbon dioxide, and hydrogen), pyrolysis gases are applied for energy source[5, 81]. The pyrolysis gases are also used for fluidization [82]

Reaction temperature provides a significant role in the distribution and composition of gas production formed during the pyrolysis process[83]. Increasing temperature pyrolysis will increase thermal decomposition and devolatilization of biomass. Moisture content also has a significant formation effect of pyrolysis gas. High moisture content enhances the extraction of water-soluble components from the gaseous phase, leading to a substantial reduction in the production of the pyrolysis gas[84]. Also, small particle sizes have favoured the breaking down of the hydrogen components, leading to increase in hydrogen and carbon monoxide while decreasing carbon dioxide [79].

1.5 Liquid phase pyrolysis (LPP)

Effective pyrolysis is conducted through optimal heat transfer from either the reactor walls, gas phase, or hot sand particles. Good heat transfer is one of the most important factors to increase the yield of bio-oil. During the pyrolysis process, heat is transferred to the biomass's outer surface via radiation and convection. Heat is then transferred to the interior of the biomass via conduction and convection. Heat reaction with high heat transfer is required to obtain through heating rate conditions. Since heat transfer

to interior of the biomass particles is a key factor of pyrolysis reaction, it is necessary to achieve the high thermal conductivity of the pyrolysis process.

One recent idea has been to conduct pyrolysis in the liquid phase as an effective method of reducing heat transfer issues. Liquid phase pyrolysis (LPP) uses a high boiling point carrier oil as heat transfer medium which requires the temperature of the reaction to be reduced to avoid evaporating the solvent[85, 86]. The idea is that as the biomass breaks down into small MW, and therefore lower boiling point products these can be collected through condensation of the reactor exhaust.

Liquid pyrolysis phase has been demonstrated at the OMV refinery in Vienna started running with a 100 kg of biomass per hour. The process is performed at atmospheric pressure, with the bio-oil collected through continuous distillation. The oil is then upgraded with standard hydrotreatment [87]. It was found that LPP process was greatly significant for heat capacity and improvement of heat conductivity for the isothermal process. LPP biochar provided the high-quality product which have benefits for many applications of the industry. The highest liquid oil yield was found to be 25–28% at a temperature of 350°C [87]. Pucher *et al.* [88] investigated the catalytic hydrogenation of dehydrated liquid phase pyrolysis oil. They found that pyrolysis oil from the liquid pyrolysis phase resulted in a lower transportation cost with increasing the density and productivity of future upgrading pyrolysis process. They also studied the activity of catalysts in the HDO process of dehydrated LPP including Ru/C, and Pd/C. The results showed that the Pt/C provided the best catalyst to produce pyrolysis oil with the highest yield of 56%. Berrchtold *et al.* [89] also investigated upgrading liquid-phase pyrolysis via fluid catalytic cracker from biomass (spruce and wheat straw). Vacuum gas oil was used as heat carrier oil in fluid catalyst cracking which allow a definite component of hydrocarbon transferred into carrier oil during the process.

1.6 pressure less catalytic depolymerisation

Due to an attempt of reducing the processing cost of pyrolysis bio-oil products, a company, AlphaKat, developed a technology termed pressureless catalytic depolymerisation (KDV in the original German) which has been considered as an alternative technology to pyrolysis, incineration, and gasification. The KDV system runs at lower temperatures to the LPP process, and reportedly uses a catalyst to aid

in the production of hydrocarbons from biomass. KDV pilot plants have been constructed in Germany, Mexico, Japan, and Korea [90]. The KDV process is reported to convert all kinds of organic substances. This process has been claimed to be successful at atmospheric pressure and temperature between 280-320 °C [91].

The major difference of this process compared to the LPP process is the addition of a binding cracking catalyst with hot heat transfer medium which can be reused again after going through the process. This is coupled to circulating the medium through a high friction turbine, that reportedly gives the required energy to break the biomass down in to smaller molecules. Reportedly, the catalyst acts as ion exchanger which deoxygenates the feedstock [90]. All of the materials are then mixed and heated up to around 250 °C in the friction turbine. Biomass then is separated by the KDV-process along with some carrier oil in the 'Ash-plant' where the hydrocarbons are vaporised for asphalt production (**Figure 1.6-1**).

Catalytic depolymerisation is thought to take place at the temperature between 280 and 320°C [91]. The company claim that during the reaction, hydrogen is generated from the biomass and aids the production of hydrocarbons [92]. The company reports claim that the KDV process occurs in the closed system which there is no gas emission to environment. Condensation observed in the KDV process is estimated in three fractions, consisting of the boiling point from 50 to 150 °C resulting in petrol, 150 and 350°C similar in diesel boiling point, and non-condensable gases. However, there are no peer-reviewed effective, scientific studies supporting these claims for the KDV technology.

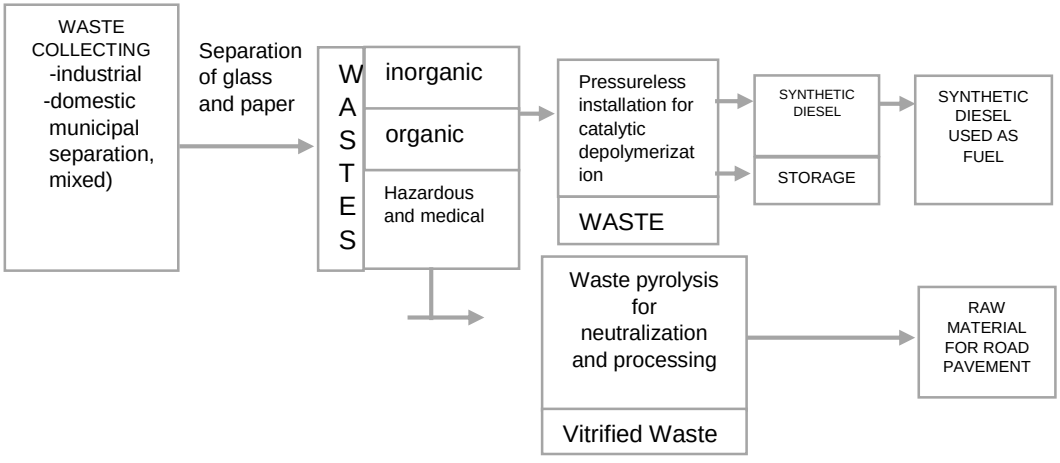

Figure 1.6- 1-Description of catalytic pressure-less depolymerization process

1.7 Hydrothermal liquefaction (HTL)

Pyrolysis requires a dry feed to be effective, and even then, the bio-oil produced is a water emulsion. However, all biomass is inherently wet, and drying is therefore an energy intensive part of any process. This inherent wetness, is especially true of algal or third generation processes which are grown in water. Similar to the LPP process however, biomass can also be processed in water at lower temperatures than pyrolysis but with the water being maintained in the liquid phase through using a pressurized reactor. This type of conversion is termed Hydrothermal Liquefaction (HTL). During the HTL process, the polymeric structure of biomass breaks down into a bio-crude oil, a gas fraction, a carbon rich aqueous fraction and solid fraction in subcritical water or organic solvent medium [93]. HTL is similar to pyrolysis in terms of the target products though the operating processing is markedly different. For example, HTL provides some benefits over the pyrolysis process as it removes the need for a drying stage directly converting wet biomass without the need for an energy use for the drying process and thus leads to a significant reduction of costs associated with pyrolysis [93]. Typical HTL processing conditions are relatively low temperature (280-370°C) and operating high pressure (10-25 MPa) keeping the water below the critical point (**Figure 1.7-1**).

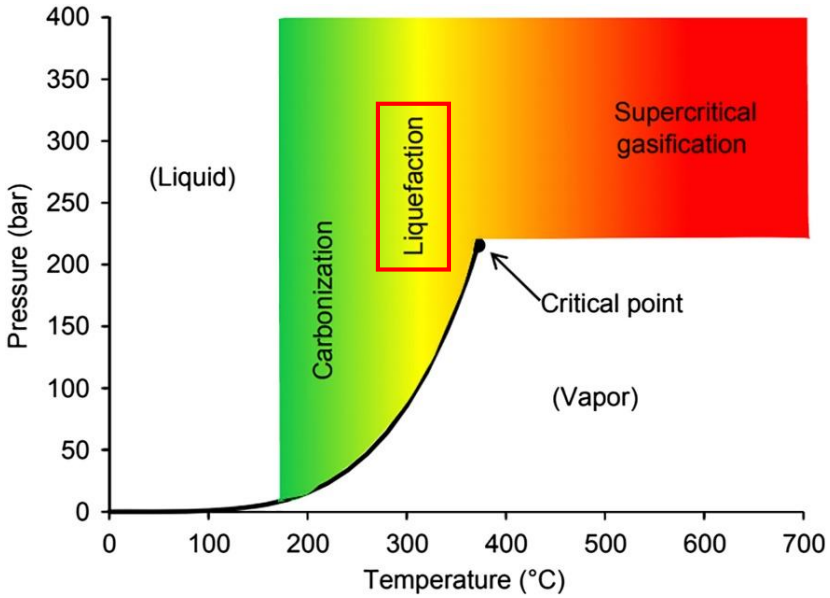

Figure 1.7- 1– Water phase diagram

Water provides key benefits as it is abundant, non-toxic, non-combustible and inexpensive [94]. Under HTL conditions water also plays an important role as a solvent, a reactant, and catalyst resulting in opportunities for separation and chemical reaction. A low viscosity, density, and permittivity, of water also means that under HTL conditions, water has a high solubility to attract hydrophobic components The viscosity of water also decreases substantially with temperature, making water an effective medium for homogeneous reactions. The dielectric constant also decreases from 78.5 Fm^{-1} to 10.5 Fm^{-1}, the solubility of an organic compound such as free fatty acids are enhanced. This results in 100 times of the concentration of protons and hydroxide ions in sub/supercritical water higher than ordinary water [95]. Acid and base-catalyst reactions are processed with non-catalytic HTL to break biomass in sub/supercritical conditions [96]. This result leads to the degradation of macromolecules and the polymerisation of smaller into larger compounds.

Converting the biomass through HTL presents a comparably lower energy consumption for bio-crude production because the water is kept in the liquid phase which avoids the large enthalpic penalty of the phase change to steam. [53, 97]. Also, the single-phase fluid found in sub/supercritical conditions excellently eliminates mass transfer limitations [97] [53].

Table 1.7- 1–Properties of sub/supercritical water condition [96]

Fluid	**Ordinary water**	**Subcritical water**		**Supercritical water**	
Temperature (K)	298	523	623	673	673
Pressure (bar)	1	50	250	250	500
Density, ρ (g cm^3)	1	0.80	0.6	0.17	0.58
Dielectric constant, ϵ (F m^{-1})	78.5	27.1	14.07	5.9	10.5
Ionic product pKw	14.0	11.2	12	19.4	11.9
Heating capacity, Cp (KJ kg^{-1} K^{-1})	4.22	4.86	10.1	13	6.8
Viscosity, (mPa s)	0.89	0.11	0.064	0.03	0.07

The bio-crude oil produced from the HTL process contains multiple products composed of aliphatic and aromatic compounds, and also a high content of oxygen and nitrogen. The bio-crude is also more stable than pyrolysis oil and could possibly be refined in existing fossil refineries to increase the biogenic carbon in the traditional liquid energy and chemical products. An aqueous phase, as well as a fraction of solid residue and gaseous products are also produced (**Figure 1.7-2**).

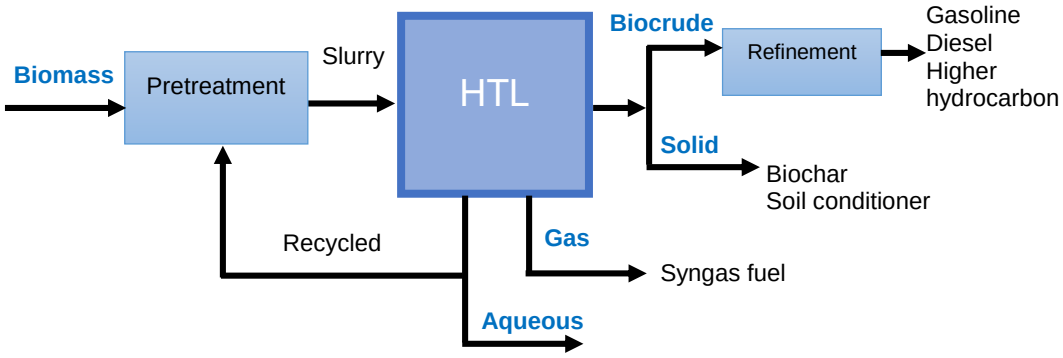

Figure 1.7- 2–HTL process for biomass

1.8 Hydrothermal liquefaction products

1.8.1 Bio-crude

The main product of the liquefaction of biomass is a bio-oil component that is normally termed bio-crude. HTL bio-crudes are compositionally similar to pyrolysis bio-oils, however, they have a far lower O content, H_2O content and tend to be far mor[98]e stable. HTL bio-crudes are a dark viscous liquid, and energy-dense constituents differ from 70 to 95% of petroleum fuel oil [99, 100]. HTL bio-crude generally contains a diverse chemical compound of aliphatic compounds, aromatics and phenolic derivative, carboxylic acids, esters, and nitrogenous ring structures [101, 102]. The chemical compound of bio-crudes has been identified by gas chromatography-mass spectrometry (GC/MS). However, the huge number of chemical compositions of the bio-crude interrupt effective chromatographic separation [103]. Nuclear magnetic resonance (NMR) spectroscopy are also worked for the characterization of bio-oils, which can provide the concentrations of chemical functionalities and indications of highly substituted aromatic groups[103].

Bio-crude composition is influenced by the HTL operating conditions such as temperature, solvent, and residence time. For instance, bio-crude compositions are

influenced by reaction temperatures: HTL bio-crude from loblolly process at 300°C reached to the highest content of acetone and cyclohexane extraction compared to reaction temperature at 250°C, and 275°C, which suggests more further fragment degradation at an increase in the reaction time [104]. The use of different feedstocks significantly affects bio-crude properties. HTL bio-crude oils contain higher nitrogen contents compared to petroleum crudes, especially when the parent biomass contains high levels of protein (such as microalgae), this gives rise to undesirably high nitrogen content and the N-containing compounds in the HTL bio-crude. Yang et al [105] found the individual protein compound in the bio-crude with the addition of nitrogen-containing compounds (such as DKP, amine and amide). Nitrogenous compounds were also observed via GC-MS when bio-crude was produced from swine manure [106]. The high nitrogen content has been found when HTL bio-crude derived from microalgal biomass because it has a 70% protein content but has been not found for the HTL bio-crude derived from lignocellulosic biomass. However, HTL biocrude derived from lignocellulosic biomass results in lower yield and higher viscosities than bio-crude derived from microalgal biomass, but carbon efficiencies of >50% has been found [107].

The higher heating value (HHV) is defined as the amount of bio-crude's energy content, which can be determined by the proficiency of producing raw material to fuel [108]. Bio-crude HHV values show a significant improvement for biomass feedstock due to about 50% of oxygen removal from biomass during the HTL process, resulting in HHV bio-crude of 30-40 MJ kg^{-1}.

Viscosity is an important measurement factor to regulate the flow behaviour of liquid fuel. The typical viscosity of HTL bio-crudes is very high, 10-1000 times higher than petroleum diesel. Bio-crudes with lower viscosity tend to have lower amounts of polymeric species which is important for future application of bio-crude in fuel refining and direct application. The presence of catalyst could reduce the viscosity and produce more light-fraction in bio-crude[109]. Bio-crude produced from various feedstock and their properties are shown in **Table 1.8-1**.

Table 1.8-1– Physical properties of bio-crude produced from various feedstock

Material	Viscosity (cP)	Density (kg/L)	HHV (MJ/kg)	Ref.
Lignocellulose				
Aspen wood and glycerol mixture	-	-	34.3	[110]
Aston wood	210, 40 °C	1.076	37.4	[111]
Forestry residue waste (in the addition of CoMo and NiMo)	78, 40 °C	0.966	41.1	[112]
Algae				
Nannochloropsis	187, 40 °C 48, 60 °C	-	33-36	[109]
Spirulina platensis	190, 40 °C	0.970	34	[113]
Fuel				
Diesel	1.1–3.5, 40 °C	0.850	45.1	
Biodiesel	1.7–5.3, 40 °C	0.880	40.5	

Bio-crudes tend to have a high metal composition, with Ca, Mg, K, Na, Al, Fe all present, especially for bio-crudes produced from high-ash biomass such as macroalgae. Previous investigates have reported that the presence of alkaline earth metals and calcium carbonates can have a positive effect during HTL of algae [114, 115]. High metal content can bring impacts in refining of bio-crude, for example, decreasing catalyst activity, destroying, and coking [116, 117].

1.8.1.1 Bio-crude upgrading to transportation fuels

Solvent extraction is widely used for the purification of bio-crudes in the lab. An extensive range of extraction solvents has been studied, particularly with differing polarities such as tetrahydrofuran, chloroform, dichloromethane, ethyl acetate, and ethanol. Recently, Watson *et al.* [118] studied the effects of the extraction solvent (acetone, dichloromethane, and toluene) on HTL bio-crude, they found that the presence of dichloromethane resulted in the maximum production of bio-crude

for *Chlorella* sp. (48.8%), toluene for *Nannochloropsis* sp. (23.3%), and acetone for *Enteromorpha* pr. (9.8%). Besides, a nonpolar solvent is more effective for separation of HTL bio-crude produced from high protein content feedstock [119]. These results are due to the increased addition of cyclic nitrogen compounds produced by the Maillard reaction between amines and sugars during the liquefaction of high-protein content feedstocks, which can act as radical scavengers and prevent radical chain reaction [120].

Fractional distillation has been used to enhance the properties of bio-crude via separation based on their boiling point. Useful mixtures of bio-crudes are separated into liquefied petroleum gas (LPG), gasoline, kerosene, and diesel. Fractional distillations for producing bio-crude of *Spirulina* sp. and *Tetraselmis* sp. were conducted by vacuum distillation [121]. Results showed that bio-crude properties were improved with the reduction of oxygen and metallic content. The oxygen content from *Spirulina* sp. reduced from 7.9 wt.% for bio-crude to 1.3% wt.% for distilled bio-crude, while the oxygen content from *Tetraselmis* sp. reduced from 12.5 wt.% for bio-crude to 0.4% wt.% for distilled bio-crude at 350°C. On the *Spirulina* sp., the nitrogen content decreased slightly from 6.9 wt.% for bio-crude to 3.8 wt.% for distilled bio-crude, and a slightly decreased nitrogen content was also seen for *Tetraselmis* sp at 350°C (from 5.7 wt.% to 3.9 wt.%). Bio-crude derived from food processing waste and animal manure was also investigated, it was found that bio-crude could be refined into fractions with similar heating value to petroleum diesel [122].

However, the most common bio-crude upgrading process is through hydrodeoxygenation (HDO), which involves hydrogenation and oxygen-removal. Pacific Northwest National Laboratory [123] conducted catalytic hydrotreatment of high pressure and pyrolyzate biomass liquefaction products using model compounds (alkyl phenol and naphthol). Results observed that the presence of sulphide CoMo and Ni provided the greatest effect for the process because they gave high specificity with less saturation of aromatic, this is expected to be useful for producing fuel similar to gasoline. However, the use of sulphide catalysts resulted in sulphur in HDO products. Ru/C was reported to a HDO products with the lowest sulphur, highest hydrocarbon content, and highest heating value (compared to Ru/C, Pd/C, Pt/C, Pt/γ-Al_2O_3, Pt/C-sulphide, Rh/γ-Al_2O_3)[124].

Besides, catalytic cracking can be achieved with moderate conditions with reducing gases and coke and improving the yield of liquid products. Catalysts used in cracking are zeolite, silica-alumina and molecular sieves. There have been a few investigated on cracking bio-oils with zeolites [125, 126].

The co-processing of blending bio-crudes with conventional petroleum refining could be considered as an alternative method to hydrotreatment. Lavanya *et al.* was the first to study the blending of 10% algal biocrude with Narimanam crudes for co-processing to produce biofuels [127]. S and N content skewness were higher in the presence of marine and fresh water algal blends related to pure Narimanam fuel. A 10% blend of biocrude with Narimanam crudes was observed to be effective to reduce the negative effect of impurities in the refining process. Lavanya *et al.* also reported that this process can be applied for downstream processing of bio-crude with reducing capital costs and can be applied in the vehicles without the need for engine change.

1.8.2 Aqueous phase

Other important products are produced alongside the bio-crude in the HTL process. As the reaction is performed in water, the aqueous stream is large and has potential for value utilisation. In general, the compound identified in aqueous contains large quantities of organic carbon, nitrogen, as well as toxic components such as heavy metals and cyclic nitrogenous compounds [128].

Various essential nutrients in aqueous phase at appropriate concentration could successfully support plant and microorganism growth. Jena *et al*[129], for example, used the aqueous phase for cultivating *Chlorella minutissima* without the addition of any external nutrients. It was found that 50% of biomass production increased compared to those obtained in a synthetic medium. The high content of N, P, K, Fe, Ca, and Mg in the aqueous phase can be used as a potential medium for microalgal cultivation [128, 130, 131]. The aqueous phase can be recycled to use as a source for nutrients for algae cultivation, with exploiting bioenergy production of nutrient input derived aqueous phase. The amount of nitrogen from aqueous containing medium to biomass is usually more than 50%, with a high concentration of 78.39% nitrogen content in the HTL aqueous phase produced from microalgal found by Jena *et al*.[129]. A high 99% of phosphorous and 40-100% of ammonium can be recovered by struvite

precipitation [132] and can be used for various applications including algal culture[133].

The aqueous phase has also been recirculated for utilization as co-solvent to investigate the possibility of employing wastewater reuse for bio-crude oil production. In general, all previous studies reported an improvement in bio-crude products and organic carbon content in the aqueous phase. Zhu *et al.* found an increase in bio-crude yields derived from barley straw which increase slightly by 3% after using three cycles of aqueous recycle, the HHVs biocrude production also slightly increased with no apparent differences in elemental distribution[134]. This finding is similar to the study of using three rounds of aqueous recycle from *Salix psammophila* [135]. The large total carbon organic increase was found in co-liquefied aspen wood with glycerol, which increased from 54 to 136 g/L [110]. Recently, Shah *et al.* reported that the energy recovery in the form of bio-crude of sewage sludge increase by 50% with the use of aqueous product recirculation, while nitrogen content in the bio-crude was doubled after eight rounds of aqueous recycle [136]. Recycling aqueous phase also has been reported successfully for microalgal biomass (*Chlorella vulgaris*), with the biocrude products increased by about 33 wt.% and 16 wt.% for Na_2CO_3 and formic acid catalyst, respectively [137]. However, the high organic carbon content and toxic substances are accumulated which required the treatment for recalcitrant contaminants [138, 139].

The aqueous phase has been suggested as a resource for energy recovery. Elliott *et al.* [140] applied the aqueous phase to use as catalytic hydrothermal gasification (CHG) for HTL continuous processing of *Saccharina* spp., resulted in high methane and carbon dioxide gas production. Nitrogen in CHG feedstock remains recovered in the aqueous effluent. Gas produced from the CHG process can be used in combined heat and power applications. Hydrothermal gasification has also been demonstrated for hydrogen production to achieve the need of hydrogenation for the bio-crude [141]. Anaerobic digestion of aqueous phase of HTL also reported as the potential pathway to increase energy recovery. Chen *et al.* investigated methane potentials of the aqueous phase from rice straw [142], they found the highest methane of the aqueous production of 314 mL CH_4/g COD with a lower amount of furans and phenols. Combining HTL with anaerobic digestion of food waste has also resulted in higher energy product recovery [143]. Supercritical water gasification of aqueous phases

from HTL macroalgae species was demonstrated by Duan *et al.* It was found that this process could enhance the energy recovery from algal biomass which consisted of mainly fuel gas, H_2 and CH_4 [144].

1.8.3 Solid residue

HTL conversion of biomass into biofuel also produces a solid residue. Though the composition is different from solid residue derived from high temperature pyrolysis. HTL solid residue, for instance, contains less quantities of heavy and alkaline earth metals as a significant amount of carbon can deposit in this phase depending on the feedstock [145]. HTL solid char derived from lignocellulosic material contains high content of carbon, hydrogen, and nitrogen, while the high nitrogen content is found in a microalgal biomass. The heating value observes to be relatively low for macroalgal biomass (e.g. 4.0 MJ kg^{-1} for marine *Ulva* [117]), but an HHV increase has been observed for oil palm bio-char (e.g. 20.3 $MJkg^{-1}$)[146].

HTL bio-char has a high surface area and pore volume but is rich in surface functional groups [147, 148]. Bio-char with specific surface acts as a remediation implement to absorb organic and inorganic contaminants. For example, HTL bio-char produced from pinewood and rice husk were effective to remove lead from water [149]. HTL bio-char produced from *C. vulgaris* biomass also was activated as an adsorbent in wastewater treatment technology for removing organic pollutants (COD, NO_3, NH_3 and PO_4). These investigations have revealed HTL biochar as one of the potentials for target pollutants.

Based on their composition, bio-char can also be used as co-fired with coal or used for soil amendment [150]. Bio-char has been used for carbon sequestration by Jain *et al*., who presented an improvement of reactivity (oxygen functional group) and mesopore area for coconut shell hydrothermal biochar [151]. H_2O_2 could be used to enhance the oxygen functional groups on the solid char to further improvement for the porosity of activated carbons [152].

1.8.4 Gas-phase production

The gaseous products obtained from HTL consists mainly of CO_2 [153], small quantities of CO, H_2, and CH_4 [154]. Brown et al. produced the gas molar composition consisting of 66.2 mol% CO_2 and 29.7 mol% H_2, and small quantities of CH_4 (1.9

mol%), N_2 (0.43 mol%), C_2H_4 (1.2 mol%) and C_2H_6 (0.6 mol%)[155]. The CO_2 content decreased once the critical point of water was exceeded, while the CH_4 and CO contents increased. HTL gas has low CO content due to the oxygen removal in HTL via decarboxylation, instead of decarboxylation, and the CO produced reacts readily and generates CO_2 and H_2 through the water-gas shift reaction [156].

The gaseous products that contain largely CO_2 may be recirculated for the algae cultivation [130], while the H_2 may be utilized for future hydrotreating of the production of bio-crude [95]. Therefore, gas production is also another useful by-product for a biorefinery.

1.9 HTL process mechanism

The general mechanism of the HTL process is extremely complex and as such has not been identified extensively in the literature. This is mainly due to the difficulties in online monitoring under these conditions, and the rapid conversion of the components in the slurry on reaction. However, many complex reactions are known to occur during the conversion of biomass into bio-crude [157], which leads to the formation of solid, liquid, and gas intermediates, and the interaction between solvent and reaction intermedia. Under HTL conditions, overall, the biomass is broken down into smaller molecules that are repolymerized into a hydrophobic, crude component [158]. Although the biomass contains carbohydrate (cellulose, hemicellulose, starch) lignin, lipid, and protein which are reported HTL reactions individually, the overall HTL reaction kinetics and mechanism are different for actual biomass than just the sum of the single species. Generally, the decomposition of biomass components in subcritical water conditions, however, follow three main reaction stages[96]:

i) Hydrolysis or depolymerization of the biological polymers
ii) Degradation of monomer by cleavage, dehydration, decarboxylisation and deamination
iii) Condensation, polymerization, isomerization, and recombination

The HTL reaction starts with hydrolysis, where the protein and carbohydrate macromolecules form water-soluble oligomers and monomers. The oligomers and monomer can undergo further degradation, repolymerization or have their functional groups reduced.

Cellulose, the most prevalent polysaccharide in biomass, is a linear polysaccharide of glucose monomers, connected by β-1→4 glycosidic bonds. Hydrothermal degradation of cellulose consists of two major steps: saccharification and carbonization [159]. Water-soluble sugars are the major intermediates in saccharification, carbohydrate intermedia such as fructose and glucose are detectable at a low operating temperature for example. These sugars are then decomposed through dehydration, decarboxylation, and aromatization leading to acetic acid, acetaldehyde, glyceraldehyde, glycoaldehyde, furfural derivatives. Repolymerization of water insoluble products results in production of solid-char [53]. The overall degradation route of glucose is shown in **Figure 1.9-1**.

Another large saccharide portion in biomass is hemicellulose. This polysaccharide is highly varied and consists of a wide range of sugar monomers such as xylose and mannose monomers, glucose and galactose. Hemicelluloses have different crystal structure and resistance comparing to cellulose. This leads them to be more conducive to hydrolysis and they can be solubilized and hydrolyzed in water at 180ºC. Xylose is a major breakdown product of the hemicellulose and further degrades to form a pyranose ring, a furanose ring or an open chain structure. The pyranose ring can produce furfural, while its open chain form can react to form glyceraldehyde, pyruvaldehyde, formic and lactic acids.

The carbohydrates in biomass are fundamentally polymers of monosaccharides that are rapidly hydrolysed under subcritical conditions. Glucose is the main hydrolysis product. Glucose itself reversibly isomerizes into fructose. The rate of glucose isomerization to fructose was essential in hydrothermal media. The fructose itself is rapidly decomposed at 300-400ºC and pressure of 25-40 MPa through isomerization, dehydration, defragmentation, rearrangement and recombination resulting in the production of phenols, furans, acids and aldehydes. Phenols are a second possible product formed from short-chain degradation products [96].

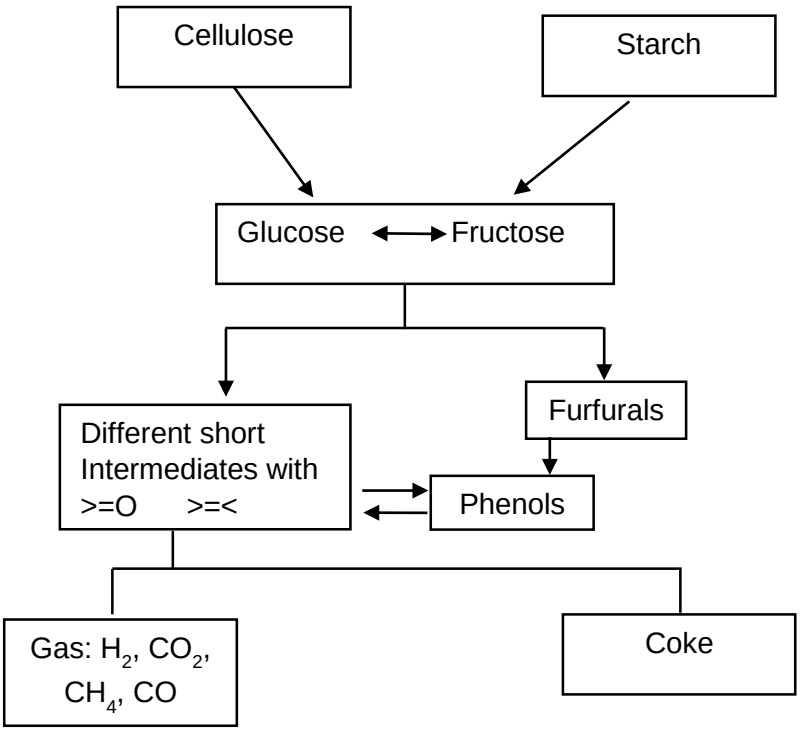

Figure 1.9- 1–A simplified reaction mechanism for carbohydrate degradation at subcritical/supercritical conditions [96]

Lignin is another main component contained in the structure of lignocellulose which is more irregular in structure and higher molecular weight than hemicellulose. Lignin consists of an aromatic heteropolymer containing p-hydroxyphenyl (H), guaiacly (G), and syringyl (S) monomers. Lignin is a phenolic compound consisting of a variety of linkages connecting three phonylpropane units connected by α-O→4 and β-O→4 bonds [160]. Due to the decrease in the density of water and an increase in ionic products under HTL conditions, hydrolysis of lignin increases and leads to the deposition of lignin to its low molecular weight components, consisting of phenols and methoxy phenols which are decomposed through hydrolysis of ether-bonds and can also be further degraded via hydrolysis of methoxy groups. However, benzyl aryl ethers, benzonitriles, pyridine carbonitriles, benzamides, and cyclohexyl phenyl compounds remain bound in the crosslinked structure of lignin below 260ºC. Hydrothermal liquefaction of lignin results in a substantial production of solid residue.

Proteins are an essential component in some lignocellulosic materials, and in third generation resources such as macroalgae. Proteins are polymers of amino acids, each linked to its neighbour through a covalent peptide bond. During the hydrolysis of

biomass, protein is firstly hydrolyzed to peptides and amino acid through two main paths including deamination and decarboxylation [96]. A considerable fraction of the nitrogen in proteins is incorporated into the bio-crude products during subcritical temperature, while nitrogen as ammonia is incorporated into the aqueous phase products. Maillard reactions between amines and sugars lead to the formation of nitrogen containing cyclic organic compounds such as pyridines and pyrroles. The formation of these compounds can act as radical scavengers and inhibit radical chain reactions that are extremely relevant for gas production at sub/supercritical conditions (**Figure 1.9-2**) [161].

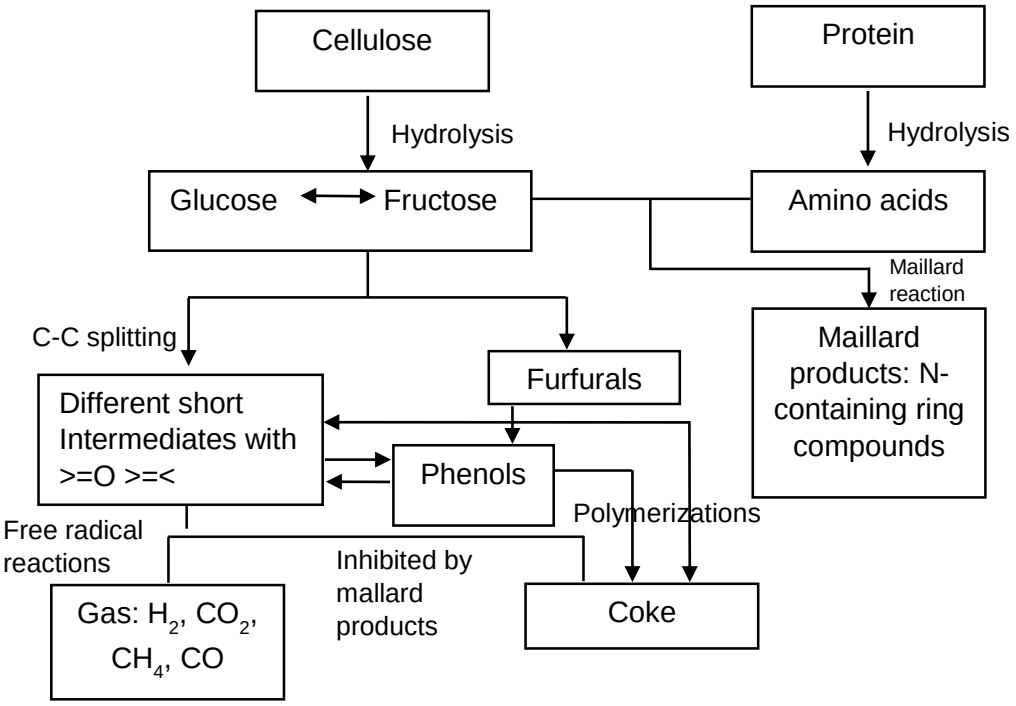

Figure 1.9- 2–A reaction mechanism for cellulose and protein degradation at subcritical/supercritical conditions [79]

1.10 HTL operational parameters

1.10.1 Temperature

Reaction temperature has been identified as one of the most essential operating parameters in HTL processing and strongly effects bio-crude yield and properties. The temperature enhances the synergetic effect on the yield of bio-crude oils due to

extended biomass fragmentations with an increase in temperature. The depolymerization of biomass occurs when the temperature is higher than the activation energy for the bond cessation. The effect of the reaction of temperature on the product yields is sequential. Firstly, the increase in temperature activates the biomass and the polymeric structure begins to depolymerize. A series of reactions then yield liquid fuel production, however, at these high temperatures the crude components will themselves begin to degrade, leading to the formation of gaseous components. In addition, at high reaction temperature, the concentrations of free radicals are high, and the recombination of free radial reactions contributes to a large char deposition in the solid residue. For example, a temperature below 280°C leads to incomplete decomposition of individual biomass components (lignin and cellulose fragments). Whereas 300–350 °C is optimal for bio-crude production.

Figure 1.10-1 shows the difference in terms of bio-crude oil produced from biomass as a function of temperature. 300-315°C was observed to be optimal operation conditions for bio-crude oil by the investigations of Zhou *et al*. [102], Yin *et al*.[101], Sugano *et al.* [162], and Qu *et al*. [163]. Biomass feedstocks reported were macroalgae, cattle manure, wastewater, and *Cunninghamia lanceolate*, respectively. Xiu *et al.* found that bio-crude yield of manure increased when increasing temperature from 260 to 340 °C [164]. The synergetic effect of bio-crude yield increase with temperature increase were also reported by the study of Karagöz *et al*. The bio-crude oil yields were observed to be 3.7%, 7.6%, and 8.5% at 180°C, 250°C and 280°C, respectively, but gas formation increased when temperature higher than 374°C used [165].

Reddy *et al.* also reported that the bio-crude yield obtained from the HTL of *Nannochloropsis gaditana and Chlorella* sp. increased when the temperature increased, increasing from 16.85% to 47.5% at a temperature from 180 to 330°C for *Nannochloropsis gaditana* [166]. However, 79% of energy in the *Nannochloropsis* sp. was recovered at 330 °C, while 62% of energy recovery from *Chlorella* sp. was recovered at 200 °C. Zhu *et al.* conducted HTL of barley straw at 280°C and 400°C, the result showed that quality of the bio-crude oil had been enhanced due to low oxygen content and higher HHVs at high temperature [134].

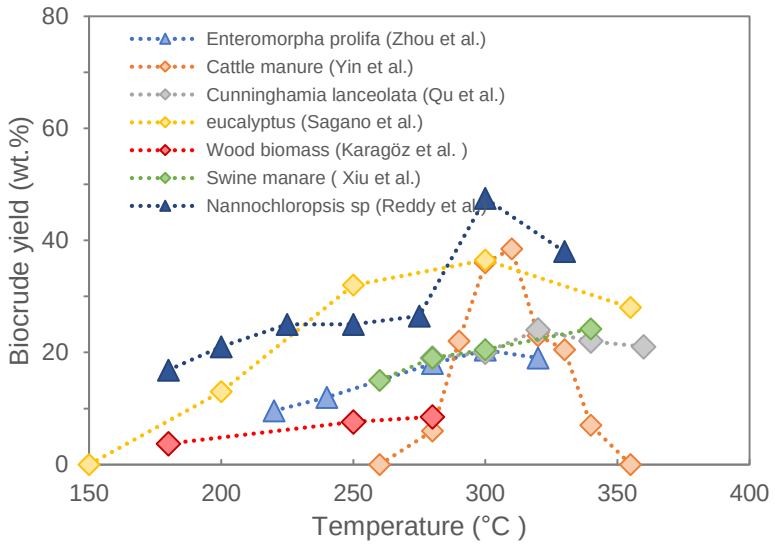

Figure 1.10- 1–Bio-crude oil yields as a function of temperature

1.10.2 Heating rate and residence time

As temperature has a large effect on bio-crude yield, the optimal temperature for bio-crude production will also lead to a reduction in the crude yield if the reaction mixture is held under conditions for too long, therefore heating rate is key to the successful operation. As such, heating rates have been reported as one of the most significant factors affecting bio-crude oil yields. Several researchers indicated that higher heating rates and short residence times tend to increase the production of bio-crude oil. For instance, Nelson *et al.* suggested that faster heating rates reduced the unavoidable disconnection and recombination of the initial products [167]. For example, when the heating rate increased from 5 to 140°C min^{-1} , the bio-crude yield increased from 50 wt.% to 70 wt.%, while gas and solid formation decreased [168]. However, the heating rate had no significant effect on the chemical composition of the HTL products [168], the composition of bio-crude products is dependent on biomass species. The fast heating rate has also been found to be beneficial on the yield of bio-crude by Xiu *et al*. The maximum bio-crude oil obtained of 21 wt.% at a retention time of 15 min, while the bio-crude oil decreased to 12.5 wt.% at a residence time of 90 min [164].

The formation of bio-crude oil during HTL reactions consists of beneficial primary reactions (pyrolytic and hydrolytic degradation) and non-beneficial secondary reactions (recombination and secondary cracking) [169]. Secondary reactions gradually become predominate at high heating rates which lead to high gaseous

formations especially under supercritical conditions. Appropriate heating rates tend to bring extensive fragmentation and insignificant secondary reactions. Furthermore, fast heating rates are sufficient to succeed in heat transfer restrictions to increase in bio-crude productions [170].

However, a very rapid heating rate and short residence time leads to high levels of oxygen in the crude product, which must be removed through hydrogenation. Long residence times on the other hand, tend to favour polymerisation reactions resulting in lower bio-crude oxygen content and higher carbon content and leading to higher high heating values. For instance, Julia et. al. found that the oxygen content for *Nannochloropsis* sp. decreased from 12.21% to 8.48% for 10 to 90 min reaction times, respectively at HTL temperature of 350 °C [171]. The properties of the liquid fuels tend to be better when processing at the long residence times, meaning that long residence times become more appropriate for bio-crude upgrading due to low hydrogen needed for hydrodeoxygenation. The higher heating value observed at long residence time also leading to higher overall energy recovery.

1.10.3 Particle size

In pyrolysis, where heat transfer is key, small particles are vital to increase the surface area and reduce char formation. In HTL, there is less of an effect, due to the water medium that the reaction is undertaken in. However, small particle sizes have some benefit particularly for continuous processing because it is beneficial for the biomass-water-bio-crude slurries pumpability [172]. It also has been observed that the size reduction of biomass costs a considerable amount of energy.

However, pumping aside, particle size is relatively insignificant. For example, Raikova *et al* investigated the particle size between 125 μm < *n* < 1.4 mm on the bio-crude yield of macroalgae at 350°C. It was found that the particle size did not have a significant effect on bio-crude products, using the largest particle size seems to enhance the high-cost and energy saving [173]. Similarly, Zhang *et al.* investigated the effect of 1 inch, 2 mm and 0.5 mm on the bio-crude oil yield in HTL of grass perennials. Again particle size had no effect on the bio-crude oil yield at 350 °C [174].

However, reducing particle size comes at a large energy penalty. Coarse grinding needs less energy whereas fine grinding needs large energy inputs with a slight increase in surface area. Mani *et al*. investigated grinding performance and physical properties. It was found that grinding cost was reduced from 27.6 $kWht^{-1}$ to 11.0 $kWht^{-1}$ when processing particle size from 3.2mm to 0.8 mm (during dry grinding of wheat straw, barley straw, and switch grass) [175]. The biomass particle sizes of 4-10 mm are suggested for overcoming heat and mass transfer restrictions for appreciate grinding costs [170]. This is another advantage in using HTL over pyrolysis.

1.10.4 Reducing gas/hydrogen donor

Reducing gases are used in HTL reactions to stabilise the fragmented products of liquefaction. Reducing species inhibit the condensation, cyclization, or repolymerization of free radicals, and results in reducing char formation. H_2 appears to be a potential reducing agent, but it presents a costly option. CO, N_2, and Ar have also been applied to offer a reducing environment. The effects of various reducing agents (CO, H_2, N_2, and air) on the bio-crude products of cattle manure were studied through HTL process by Yin *et al*. [101]. The result showed that CO and H_2 were the most potential reducing agent and provided the highest bio-crude oil yield of 50% at 310°C. Reducing gases (CO, H_2) give higher bio-crude products than inert gas (nitrogen and argon). However, the hazardous nature of reducing gas need specific pyrolyzers to prevent the gas channelling and maldistribution during operation [170].

Hydrogen donor solvents have also been reported as an alternative to reducing gases, proving a more desirable option to hydrogenate the biomass fragments compared to reducing gas. Many solvents can be used as effective hydrogen donors as long as they can donate hydrogen to unstable biomass fragments [176]. For example, the presence of alcohol has been shown to result in reducing low-rank coal into bio-crude oil [177, 178]. These suggest that alcohol is connected to the action of the hydrogen donor and its alkylating ability. A reduction of viscosity of bio-crude oil derived-biomass was observed in the presence of organic solvent by Demirbas [179].

Acids such as formic acid can also act as a hydrogen donor to convert bio-crudes to hydrocarbons via following reaction, Bio-Oil + HCOOH → hydrocarbon + H_2O + CO_2. Solvolysis on lignin using formic acid and ethanol has been studied, with the combination of solvents obtaining high-quality liquid oil products [180].

Hydrogen donor solvents such as tetralin and decalin have more substantial enhancement in terms of conversion and contribution to bio-crude products, resulting from the increasing of hydrogenation and hydrocracking reaction with inhibition of polycondensation. Another key benefit of a hydrogen donors is a lower energy bonds of C-H in comparison to H-H bond [176]. For example, the presence of tetralin was more effective than toluene solvent (non-hydrogen donor) and reducing gas (H_2) in terms of enhancing the bio-crude yield with low oxygen contents, with bio-crude yields of 58.9%, 42%, and <40%, respectively. Resulting in increased higher heating values and improved bio-crude properties [181].

1.10.5 Catalysts for the hydrothermal liquefaction reaction

There have been efforts to study various catalysts to increase the yield and improve the properties of the bio-crude through HTL processing. Most research has focussed on heterogeneous catalysts due to the ease of recovery, low corrosion effects, and high catalytic performance [182, 183]. Heterogeneous catalysts such as Ni–Mo sulphide, MoS_2 in the hydrothermal upgrading have been investigated for the hydrodeoxygenation of model compounds such as phenol [184, 185]

One of the most researched heterogeneous systems are inorganic salts. For example, Kong *et al.* suggested that lactic acid could be produced from the catalytic HTL of lignocellulosic biomass in the presence of $ZnSO_4$, $CoSO_4$, $NiSO_4$, $Cr_2(SO_4)_3$ [186]. The effect of metal oxide catalysts on supercritical water conversion of empty fruit bunch derived from oil palm residues was investigated, the authors found that CaO, MnO, La_2O_3 and CeO_2 gave the highest bio-crude (~1.40 times that non-catalytic run) [187]. Raikova *et al*. investigated the suitability of using HTL to process metal contaminated *Spirulina*. This resulted in a positive catalyst effect, metal in the bio-crude oil increased with increasing addition of Mg, Zn and Fe at 310 °C (bio-crude increased from ~36 % for non-additional metal to ~45% for high uptake metal content). Rojas-Perez *et al*. studied the effect of an ultrananocrystalline Fe_3O_4 (UNCFO) catalyst on the production of refined bio-crude via a HTL process using *Ulva fasciata* macroalgae as biomass [188]. It was found that the bio-crude yield substantially increased as the use of UNCFO increased, resulting in the bio-crude yield increasing from 23.3% for non-catalytic HTL to 32.4% for 1.2 wt.% UNCFO loading. Fang *et al.* found that adding 10 %(w/w) iron (III) chloride as co-catalyst in 60% ethanol positively affected bio-crude yield in liquefaction of untreated switchgrass, increasing from 55.7 ± 1.5 to 67.6 ± 2.5%

at 200 psi, 210 °C, 24 hour [189]. This improvement was thought to occur because the acidity provided by $FeCl_3$ in aqueous ethanol promotes further decomposition of hemicellulose and lignin due to chelation with Fe (III).

Recently, Egesa *et al.* studied the efficiency of ferrite magnetic nanoparticles in efficient spirulina separation from a culture medium, finding that magnetic nanoparticles gave a separation efficiency while extracting algae from an aqueous solution of 99%. They also used magnetic nanoparticles as an HTL catalyst, results showed an increase in production of bio-crude oil from 23.2% for pure spirulina to 37.1% for that with the magnetic nanoparticles. Also, recycled magnetic nanoparticles were still effective in microalgal-separation and HTL catalysts, with a separation efficiency of 96.1% and bio-crude yield was increased by 7%[190]. This finding could potentially reduce the cost of advanced algal biofuels leading this process to be preferred compared to petroleum fuels.

Duan and Savage systematically investigated noble metals supported on carbon (Pt/C, Ru/C, Pd/C, Ni/SiO_2-Al_2O_3, CoMo/γ-Al_2O_3, and zeolite) in the liquefaction of *Nannochloropsis* sp. The authors found that Pt/C increased bio-crude yields with the highest carbon and hydrogen contents and HHV. The presence of Ru and Ni catalysts were observed to give an increase in methane, while significant amounts of N_2 was observed in the addition of zeolite catalyst [182]. This indicated that the interaction between ammonia and cationic zeolite is dominated by an electrostatic reaction between counter-ions and the lone-electron pair of nitrogen atoms[191]. Robin *et al.* investigated the activity of HZSM-5 doped with metal (Mo, Ni, Cu, and Fe) in the liquefaction of *P. ellipsoidea.* sunflower oil, *Chlorella vulgaris* and soy protein [192]. Although the presence of metal/HZSM-5 gave an overall decrease in the bio-crude yield, the bio-crude properties were found to be improved. For example, MoZSM-5 increased the production of aromatic compounds, while NiZSM-5 and CuZSM-5 enhanced the deoxygenation. This observation will be important for further investigation of the performance of metal/zeolites for bio-crude upgrading in sub/supercritical conditions.

Homogenous catalysts have also been examined in the hydrothermal liquefaction of biomass. K_2CO_3, KOH, Na_2CO_3, and NaOH of wood biomass were investigated, the bio-crude oil yield with non-catalytic HTL was observed at 8.6 wt.% and was found to increase bio-crude oil to 33.7 wt.% for 0.94 M of K_2CO_3. The catalytic activity was

observed in the following order; K_2CO_3> KOH,>Na_2CO_3 >NaOH [193]. The presence of K_2CO_3 also had a positive effect on the production of bio-crude of barley with an improvement in energy efficiency reported [134]. Jena *et al*, investigated the liquefaction of microalgae *Spirulina platensis* by using Na_2CO_3, $Ca_3(PO_4)_2$, and NiO. Results observed that Na_2CO_3 gave a positive effect on production bio-crude, which was ~29%, ~71% and ~50% higher than non-catalytic, NiO and $Ca_3(PO_4)_2$ catalysts respectively [194]. 5% Na_2CO_3 in the liquefaction of marine macroalgae *Enteromorpha prolifera* also produced the highest bio-crude yield (23.0 wt.%) [102]. However, Li *et al.* investigated 5% Na_2CO_3 in the liquefaction of *Sargassum patens* C. Agardh. Results showed the presence of Na_2CO_3 led to a decreasing of the bio-crude products and an increase of gas and aqueous phase products [195]. The similar findings were reported for KOH catalysis of the brown macroalga *Laminaria saccharina* ,a maximum bio-crude yield of 19.3 wt.% was obtained for non-additional catalyst at 350°C [196].

1.11 HTL continuous processing

Continuous processing is the key to making HTL an industrial process. The benefits of continuous processing include a high throughput and enhanced energy recovery, both key to a biofuel production platform. Continuous reactors require a feeding system that operates under pressure and consist of either slurry pump or lock hopper systems [107]. Forming water slurries of biomass particles are required to maintain a continuous flow. For microalgal biomass, pre-treatment is imperative as their particle size is relatively small, this means that they need the complexities of pumping slurries to the reactor. The processing of lignocellulosic biomass may require grinding or maceration. Algae needs dewatering prior to processing due to their high moisture biomass contents. High moisture content and low biomass feed concentrations have negative effects on HTL product recovery [197]. This can lead to an increase of unnecessary costs for processing excess water [121]. The slurries with small particle biomasses can affect an energetic cost in biomass pre-processing. Low operational cost can be achieved in the utilisation of high slurry concentrations and large particle sizes, but this complicates the logistics of pumping. Higher efficiency pumps can be used to enhance biomass heating rates which have been reported to increase bio-crude conversion [197]. Complex reaction processes are not needed for lignocellulosic biomass as the bio-crude produced contains a small amount in moisture, and oxygen content [198].

Although continuous HTL processes are regularly conducted as tubular reactors, there are also studies where the same conditions were carried out in a continuous stirred tank (CSTR). It has been suggested that fouling and plugging problems could be minimised by using CSTR [199]. This contributes to efficient mass transfer that may support improved biomass conversion. CSTR was chosen over PER for the luxury of handling, to reduce plugging, and to have a temperature control of reaction vessel [200]. However, the plug flow type reactor is more economical at the given design for a large-scale system [201].

Previous batch experiments use hydrophobic solvents through the work-up, with the solids phase collected through filtration. The separation of HTL product and recovery of bio-crude from the reaction mixture in continuous liquefaction can be enhanced by applying organic co-solvents [202].

A high heating value through the continuous process was observed by Elliott *et al.,* bio-crude yield of 82 wt.% on a carbon basis was achieved with high slurry contents of 34 wt.% on dry solids [140]. The study of Pedersen *et al.* found bio-crude oil properties of aspen wood similarly to gasoline [110]. Mørup *et al.* also reported the advantage of processing the continuous flow reactor enhanced HTL product conversions compared to the conventional batch systems [203].

1.12 Co-processing of plastic with biomass

The three thermochemical techniques (fast pyrolysis, liquid phase pyrolysis, and hydrothermal liquefaction), presented are therefore suitable for the processing of biomass or plastics into liquid fuels. However, the co-processing of both sources together has only really been investigated heavily in the area of pyrolysis. Plastics are organic polymers that originated from petrochemicals and generally contain high carbon and hydrogen content. Polyoelfins have little or no oxygen, and HHV similar to petroleum fuels.

1.12.1 Co-pyrolysis of fossil derived plastics with biomass

Co-pyrolysis of biomass with a hydrogen-rich feedstock, such as a polyolefin, is an ideal processing strategy, potentially allowing the stabilisation of the pyrolysis vapour and lowering of the overall oxygen content. Co-pyrolysis of biomass and plastic mixtures have gained much attention over the last 20 years, demonstrating an alternative technique to recycle polyolefins alongside lignocellulosic material,

producing a range of high-value products, the recovery of bulk chemicals as well as generating renewable energy [204]. The co-pyrolysis also produces superior pyrolysis oil with an increase in the yield and producing better properties such as elevated HHV. The co-pyrolysis processes are more cost-effective than other conventional technologies for improving biofuel due to avoiding the use of solvent, catalyst, or hydrogen.

The available literature on the non-catalytic co-pyrolysis of different biomass types with plastic blends is summarised in **Table 1.12-1.** There has been found that polyethylene is widely used for co-materials with biomass, while waste plastics such as polypropylene, polystyrene, polyvinyl chloride, and polyethylene terephthalate have also been reported[205]. Co-processing of biomass and plastic have been conducted in a range of reactors including batch and fixed bed.

For example, Pinto *et al*. aimed to valorise of rice crop waste mixture (rice husk and rice straw) by co-pyrolysis with PE to produce energy products [206]. A higher yield of bio-oil was produced in the co-pyrolysis of rice husk with PE, while more gas products were obtained in the co-pyrolysis of rice straw with PE. The pyrolysis oil products consisted mainly of aliphatic hydrocarbon (alkanes and alkenes). Aliphatic hydrocarbons were also the main component in the bio-oil produced from the co-processing of an almond shell with HDPE [207, 208]. Xue *et al*. also found the positive synergy between red oak and HDPE in continuous fluidized bed reactor, the result obtained with the higher heating value and aliphatic hydrocarbon formation [209]. In these studies, the co-pyrolysis with HDPE also seemed to reduce the solid residue, presumably as the plastics fragments mainly distributed into the oil phase. Costa et. al. reasoned that the presence of HDPE enhanced the biomass conversion and improved heat and mass transfer in the pyrolysis reaction [18]. The HHV of the pyrolysis oil produced from the co-processing process were all improved in these studies [210]. Zhou et al. investigated the kinetics of co-pyrolysis of plastic (HDPE and LDPE) and biomass (pine wood sawdust) by using the thermogravimetric method. The investigation identified that the thermal degradation temperature of plastic was 438-521°C, while the thermal degradation temperature of biomass is 292-480 °C [211].

The co-pyrolysis of polypropylene with biomass created a more varied pyrolysis oil. For example, producing a range of long-chain alcohols (C8-C20). The authors reasoned that these were obtained from the interaction between cellulose and

polypropylene. The highest yield of alcohol was 36 % of the total pyrolysis oil, and the highest HHV of 41 $MJkg^{-1}$ were also obtained for the co-pyrolysis of cellulose and polypropylene [212]. The positive synergetic of alder wood, pine wood, and pine wood sawdust with PP in the co-pyrolysis has also been reported [213]. Due to these reactions, the presence of polypropylene as a co-feedstock did not only generally improve the biofuel quality, but also decreased the solid residue forming.

For the co-pyrolysis with polystyrene, which has a far lower hydrogen to carbon ratio, the pyrolysis oil is not as well stabilised, however, in the presence of cellulose a substantial increase from 45.5 wt.% yield to 80.10 wt.% yield, compared to cellulose alone was observed with 3:1 (cellulose: PS) added to the feed [214]. The substantial pyrolysis oil increase was also found in the co-pyrolysis of pine and cellulose with PS (from 47.5 wt.% to 69.7 wt.%) for the presence of pine core, and from 46 wt.% to 62 wt.% for the presence of palm shell [210, 215]. The addition of PS led to the pyrolysis oil properties enhanced by decreasing of acid number, pour point, and density. The improvement of HHV was also found in the co-pyrolysis of palm shell and polystyrene, with the HHV improved from 11.94 MJ kg^{-1} to 38.01 MJ kg^{-1}.

The co-pyrolysis of rice straw with PET has also been examined. It was found that the pyrolysis oil product was obtained with a higher water content (52.46 wt.%) leading to a lower high heating value (14 $MJkg^{-1}$)[216]. The pyrolysis solid phase produced from the co-pyrolysis of wood sawdust and PET might be suitable to apply for soil separation [217].

The effect of co-pyrolysis of the biomass component (cellulose, xylan, and lignin) with PVS on the formation of polycyclic aromatic hydrocarbon (PHA) was conducted at 800°C in a fixed bed reactor coupled with a hydrochloric acid (HCl) absorption system. This resulted in an overall decrease of PAH components (polycyclic aromatic hydrocarbon) in the tar. It was also observed that the liquid yield was substantially increased and HCl yields decreased. In addition, solid residue obtained from lignin alone and PVC was examined under the same conditions, the result found that tar yield derived from PVC mixed with lignin residue increased and HCl decreased substantially. This suggests that lignin bio-char can act as a catalyst which inhibits the dehydrochlorination process or promotes the chain scission of PVC [218]. As a result, the dehydrochlorination process might not be completed resulting in the production of chlorinated oil compounds, which leads to a decrease in PHA concentration [218].

Table 1.12- 1– Summary of studies on co-pyrolysis biomass with plastic.

Material		Reaction condition	Oil yield (wt.%)		HHV (MJ kg^{-1})	Ref.
Biomass	Plastic		Biomass	Mixed		
Rice husk	PE	Parr reactor, 350-430°C, plastic: biomass 4:1-1:1	NA.	72	27	[206]
Rice straw				66	32	
Pine cone	LDPE	Semi-batch glass reactor, 500 °C, plastic: biomass 1:1	47.5	63.9	46.3	[210]
	PP			64.7	45.6	
	PS			69.7	46.4	
Almond shell	HDPE	Fixed bed reactor, 500°C plastic: biomass 1:2-2:1	NA.	50.9	45.6	[208]
Red oak	HDPE	Continuous fluidized bed reactor, 625 °C, plastic: biomass 1:4	50.3	57.6	36.7	[209]
Potato shell	HDPE	Stainless steel retort, 400-550 °C, plastic: biomass 1:2-2:1	∽26.00	51.0	45.6	[207]
Cellulose	PP	Pyroprobe reactor, 500-800 °C, plastic: biomass 1:3-3:1	21.21	NA.	41	[212]
Alder wood	PP	Steel batch retort, 500-700 °C, plastic: biomass 1:9-1:1	50.3	73.2	NA.	[213]
Pine wood			∽26.00	70.6	NA.	
Pine wood sawdust	PP	Pyrex reactor, 450°C, plastic: biomass 1:3-3:1	NA.	61	NA.	[219]
	PS		NA.	67	NA.	
Cellulose	PS	Pyrex reactor, 500°C, plastic: biomass 1:3-3:1	NA.	80.1	38.0	[214]
Palm shell	PS	Fixed bed reactor, 500°C, plastic: biomass 1:1	52.50	61.63	38.01	[215]
Cellulose	PVC	Fixed bed reactor, 800°C plastic: biomass 1:1	NA.	45	NA.	[218]
Xylan				40	NA.	
Lignin				37	NA.	

Material		Reaction condition	Oil yield (wt.%)		HHV (MJ kg^{-1})	Ref.
Biomass	Plastic		Biomass	Mixed		
Rice straw	PET	Fixed bed reactor, 400-600 °C, plastic: biomass 1:1	NA.	36	≈14 high water content (52.46 wt.%)	[216]
Wood sawdust	PET	600 °C,	NA.	NA.	biochar ≈30-31	[217]
Paulownia wood	PET	Drop tube fixed-bed reactor, 600-1000 °C	NA.	NA.	NA.	[220]

1.12.2 Catalytic co-pyrolysis of plastics and biomass

An alternative route for upgrading pyrolytic volatiles directly is through catalytic pyrolysis. Catalytic pyrolysis has been demonstrated to convert biomass-plastic mixtures into higher value pyrolysis oils with enhanced stability, since they can reduce the problem of polymerization and re-evaporation of the pyrolysis oil products [221-224]. Catalytic co-pyrolysis processes have been widely investigated to improve the carbon content of petrochemicals (particularly the monocyclic and aromatic hydrocarbon), increase the efficiency of carbon in aromatics and reduce coke production. The addition of catalyst has enhanced the target product conversion and selection via catalytic cracking and refineries [225]. However, researchers found that the short lifetime of zeolite catalysts could present the heteroatom via the catalytic process. This leads to a large amount of coke formation and deactivates the catalyst. Therefore, the investigations of a suitable catalyst with suitable acid sites and acidity are the challenges in the concept of commercial production of renewable stabilised oils through this route.

Zeolite-based catalysts have been recognized as arguably the most effective catalysts to produce petrochemicals [19, 114, 226, 227]. For example, most studies report the use of HZSM-5 in the catalytic co-pyrolysis of biomass with PE, PP, and PS with the researchers generally finding a synergy effect in the improvement of aromatic product and selectively and reducing coke formation. The summary of the study on catalytic co-pyrolysis of biomass with plastics is shown in **Table 1.12-2.**

The most well-researched catalytic co-pyrolysis processes are conducted with cellulose as a representative material for lignocellulosic biomass. Li *et al*. [226] found the co-pyrolysis of cellulose with LDPE in catalytic fast pyrolysis leads to a substantial increase in aromatics than the catalytic pyrolysis with LDPE alone, and the catalytic co-pyrolysis resulted in lower coke formation. In addition, 85.1% of mono-cyclic aromatics were observed. The blending of cellulose and LDPE in the addition of ZSM-5 provided a more obvious synergy due to the Diels–Alder reaction between cellulose-derived furans reacted with linear olefins LDPE-derived during pyrolysis reaction [228]. Dorado *et al*. studied co-processing of mixtures of biomass and plastics at 650°C by using H-ZSM5 and determined the biofuel compositions using a micro-pyrolyzer coupled with GC/MS (py-GC/MS). This showed that in the addition of PE and PP contributed to the aliphatic products, while PET led to the aromatic formations significantly increasing [227]. Moreover, the presence of HZSM-5 in co-pyrolysis of switchgrass, corn stalk, and HDPE promoted the carbon efficiency of aromatic hydrocarbons. Torrefiled wood was also employed with PS by using HZSM-5 to enhance the aromatic production. It was found that oxygenated phenolic compounds decreased and aromatic hydrocarbon increased [229]

Zhang *et al*. [230] performed the thermal decomposition behaviour and kinetics of cellulose/Douglas fir sawdust and LDPE by using ZSM-5 as a catalyst. The authors found a synergistic effect existed between biomasses and plastic, which led to an improvement in the properties of the pyrolysis oil and reduction in the formation of char residue. Kim *et al*. [231] studied catalytic co-pyrolysis of cellulose and plastics (PP, LLDPE) using HZSM-5 and HY. The aromatic hydrocarbon formation was simply produced by using HY for both PP and LDPE, while HZSM-5 needed the high temperature and high catalyst feed ratio to produce aromatic hydrocarbons.

Zhou *et al.* studied the properties of ZSM-5 impregnation with boron on its catalytic properties of cellulose and LDPE [232]. This catalyst however had a slight decrease in the effective pore size of the zeolites. Li *et al.* [233] investigated a series of gallium-containing catalysts (Ga/ZSM-5) and Ga bound into the framework (Ga–Al–Si, and Ga–Si MFI) as catalysts for the co-pyrolysis of pine wood sawdust with LDPE. Ga/ZSM-5 showed an increase in carbon yield of monocyclic aromatic and olefin hydrocarbon but the formation of polycyclic aromatics and alkanes were decreased. For Ga–Al–Si and Ga–Si MFI catalysts, it was found that higher yield of aromatics and

more valuable products were produced during catalytic co-pyrolysis processing. Yao *et al.* [234] investigated phosphorus and phosphorus/nickel modified ZSM-5 zeolites of pine wood with LDPE. It was found that the yield of olefins and aromatic hydrocarbon showed an increase from 42.9 C% to 52 % for ZSM-5 and 54.8 C% for P-and P/Ni-modified ZSM-5, respectively. Products decreasing was found in low-value alkanes (17.3 C% to 9.6-10.2 C%) and char formation (22.6 C% to18.9-15.7 C%). This finding was similar to the investigation of Lin *et al.* [235], HZSM-5 favoured the production of aromatic, p/HZSM-5 favoured the production of aliphatic hydrocarbons (C4-C12).

Furthermore, Solak *et al*. studied the product distribution in the pyrolysis of cellulose with LDPE over K10, KSF, and bentonite as catalysts. The highest bio-oil yield (79.5 wt.%) was obtained with non-catalyst fast pyrolysis at 500 °C [236]. The gas formation was enhanced by the addition of catalysts. This suggested that the main production could be attributed to the catalytic cracking reactions of primary vapours on the acid centres of the catalyst.

Alternative reactors have also been reported on in the catalytic co-pyrolysis, for example the catalytic pyrolysis of cellulose and Douglar fir pellets with LDPE by using ZSM-5 and a microwave reactor was demonstrated by Zhang *et al.* [230, 237]. In this study cellulose with LDPE enhanced aromatic hydrocarbons and reduced pyrolysis char. The aromatic yields were found in the jet fuel (C8-C16 hydrocarbon) in both cases of cellulose and Douglas fir pellets. A continuous fluidized bed reactor of the catalytic co-pyrolysis was carried out of pine sawdust [114] and black-liquor lignin [225] with plastics (PE, PP, and PS). Results showed that LOSA-1 improved catalytic performance compared with spent FCC, γ-Al_2O_3, and sand. Similar results were also observed from the co-pyrolysis of black-liquor lignin with PE. The highest of petrochemical yield for the co-feeding of plastics was PS >PE > PP. Meanwhile, the maximum aromatic products (55.3%) was observed in the presence of lignin with PS, while the highest carbon products of aromatics (47%) was found for pine sawdust with PS.

Table 1.12- 2–Summary of studies on the catalytic co-pyrolysis biomass with plastic.

Material		Condition		Pyrolysis-oil	Ref.
Biomass	**Plastic**	**catalyst**	**Temp (°C)**	**(wt.%)**	
Cellulose	LDPE	HZSM-5	650	47 C wt.% of aromatic	[226]
Mixture of biomass (switchgrass, cellulose, xylan, and lignin)	PET	HZSM-5	650	NA.	[227]
	PP				
	LDPE				
	HDPE				
Cellulose	LDPE	HZSM-5	590	33-34	[232]
		B/HZSM-5	590	27-31	
Cellulose	LDPE	HZSM-5	550	48	[228]
	PP	HZSM-5		38	
	PS	HZSM-5		54	
Cellulose	LDPE	K10	500	53-70[a]	[236]
		KSF	400-500	52-69 [a]	
		Bentonite	400-500	62-64 [a]	
Cellulose	LDPE	HZSM-5	250-500	36-46	[230]
Cellulose	PP	HY	500-600	12-33	[231]
		HZSM-5		10-17 [b]	
	LDPE	HZSM-5		8-27 [b]	
		HY		9-15 [b]	
Cellulose	PE	HZSM-5	500	25	[238]
Xylan	PE	HZSM-5	500	18	
Wood	PE	HZSM-5	500	15	
Red oak	PE	HZSM-5	500	16-21	
Black-liquor lignin	PE	LOSA-1	450-650	29.9, 14 (aromatic, olefin)	[225]
		Spent FCC		≈20	

Material		Condition		Pyrolysis-oil	Ref.
Biomass	Plastic	catalyst	Temp (°C)	(wt.%)	
		γ-Al2O3,		≈17	
		Sand		≈13	
	PP	LOSA-1		≈19, ≈8 (aromatic) olefin)	
	PS	LOSA-1		53.5, ≈7 (aromatic olefin)	
Douglas fir pellets	LDPE	HZSM-5	200-500	34-43	[237]
Pine sawdust	PE	LOSA-1	600	43	[114]
		Spent FCC	400-650	15-38	
		γ-Al2O3	600	26	
		Sand	600	20	
	PP	Spent FCC	600	35	
	PS	Spent FCC	600	47	
Pine wood sawdust	LDPE	HZSM-5	550	29	[233]
		Ga/HZSM-5	550	30	
		Ga–Al–Si	550	28-30	
		Ga–Si MFI	550	25-28	
		ZSM-5		42.9 C%	[234]
Pine wood	LDPE	P/ZSM-5	550	52.8 C%	
		P/Ni/ZSM-5		54.1 C%	
Corn stalk	HDPE	HZSM-5	550-800	NA	[239]
Poplar wood	HDPE	P/HZSM-5	450-650	NA	[235]
Lignocellulosic biomass	PP	FCC catalyst	510	73% (aromatic yield)	[240]

Material		Condition		Pyrolysis-oil	Ref.
Biomass	Plastic	catalyst	Temp (°C)	(wt.%)	
	PS	(Si/Al, 1.29)		82% (aromatic yield)	
Torrefied wood	PS	HZSM-5	500-650	NA	[229]
Sugarcane	PET	HZSM-5/ Na_2CO_3/ γ-Al_2O_3	700	NA.	[241]

1.12.3 Hydrothermal liquefaction of biomass with plastic

Although the use of co-pyrolysis of biomass and plastic is able to improve the characteristic of pyrolysis oil such as increase the oil yield, reduce the water content, and increase the caloric value of oil, HTL on the other hand has not widely been investigated for the conversion of plastic. Polyethylene has been studied as co-feedstock in HTL to investigate their synergy in the process. Yuan *et al*. [242] employed the co-liquefaction of biomass (sawdust and rice straw) with HDPE in supercritical water medium at 380 °C for 80 min. Co-liquefaction of sawdust with HDPE blend resulted in an improvement in HHV compared to the HTL of biomass individuals. Blending to HDPE was also found to increase oil yield, which achieved the highest yield of 60 wt.% at 80/20 HDPE/biomass mass ratio. The co-liquefaction reaction could also promote the chemical formation observed through GC–MS results, the presence of 9-heptadecanol was only found in HDPE/sawdust oils. This suggests that the radical interactions contributed to the positive synergistic effect during process reaction. Co-liquefaction of microalgae (*Spirulina*) and HDPE in sub/supercritical was investigated. Results showed that the addition of *Spirulina* led to the milder conversion of HDPE, the oil increased by 44.81 wt.% when *Spirulina*/HDPE ratio was increased from 1/10 to 4/6. Besides, the synergistic effect between HDPE and *Spirulina* was enhanced. Co-liquefaction of *Spirulina* with HDPE was also found to decrease the oxygen content of bio-crude oil [243]. Moreover, the liquefaction of Vietnamese *Ulva intestinalis* with polypropylene gave bio-crude with decreased nitrogen contents and increased HHV, this leads to overall improvement in fuel properties[244]. Recently, macroalgae was

co-liquefied with polyethylene at 350 °C for 10 min to investigate the synergistic effect on product yield and composition. Oil product derived from PE contained olefinic species, as well as oxidative depolymerization was observed to form ketone, the bio-crude obtained with high HHV and carbon content [153].

The utilization of polypropylene has also attracted attention for the co-liquefaction. Wu *et al*. [245] employed the co-liquefaction process of *Dunaliella tertiolecta* (*D. tertiolecta*) and PP. Results showed that 3.3 % synergistic effect was observed for co-liquefaction of 80:20 *D. tertiolecta* /PP, as well as the acid content in oil was reduced in the presence of PP. In addition, the blending of PP also improved the quality oil which was observed through GC-MS, the bio-crude products mainly composed of cyclopentenone derivatives. This presumably was a result of the Maillard reaction between carbohydrates and proteins or their hydrolysates. Polypropylene co-liquefaction with macroalgal was also investigated. It was observed that the co-liquefaction depolymerized more readily formed gaseous propylene and the energy content of oil was represented by an HHV increase, however in all of these reports the actual conversion of PP was less than 10% [153].

Polyethylene terephthalate (PET) was added to lignite, wheat straw, in the co-liquefaction. The co-processing was conducted through an autoclave reactor at 300°C for 30 min [246]. It was found that blending feedstock with PET provided the positive synergy between biomass and polymer HTL reaction. The blending ratio of lignite, wheat straw, and plastic waste of 5:4:1 showed the total conversion and oil yield were all the highest, while the preasphaltene yield was lowest. They also found that co-liquefaction of lignite, wheat straw and plastic wastes enhanced bio-crude products, product distributions and property of oil compared to the process was conducted with the traditional catalyst.

The utilization of nylon has also attracted attention for co-liquefaction. Nylon was used with macroalgal biomass (*L. digitata*, *U. lactuca*, *F. serratus* and *S. muticum*) in co-liquefaction at 350 °C in a batch reactor to study synergistic plastic conversion. It was found that nylon depolymerized almost completely to form ϵ-caprolactam *via* an ϵ-aminocaproic acid intermediate, largely partitioning into the aqueous phase and oil, increasing oil nitrogen. They also suggested that plastic contaminants could be a representative opportunity to the improvement of HTL macroalgal biorefinery.

1.13 Conclusion and gap in the literature

Co-processing of biomass with plastics is a promising route to the production of higher value oils that could form the basis of a renewable refinery. The addition ofplastics into a biomass stream for liquefaction could also have multiple benefits including creating a superior bio-crude, the recovery of monomers in a biorefinery concept, or stabilisation of the aqueous fractions. Plastic waste, especially low-quality, mixed and contaminated wastes, are difficult to recycle and currently are either incinerated or landfilled. As such opening up further routes to production offers a promising method for waste management.

A substantial number of studies on plastic as a potential co-feedstock with biomass through pyrolysis have been published; however, most require expensive and energy-intensive post-processing. In addition, the oxygen content of the pyrolysis is high and has been identified to exist in several forms of oxygenated compounds, and is mostly found as water. Therefore, co-processing of plastic and biomass with minimised energy input, and improved oil product throughout the production process, are the major challenges. This may come with the implementation of co-processing at below the decomposition point of the plastic, conducted in liquid media in either a high boiling point oil (LPP) or water (HTL), which have been researched less extensively. This is challenging, however the liquefaction routes do not require the extensive drying that pyrolysis does, which could pave the way to lower overall energy input.

The LPP process has been claimed to depolymerise organic feed stocks to produce a hydrocarbon biofuel in one step, without the need for hydrogen or chemical upgrading. Although a number of pilot plants have been built to demonstrate the KDV process, there are currently no lab scale examples in the literature of this process, or any investigations actually detailing the mechanism of how this process could possibly produce such high-grade hydrocarbon products without the addition of hydrogen. As such, much of the chemistry and fundamental engineering remains unclear.

HTL of biomass has been shown to be a promising route to the production of bio-crude and a wide range of HTL conditions have been examined by different researchers across the globe, however there are currently no reports of co-liquefaction of biomass and plastics via hydrothermal liquefaction, particularly pistachio hulls which are a common agricultural waste material, that are also a rich source of natural phenolics

and lipids. Furthermore, few studies have addressed the use of catalyst and alternative organic additives for improving the conversion of plastic through liquefaction.

In addition, there is evidence that monomers of nylon 6 could significantly add to the value of a marine biorefinery by being able to effectively chemically recycle the waste nylon alongside producing bio-crude and fertiliser product. This is of vital importance in order to investigate a wider range of nylons commonly found in maritime plastics that will affect macroalgal HTL processing.

1.14 Aims and objectives

The overall aim of this thesis is to explore the valorisation of plastic waste, through co-processing with biomass. Specifically, the projects focused on two technologies: the catalytic pressure-less depolymerisation (KDV, in the original German), and hydrothermal liquefaction (HTL).

In order to achieve these aims, the core objectives of the project were defined as follows:

- To assess the suitability of producing advanced biofuels through the KDV process on the laboratory- and pilot-scale with pistachio hulls, with an assessment of whether the co-processing with plastics is viable.
- To assess pistachio hulls as a feedstock in the HTL process and determine whether the co-liquefaction of the feedstock with a range of plastics is viable.
- To assess the effect of the addition of a range of organic and inorganic catalysts and the mechanism of conversion, extrapolated to determine whether a typical thermochemical catalyst could be further utilised to aid the breakdown of polypropylene in the co-liquefaction of biomass and PP and aid the production of further valuable products from this stream.
- To investigate range of different nylons including an actual sample of marine macroalgae collected at sea, entangled with nylon fishing line to demonstrate the concept of effectively chemically recycling the waste nylon alongside producing bio-crude and fertiliser product.

1.15 References

[1] C. Liu, H. Wang, A.M. Karim, J. Sun, Y. Wang, Catalytic fast pyrolysis of lignocellulosic biomass, Chemical Society Reviews, 43 (2014) 7594-7623.
[2] J.C. Serrano-Ruiz, J.A. Dumesic, Catalytic routes for the conversion of biomass into liquid hydrocarbon transportation fuels, Energy & Environmental Science, 4 (2011) 83-99.
[3] G.-J. Zhou, W.-Y. Wong, Organometallic acetylides of PtII, AuI and HgII as new generation optical power limiting materials, Chemical Society Reviews, 40 (2011) 2541-2566.
[4] F. Abnisa, W.M.A. Wan Daud, A review on co-pyrolysis of biomass: An optional technique to obtain a high-grade pyrolysis oil, Energy Conversion and Management, 87 (2014) 71-85.
[5] P. McKendry, Energy production from biomass (part 1): overview of biomass, Bioresource Technology, 83 (2002) 37-46.
[6] A. Ahtikoski, J. Heikkilä, V. Alenius, M. Siren, Economic viability of utilizing biomass energy from young stands—The case of Finland, Biomass and Bioenergy, 32 (2008) 988-996.
[7] J. Aguado, J. Carlos, D. Serrano, European trends in the feedstock recycling of plastic wastes, Global Wastes NEST Journal, 9 (2007).
[8] D.B.-T. Hoornweg, Perinaz., What a Waste : A Global Review of Solid Waste Management. , Urban development series;knowledge papers no. 15. World Bank, Washington, DC. © World Bank., (2012).
[9] T.E.a.L. Elliott, UK Plastic Waste Generation, A PLASTIC FUTURE PLASTICS CONSUMPTION AND WASTE MANAGEMENT IN THE UK, (2019).
[10] A. Joshi, R. Punia, CONVERSION OF PLASTIC WASTES INTO LIQUID FUELS – A REVIEW, in, 2013, pp. 10.
[11] R.C. Thompson, S.H. Swan, C.J. Moore, F.S.v. Saal, Our plastic age, Philosophical Transactions of the Royal Society B: Biological Sciences, 364 (2009) 1973-1976.
[12] T. Yamamoto, H. Shiraishi, O. Nakasugi, Bisphenol A in hazardous waste landfill leachates, Chemosphere, 42 (2001) 415-418.
[13] S. Ma, J. Lu, J. Gao, Study of the low temperature pyrolysis of PVC, Energy and Fuels, 16 (2002) 338-342.
[14] F. Kreith, Handbook of energy efficiency and renewable energy, Boca Raton, Florida, Taylor and Francis (2007).
[15] R. Saidur, E.A. Abdelaziz, A. Demirbas, M.S. Hossain, S. Mekhilef, A review on biomass as a fuel for boilers, Renewable and Sustainable Energy Reviews, 15 (2011) 2262-2289.
[16] Z.-y. Zhao, H. Yan, Assessment of the biomass power generation industry in China, Renewable Energy, 37 (2012) 53-60.
[17] F. Abnisa, W. Daud, A review on co-pyrolysis of biomass: An optional technique to obtain a high-grade pyrolysis oil, Energy Conversion and Management, 87 (2014) 71–85.
[18] P. Costa, F. Pinto, M. Miranda, R. André, M. Rodrigues, Study of the experimental conditions of the co-pyrolysis of rice husk and plastic wastes, Chemical Engineering Transactions, 39 (2014) 1639-1644.
[19] S. Wang, Y. Hu, B.B. Uzoejinwa, B. Cao, Z. He, Q. Wang, S. Xu, Pyrolysis mechanisms of typical seaweed polysaccharides, Journal of Analytical and Applied Pyrolysis, 124 (2017) 373-383.

[20] M. Sajdak, R. Muzyka, J. Hrabak, K. Słowik, Use of plastic waste as a fuel in the co-pyrolysis of biomass: Part III: Optimisation of the co-pyrolysis process, Journal of Analytical and Applied Pyrolysis, 112 (2015).
[21] M.H. Hassan, M.A. Kalam, An Overview of Biofuel as a Renewable Energy Source: Development and Challenges, Procedia Engineering, 56 (2013) 39-53.
[22] J. Popp, Z. Lakner, M. Harangi-Rákos, M. Fári, The effect of bioenergy expansion: Food, energy, and environment, Renewable and Sustainable Energy Reviews, 32 (2014) 559-578.
[23] K. Açıkalın, F. Karaca, E. Bolat, Pyrolysis of pistachio shell: Effects of pyrolysis conditions and analysis of products, Fuel, 95 (2012) 169-177.
[24] A. Tomaino, M. Martorana, T. Arcoraci, D. Monteleone, C. Giovinazzo, A. Saija, Antioxidant activity and phenolic profile of pistachio (Pistacia vera L., variety Bronte) seeds and skins, Biochimie, 92 (2010) 1115-1122.
[25] A.H. Goli, M. Barzegar, M.A. Sahari, Antioxidant activity and total phenolic compounds of pistachio (Pistachia vera) hull extracts, Food Chemistry, 92 (2005) 521-525.
[26] P. Gegg, V. Wells, The development of seaweed-derived fuels in the UK: An analysis of stakeholder issues and public perceptions, Energy Policy, 133 (2019) 110924.
[27] D. Aitken, C. Bulboa, A. Godoy-Faundez, J.L. Turrion-Gomez, B. Antizar-Ladislao, Life cycle assessment of macroalgae cultivation and processing for biofuel production, Journal of Cleaner Production, 75 (2014) 45-56.
[28] T. Matsui, Y. Koike, Methane fermentation of a mixture of seaweed and milk at a pilot-scale plant, Journal of Bioscience and Bioengineering, 110 (2010) 558-563.
[29] N. Schultz-Jensen, A. Thygesen, F. Leipold, S.T. Thomsen, C. Roslander, H. Lilholt, A.B. Bjerre, Pretreatment of the macroalgae Chaetomorpha linum for the production of bioethanol – Comparison of five pretreatment technologies, Bioresource Technology, 140 (2013) 36-42.
[30] F. Abeln, J. Fan, V.L. Budarin, H. Briers, S. Parsons, M.J. Allen, D.A. Henk, J. Clark, C.J. Chuck, Lipid production through the single-step microwave hydrolysis of macroalgae using the oleaginous yeast Metschnikowia pulcherrima, Algal Research, 38 (2019) 101411.
[31] S. Raikova, M.J. Allen, C.J. Chuck, Hydrothermal liquefaction of macroalgae for the production of renewable biofuels, Biofuels, Bioproducts and Biorefining, 13 (2019) 1483-1504.
[32] S.D. Anuar Sharuddin, F. Abnisa, W.M.A. Wan Daud, M.K. Aroua, A review on pyrolysis of plastic wastes, Energy Conversion and Management, 115 (2016) 308-326.
[33] A.K. Panda, R.K. Singh, D.K. Mishra, Thermolysis of waste plastics to liquid fuel: A suitable method for plastic waste management and manufacture of value added products—A world prospective, Renewable and Sustainable Energy Reviews, 14 (2010) 233-248.
[34] B. Kunwar, H.N. Cheng, S.R. Chandrashekaran, B.K. Sharma, Plastics to fuel: a review, Renewable and Sustainable Energy Reviews, 54 (2016) 421-428.
[35] A.G. Buekens, H. Huang, Catalytic plastics cracking for recovery of gasoline-range hydrocarbons from municipal plastic wastes, Resources, Conservation and Recycling, 23 (1998) 163-181.
[36] C. Zhou, W. Fang, W. Xu, A. Cao, R. Wang, Characteristics and the recovery potential of plastic wastes obtained from landfill mining, Journal of Cleaner Production, 80 (2014) 80-86.

[37] N. Miskolczi, L. Bartha, G. Deák, B. Jóver, Thermal degradation of municipal plastic waste for production of fuel-like hydrocarbons, Polymer Degradation and Stability, 86 (2004) 357-366.
[38] N. Miskolczi, L. Bartha, G. Deák, Thermal degradation of polyethylene and polystyrene from the packaging industry over different catalysts into fuel-like feed stocks, Polymer Degradation and Stability, 91 (2006) 517-526.
[39] S.M. Gospe, CHAPTER 36 - Other Organic Chemicals, in: M.R. Dobbs (Ed.) Clinical Neurotoxicology, W.B. Saunders, Philadelphia, 2009, pp. 415-420.
[40] T.H. Begley, H.C. Hollifield, High-performance liquid chromatographic determination of migrating poly(ethylene terephthalate) oligomers in corn oil, Journal of Agricultural and Food Chemistry, 38 (1990) 145-148.
[41] J.R. Jambeck, R. Geyer, C. Wilcox, T.R. Siegler, M. Perryman, A. Andrady, R. Narayan, K.L. Law, Plastic waste inputs from land into the ocean, Science, 347 (2015) 768-771.
[42] M. Eriksen, L.C.M. Lebreton, H.S. Carson, M. Thiel, C.J. Moore, J.C. Borerro, F. Galgani, P.G. Ryan, J. Reisser, Plastic Pollution in the World's Oceans: More than 5 Trillion Plastic Pieces Weighing over 250,000 Tons Afloat at Sea, PLOS ONE, 9 (2014) e111913.
[43] M.R. Gregory, Environmental implications of plastic debris in marine settings—entanglement, ingestion, smothering, hangers-on, hitch-hiking and alien invasions, Philosophical Transactions of the Royal Society B: Biological Sciences, 364 (2009) 2013-2025.
[44] M. Eriksen, S. Mason, S. Wilson, C. Box, A. Zellers, W. Edwards, H. Farley, S. Amato, Microplastic pollution in the surface waters of the Laurentian Great Lakes, Marine Pollution Bulletin, 77 (2013) 177-182.
[45] A.L. Andrady, Microplastics in the marine environment, Marine Pollution Bulletin, 62 (2011) 1596-1605.
[46] S.N. Thomas, C. Hridayanathan, The effect of natural sunlight on the strength of polyamide 6 multifilament and monofilament fishing net materials, Fisheries Research, 81 (2006) 326-330.
[47] J.R. Michael Topham, Simon Rutledge, Plastic Surgery: Managing Waste Plastics, biffa.co.uk/publications, September 2019 (2019).
[48] R. Thahir, A. Altway, S.R. Juliastuti, Susianto, Production of liquid fuel from plastic waste using integrated pyrolysis method with refinery distillation bubble cap plate column, Energy Reports, 5 (2019) 70-77.
[49] Y. Lin, S. Tanaka, Ethanol fermentation from biomass resources: current state and prospects, Applied Microbiology and Biotechnology, 69 (2006) 627-642.
[50] J. Mata-Alvarez, S. Macé, P. Llabrés, Anaerobic digestion of organic solid wastes. An overview of research achievements and perspectives, Bioresource Technology, 74 (2000) 3-16.
[51] D.C. Elliott, D. Beckman, A.V. Bridgwater, J.P. Diebold, S.B. Gevert, Y. Solantausta, Developments in direct thermochemical liquefaction of biomass: 1983-1990, Energy & Fuels, 5 (1991) 399-410.
[52] Y. Matsumura, T. Minowa, B. Potic, S.R.A. Kersten, W. Prins, W.P.M. van Swaaij, B. van de Beld, D.C. Elliott, G.G. Neuenschwander, A. Kruse, M. Jerry Antal Jr, Biomass gasification in near- and super-critical water: Status and prospects, Biomass and Bioenergy, 29 (2005) 269-292.
[53] A.A. Peterson, F. Vogel, R.P. Lachance, M. Fröling, J.M.J. Antal, J.W. Tester, Thermochemical biofuel production in hydrothermal media: A review of sub- and supercritical water technologies, Energy & Environmental Science, 1 (2008) 32-65.

[54] S. Parsons, M.J. Allen, C.J. Chuck, Coproducts of algae and yeast-derived single cell oils: A critical review of their role in improving biorefinery sustainability, Bioresource Technology, 303 (2020) 122862.
[55] K. Kositkanawuth, M.L. Sattler, B. Dennis, Pyrolysis of Macroalgae and Polysytrene: A Review, Current Sustainable/Renewable Energy Reports, 1 (2014) 121-128.
[56] M. Van de Velden, J. Baeyens, A. Brems, B. Janssens, R. Dewil, Fundamentals, kinetics and endothermicity of the biomass pyrolysis reaction, Renewable Energy, 35 (2010) 232-242.
[57] J.E. White, W.J. Catallo, B.L. Legendre, Biomass pyrolysis kinetics: A comparative critical review with relevant agricultural residue case studies, Journal of Analytical and Applied Pyrolysis, 91 (2011) 1-33.
[58] A. Demirbas, Pyrolysis of Biomass for Fuels and Chemicals, Energy Sources, Part A: Recovery, Utilization, and Environmental Effects, 31 (2009) 1028-1037.
[59] S. Jones, C. Drennan, C. Walton, D. Elliott, J. Holladay, D. Stevens, C. Kinchin, S. Czernik, Production of Gasoline and Diesel from Biomass Via Fast Pyrolysis, Hydrotreating and Hydrocracking: A Design Case, Richland, WA: Pacific Northwest National Laboratory, (2009).
[60] P.T. Williams, S. Besler, The influence of temperature and heating rate on the slow pyrolysis of biomass, Renewable Energy, 7 (1996) 233-250.
[61] S.N. Naik, V.V. Goud, P.K. Rout, A.K. Dalai, Production of first and second generation biofuels: A comprehensive review, Renewable and Sustainable Energy Reviews, 14 (2010) 578-597.
[62] M. Saidi, F. Samimi, D. Karimipourfard, T. Nimmanwudipong, B.C. Gates, M.R. Rahimpour, Upgrading of lignin-derived bio-oils by catalytic hydrodeoxygenation, Energy & Environmental Science, 7 (2014) 103-129.
[63] J. Waluyo, I.G.B.N. Makertihartha, H. Susanto, Pyrolysis with intermediate heating rate of palm kernel shells: Effect temperature and catalyst on product distribution, AIP Conference Proceedings, 1977 (2018) 020026.
[64] A.V. Bridgwater, Review of fast pyrolysis of biomass and product upgrading, Biomass and Bioenergy, 38 (2012) 68-94.
[65] Q. Lu, W.-Z. Li, X.-F. Zhu, Overview of fuel properties of biomass fast pyrolysis oils, Energy Conversion and Management, 50 (2009) 1376-1383.
[66] A.V. Bridgwater, D. Meier, D. Radlein, An overview of fast pyrolysis of biomass, Organic Geochemistry, 30 (1999) 1479-1493.
[67] S. Czernik, A.V. Bridgwater, Overview of Applications of Biomass Fast Pyrolysis Oil, Energy & Fuels, 18 (2004) 590-598.
[68] K. Sipilä, E. Kuoppala, L. Fagernäs, A. Oasmaa, Characterization of biomass-based flash pyrolysis oils, Biomass and Bioenergy, 14 (1998) 103-113.
[69] Z. Luo, S. Wang, Y. Liao, J. Zhou, Y. Gu, K. Cen, Research on Biomass Fast Pyrolysis for Liquid Fuel, 2004.
[70] D. Mohan, C.U. Pittman, P.H. Steele, Pyrolysis of Wood/Biomass for Bio-oil: A Critical Review, Energy & Fuels, 20 (2006) 848-889.
[71] J. Carrasco, S. Gunukula, A. Boateng, C.A. Mullen, W. Desisto, M. Wheeler, Pyrolysis of forest residues: An approach to techno-economics for bio-fuel production, Fuel, 193 (2017) 477-484.
[72] D.C. Elliott, H. Wang, M. Rover, L. Whitmer, R. Smith, R. Brown, Hydrocarbon Liquid Production via Catalytic Hydroprocessing of Phenolic Oils Fractionated from Fast Pyrolysis of Red Oak and Corn Stover, ACS Sustainable Chemistry & Engineering, 3 (2015) 892-902.

[73] E.G. Baker, D.C. Elliott, Catalytic Hydrotreating of Biomass-Derived Oils, in: Pyrolysis Oils from Biomass, American Chemical Society, 1988, pp. 228-240.
[74] R.V. Pindoria, A. Megaritis, A.A. Herod, R. Kandiyoti, A two-stage fixed-bed reactor for direct hydrotreatment of volatiles from the hydropyrolysis of biomass: effect of catalyst temperature, pressure and catalyst ageing time on product characteristics, Fuel, 77 (1998) 1715-1726.
[75] R.J. French, J. Hrdlicka, R. Baldwin, Mild hydrotreating of biomass pyrolysis oils to produce a suitable refinery feedstock, Environmental Progress & Sustainable Energy, 29 (2010) 142-150.
[76] M. Ahmad, A.U. Rajapaksha, J.E. Lim, M. Zhang, N. Bolan, D. Mohan, M. Vithanage, S.S. Lee, Y.S. Ok, Biochar as a sorbent for contaminant management in soil and water: A review, Chemosphere, 99 (2014) 19-33.
[77] D. Mohan, A. Sarswat, Y.S. Ok, C.U. Pittman, Organic and inorganic contaminants removal from water with biochar, a renewable, low cost and sustainable adsorbent – A critical review, Bioresource Technology, 160 (2014) 191-202.
[78] D.A. Laird, R.C. Brown, J.E. Amonette, J. Lehmann, Review of the pyrolysis platform for coproducing bio-oil and biochar, Biofuels, Bioproducts and Biorefining, 3 (2009) 547-562.
[79] X. Hu, M. Gholizadeh, Biomass pyrolysis: A review of the process development and challenges from initial researches up to the commercialisation stage, Journal of Energy Chemistry, 39 (2019) 109-143.
[80] P. Abhijeet, G. Swagathnath, S. Rangabhashiyam, M. Asok Rajkumar, P. Balasubramanian, Prediction of pyrolytic product composition and yield for various grass biomass feedstocks, Biomass Conversion and Biorefinery, 10 (2020) 663-674.
[81] T.K. Patra, P.N. Sheth, Biomass gasification models for downdraft gasifier: A state-of-the-art review, Renewable and Sustainable Energy Reviews, 50 (2015) 583-593.
[82] M. Ringer, V. Putsche, J. Scahill, Large-Scale Pyrolysis Oil Production: A Technology Assessment and Economic Analysis, (2006).
[83] D. Czajczyńska, L. Anguilano, H. Ghazal, R. Krzyżyńska, A.J. Reynolds, N. Spencer, H. Jouhara, Potential of pyrolysis processes in the waste management sector, Thermal Science and Engineering Progress, 3 (2017) 171-197.
[84] D. S, P. Paul, H. Mukunda, R. N K S, S. Gururaja Rao, S. H V, Biomass gasification technology - A route to meet energy needs, Current Science, 87 (2004).
[85] H. Pucher, N. Schwaiger, R. Feiner, L. Ellmaier, P. Pucher, B.S. Chernev, M. Siebenhofer, Lignocellulosic Biofuels: Phase Separation during Catalytic Hydrodeoxygenation of Liquid Phase Pyrolysis Oil, Separation Science and Technology, 50 (2015) 2914-2919.
[86] K. Treusch, N. Schwaiger, K. Schlackl, R. Nagl, P. Pucher, M. Siebenhofer, Temperature Dependence of Single Step Hydrodeoxygenation of Liquid Phase Pyrolysis Oil, Frontiers in Chemistry, 6 (2018).
[87] N. Schwaiger, R. Feiner, K. Zahel, A. Pieber, V. Witek, P. Pucher, E. Ahn, P. Wilhelm, B. Chernev, H. Schröttner, M. Siebenhofer, Liquid and Solid Products from Liquid-Phase Pyrolysis of Softwood, 2011.
[88] H. Pucher, R. Feiner, N. Schwaiger, P. Pucher, M. Siebenhofer, 316875 Biomasspyrolysisrefinery: Hydrodeoxygenation of Liquid Phase Pyrolysis Oil, 2013.
[89] M. Berchtold, J. Fimberger, A. Reichhold, P. Pucher, Upgrading of heat carrier oil derived from liquid-phase pyrolysis via fluid catalytic cracking, Fuel Processing Technology, 142 (2016) 92-99.
[90] E. Butler, G. Devlin, K. McDonnell, Waste Polyolefins to Liquid Fuels via Pyrolysis: Review of Commercial State-of-the-Art and Recent Laboratory Research, 2011.

[91] Alphakat, The KDV-Process, in.
[92] F. Wang, A LIFE CYCLE ASSESSMENT ON KDV DIESEL OIL FROM WOOD, in, 2014.
[93] L. Yang, Q. He, P. Havard, K. Corscadden, C. Xu, X. Wang, Co-liquefaction of spent coffee grounds and lignocellulosic feedstocks, Bioresource Technology, 237 (2017) 108-121.
[94] H. Huang, X.-Z. Yuan, Recent progress in the direct liquefaction of typical biomass, Progress in Energy and Combustion Science, 49 (2015).
[95] D. López Barreiro, W. Prins, F. Ronsse, W. Brilman, Hydrothermal liquefaction (HTL) of microalgae for biofuel production: State of the art review and future prospects, Biomass and Bioenergy, 53 (2013) 113-127.
[96] S.S. Toor, L. Rosendahl, A. Rudolf, Hydrothermal liquefaction of biomass: A review of subcritical water technologies, Energy, 36 (2011) 2328-2342.
[97] C. Tian, B. Li, Z. Liu, Y. Zhang, H. Lu, Hydrothermal liquefaction for algal biorefinery: A critical review, Renewable and Sustainable Energy Reviews, 38 (2014) 933-950.
[98] A. Palomino, R.D. Godoy-Silva, S. Raikova, C.J. Chuck, The storage stability of biocrude obtained by the hydrothermal liquefaction of microalgae, Renewable Energy, 145 (2020) 1720-1729.
[99] L. Cao, G. Luo, S. Zhang, J. Chen, Bio-oil production from eight selected green landscaping wastes through hydrothermal liquefaction, RSC Advances, 6 (2016) 15260-15270.
[100] M.K. Jindal, M.K. Jha, Effect of process parameters on hydrothermal liquefaction of waste furniture sawdust for bio-oil production, RSC Advances, 6 (2016) 41772-41780.
[101] S. Yin, R. Dolan, M. Harris, Z. Tan, Subcritical hydrothermal liquefaction of cattle manure to bio-oil: Effects of conversion parameters on bio-oil yield and characterization of bio-oil, Bioresour Technol, 101 (2010) 3657-3664.
[102] D. Zhou, L. Zhang, S. Zhang, H. Fu, J. Chen, Hydrothermal Liquefaction of Macroalgae Enteromorpha prolifera to Bio-oil, Energy & Fuels, 24 (2010) 4054-4061.
[103] I. Leonardis, S. Chiaberge, T. Fiorani, S. Spera, E. Battistel, A. Bosetti, P. Cesti, S. Reale, F. De Angelis, Characterization of Bio-oil from Hydrothermal Liquefaction of Organic Waste by NMR Spectroscopy and FTICR Mass Spectrometry, ChemSusChem, 6 (2013) 160-167.
[104] A. Saba, B. Lopez, J.G. Lynam, M.T. Reza, Hydrothermal Liquefaction of Loblolly Pine: Effects of Various Wastes on Produced Biocrude, ACS Omega, 3 (2018) 3051-3059.
[105] J. Yang, Q. He, H. Niu, K. Corscadden, T. Astatkie, Hydrothermal liquefaction of biomass model components for product yield prediction and reaction pathways exploration, Applied Energy, 228 (2018) 1618-1628.
[106] S. Xiu, A. Shahbazi, L. Wang, Co-liquefaction of swine manure with waste vegetable oil for enhanced bio-oil production, Energy Sources, Part A: Recovery, Utilization, and Environmental Effects, 38 (2016) 459-465.
[107] P. Biller, A.B. Ross, 17. Production of biofuels via hydrothermal conversion, in, 2016.
[108] J.A. Ramirez, R.J. Brown, T.J. Rainey, A Review of Hydrothermal Liquefaction Bio-Crude Properties and Prospects for Upgrading to Transportation Fuels, Energies, 8 (2015) 6765-6794.
[109] W. Wang, Y. Xu, X. Wang, B. Zhang, W. Tian, J. Zhang, Hydrothermal liquefaction of microalgae over transition metal supported TiO2 catalyst, Bioresource Technology, 250 (2018) 474-480.

[110] T.H. Pedersen, I.F. Grigoras, J. Hoffmann, S.S. Toor, I.M. Daraban, C.U. Jensen, S.B. Iversen, R.B. Madsen, M. Glasius, K.R. Arturi, R.P. Nielsen, E.G. Søgaard, L.A. Rosendahl, Continuous hydrothermal co-liquefaction of aspen wood and glycerol with water phase recirculation, Applied Energy, 162 (2016) 1034-1041.
[111] J. Yu, P. Biller, A. Mamahkel, M. Klemmer, J. Becker, M. Glasius, B.B. Iversen, Catalytic hydrotreatment of bio-crude produced from the hydrothermal liquefaction of aspen wood: a catalyst screening and parameter optimization study, Sustainable Energy & Fuels, 1 (2017) 832-841.
[112] P. Haghighat, A. Montanez, G.R. Aguilera, J.K. Rodriguez Guerrero, S. Karatzos, M.A. Clarke, W. McCaffrey, Hydrotreating of Hydrofaction™ biocrude in the presence of presulfided commercial catalysts, Sustainable Energy & Fuels, 3 (2019) 744-759.
[113] U. Jena, K.C. Das, Comparative Evaluation of Thermochemical Liquefaction and Pyrolysis for Bio-Oil Production from Microalgae, Energy & Fuels, 25 (2011) 5472-5482.
[114] H. Zhang, J. Nie, R. Xiao, B. Jin, C. Dong, G. Xiao, Catalytic Co-pyrolysis of Biomass and Different Plastics (Polyethylene, Polypropylene, and Polystyrene) To Improve Hydrocarbon Yield in a Fluidized-Bed Reactor, Energy & Fuels, 28 (2014) 1940-1947.
[115] W.-T. Chen, Y. Zhang, J. Zhang, G. Yu, L.C. Schideman, P. Zhang, M. Minarick, Hydrothermal liquefaction of mixed-culture algal biomass from wastewater treatment system into bio-crude oil, Bioresource Technology, 152 (2014) 130-139.
[116] Q.-V. Bach, M.V. Sillero, K.-Q. Tran, J. Skjermo, Fast hydrothermal liquefaction of a Norwegian macro-alga: Screening tests, Algal Research, 6 (2014) 271-276.
[117] N. Neveux, A.K.L. Yuen, C. Jazrawi, M. Magnusson, B.S. Haynes, A.F. Masters, A. Montoya, N.A. Paul, T. Maschmeyer, R. de Nys, Biocrude yield and productivity from the hydrothermal liquefaction of marine and freshwater green macroalgae, Bioresource Technology, 155 (2014) 334-341.
[118] J. Watson, J. Lu, R. de Souza, B. Si, Y. Zhang, Z. Liu, Effects of the extraction solvents in hydrothermal liquefaction processes: Biocrude oil quality and energy conversion efficiency, Energy, 167 (2019) 189-197.
[119] P.J. Valdez, J.G. Dickinson, P.E. Savage, Characterization of Product Fractions from Hydrothermal Liquefaction of Nannochloropsis sp. and the Influence of Solvents, Energy & Fuels, 25 (2011) 3235-3243.
[120] Y. Huang, Y. Chen, J. Xie, H. Liu, X. Yin, C. Wu, Bio-oil production from hydrothermal liquefaction of high-protein high-ash microalgae including wild Cyanobacteria sp. and cultivated Bacillariophyta sp, Fuel, 183 (2016) 9-19.
[121] B.E.-O. Eboibi, D.M. Lewis, P.J. Ashman, S. Chinnasamy, Hydrothermal liquefaction of microalgae for biocrude production: Improving the biocrude properties with vacuum distillation, Bioresource Technology, 174 (2014) 212-221.
[122] W.-T. Chen, Y. Zhang, T.H. Lee, Z. Wu, B. Si, C.-F.F. Lee, A. Lin, B.K. Sharma, Renewable diesel blendstocks produced by hydrothermal liquefaction of wet biowaste, Nature Sustainability, 1 (2018) 702-710.
[123] D.C. Elliott, E.G. Baker, Catalytic hydrotreating of biomass liquefaction products to produce hydrocarbon fuels: Interim report, in, ; Pacific Northwest Lab., Richland, WA (USA), 1986, pp. Medium: ED.
[124] C. Zhang, P. Duan, Y. Xu, B. Wang, F. Wang, L. Zhang, Catalytic upgrading of duckweed biocrude in subcritical water, Bioresource Technology, 166 (2014) 37-44.
[125] J.D. Adjaye, N.N. Bakhshi, Catalytic conversion of a biomass-derived oil to fuels and chemicals I: Model compound studies and reaction pathways, Biomass and Bioenergy, 8 (1995) 131-149.

[126] B.S. Gevert, J.-E. Otterstedt, Upgrading of directly liquefied biomass to transportation fuels: catalytic cracking, Biomass, 14 (1987) 173-183.
[127] M. Lavanya, A. Meenakshisundaram, S. Renganathan, S. Chinnasamy, D.M. Lewis, J. Nallasivam, S. Bhaskar, Hydrothermal liquefaction of freshwater and marine algal biomass: A novel approach to produce distillate fuel fractions through blending and co-processing of biocrude with petrocrude, Bioresource Technology, 203 (2016) 228-235.
[128] L. Leng, J. Li, Z. Wen, W. Zhou, Use of microalgae to recycle nutrients in aqueous phase derived from hydrothermal liquefaction process, Bioresource Technology, 256 (2018) 529-542.
[129] U. Jena, N. Vaidyanathan, S. Chinnasamy, K.C. Das, Evaluation of microalgae cultivation using recovered aqueous co-product from thermochemical liquefaction of algal biomass, Bioresource Technology, 102 (2011) 3380-3387.
[130] P. Biller, A.B. Ross, S.C. Skill, A. Lea-Langton, B. Balasundaram, C. Hall, R. Riley, C.A. Llewellyn, Nutrient recycling of aqueous phase for microalgae cultivation from the hydrothermal liquefaction process, Algal Research, 1 (2012) 70-76.
[131] L. Garcia Alba, C. Torri, D. Fabbri, S.R.A. Kersten, D.W.F. Brilman, Microalgae growth on the aqueous phase from Hydrothermal Liquefaction of the same microalgae, Chemical Engineering Journal, 228 (2013) 214-223.
[132] S.R. Shanmugam, S. Adhikari, R. Shakya, Nutrient removal and energy production from aqueous phase of bio-oil generated via hydrothermal liquefaction of algae, Bioresource Technology, 230 (2017) 43-48.
[133] E. Barbera, A. Teymouri, A. Bertucco, B.J. Stuart, S. Kumar, Recycling Minerals in Microalgae Cultivation through a Combined Flash Hydrolysis–Precipitation Process, ACS Sustainable Chemistry & Engineering, 5 (2017) 929-935.
[134] Z. Zhu, L. Rosendahl, S.S. Toor, D. Yu, G. Chen, Hydrothermal liquefaction of barley straw to bio-crude oil: Effects of reaction temperature and aqueous phase recirculation, Applied Energy, 137 (2015) 183-192.
[135] C. Li, X. Yang, Z. Zhang, D. Zhou, L. Zhang, S. Zhang, J.-M. Chen, Hydrothermal Liquefaction of Desert Shrub Salix psammophila to High Value-added Chemicals and Hydrochar with Recycled Processing Water, Bioresources, 8 (2013) 2981-2997.
[136] A.A. Shah, S.S. Toor, T.H. Seehar, R.S. Nielsen, A. H. Nielsen, T.H. Pedersen, L.A. Rosendahl, Bio-Crude Production through Aqueous Phase Recycling of Hydrothermal Liquefaction of Sewage Sludge, Energies, 13 (2020) 493.
[137] Y. Hu, S. Feng, Z. Yuan, C. Xu, A. Bassi, Investigation of aqueous phase recycling for improving bio-crude oil yield in hydrothermal liquefaction of algae, Bioresource Technology, 239 (2017) 151-159.
[138] P. Biller, R.B. Madsen, M. Klemmer, J. Becker, B.B. Iversen, M. Glasius, Effect of hydrothermal liquefaction aqueous phase recycling on bio-crude yields and composition, Bioresource Technology, 220 (2016) 190-199.
[139] R.B. Madsen, M.M. Jensen, A.J. Mørup, K. Houlberg, P.S. Christensen, M. Klemmer, J. Becker, B.B. Iversen, M. Glasius, Using design of experiments to optimize derivatization with methyl chloroformate for quantitative analysis of the aqueous phase from hydrothermal liquefaction of biomass, Analytical and bioanalytical chemistry, 408 (2016) 2171-2183.
[140] D.C. Elliott, T.R. Hart, A.J. Schmidt, G.G. Neuenschwander, L.J. Rotness, M.V. Olarte, A.H. Zacher, K.O. Albrecht, R.T. Hallen, J.E. Holladay, Process development for hydrothermal liquefaction of algae feedstocks in a continuous-flow reactor, Algal Research, 2 (2013) 445-454.

[141] R. Cherad, J.A. Onwudili, P. Biller, P.T. Williams, A.B. Ross, Hydrogen production from the catalytic supercritical water gasification of process water generated from hydrothermal liquefaction of microalgae, Fuel, 166 (2016) 24-28.
[142] H. Chen, C. Zhang, Y. Rao, Y. Jing, G. Luo, S. Zhang, Methane potentials of wastewater generated from hydrothermal liquefaction of rice straw: focusing on the wastewater characteristics and microbial community compositions, Biotechnology for Biofuels, 10 (2017) 140.
[143] R. Posmanik, R.A. Labatut, A.H. Kim, J.G. Usack, J.W. Tester, L.T. Angenent, Coupling hydrothermal liquefaction and anaerobic digestion for energy valorization from model biomass feedstocks, Bioresource Technology, 233 (2017) 134-143.
[144] P.-G. Duan, S.-K. Yang, Y.-P. Xu, F. Wang, D. Zhao, Y.-J. Weng, X.-L. Shi, Integration of hydrothermal liquefaction and supercritical water gasification for improvement of energy recovery from algal biomass, Energy, 155 (2018) 734-745.
[145] L. Cao, C. Zhang, H. Chen, D.C.W. Tsang, G. Luo, S. Zhang, J. Chen, Hydrothermal liquefaction of agricultural and forestry wastes: state-of-the-art review and future prospects, Bioresource Technology, 245 (2017) 1184-1193.
[146] A. Jadhav, I. Ahmed, A.G. Baloch, H. Jadhav, S. Nizamuddin, M.T.H. Siddiqui, H.A. Baloch, S.S. Qureshi, N.M. Mubarak, Utilization of oil palm fronds for bio-oil and bio-char production using hydrothermal liquefaction technology, Biomass Conversion and Biorefinery, (2019).
[147] Z. Liu, F.-S. Zhang, J. Wu, Characterization and application of chars produced from pinewood pyrolysis and hydrothermal treatment, Fuel, 89 (2010) 510-514.
[148] L.-j. Leng, X.-Z. Yuan, H. Huang, W. Hou, Z. Wu, L.-h. Fu, X. Peng, X.-h. Chen, L. Leng, Characterization and application of bio-chars from liquefaction of microalgae, lignocellulosic biomass and sewage sludge, Fuel Processing Technology, 129 (2015) 8–14.
[149] Z. Liu, F.-S. Zhang, Removal of lead from water using biochars prepared from hydrothermal liquefaction of biomass, Journal of Hazardous Materials, 167 (2009) 933-939.
[150] P. Biller, A.B. Ross, Hydrothermal processing of algal biomass for the production of biofuels and chemicals, Biofuels, 3 (2012) 603-623.
[151] A. Jain, S. Jayaraman, R. Balasubramanian, M.P. Srinivasan, Hydrothermal pre-treatment for mesoporous carbon synthesis: enhancement of chemical activation, Journal of Materials Chemistry A, 2 (2014) 520-528.
[152] A. Jain, R. Balasubramanian, M.P. Srinivasan, Production of high surface area mesoporous activated carbons from waste biomass using hydrogen peroxide-mediated hydrothermal treatment for adsorption applications, Chemical Engineering Journal, 273 (2015) 622-629.
[153] S. Raikova, T.D.J. Knowles, M.J. Allen, C.J. Chuck, Co-liquefaction of Macroalgae with Common Marine Plastic Pollutants, ACS Sustainable Chemistry & Engineering, 7 (2019) 6769-6781.
[154] A. Kruse, Supercritical water gasification, Biofuels, Bioproducts and Biorefining, 2 (2008) 415-437.
[155] T.M. Brown, P. Duan, P.E. Savage, Hydrothermal Liquefaction and Gasification of Nannochloropsis sp, Energy & Fuels, 24 (2010) 3639-3646.
[156] D.C. Elliott, L.J. Sealock, Aqueous catalyst systems for the water-gas shift reaction. 1. Comparative catalyst studies, Industrial & Engineering Chemistry Product Research and Development, 22 (1983) 426-431.
[157] A.R.K. Gollakota, M. Reddy, M.D. Subramanyam, N. Kishore, A review on the upgradation techniques of pyrolysis oil, Renewable and Sustainable Energy Reviews, 58 (2016) 1543-1568.

[158] L. Zhang, C. Xu, P. Champagne, Overview of recent advances in thermo-chemical conversion of biomass, Energy Conversion and Management, 51 (2010) 969-982.
[159] T. Sakaki, M. Shibata, T. Miki, H. Hirosue, N. Hayashi, Decomposition of Cellulose in Near-Critical Water and Fermentability of the Products, Energy & Fuels, 10 (1996) 684-688.
[160] S. Kang, X. Li, J. Fan, J. Chang, Classified Separation of Lignin Hydrothermal Liquefied Products, Industrial & Engineering Chemistry Research, 50 (2011) 11288-11296.
[161] A. Kruse, P. Maniam, F. Spieler, Influence of Proteins on the Hydrothermal Gasification and Liquefaction of Biomass. 2. Model Compounds, Industrial & Engineering Chemistry Research, 46 (2007) 87-96.
[162] M. Sugano, H. Takagi, K. Hirano, K. Mashimo, Hydrothermal liquefaction of plantation biomass with two kinds of wastewater from paper industry, Journal of Materials Science, 43 (2008) 2476-2486.
[163] Y. Qu, X. Wei, C. Zhong, Experimental study on the direct liquefaction of Cunninghamia lanceolata in water, Energy, 28 (2003) 597-606.
[164] S. Xiu, A. Shahbazi, V. Shirley, D. Cheng, Hydrothermal pyrolysis of swine manure to bio-oil: Effects of operating parameters on products yield and characterization of bio-oil, Journal of Analytical and Applied Pyrolysis, 88 (2010) 73-79.
[165] S. Karagöz, T. Bhaskar, A. Muto, Y. Sakata, Hydrothermal upgrading of biomass: Effect of K2CO3 concentration and biomass/water ratio on products distribution, Bioresource Technology, 97 (2006) 90-98.
[166] H.K. Reddy, T. Muppaneni, S. Ponnusamy, N. Sudasinghe, A. Pegallapati, T. Selvaratnam, M. Seger, B. Dungan, N. Nirmalakhandan, T. Schaub, F.O. Holguin, P. Lammers, W. Voorhies, S. Deng, Temperature effect on hydrothermal liquefaction of Nannochloropsis gaditana and Chlorella sp, Applied Energy, 165 (2016) 943-951.
[167] D.A. Nelson, P.M. Molton, J.A. Russell, R.T. Hallen, Application of direct thermal liquefaction for the conversion of cellulosic biomass, Industrial & Engineering Chemistry Product Research and Development, 23 (1984) 471-475.
[168] B. Zhang, M. Von Keitz, K. Valentas, Thermal Effects on Hydrothermal Biomass Liquefaction, Applied biochemistry and biotechnology, 147 (2008) 143-150.
[169] K.Q. Tran, Fast hydrothermal liquefaction for production of chemicals and biofuels from wet biomass - The need to develop a plug-flow reactor, Bioresour Technol, 213 (2016) 327-332.
[170] J. Akhtar, N.A.S. Amin, A review on process conditions for optimum bio-oil yield in hydrothermal liquefaction of biomass, Renewable and Sustainable Energy Reviews, 15 (2011) 1615-1624.
[171] J.L. Faeth, P.J. Valdez, P.E. Savage, Fast Hydrothermal Liquefaction of Nannochloropsis sp. To Produce Biocrude, Energy & Fuels, 27 (2013) 1391-1398.
[172] I.M. Dãrãban, L.A. Rosendahl, T.H. Pedersen, S.B. Iversen, Pretreatment methods to obtain pumpable high solid loading wood–water slurries for continuous hydrothermal liquefaction systems, Biomass and Bioenergy, 81 (2015) 437-443.
[173] S. Raikova, C.D. Le, T.A. Beacham, R.W. Jenkins, M.J. Allen, C.J. Chuck, Towards a marine biorefinery through the hydrothermal liquefaction of macroalgae native to the United Kingdom, Biomass and Bioenergy, 107 (2017) 244-253.
[174] B. Zhang, M. von Keitz, K. Valentas, Thermochemical liquefaction of high-diversity grassland perennials, Journal of Analytical and Applied Pyrolysis, 84 (2009) 18-24.

[175] S. Mani, L.G. Tabil, S. Sokhansanj, Grinding performance and physical properties of wheat and barley straws, corn stover and switchgrass, Biomass and Bioenergy, 27 (2004) 339-352.
[176] K.M. Isa, T.A.T. Abdullah, U.F.M. Ali, Hydrogen donor solvents in liquefaction of biomass: A review, Renewable and Sustainable Energy Reviews, 81 (2018) 1259-1268.
[177] P. Nordon, B.C. Young, N.W. Bainbridge, The rate of oxidation of char and coal in relation to their tendency to self-heat, Fuel, 58 (1979) 443-449.
[178] M. Makabe, K. Ouchi, Effect of pressure and temperature on the reaction of coal with alcohol-alkali, Fuel, 60 (1981) 327-329.
[179] A. Demirbaş, Mechanisms of liquefaction and pyrolysis reactions of biomass, Energy Conversion and Management, 41 (2000) 633-646.
[180] M. Kleinert, J.R. Gasson, T. Barth, Optimizing solvolysis conditions for integrated depolymerisation and hydrodeoxygenation of lignin to produce liquid biofuel, Journal of Analytical and Applied Pyrolysis, 85 (2009) 108-117.
[181] G. Wang, W. Li, B. Li, H. Chen, Direct liquefaction of sawdust under syngas, Fuel, 86 (2007) 1587-1593.
[182] P. Duan, P.E. Savage, Hydrothermal Liquefaction of a Microalga with Heterogeneous Catalysts, Industrial & Engineering Chemistry Research, 50 (2011) 52-61.
[183] P. Biller, R. Riley, A.B. Ross, Catalytic hydrothermal processing of microalgae: Decomposition and upgrading of lipids, Bioresource Technology, 102 (2011) 4841-4848.
[184] Y.Q. Yang, C.T. Tye, K.J. Smith, Influence of MoS2 catalyst morphology on the hydrodeoxygenation of phenols, Catalysis Communications, 9 (2008) 1364-1368.
[185] B. Yoosuk, D. Tumnantong, P. Prasassarakich, Amorphous unsupported Ni–Mo sulfide prepared by one step hydrothermal method for phenol hydrodeoxygenation, Fuel, 91 (2012) 246-252.
[186] L. Kong, G. Li, H. Wang, W. He, F. Ling, Hydrothermal catalytic conversion of biomass for lactic acid production, Journal of Chemical Technology & Biotechnology, 83 (2008) 383-388.
[187] S.C. Yim, A.T. Quitain, S. Yusup, M. Sasaki, Y. Uemura, T. Kida, Metal oxide-catalyzed hydrothermal liquefaction of Malaysian oil palm biomass to bio-oil under supercritical condition, The Journal of Supercritical Fluids, 120 (2017) 384-394.
[188] A. Rojas-Pérez, D. Diaz-Diestra, C.B. Frias-Flores, J. Beltran-Huarac, K.C. Das, B.R. Weiner, G. Morell, L.M. Díaz-Vázquez, Catalytic effect of ultrananocrystalline Fe3O4 on algal bio-crude production via HTL process, Nanoscale, 7 (2015) 17664-17671.
[189] F. Deng, A.S. Amarasekara, Iron(0)-Catalyzed Hydrothermal Liquefaction of Switchgrass: the Effects of Co-Catalysts and Reductive Conditions, BioEnergy Research, (2020).
[190] D. Egesa, C.J. Chuck, P. Plucinski, Multifunctional Role of Magnetic Nanoparticles in Efficient Microalgae Separation and Catalytic Hydrothermal Liquefaction, ACS Sustainable Chemistry & Engineering, 6 (2018) 991-999.
[191] F. Gilles, J.L. Blin, H. Toufar, M. Briend, B.L. Su, Double interactions between ammonia and a series of alkali-exchanged faujasite zeolites evidenced by FT-IR and TPD-MS techniques, Colloids and Surfaces A: Physicochemical and Engineering Aspects, 241 (2004) 245-252.
[192] T.F. Robin, A.B. Ross, A.R. Lea-Langton, J.M. Jones, Stability and Activity of Doped Transition Metal Zeolites in the Hydrothermal Processing, Frontiers in Energy Research, 3 (2015).

[193] S. Karagöz, T. Bhaskar, A. Muto, Y. Sakata, T. Oshiki, T. Kishimoto, Low-temperature catalytic hydrothermal treatment of wood biomass: analysis of liquid products, Chemical Engineering Journal, 108 (2005) 127-137.
[194] U. Jena, K.C. Das, J.R. Kastner, Comparison of the effects of Na2CO3, Ca3(PO4)2, and NiO catalysts on the thermochemical liquefaction of microalga Spirulina platensis, Applied Energy, 98 (2012) 368-375.
[195] D. Li, L. Chen, D. Xu, X. Zhang, N. Ye, F. Chen, S. Chen, Preparation and characteristics of bio-oil from the marine brown alga Sargassum patens C. Agardh, Bioresource Technology, 104 (2012) 737-742.
[196] K. Anastasakis, A.B. Ross, Hydrothermal liquefaction of the brown macro-alga Laminaria Saccharina: Effect of reaction conditions on product distribution and composition, Bioresource Technology, 102 (2011) 4876-4883.
[197] C. Jazrawi, P. Biller, A.B. Ross, A. Montoya, T. Maschmeyer, B.S. Haynes, Pilot plant testing of continuous hydrothermal liquefaction of microalgae, Algal Research, 2 (2013) 268-277.
[198] A.R.K. Gollakota, N. Kishore, S. Gu, A review on hydrothermal liquefaction of biomass, Renewable and Sustainable Energy Reviews, 81 (2018) 1378-1392.
[199] D. Castello, T. Pedersen, L. Rosendahl, Continuous Hydrothermal Liquefaction of Biomass: A Critical Review, Energies, 11 (2018) 3165.
[200] S. Raikova, C.D. Le, J.L. Wagner, V.P. Ting, C.J. Chuck, Chapter 9 - Towards an Aviation Fuel Through the Hydrothermal Liquefaction of Algae, in: C.J. Chuck (Ed.) Biofuels for Aviation, Academic Press, 2016, pp. 217-239.
[201] Y. Zhu, M.J. Biddy, S.B. Jones, D.C. Elliott, A.J. Schmidt, Techno-economic analysis of liquid fuel production from woody biomass via hydrothermal liquefaction (HTL) and upgrading, Applied Energy, 129 (2014) 384-394.
[202] Y. He, X. Liang, C. Jazrawi, A. Montoya, A. Yuen, A.J. Cole, N. Neveux, N.A. Paul, R. de Nys, T. Maschmeyer, B.S. Haynes, Continuous hydrothermal liquefaction of macroalgae in the presence of organic co-solvents, in.
[203] A.J. Mørup, J. Becker, P.S. Christensen, K. Houlberg, E. Lappa, M. Klemmer, R.B. Madsen, M. Glasius, B.B. Iversen, Construction and Commissioning of a Continuous Reactor for Hydrothermal Liquefaction, Industrial & Engineering Chemistry Research, 54 (2015) 5935-5947.
[204] N. Marin, S. Collura, V.I. Sharypov, N.G. Beregovtsova, S.V. Baryshnikov, B.N. Kutnetzov, V. Cebolla, J.V. Weber, Copyrolysis of wood biomass and synthetic polymers mixtures. Part II: characterisation of the liquid phases, Journal of Analytical and Applied Pyrolysis, 65 (2002) 41-55.
[205] X. Zhang, H. Lei, S. Chen, J. Wu, Catalytic co-pyrolysis of lignocellulosic biomass with polymers: a critical review, Green Chemistry, 18 (2016) 4145-4169.
[206] F. Pinto, M. Miranda, P. Costa, Production of liquid hydrocarbons from rice crop wastes mixtures by co-pyrolysis and co-hydropyrolysis, Fuel, 174 (2016) 153-163.
[207] E. Önal, B.B. Uzun, A.E. Pütün, An experimental study on bio-oil production from co-pyrolysis with potato skin and high-density polyethylene (HDPE), Fuel Processing Technology, 104 (2012) 365-370.
[208] E. Önal, B.B. Uzun, A.E. Pütün, Bio-oil production via co-pyrolysis of almond shell as biomass and high density polyethylene, Energy Conversion and Management, 78 (2014) 704-710.
[209] Y. Xue, S. Zhou, R.C. Brown, A. Kelkar, X. Bai, Fast pyrolysis of biomass and waste plastic in a fluidized bed reactor, Fuel, 156 (2015) 40-46.
[210] M. Brebu, S. Uçar, C. Vasile, J. Yanik, Co-pyrolysis of pine cone with synthetic polymers, Fuel, 89 (2010) 1911-1918.

[211] L. Zhou, Y. Wang, Q. Huang, J. Cai, Thermogravimetric characteristics and kinetic of plastic and biomass blends co-pyrolysis, Fuel Processing Technology, 87 (2006) 963-969.
[212] D.K. Ojha, R. Vinu, Fast co-pyrolysis of cellulose and polypropylene using Py-GC/MS and Py-FT-IR, RSC Advances, 5 (2015) 66861-66870.
[213] M. Sajdak, R. Muzyka, J. Hrabak, K. Słowik, Use of plastic waste as a fuel in the co-pyrolysis of biomass: Part III: Optimisation of the co-pyrolysis process, Journal of Analytical and Applied Pyrolysis, 112 (2015) 298-305.
[214] P. Rutkowski, A. Kubacki, Influence of polystyrene addition to cellulose on chemical structure and properties of bio-oil obtained during pyrolysis, Energy Conversion and Management, 47 (2006) 716-731.
[215] F. Abnisa, W.M.A.W. Daud, J.N. Sahu, Pyrolysis of mixtures of palm shell and polystyrene: An optional method to produce a high-grade of pyrolysis oil, Environmental Progress & Sustainable Energy, 33 (2014) 1026-1033.
[216] N.I. Izzatie, M.H. Basha, Y. Uemura, M.S.M. Hashim, N.A.M. Amin, M.F. Hamid, Co-pyrolysis of rice straw and Polyethylene Terephthalate (PET) using a fixed bed drop type pyrolyzer, Journal of Physics: Conference Series, 908 (2017) 012073.
[217] M.R. Kim, P.R. Bonelli, A.L. Cukierman, Co-pyrolysis of polyethylene terephthalate (PET) bottle waste and poplar wood sawdust: Kinetics and char characterization, in, 2018, pp. 99-132.
[218] H. Zhou, C. Wu, J.A. Onwudili, A. Meng, Y. Zhang, P.T. Williams, Effect of interactions of PVC and biomass components on the formation of polycyclic aromatic hydrocarbons (PAH) during fast co-pyrolysis, RSC Advances, 5 (2015) 11371-11377.
[219] P. Rutkowski, Influence of zinc chloride addition on the chemical structure of bio-oil obtained during co-pyrolysis of wood/synthetic polymer blends, Waste Management, 29 (2009) 2983-2993.
[220] L. Chen, S. Wang, H. Meng, Z. Wu, J. Zhao, Study on Gas Products Distributions During Fast Co-pyrolysis of Paulownia Wood and PET at High Temperature, Energy Procedia, 105 (2017) 391-397.
[221] E. Taarning, C.M. Osmundsen, X. Yang, B. Voss, S.I. Andersen, C.H. Christensen, Zeolite-catalyzed biomass conversion to fuels and chemicals, Energy & Environmental Science, 4 (2011) 793-804.
[222] T.R. Carlson, T.P. Vispute, G.W. Huber, Green Gasoline by Catalytic Fast Pyrolysis of Solid Biomass Derived Compounds, ChemSusChem, 1 (2008) 397-400.
[223] T.R. Carlson, G.A. Tompsett, W.C. Conner, G.W. Huber, Aromatic Production from Catalytic Fast Pyrolysis of Biomass-Derived Feedstocks, Topics in Catalysis, 52 (2009) 241.
[224] Y.-T. Cheng, G.W. Huber, Chemistry of Furan Conversion into Aromatics and Olefins over HZSM-5: A Model Biomass Conversion Reaction, ACS Catalysis, 1 (2011) 611-628.
[225] H. Zhang, R. Xiao, J. Nie, B. Jin, S. Shao, G. Xiao, Catalytic pyrolysis of black-liquor lignin by co-feeding with different plastics in a fluidized bed reactor, Bioresource Technology, 192 (2015) 68-74.
[226] X. Li, H. Zhang, J. Li, L. Su, J. Zuo, S. Komarneni, Y. Wang, Improving the aromatic production in catalytic fast pyrolysis of cellulose by co-feeding low-density polyethylene, Applied Catalysis A: General, 455 (2013) 114-121.
[227] C. Dorado, C.A. Mullen, A.A. Boateng, H-ZSM5 Catalyzed Co-Pyrolysis of Biomass and Plastics, ACS Sustainable Chemistry & Engineering, 2 (2014) 301-311.
[228] X. Li, L. Su, Y. Wang, Y. Yu, C. Wang, X. Li, Z. Wang, Catalytic fast pyrolysis of Kraft lignin with HZSM-5 zeolite for producing aromatic hydrocarbons, Frontiers of Environmental Science & Engineering, 6 (2012) 295-303.

[229] E.B. Hassan, I. Elsayed, A. Eseyin, Production high yields of aromatic hydrocarbons through catalytic fast pyrolysis of torrefied wood and polystyrene, Fuel, 174 (2016) 317-324.
[230] X. Zhang, H. Lei, L. Zhu, X. Zhu, M. Qian, G. Yadavalli, D. Yan, J. Wu, S. Chen, Optimizing carbon efficiency of jet fuel range alkanes from cellulose co-fed with polyethylene via catalytically combined processes, Bioresource Technology, 214 (2016) 45-54.
[231] B.-S. Kim, Y.-M. Kim, H.W. Lee, J. Jae, D.H. Kim, S.-C. Jung, C. Watanabe, Y.-K. Park, Catalytic Copyrolysis of Cellulose and Thermoplastics over HZSM-5 and HY, ACS Sustainable Chemistry & Engineering, 4 (2016) 1354-1363.
[232] G. Zhou, J. Li, Y. Yu, X. Li, Y. Wang, W. Wang, S. Komarneni, Optimizing the distribution of aromatic products from catalytic fast pyrolysis of cellulose by ZSM-5 modification with boron and co-feeding of low-density polyethylene, Applied Catalysis A: General, 487 (2014) 45-53.
[233] J. Li, Y. Yu, X. Li, W. Wang, G. Yu, S. Deng, J. Huang, B. Wang, Y. Wang, Maximizing carbon efficiency of petrochemical production from catalytic co-pyrolysis of biomass and plastics using gallium-containing MFI zeolites, Applied Catalysis B: Environmental, 172-173 (2015) 154-164.
[234] w. Yao, J. Li, Y. Feng, W. Wang, X. Zhang, Q. Chen, S. Komarneni, Y. Wang, Thermally stable phosphorus and nickel modified ZSM-5 zeolites for catalytic co-pyrolysis of biomass and plastics, RSC Advances, 5 (2015) 30485-30494.
[235] X. Lin, Z. Zhang, Z. Zhang, J. Sun, Q. Wang, C.U. Pittman, Catalytic fast pyrolysis of a wood-plastic composite with metal oxides as catalysts, Waste Management, 79 (2018) 38-47.
[236] A. Solak, P. Rutkowski, The effect of clay catalyst on the chemical composition of bio-oil obtained by co-pyrolysis of cellulose and polyethylene, Waste Management, 34 (2014) 504-512.
[237] X. Zhang, H. Lei, L. Zhu, M. Qian, X. Zhu, J. Wu, S. Chen, Enhancement of jet fuel range alkanes from co-feeding of lignocellulosic biomass with plastics via tandem catalytic conversions, Applied Energy, 173 (2016) 418-430.
[238] Y. Xue, A. Kelkar, X. Bai, Catalytic co-pyrolysis of biomass and polyethylene in a tandem micropyrolyzer, Fuel, 166 (2016) 227-236.
[239] B. Zhang, Z. Zhong, K. Ding, Z. Song, Production of aromatic hydrocarbons from catalytic co-pyrolysis of biomass and high density polyethylene: Analytical Py–GC/MS study, Fuel, 139 (2015) 622-628.
[240] K. Praveen Kumar, S. Srinivas, Catalytic Co-pyrolysis of Biomass and Plastics (Polypropylene and Polystyrene) Using Spent FCC Catalyst, Energy & Fuels, 34 (2020) 460-473.
[241] P. Ghorbannezhad, S. Park, J.A. Onwudili, Co-pyrolysis of biomass and plastic waste over zeolite- and sodium-based catalysts for enhanced yields of hydrocarbon products, Waste Management, 102 (2020) 909-918.
[242] X. Yuan, H. Cao, H. Li, G. Zeng, J. Tong, L. Wang, Quantitative and qualitative analysis of products formed during co-liquefaction of biomass and synthetic polymer mixtures in sub- and supercritical water, Fuel Processing Technology, 90 (2009) 428-434.
[243] X. Pei, X. Yuan, G. Zeng, H. Huang, J. Wang, H. Li, H. Zhu, Co-liquefaction of microalgae and synthetic polymer mixture in sub- and supercritical ethanol, Fuel Processing Technology, 93 (2012) 35-44.
[244] L. Zhou, F. Santomauro, J. Fan, D. Macquarrie, J. Clark, C.J. Chuck, V. Budarin, Fast microwave-assisted acidolysis: a new biorefinery approach for the zero-waste

utilisation of lignocellulosic biomass to produce high quality lignin and fermentable saccharides, Faraday Discussions, 202 (2017) 351-370.
[245] X. Wu, J. Liang, Y. Wu, H. Hu, S. Huang, K. Wu, Co-liquefaction of microalgae and polypropylene in sub-/super-critical water, RSC Advances, 7 (2017) 13768-13776.
[246] B. Wang, Y. Huang, J. Zhang, Hydrothermal liquefaction of lignite, wheat straw and plastic waste in sub-critical water for oil: Product distribution, Journal of Analytical and Applied Pyrolysis, 110 (2014) 382-389.

Chapter 2

Liquid hydrocarbon via liquid phase pyrolysis from pistachio hulls phase steam

2.1 Introduction

Due to its resistance to degradation, substantial quantities of plastics have accumulated in the natural environment and landfills for a century. The main sources of plastic entering the environment are land-and-sea-based sources, with domestic, industrial, and fishing activities also a major contributor. Minimisation of this waste has been considered as part of the solution, however the disposal of plastic waste in landfills provides habitats for insects and rodents that may cause different types of diseases. Waste plastic recycling processes that include reprocessing to form new products tend to result in a low-quality product. The transportation, constraints on water contamination and inadequate prior separation increase the cost of the recycling process. An alternative is the thermal processing of converting waste plastic into biofuel and chemicals, which has gained a lot of attention in recent years as a promising technique to eliminate the refuse that is harmful to the environment.

Second-generation biofuels produced from lignocellulosic biomass have been identified as some of the most promising liquid fuels, as they provide a way to simplify the waste disposal process as well as providing energy-rich useful products. In one promising example from the industrial sector, pistachio hulls offer a promising source of waste lignocellulosic biomass. In this study of a food industry waste stream, pistachio hulls provided by Wonderful™ snack company were used as a feedstock for biofuel production. The soft outer shell of pistachio nuts is removed during processing and creates a considerable waste stream.

Thermochemical conversion technologies currently being developed include direct combustion, gasification, pyrolysis and hydrothermal liquefaction, which can convert biomass into heat, syngas, and crude oil respectively. However, the biofuel products require expensive and energy-intensive post processing [1]. For instance, pyrolysis fuels obtained from biomass are deoxygenated in the presence of hydrogen under a high-pressure (~10 MPa) catalytic reactor operated at temperatures of ~350−400°C [2, 3]. Technological progress is essential to cover energy demands and society's concern over environmental pollution. This chapter focuses on assessing an alternative catalytic process, used industrially on the pilot scale, in which organic wastes are claimed to be potentially liquefied and deoxygenated in a single step at low operational conditions.

Liquid phase pyrolysis (LPP), where biomass is heated in a high boiling point carrier oil, offers the opportunity to reduce the temperature and increase the mass transfer by undertaking the reaction in a liquid medium [4], and has been shown to be an effective method of conversion at suitably high temperatures. The liquid medium can be employed to transfer heat to the feedstocks and the process is characterised by a very good heat transfer rate. The process uses refined petroleum 'carrier oil' as the heat carrier. Thus, the process temperature of LPP is restricted to the boiling point of the carrier oil. During LPP, particles are retained via heating of the carrier oil, leading to a bio-fuel oil without particles or inorganics [5]. The lignocellulosic biomass is converted into shorter chain oxygenates which can dissolve in the liquid fraction aiding further processing. There are several clear advantages of the LPP process in cooperation with pyrolysis. The temperature of the LPP process is lower (400-500 °C) than fast pyrolysis (500-850 °C) which can reduce the operating cost.

A related catalytic process has also been developed recently by combining LPP with catalytic cracking, which claims to need no additional hydrogen source. This process is termed catalytic pressure-less depolymerisation (CPD), or Katalytische Drucklose Verölung (KDV) in the original German. KDV is a patented technology developed by Alphakat GmbH [2]. During the KDV process, the company claim that the organic feedstock undergoes depolymerisation reactions to produce a fossil oil, as with LPP, but in the presence of a neutraliser ($CaOH_2$) and a zeolite catalyst. It is claimed that the lignocellulose is pyrolyzed at temperatures between 250-320°C at atmospheric pressure to produce a high-grade hydrocarbon fuel suitable for road transport [2, 6, 7]. The volatile products are then collected continuously from the reaction vessel through distillation, and separated from a large aqueous fraction [8]. The claimed benefit of the KDV process is in converting all kinds of organic substances at atmospheric pressure and temperatures between 280-320 °C [8].

In addition to the catalysts, the KDV process also uses intensive mixing of the carrier oil with the solid materials. This is achieved by replacing conventional heating through the reactor wall with generating the heat through a high-shear in-line mixer. The temperature of the reaction is substantially lower than the typical uses for other thermochemical processes and is limited by this method of heating. Consequently, the company claim that this technology removes non-uniformities in temperature and heat flux. The coke formation thus does not impact the KDV process. Surprisingly, as there

are no reports of the mechanism, pilot plants based on KDV technology have been established in Germany, Mexico, Japan and Korea.

Gonzalez-Quiroga *et al.* studied the production of demolition and municipal solid wastes to diesel using a KDV pilot plant. They found that the KDV showed successful liquefaction together with the deoxygenation of the product, with low oxygen content and a high share of paraffins [1]. However, in this publication there was no mass balance given, and no indication of how this could possibly be achieved. Al-Rousan *et al.* studied the possibilities of biodiesel potential from various bio-wastes, including olive cake, activated sludge, digested sludge, sheep manure, poultry manure, and laying hens manure in a KDV pilot plant from ALPHAKAT Company. The results showed that olive cake gave the best option for bio-oil yield (39%). A strong linear relationship between the percentage of organic content and caloric value and bio-oil output was observed [6]. However, the work makes no reference how much of cracked carrier oil adds to the bio-oil and how much is derived from biomass. Therefore, the yields given are almost certainly an overestimate.

While a number of pilot plants have been built to demonstrate the KDV process, there are currently no lab-scale examples in the literature of this process or any investigations actually detailing the mechanism of how this process could possibly produce such high-grade hydrocarbon products without the addition of hydrogen. As such much of the chemistry and fundamental engineering remains unclear.

The aim of this chapter was to investigate the KDV process further, and through collaboration with the Wonderful Company and Ekotrend assess the pilot scale mass balance and determine the suitability of this approach for producing hydrocarbons from biomass. To this end pistachio hulls were investigated as the biomass source. To achieve the aim the following objectives were identified:

1. Data will be collected data from a KDV pilot plant run in batch mode and complete a full mass balance to assess the suitability of producing advanced biofuels through this process.
2. The process will be mimicked on the lab scale, on both 1L and 5L scales and test the optimal catalyst type and loading.
3. The mechanism that allows high grade hydrocarbons to be created from the KDV process will be assessed.

4. Building on suitable results achieved in the first 3 objectives the possibility of co-processing polypropylene and pistachio hulls will be investigated.

2.2 Materials and methods

2.2.1 Materials

Waste pistachio hulls were provided by Wonderful Snack Company. The shell of pistachio nuts removed during processing creates a considerable waste stream with a particle size of 2-5mm. Properties of pistachio hulls is present in **Table 2.1-1**

Table 2.1- 1 Properties of pistachio hulls

Properties	Result	Method
Moisture	14.31 wt %	ASTM E1755
Ash	4.24 wt %	ASTM E1755
Volatile Matter	70.09 wt %	ASTM E1755
Fixed Carbon	11.35 wt %	ASTME1755
Carbon	41.22 wt %	ASTM D5291
Sulfur	0.13 wt %	ASTM E3177
Hydrogen	6.98 wt %	ASTM D5291
Nitrogen	1.34 wt %	ASTM D5291
Oxygen by Difference	46.08 wt %	ASTM D5291
Low Heat Value	7508 BTU/lb	ASTM E711
High Heat Value	8155 BTU/lb	ASTM E711

Faujasite zeolite-type were applied to catalyse the deoxygenation reactions including 4A zeolite, aluminosilicate, and ZSM-5 zeolites. All zeolite catalysts were purchased in powder form, with a particle size of 0.8-8 µm. All the catalysts were purchased from Zeolyst International and used without further treatment or purification. Calcium Hydroxide $Ca(OH)_2$, brand name ALPOL 120 was purchased from the Polish supplier, ALPOL and was used without further purification.

Two types of carrier oils were used, a light carrier oil (N200 oil) and heavy oil (LAN-150). N200 oil is significantly more volatile and provides a low density and flows freely at ambient temperature. The kinetic viscosity of LAN-150 oil at 40 °C and 100 °C were

131.4 and 13.20 mm^2 s^{-1} respectively. The density of LAN-150 oil was 887.1 kg/m^3. The boiling point of N200 and LAN-150 oil were 180°C and 272 °C respectively. The element composition of carrier oils is shown in **Table 2.2-2**

Table 2.1- 2–Elemental composition of light carrier oil (N200) and heavy oil (LAN-150)

Analysis parameter	N200 carrier oil	LAN-150 carrier oil
C (wt%)	86.01	85.09
H (wt%)	13.87	13.09
N (wt%)	0.15	0.59
S (wt%)	-	1.04

2.2.2 Methodology

Laboratory Batch Liquid Phase Pyrolysis: 1L Reaction

Liquid phase pyrolysis of pistachio hull was carried out in a 1 L 316 stainless steel batch reactor with a diameter 10 cm allowing a sample bed depth of around 25 cm. A pressure gauge was connected to the top of the reactor to monitor and control the pressure in the case of excess pressure generated. The system was heated via an infra-red furnace and a thermocouple was inserted to measure the reactor temperature. In a typical experiment, the reactor was loaded with a mixture of pistachio: carrier oil (5:1, 5:2, with respect to 100 g of carrier oil) and catalyst ranged between 5 and 150 wt.% of either 4A zeolite, aluminosilicate, and ZSM-5. The feedstock was then mixed with 2-10 wt.% of $Ca(OH)_2$) as co-catalyst to enhance the reaction.

The system started at the room temperature at 25°C and the heating rate to reach the pyrolysis temperature was set to be around 4.17°C s^{-1}. After the temperature reached pyrolysis temperature of 300 °C, the reaction was maintained for 1.5 hours. All condensable vapours were condensed to liquid product using a system of condensers. While the uncondensed product was collected from a pipe at the bottom. The condenser temperature was maintained by water cooling at about 10 °C. After the pyrolysis reaction was completed, the system was quickly cooled to ambient

temperature. Bio-oil was then separated from the liquid product through condenser and the yield of bio-oil product determined.

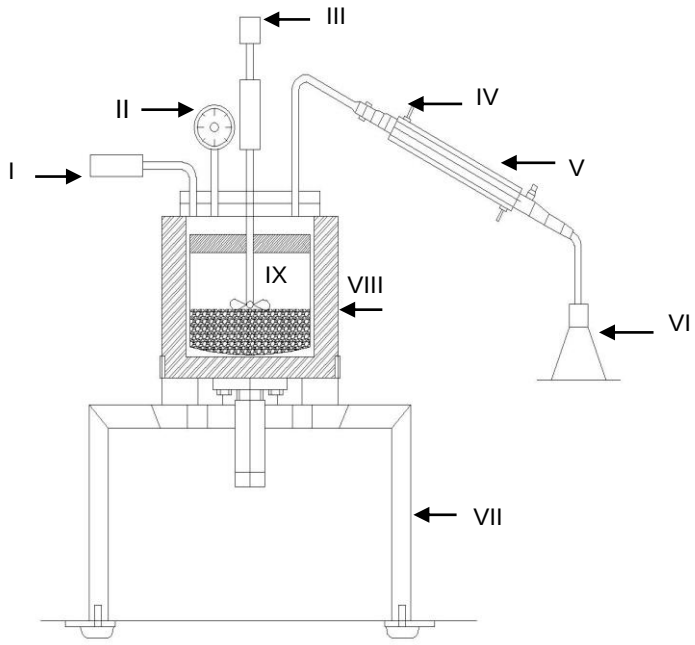

I. Thermocouple

II. pressure gauge

III. Stirrer motor

IV. Cooling water,

V. Condenser

VI. Liquid product collector

VII. Shelf

VIII. Heater

IX- Reactor

Figure 2.2- 1–Experiment set up of batch liquid phase pyrolysis

Laboratory Batch Liquid Phase Pyrolysis: 5L Reaction

Although the 1L reactor could be used to convert the biomass to bio-oil, there were several errors during the process such as the short path distillation and lack of head space in the reactor. The reactor provided lower efficiency as the limited momentum of the solid mixture which might easily result in blocking of reactor vessels. In order to meet the representative process, the process was then conducted in the larger reactor (5L) which provided a longer distillation pathway and better efficiency. The preparation was the same as presented in the 1L reactor. The reaction was carried out under stirring at 450-500 rpm and the reaction started at 90 °C for 30 minutes to minimize foaming. The temperature was then slowly increased to 300 °C at a heating rate of 4.17 °C/min. The reaction was held time at maximum temperature for 3 hours. The sample vapours were condensed and collected in the bottom collector continually throughout the experiment.

2.2.3 Distillate bio-oil analysis

The chemical composition of the volatile fraction of the reaction was identified using Agilent Technologies 7890A GC system fitted with a 30 m × 250 µm × 0.25 µm HP5-MS column, coupled to a 5975C inert MSD. The sample obtained from the pyrolysis experiment was dissolved in hexane. Helium was used as carrier gas in a constant rate at 1.3 ml min^{-1}. The initial temperature of oven temperature program was set at 50°C which increased 5 °C min^{-1} until 250 °C. The injector temperature and sample injection volume were 250°C and 1 µL, respectively. Library and residence times of known species injected in the chromatography was determined using the NIST mass spectral database.

Thermal decomposition characteristics and the weight reduction characteristic were determined of solid phase through thermogravimetric analyser (TGA). The high purity nitrogen was used as the carrier with volume flowrate at 5.0 min^{-1}. The heating rate was 10°C min^{-1}. The weight of sample powder was approximately 2.5 mg. The sample was loaded in an alumina crucible. The sample was heated over the range 20 °C to 1000°C.

CHN element analysers are the methods to rapidly determine carbon, hydrogen and nitrogen in the organic matrices. The simplest forms CHN analysis was conducted with high temperature combustion. In the combustion process (1000 °C), the sample is broken down into its elemental components, N_2, CO_2, and H_2O. CHN elements of this work were determined at the London Metropolitan University on a Carlo Erba Flash 2000 Elemental Analyzer to determine CHN content.

The amount of bio-content in the fuels was determined through a simplified radiocarbon (^{14}C) analytical technique. Radiocarbon dating is rate of decay of radioactive ^{14}C, which generated in the upper atmosphere via a cosmogenic isotope and its subsequent decay to ^{14}N. ^{14}C is formed continuously in the earth's upper atmosphere. Thus, there is ^{14}C remains present in atmospheric CO_2. ^{14}C reacts with oxygen to generate CO_2, which is the absorbed through plants during photosynthesis. Plants and animals use carbon in food chain take up ^{14}C throughout their lifetimes. Once the plant or animal dies, they stop exchanging carbon and their ^{14}C is no longer replaced by the atmosphere, and the constant decay of ^{14}C back to 14N and beta particle begins. Thus, the ratio of ^{14}C in a decreased organism decreases at a constant

rate over time. Because ^{14}C has haft-life of 5,730 years, ^{14}C is almost absent from fossil products older than 20,000 to 30,000 years.

Radiocarbon dating is essentially a technique which is completed via reducing the quantity of radiocarbon (^{14}C) in a sample to a modern reference standard. In order to know how much ^{14}C remains in the sample, the ^{14}C of the sample has to be compared with the ^{14}C value of the reference value. The ^{14}C reference value applied to determine the bioC quantity varies of different biogenic material. Samples with high bio-oil obtained were determined using 'Beta Analytic' radiocarbon analysis labs for bio-carbon content determination. ^{14}C was carried out in accordance with ASTM D6866.

2.3 Results and Discussion

2.3.1 Initial plant operation

In the operation of both the lab and pilot system a distillate contains both water and the distillate oil. This is separated giving the non-water-soluble fraction, termed the distillate oil. This is made up of the bio-component (bio-oil) and any cracked or light boiling point carrier oil from the system. There are a few key differences in the operation on the pilot plant than is available in a simpler lab-based system. The differences between pilot plant scale and lab scale reactor in this study can be summarized as:

- The difference in heating apparatus. Both of 1L and 5L reactor heat is conventional electric heating, while the plant process uses recirculation of the oil-solids slurry through a friction turbine pump to generate the heat. In addition, the plant uses a pre-treatment section which requires loading and heating at a lower reaction temperature.
- The pre-treatment section on the pilot plant preheats all reaction components at around 90 °C. Raw materials are then transferred into the reaction vessel, termed KDV vessel, where the pyrolysis reaction could potentially take place.
- Two turbines (turbine A and B) are used in the pilot plant process. Turbine A is used for mixing reactants together at a temperature of 90 °C, before transfer to B100 and B200, while turbine B is used as heat generator for B200, the temperature inside B200 are controlled in the range of around 290-320 °C.

A schematic of the KDV pilot plant is shown in **Figure 2.3-1.** The KDV pilot plant consists of the following components including (a) feed system; pre-heater section, pyrolysis reactor, (b) condensation section; control section. The carrier oil is added to the system and the solids (catalyst, neutraliser, biomass) then fed into the premix. As the raw material contain moisture, the slurry was held at 90 °C to remove the water. After moisture removal, the slurry was transferred to the reaction KDV vessel to complete the pyrolysis reaction. At this point, the reaction section is heated via turbine A and slowly heats up to 300 °C. Under these temperatures, the assumption is that the heterogeneous catalyst starts working and the biomass is cracked into a gas, liquid vapour and solids. The reactor vapour produced is removed through a distillation column, effecting continuous removal of the liquid products as vapour. The formed liquid products (water, pyrolysis oil) leaves the process at the top through the condenser section. The remaining solution after reaction is then returned to the preheat section to cool down and then are carried to the centrifuge system to separate waste solids and carrier oil. In this section, the waste stream is centrifuged immediately after it has been cooled to prevent waste settling and becoming too thick. The carrier oil is used as the recycled oil which is mixed with the new carrier oil where the cycle starts again. Prior to the PhD, the pilot plant was producing 150 L of distillate per tonne of biomass.

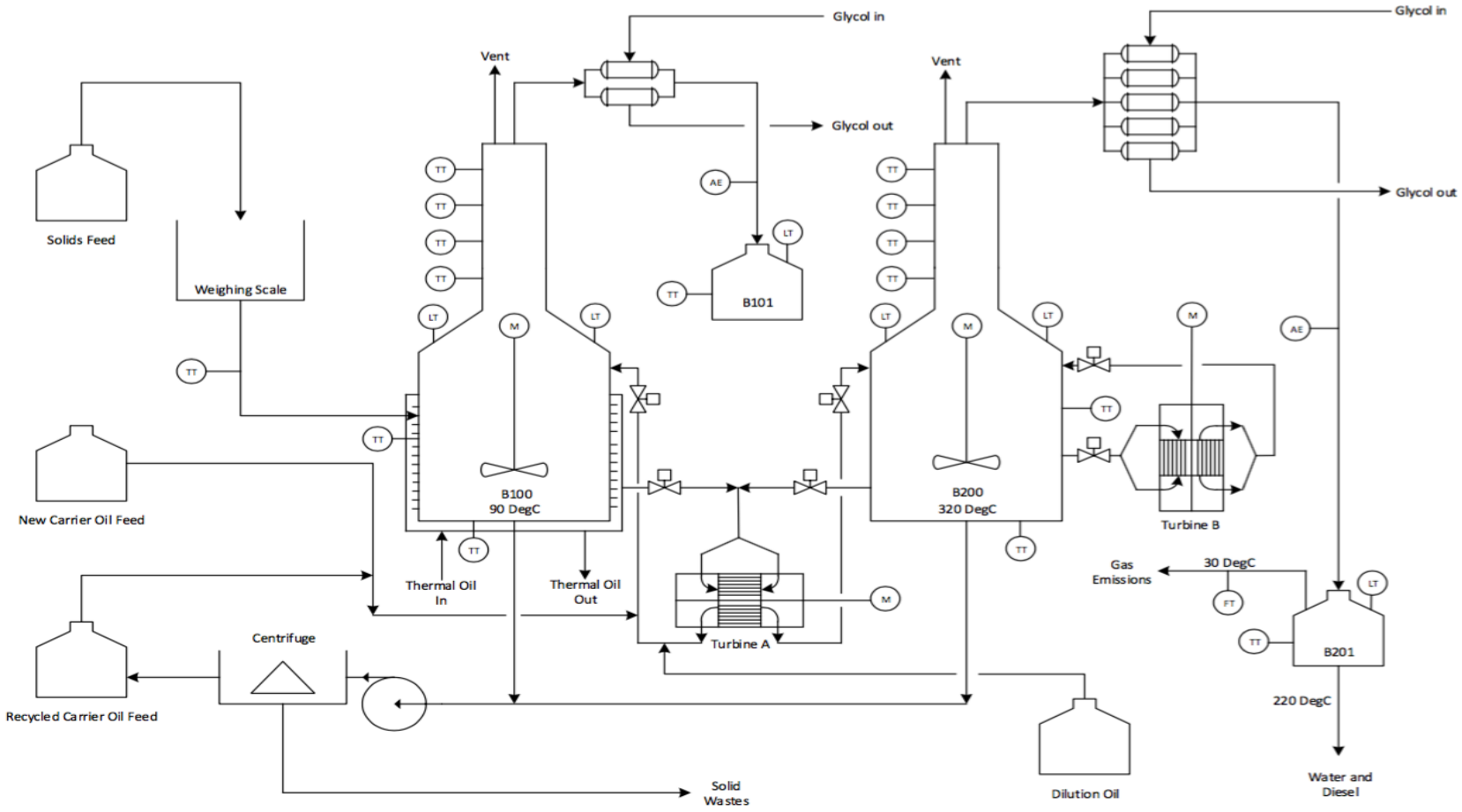

Figure 2.3- 1–Design basic and process description (F1-solid feed, F2-New carrier oil, F3-solid after pre-treatment, F4-mojerizer collection, F5-feed stock after increasing temperature, F6-gas production, F7-gas production after condensed, F8-liquid production, F9-wasted carrier oil collection, F10-wasted production, F11-solid wastes, 1-pretreatment system, 2–batch reactor, 3–condensed system)

To determine the suitability of this process for bio-oil production, an initial mass balance was completed, based on the direct measurement of each of the process inputs and outputs. This run gave the operating conditions of KDV technology as 300-320 °C and pre-treatment 90°C. A higher boiling point carrier oil, LAN-150, was used in this test to reduce the amount of carrier oil in the product. The result based on the moisture content of catalyst, and pistachio hulls are 12% and 10% respectively. The overall mass balance demonstrated that only 32.8 L distillate oil was produced using 1,000 kg of biomass (3.28 %) which was much lower than previously reported [1] though crucially no mention in any of the reports is given to how much of the carrier oil simply cracked and added to the product. To this end ^{14}C analysis was undertaken to determine the bio-content in the product, the yield of bio-content in the product oil was 49%. Meaning the yield of bio-oil from the system was approximately 16 kg per 1000 kg of biomass used, or 1.6%. This is akin to a slow pyrolysis process undertaken under those temperatures [9]. The mass balance data is given in **Table 2.3-1** for material fraction composition and production value, respectively.

The energy balance was determined from the heat feed and heat consumption of the process. Heat input included a capacity up to 992 kg of biomass and carrier oil 2113.5 kg. The core of the plant is a batch reactor which was designed based on the previous study. The energy balances enabled the determination of the energy consumption for biomass is 5.4×10^6 kJ, and the energy consumption for the carrier oil is 1.18×10^7 kJ (**Table 2.3-2**).

Previously to the PhD, and in the few reports available, only a light oil was used as the carrier oil. With the application of a much heavier oil, and the calculation of the bio content present, it seems extremely unlikely that this process is a suitable method for biofuel production and rather the light fraction of the carrier oil and the cracked carrier oil adds to the product, just making it seem so.

To validate these observations, and understand the underlying chemical process, the reaction was scaled down to the laboratory scale.

Table 2.3- 1–Material fraction composition of inputs and outputs in plant operation converting pistachio hulls with a pre-mix temperature of 90 °C, KDV temperature of 300-320 °C using LAN-500 carrier oil

	Mass [kg]	**Moisture content [%]**	**Dry Mass [kg]**
Carrier oil LAN150	2,113.5	0	2,113.5
Catalyst 4A	249	6.85	231.9
Neutralizer	149	1.25	147.1
Biomass (pistachio)	992	10.66	886.3
Total Outputs	**3,503.5**		**3,378.8**
Product oil	66.5	-	-
Water	319.5	-	-
Waste oil with solids	3013	-	-
Waste oil	2,146.6	-	-
Solid waste	866.4	-	-
Exhaust gases	85.4	-	-
Total	**3,484.4**		
Different in mass balance	**19.1 (0.5%)**		

Table 2.3- 2–Production values and resultant bio-oil production figures. Generated cross referencing all radiocarbon data, plant production data & biomass analysis data.

Description	Value
Biomass in (kg)	992
Ash @ 11%	109
Moisture (kg)	105
Carrier oil (L)	2,113
Utilisable biomass (kg)	777
Bio-oil in carrier @3.7% (L)	63.39
Total distillate oil Product (L)	66.5
Bio-content of oil Product	49%
Produced bio-oil (L) present in any oil phase	95
Produced bio-oil (L/tonne biomass)	96.75
Bio-oil relative to original biomass loading present in any oil phase (wt.%)	**9.67%**
Bio-oil Present in the distillate product only (L/tonne biomass)	32.85
Bio-oil product present in the distillate product, relative to original biomass loading (wt.%)	**3.28%**
Conversion of dry, ash free biomass to bio-oil in any oil phase (L/ tonne)	123.50
Bio-oil present in oil phase, relative to utilisable biomass (wt.%)	**12.35%**

Table 2.3- 3–Energy of inputs and outputs were used in plant test

Component	Delta Hf (kJ/mol)	Energy Consumption (kJ)
Biomass	20,000	5.4×10^6
Carrier oil	45,000	8.32×10^6

2.3.2 Laboratory liquid phase pyrolysis: 1L reaction

The reaction was studied on the lab scale where pistachio hulls were converted in carrier oil using either 4A zeolite, ZSM-5 or an aluminosilicate catalyst. As the pilot plant operation involves holding the reaction mixture at 150 °C, this temperature was examined to determine if the pistachio hulls are starting to degrade in the pre-mix vessel. The temperature of the KDV system was reported to be achieved at between 250-300°C as mentioned in the literature, so the reaction was also studied at these temperatures on the lab scale.

During the KDV process, heat transfer between components was accomplished via the carrier oil. Liquid phase was collected once the temperature reached at around 120°C which related to extraction of moisture from the pistachio hull and the catalyst. Amount of biomass breakdown product was found in the distillate phase when the temperature was above 200°C. Substantial degradation reactions were observed at the temperature above 280°C. Two main liquid phases were obtained as the product: one yellow wastewater (aqueous phase) and one dark brown oil (distillate oil) with a smoky smell. The dark brown oil phase was separated on the top of the water, and was defined as the distillate oil from the process (**Figure 2.3-2**). The yields of product liquids and chars were calculated by weighing. Distillation of total distillate and distillate oil at different temperatures, with no catalyst is shown in **Figure 2.3-3**. Each experiment was repeated three times to determine experimental error and test the repeatability of experimental results.

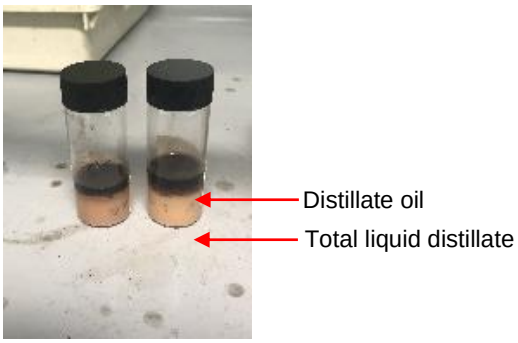

Figure 2.3- 2–Liquid distillate from 4A zeolite after KDV reaction at 300 °C.

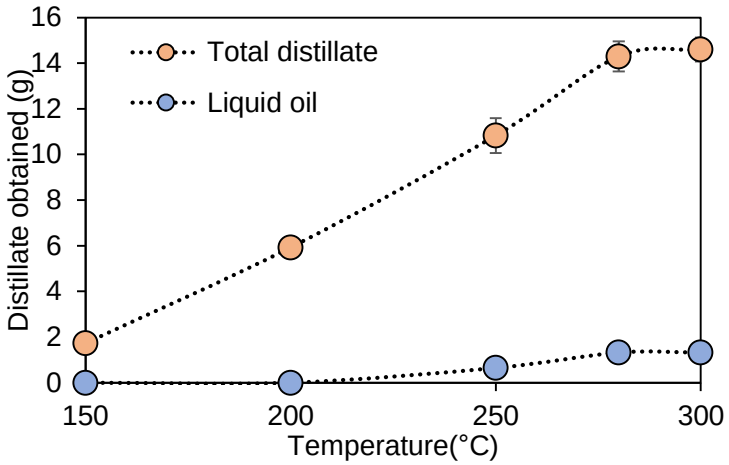

Figure 2.3- 3–Distillation of total distillate and distillate oil at different temperatures, with no catalyst

2.3.2.1 4A Zeolite catalyst

Initially, the 4A zeolite used in the KDV process was applied to the laboratory process. In order to study the effect of the 4A zeolite in the liquid phase pyrolysis reaction, the experiments were performed with 20 g of biomass with catalyst loadings of 33.3 wt%, 50 wt% and 75 wt%, (10 g, 20 g, and 30 g). Carrier oil (N-200): biomass weight ratio was also examined with a 5:1 and 5:2 weight ratio investigated. Neutraliser ($Ca(OH)_2$) was also included (10 wt%, 2 g for all reactions). The pyrolysis reaction was carried out at a controlled temperature of 300 °C and held for 90 minutes, which was sufficient in all cases to collect the distillate formed.

At a loading of 100g of carrier oil and 20g of biomass, 8.5g of distillate was obtained, when the amount of carrier oil was increased to 200g, then the amount of distillate increased accordingly. For all carrier oil loadings, both the 33.3 wt% and 75 wt%

catalyst loadings gave similar levels of distillate with the 50 wt% of catalyst being optimal at both loadings, producing 14.6g and 20.6g of distillate in the 100g and 200g carrier oil respectively (**Figure 2.3-4**).

The distillate oil was found to increase with carrier oil increased, 1.3 g of distillate oil was obtained at 100 g of carrier oil, increasing to 1.6 g at 200 g of carrier oil. The distillate oil obtained was analysed to 6.5 vol% and 8.0 vol% for 100 g and 200 g of carrier oil respectively. The distillate oil yields obtained were less compared to slow pyrolysis from pistachio shells at 300 °C (15.5 wt%) [10]. For all carrier oil loading, both the 33.3 wt% and 75 wt% catalyst loading decreased the distillate oil. The distillate oil decreased slightly from 1.3 g for 100 g carrier oil to 0.5 wt% and 0.2 wt% for the 33.3 wt% and 75 wt% catalyst loading respectively, this gave similar levels of distillate oil with 200 g carrier oil. These yields are similar to the bio-oil obtained from pilot plant.

The ^{14}C demonstrated that the liquid oil product was mainly derived from the carrier oil. The efficiency of biomass conversion by KDV process does not appear to have significant benefit in terms of bio-oil production from pistachio hulls, with an average of approximately 16% for bio-oil carbon content derived from biomass was found in the presence of 50 wt% catalyst and 100 g carrier oil (**Table 2.3-4**).

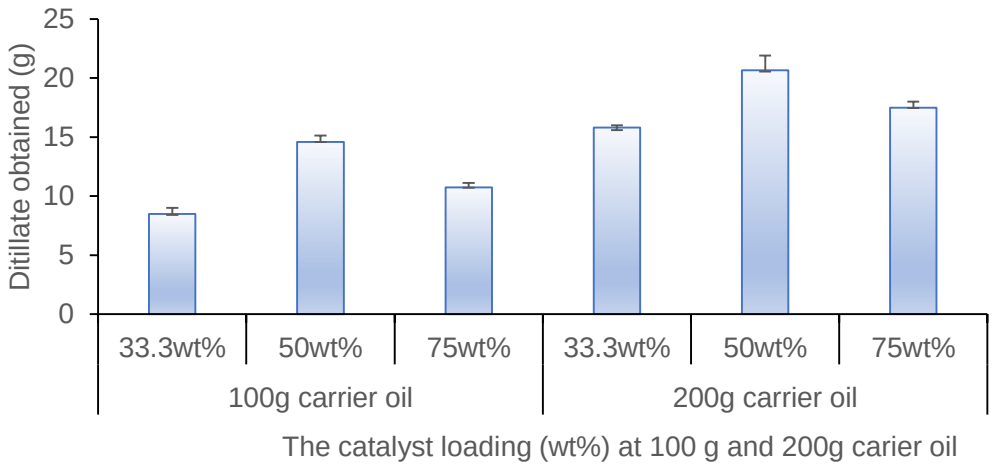

Figure 2.3- 4–Distillation of total liquid product from liquid phase pyrolysis with 4A catalyst at 100g and 200g of N200 carrier to biomass.

Table 2.3- 4 –The distillate oil, and bio-carbon content at different 4A zeolite loading at 100g carrier oil (N200)

4A zeolite (g)	Distillate (g)	Distillate oil product (g)	Biocarbon content of oil product (%)
10	8.5	0.47	10.77 +/- 0.06 pCM
20	14.6	1.32	15.98 +/- 0.08 pCM
30	10.2	0.166	4.34 +/- 0.05 pCM

In the initial description of this work, $Ca(OH)_{2,}$ was added to control the pH, which was then claimed to prolong the life of the catalyst. The effect of the neutralizer was therefore investigated on this scale. Different $Ca(OH)_2$ concentrations of 0 g, 2 g, and 5 g relative to 20 g biomass were prepared. The mass ratio of carrier oil: biomass was carried at 5:1, the reaction temperature was kept at 300 °C, and held for 90 minutes. Blending feedstock with neutraliser did not have a significant impact with slight yield increases observed of 0.3-0.6 for 5 g and 2 g respectively (**Figure 2.3-5)**.

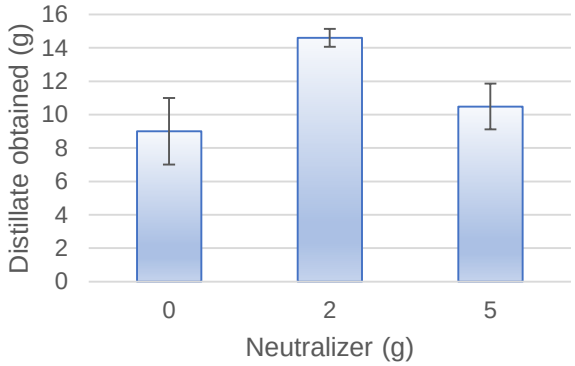

Figure 2.3- 5– Distillation of liquid product from liquid phase pyrolysis with different neutralizer loading in biomass at 20g of catalyst loading and 100g of carrier oil (N200).

Table 2.3- 5–The distillate oil, bio-oil yield, bio-carbon content at different neutralizer loading at 20 g 4A zeolites and 100g carrier oil (N200)

Neutralizer (g)	Distillate (g)	Distillate oil product (g)	Biocarbon content of oil product (%)
0	9	0.7	-
2	1.6	1.32	15.98 +/- 0.08 pMC
5	10.5	0.97	4.34 +/- 0.05 pMc

There was some indication in the pilot plant that an excess of water in the reaction would help to strip products out of the carrier oil. This is used in some fuel processing applications, including steam cracking on standard fuel refineries [11]. To increase liquid product conversion, this effect was examined by soaking all of the raw materials (2 g of neutraliser, 20 g biomass, 20 g 4A zeolite, and 100 g of carrier oil) in 20 ml of water for 24 hours before use in the KDV process. The results showed a substantially increase in the total liquid product distillation from 14.8 g for non-soaking solid material to 27.0 g for soaking solid in the water but liquid oil distillates were similar to those produced from non-soaking material. There is therefore no evidence additional moisture in the materials aids the reaction yield.

Table 2.3- 6– The distillate oil with soaking solid material in the water at 20g catalyst loading and 100g of carrier oil (N200).

	Distillate (g)	**Distillate oil (g)**
Non-soaking solid material	14.8	0.7
Soaking solid material	27	1.32

2.3.2.4 Aluminosilicate catalyst

It seems highly unlikely that under this water loading or temperature that 4A zeolite would retain its structure. Therefore, an amorphous aluminosilicate was tested to assess whether the same yields could be achieved. The amorphous species is over 100x cheaper than 4A, but if active would also indicate what is happening to the catalyst in this reaction. The acid sites of aluminosilicate can catalyse pyrolysis intermediates which provide fewer oxygenated phenols and aromatic hydrocarbons. In this work, 50 wt% and 75 wt% (20 g and 30 g) of catalyst were prepared with 100 g of carrier oil to biomass and 20 g of neutraliser. The aluminosilicate produced approximately as much distillate oil as the 4A catalyst suggesting that the 4A catalyst was not retaining its structure (**Table 2.3-7**)

Table 2.3- 7–The distillate oil, bio-oil yield and bio-carbon content at different 4A zeolite loading at 100g carrier oil (N200)

Catalyst	Catalyst loading (wt%)	Distillate (g)	Distillate oil product (g)
Aluminosilicate	50 wt%	12	0.4
	75 wt%	12	0.2
4A zeolite	50 wt%	14.6	1.3
	75 wt%	10.75	0.2

2.3.2.5 ZSM-5 zeolite catalyst

ZSM-5 is a standard catalyst used in alternative fuel production processes, though to date has not been investigated in this reaction. ZSM-5 has been reported to produce more aromatic hydrocarbon compounds under suitable conditions. It shows to be an effective catalyst to crack the heavy aromatic compounds in to transport fuel range hydrocarbons, with increasing the desirable chemical species as well as decreasing the undesired molecules. The microporous nature of zeolite plays an important role in thermal cracking by adsorbing selective large chain molecules to produce liquid oil. To study the activity of ZSM-5, the experiments were carried out by using either 100 g of light carrier oil (N200 oil) or heavy carrier oils (LAN-150 oil). The experiments contained 20 g pistachio hull, ZSM-5 either 5 wt%, 10 wt% or 20 wt% compared to the biomass loading. These ratios were fixed based on recently published research [12].

Similar to 4A zeolite, there was no significant increase in the yield production as increasing catalyst loading in biomass. The highest bio-oil yield conversion was found at 1.16 g in the presence of light oil. The yield of liquid oil decreased slightly from 1.16 g for 2 g ZSM-5 added to 0.69 g for 5 g ZSM-5 added. A high concentration catalyst loading resulted in difficult downstream separations. The control reaction, without catalyst, was also successful in converting pistachio hulls to liquid oil products (distillate oil products of 0.89 g). This suggests that the biomass itself was converted into pyrolysis oil on cracking process.

A comparison between heavy and light carrier oil, the light oil was more suitable heat carrier oil due to its lower density which improved the increase of heat transfer and mass transfer during pyrolysis reaction.

Table 2.3- 8–The distillate oil, bio-oil yield at different ZSM-5 zeolite loading at 100 g carrier oil of N200 and LN-150

Carrier oil	ZSM-5 loading (wt%)	Distillate (g)	Distillate oil product (g)
Light carrier oil (N200)	0	4.2	0.9
	5	4.61	0.6
	10	6.23	1.2
	20	5.6	0.7
Heavy carrier oil (LN-500)	5	1.57	0.3
	10	2.4	0.3
	20	1.52	0.4

2.3.2.6 Carrier oil reuse

The use of fresh carrier oil for each reaction run is extremely uneconomic, recycling must be taken to create a more viable process. To study the effectiveness of the KDV reaction, the carrier oil from the reaction was extracted and added to fresh carrier oil to meet the total of 100 g oil usage with 20 g of biomass and 2 g of ZSM-5 **(Figure 2.3-6)**. The first reuse-carrier oil showed similar quantity of liquid product obtained with new oil respect to 65 g of carrier oil left in the reactor. On the second run of reuse-carrier oil, the yield oil had little difference with the 48 g left in the reactor. In contrast, liquid fuel was significantly decreased after the carrier oil was used on the third run. By the fourth reuse very little fuel was produced. This is potentially due to the increase in viscosity of the oil resulting in poor mass and heat transfer by this point.

However, as the oil yields are reasonably small through 1L reactor, there were several errors during the process as the short path distillation and lack of heat space in the reactor, so to continue development of the system, the reaction was scaled to a 5L reactor system, with a longer distillation path and higher efficiency.

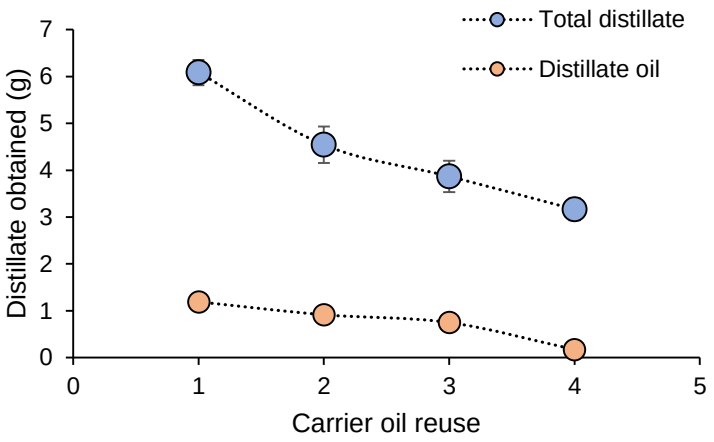

Figure 2.3- 6–Distillate production with corresponding carrier oil and solid depletion for carrier oil reuse reactions

2.3.3 Laboratory batch pyrolysis: 5L reactor

As the N200 light carrier oil added a lot to the distillate product, the heavier boiling point carrier oil was used (LAN-150) in all the testing at 5L to reduce the amount of carrier oil in the distillate product. The LAN-150 oil has a far smaller volatile fraction than the N-200 oil, and seemingly, was not easily cracked by the catalyst. This led to a greatly reduced amount of carrier oil derived product in the distillate. Though this increased the biogenic percentage in the fuel, no further increase in the total biogenic distillate fraction was observed. The yields of biogenic content in this reaction were similar to those produced from the catalyst-free slow pyrolysis of biomass. On using the LAN-150 carrier oil, the production volumes were too small on the 1L system for accurate measurement; as such further scale up to a 5L reactor was undertaken.

The reaction was scaled to 1000 ml of carrier oil (LAN-150) and up to 333 g of biomass in a 5L reactor with a longer pathway of the condensed system. As the 4A catalyst did not show suitable efficiency. The following experiments investigated the effect of ZSM-5 as an alternative catalyst. ZSM-5 was used at 33 g, 67 g, 167 g, 333 g, and 450 g with 333 g of biomass and 1,000 ml of carrier oil. The reaction was first performed at 90°C and held for 30 minutes to reduce the foaming reaction. After that, the process was slowly heated until the temperature reached 280 °C and the reaction was then maintained for 3 hours.

Similar, to the 1L reaction the effect of reaction temperature was the key factor in catalyst cracking activity of ZSM-5. The vapor was condensed from the system after around 115 °C which resulted from the initial moisture of biomass and dehydration reaction that occurred during the pyrolysis process. At a reaction temperature up to 280 °C, the liquid distillate was substantially increased. This suggests that high temperature increases the decomposition of the biomass as well as removing more carrier oil. However, the ZSM-5 zeolite action reduced substantially after holding reaction time at 280 °C for 45 minutes, this suggests that there is the formation of coke which deactivates the zeolite catalyst's shape selective-process.

The addition of catalyst did not appear to have significant benefit in terms of distillate oil production. The highest distillate oil, 19 g, was obtained for 167 g of ZSM-5 loading. The slight decrease was found in the addition of 333 g of ZSM-5 loading, with bio-oil decreased slightly from 19 g to 17 g. On the addition of 33 g ZSM-5 loading, the yield of liquid phase decreased from 180 ml to 87 ml and from 17 g to 10 g for total distillate product (**Figure 2.3-7**). In contrast, no distillate was observed for the catalyst loading at 450 g. The reaction was not completed due to the stop of heat transfer on the high catalyst loading.

The use of $Ca(OH)_2$ obtained higher total distillate yield conversion compared to non-$Ca(OH)_2$. However, the effect of $Ca(OH)_2$ did not affect the distillate oil production significantly which showed the similar result in the use of non-$Ca(OH)_2$. This is presumably due to the elevated moisture content of the neutraliser.

Although the liquid phase pyrolysis process in the 5L reactor was successful which was found to be more effective than the 1L reactor, the distillate oil yield was only approximately 6 wt./v%. The ZSM-5 was not as active as high potential catalyst for cracking in the slowing heating process at lower-temperature conditions.

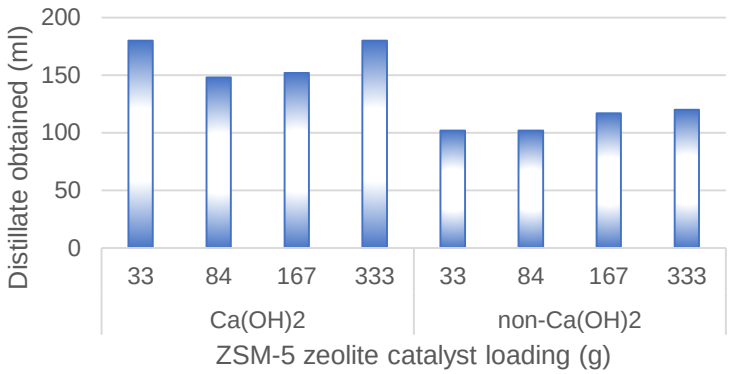

Figure 2.3- 7–The result of liquid distillate obtained from catalyst loading with $Ca(OH)_2$ and non-$Ca(OH)_2$

Table 2.3-9–The result of liquid oil distillate obtained from catalyst loading with $Ca(OH)_2$ and non-$Ca(OH)_2$

Carrier oil	ZSM-5 loading (g)	Distillate (g)	Distillate oil (g)
$Ca(OH)_2$	33	180	0.6
	84	148	17
	167	152	19
	333	180	15
Non-$Ca(OH)_2$	33	102	10
	84	102	12
	167	117	17
	333	120	15

Although the best result obtained on the KDV process on the pilot plant from pistachio hulls was in line with the company claims (120 kg/tonne) in a single step at reduced pressure and temperature without the need for hydrogen or additional chemical upgrade, the ^{14}C demonstrated that only 21% of product derived from biogenic material. This is equivalent to an approximate yield of 2.5% bio-oil. The distillate oil product, and biogenic component, was not improved through switching to the lab scale, a zeolite catalyst, or alternative carrier oil. Indeed, the results from the lab scale (1 L and 5L) slightly decreased from pilot plant and similar levels of biomass to non-catalytic CPD (7.0 wt% and 5.7 wt % for 1L and 5L respectively). This suggests that the heat carrier does not have significant effect on the biomass depolymerization. The

CPD reaction does not seem to successfully produce a distillate product with the 4A catalyst. The more stable system, using ZSM-5 zeolite produces substantially more yield, however, the presence of ZSM-5 is not appropriate to use in this process due to a high ability for cracking heat carrier oil.

2.3.4 Characterisation of bio-oil produced

2.3.4.1 CHN analysis

The elemental composition of bio-oil obtained from 4A and ZSM-5 loading are presented in **Figure 2.3-11a-2.3-11b**. Liquid phase pyrolysis of the additional catalyst had significant change from the pure pistachio hull feedstock resulting in a substantial carbon increase and oxygen decrease (carbon increasing from 41.2 wt.% to approximately 86 wt.% and oxygen decreasing from 46 wt.% to 0.7 wt.%). Hydrogen content increased which gave an increase from 7.0 wt.% to approximately 14 wt.%. This trend was observed for both 4A and ZSM-5 catalyst loading. This finding was similar to previous study of Gonzalez-Quiroga [1]. And is highly suggestive that the majority of the distillate is directly from the carrier oil.

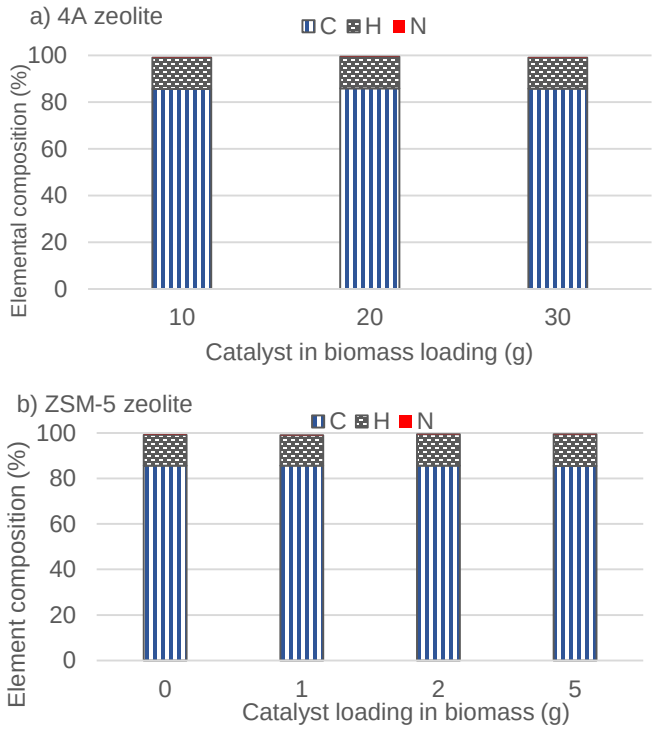

Figure 2.3- 8–The elemental composition of C, H, N with different catalysts loading in the presence of (a) 4A zeolite and (b) ZSM-5 catalyst.

2.3.4.2 Thermogravimetric analysis

To examine the proportion of biomass reached under KDV conditions, the KDV solid phase obtained from 1L and 5L reactor in the presence of ZSM-5 were analysed compared to pure pistachio through TGA. Overall, three regions are observed (**Figure 2.3-9**). The initial decomposition process was observed after sample temperature reached to 150°C with was related to extraction of moisture and waste in the pistachio hull biomass. The main decomposition process was depolymerisation, decarboxylation and cracking was found in the devolatilization temperature range from 200-430 °C. In this region, pistachio hull was considered to be three main components including hemicellulose, cellulose, and lignin. Hemicellulose and cellulose were composed in the temperature from 260°C °C and 350°C, respectively. Lignin was composed in the higher range of temperature than cellulose and hemicellulose at the temperature between 350°C and 650°C.

A degradation peak observed at around 570°C, the rate of degradation for pure pistachio hull is slightly higher than solid phase obtained from 1L and 5L reactor. For pure pistachio hull, almost no degradation is seen within 570°C which is different for the solid phase from KDV of 1L and 5L. The TGA profile of the solid phases from 5L become less marked at 570°C, suggesting that unreacted pistachio hull is present. For the 1L reactor, the TGA profile of the solid phases did not degrade within the temperature at 400 °C, however, the percent of mass reduction was lower than pure pistachio hull. This suggests that there is a quantity of unreacted pistachio hull remaining in the solid phase.

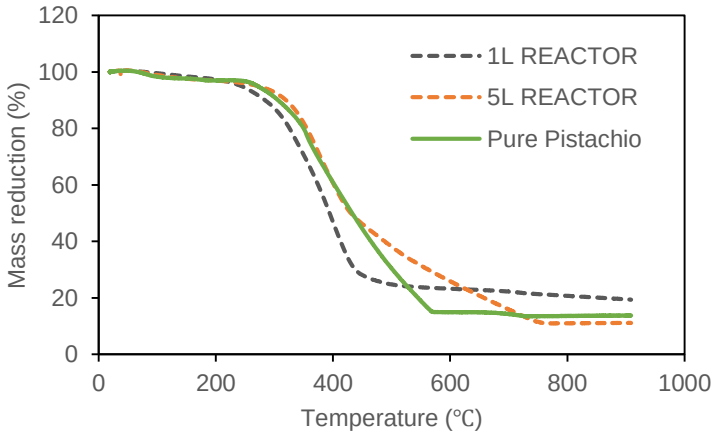

Figure 2.3- 9–TGA result of the solids left in the KDV reactions on 1L and 5L reactors

2.3.1.3 Gas chromatography-mass spectrometry (GC-MS)

The liquid oils obtained were yellow and had a low viscosity. To study the effect of the additional catalyst on bio-oil composition, the bio-oil obtained from pure pistachio, and pistachio with additional ZSM-5 (5 wt%, 10 wt%, and 25 wt% ZSM-5 loading) were characterised through gas chromatography-mass spectrometry (GC-MS). From the GC-analysis, bio-oil products contained mainly of aliphatic hydrocarbons and their derivatives including dodecane, tridecane, napthadecane, hexadecane and heptadecane. These compounds are expected to originate from the heat carrier oil. A slight increase in the benzene and alkane formation were observed in the presence of ZSM-5 catalyst, however, no increase in the abundance of phenolic compound which is the main composition originate from lignin, and major components of pistachio hulls. This suggest that ZSM-5 enhanced the activity and efficacy for aromatic and acyclic cracking but ZSM-5 did not affect the capacity of biomass cracking [13]. A summary of the most abundant compounds in the liquid oil produced, identified using GC-MS, is present in **Table A-1.**

2.4 Conclusion

It has been claimed, with little peer reviewed literature studies, that biomass can be processed in a liquid heat carrier phase that provides adequate heat ability and high heat conductivity, at low temperature (300 °C) producing a diesel like fuel.

However, an accurate mass balance on a pilot scale process as well as mimicking the process in the lab, demonstrated that the majority of the distillate is either the low boiling fraction of the carrier oil or the cracked species of this. The maximum distillate obtained when using a heavier carrier oil was relatively low (approximately 6.5v/w%) with less than half of the pistachio hull used. The liquid product contained not only pyrolysis oil but also 30-50 wt.% water. Catalyst was deactivated completely after the first use which prevented the possibility of reuse. The bio-content as determined through ^{14}C analysis was remarkably low for all reaction conditions, demonstrating that the majority of the product came from the carrier oil.

Based on these findings, there is no evidence on the lab or pilot scale that this is a suitable method for the production of hydrocarbons. The seemingly high yields of fuels in other sites seem to be predominantly due to the cracking and distillation of the fossil carrier oil. Further scaling up of the process is not recommended. In fact, the efficiency

of the biomass conversion by KDV process was less than conventional slow pyrolysis or LPP. Therefore, it can be concluded that the KDV process is not an appropriate conversion pathway when the liquid-oil is the target product, for either biomass or plastics.

2.5 Reference

[1] A. Gonzalez-Quiroga, M.R. Djokic, K.M. Van Geem, G.B. Marin, Conversion of Solid Waste to Diesel via Catalytic Pressureless Depolymerization: Pilot Scale Production and Detailed Compositional Characterization, Energy & Fuels, 30 (2016) 8292-8303.
[2] G. Labeckas, S. Slavinskas, Performance and emission characteristics of a direct injection diesel engine operating on KDV synthetic diesel fuel, Energy Conversion and Management, 66 (2013) 173-188.
[3] D. Howe, T. Westover, D. Carpenter, D. Santosa, R. Emerson, S. Deutch, A. Starace, I. Kutnyakov, C. Lukins, Field-to-Fuel Performance Testing of Lignocellulosic Feedstocks: An Integrated Study of the Fast Pyrolysis–Hydrotreating Pathway, Energy & Fuels, 29 (2015) 3188-3197.
[4] N. Schwaiger, R. Feiner, K. Zahel, A. Pieber, V. Witek, P. Pucher, E. Ahn, P. Wilhelm, B. Chernev, H. Schröttner, M. Siebenhofer, Liquid and Solid Products from Liquid-Phase Pyrolysis of Softwood, BioEnergy Research, 4 (2011) 294-302.
[5] K. Treusch, A. Huber, S. Reiter, M. Lukasch, B. Hammerschlag, J. Außerleitner, D. Painer, P. Pucher, M. Siebenhofer, N. Schwaiger, Refinery integration of lignocellulose for automotive fuel production via the bioCRACK process and two-step co-hydrotreating of liquid phase pyrolysis oil and heavy gas oil, Reaction Chemistry & Engineering, 5 (2020) 519-530.
[6] A. Al Rousan, A. Zyadin, S. Azzam, M. Hiary, Prospects of Synthetic Biodiesel Production from Various Bio-Wastes in Jordan, Journal of Sustainable Bioenergy Systems, 03 (2013) 217-223.
[7] T.L. Chew, S. Bhatia, Catalytic processes towards the production of biofuels in a palm oil and oil palm biomass-based biorefinery, Bioresource Technology, 99 (2008) 7911-7922.
[8] Alphakat.de, ALPHAKAT, onlineAvailable at http://alphakat.de/temp/index.php.
[9] S. Nanda, J. Mohammad, S.N. Reddy, J.A. Kozinski, A.K. Dalai, Pathways of lignocellulosic biomass conversion to renewable fuels, Biomass Conversion and Biorefinery, 4 (2014) 157-191.
[10] K. Açıkalın, F. Karaca, E. Bolat, Pyrolysis of pistachio shell: Effects of pyrolysis conditions and analysis of products, Fuel, 95 (2012) 169-177.
[11] P.M. Eletskii, O.O. Mironenko, G. Sosnin, O. Bulavchenko, O. Stonkus, V. Yakovlev, P. Yeletsky, Investigating the process of heavy crude oil steam cracking in the presence of dispersed catalysts. II: Investigating the effect of Ni-containing catalyst concentration on the yield and properties of products, Catalysis in Industry, 8 (2016) 328-335.
[12] M. Rehan, R. Miandad, M.A. Barakat, I.M.I. Ismail, T. Almeelbi, J. Gardy, A. Hassanpour, M.Z. Khan, A. Demirbas, A.S. Nizami, Effect of zeolite catalysts on pyrolysis liquid oil, International Biodeterioration & Biodegradation, 119 (2017) 162-175.
[13] H. Konno, T. Tago, Y. Nakasaka, R. Ohnaka, J.-i. Nishimura, T. Masuda, Effectiveness of nano-scale ZSM-5 zeolite and its deactivation mechanism on catalytic cracking of representative hydrocarbons of naphtha, Microporous and Mesoporous Materials, 175 (2013) 25-33.

2.6 Appendix

Table A- 1–Retention data and identified pyrolysis oil product from pistachio hull at the present of ZSM-5 catalyst and non-catalytic ZSM-5

Compound identified	Relative abundance			
	Non-catalytic	ZSM-5 (5 wt%)	ZSM-5 (10 wt%)	ZSM-5 (25 wt%)
Decane	82145	51204	69618	86715
Benzene, 2-ethyl-1,4-dimethyl-	34786		31218	
D-Limonene	45199	27957	40436	34605
Decane, 2-methyl-	36833	22238	29694	
Benzene, 1-methyl-4-(1-methylethenyl)-	53696		46715	61850
Benzene, (2-methyl-1-propenyl)-		38598		52817
Undecane	78141	50061	62847	42212
Benzene, 1,2,3,4-tetramethyl-	27536			
Benzene, 1-ethenyl-4-ethyl-	51983			
Benzene, 1-ethyl-2,3-dimethyl-		19711		
Heptadecane, 8-methyl-	35255			
Heptadecane, 2,6,10,15-tetramethyl-				41229
1H-Indene, 2,3-dihydro-4-methyl-		28020	39970	
1H-Indene, 2,3-dihydro-1,1,3-trimethyl-				61255
1H-Indene, 2,3-dihydro-1,6-dimethyl-				69389
2-Ethyl-1-dodecanol				46033
Methoxyacetic acid, 2-tetradecyl ester		21487		

Compound identified	Relative abundance			
	Non-catalytic	ZSM-5 (5 wt%)	ZSM-5 (10 wt%)	ZSM-5 (25 wt%)
Naphthalene, 1,2,3,4-tetrahydro-	93423	58295	77235	98912
1-Heptacosanol	48390			
Benzene, (3-methyl-2-butenyl)-	34786			
2,2-Dimethylindene, 2,3-dihydro-		19840		
Dodecane	238384	142634	191219	243496
Sulfurous acid, butyl undecyl ester				30556
1-Hexanol, 5-methyl-2-(1-methylethyl)-	37414			
Nonadecane, 9-methyl-			46023	59639
Dodecane, 3-methyl-			25152	
Benzene, (2-methyl-1-butenyl)-		25072	33978	
Benzene, (3-methyl-2-butenyl)-	36705			
Undecane, 2,6-dimethyl-	38132			42212
Naphthalene, 1,2,3,4-tetrahydro-1-methyl-	58806		44703	61569
Cyclohexane, (4-methylpentyl)-	45833			
Nonane, 5-butyl-	56423			
1H-Indene, 2,3-dihydro-5,6-dimethyl-	41779	21164		
Pentadecane, 2,6,10-trimethyl-		24921		
10-Methylnonadecane	60504			
10-Methylnonadecane	31322			
Benzene, 1-methyl-3-(1-methyl-2-propenyl)-		34795	29935	
Benzene, (3-methyl-2-butenyl)-	39137	22131		

Compound identified	Relative abundance			
	Non-catalytic	ZSM-5 (5 wt%)	ZSM-5 (10 wt%)	ZSM-5 (25 wt%)
Naphthalene, 1,2,3,4-tetrahydro-5-methyl-	54376			80861
1H-Indene, 2,3-dihydro-4,7-dimethyl-	32510	23849	1058193	71858
1H-Indene, 2,3-dihydro-5,6-dimethyl-		25088		
Tridecane	159561	92488	129187	152333
Naphthalene, 1,2,3,4-tetrahydro-6-methyl-	85476	88468	46756	
Naphthalene, 1,2,3,4-tetrahydro-1,4-dimethyl-	116027	71318	69331	112898
Naphthalene, 6-ethyl-1,2,3,4-tetrahydro-		306016		42808
Heptylcyclohexane	52998	29988	42397	52529
Phenol, 2-(1,1-dimethylethyl)-4-methyl-				40164
1-Octadecanesulphonyl chloride	41472		33542	
Octacosane	49206			
Dodecane			191219	
Undecane, 2,6-dimethyl-			34107	
Dodecane, 2,6,10-trimethyl-	37376	22235		30815
Cyclohexane, hexyl-			39820	50358
Cyclohexane, (2-methylpropyl)-		25600		
Cyclohexane, (1,3-dimethylbutyl)-				61057
Cyclohexane, 1,1'-methylenebis-	39887	31645		33194
Isobutyl nonyl carbonate				57078
Tetradecane	207046	124090	172859	186044

Compound identified	Relative abundance			
	Non-catalytic	ZSM-5 (5 wt%)	ZSM-5 (10 wt%)	ZSM-5 (25 wt%)
Naphthalene, 1,2,3,4-tetrahydro-1,4-dimethyl-	66909			
Naphthalene, 1,2,3,4-tetrahydro-5,6-dimethyl-		40199		56524
Benzimidazole, 2-ethyl-1-propyl-		24600		
Benzene, 1,3,5-trimethyl-2-(1-methylethenyl)-			30710	
Benzene, 1-(2-butenyl)-2,3-dimethyl-			53800	
Benzene, (2-methyl-1-butenyl)-				39112
Benzene, 2-ethenyl-1,3,5-trimethyl-				32421
Nonahexacontanoic acid		36269		
1-Decanol, 2-hexyl-	52642		27465	
Naphthalene, 1,2,3,4-tetrahydro-1,6,8-trimethyl-	60704	36509		
Oxalic acid, 6-ethyloct-3-yl ethyl ester		46738		
Tetratetracontane		32743		39655
Oxalic acid, cyclobutyl pentadecyl ester	59246			
1-Decanol, 2-octyl-	27011			
Pentadecane	167736	104557	149648	140476
Octadecane, 1-chloro-	36823	34126	30355	94768
Hexadecane	204691	138724	192983	167826
Hentriacontane	51373		48571	
Cyclohexane, 1,1'-(1,3-propanediyl)bis-	29121			
Heptadecane	153987	109416	142939	124713
Hexadecane, 2,6,11,15-tetramethyl-		44703		48321

Compound identified	Relative abundance			
	Non-catalytic	ZSM-5 (5 wt%)	ZSM-5 (10 wt%)	ZSM-5 (25 wt%)
Dodecane, 2,6,10-trimethyl-	56254			
Octadecane	107694	84685	112769	108928
Dodecane, 2,6,10-trimethyl-	52907	39019	30301	

Chapter 3

Co-processing of common plastics with pistachio hulls via hydrothermal liquefaction

3.1 Context

The previous chapter examined the effectiveness of producing bio-fuel oil from pistachio hulls via the KVD process. However, the maximum distillate obtained when using a heavier carrier oil was relatively low (approximately 6.5v/w%) with less than half of the pistachio hull processed. The bio-content as determined through ^{14}C analysis was remarkably low for all reaction conditions, demonstrating that the majority of the product came from the carrier oil. These findings therefore indicate the unsuitability of the KDV one-step process for fuel production.

However, an alternative promising liquefaction technology is Hydrothermal Liquefaction (HTL). This thermochemical process can convert organic solid wastes into valuable products at relatively low temperatures, albeit using high-pressure water. This leads to the possibility of being able to co-process plastics with biomass. Over the last decade, extensive research on HTL has been successful in converting algae biomass feedstock into biofuel products. However, research on HTL has been limited in studying co-liquefaction of lignocellulosic biomass and indeed plastics.

Therefore the following study, presented in full in this chapter, aimed to explore pistachio hulls as a feedstock in the HTL process and determine whether the co-liquefaction of the feedstock with a range of plastics is viable. Polyethylene, polypropylene, polyethylene terephthalate, and nylon were used as the plastic pollutants. The plastic conversion in the system was estimated through a novel FT-IR method, and the product phases were fully analysed.

This work was published in Waste management in November 2019. **Sukanya Hongthong**, Sonia Raikova, Hannah Leese, Christopher J. Chuck*. Co-processing of common plastics with pistachio hulls via hydrothermal liquefaction, Waste management (New York, N.Y.), 102 (2019) 351-361.

This chapter is submitted in an alternative format in line with Appendix 6A of the “Specifications for Higher Degree Theses and Portfolios” as required by the University of Bath.

The work completed in this paper was conducted by the author with the exception of the elemental analysis was carried out by analytical department personnel at London Metropolitan University.

3.2 Waste management paper

Co-processing of common plastics with pistachio hulls via hydrothermal liquefaction

Sukanya Hongthong, Sonia Raikova, Hannah Leese, Christopher J. Chuck*.

Department of Chemical Engineering, University of Bath, Claverton down, Bath, BA2 7AY, United Kingdom.

3.2.1 Keywords

HTL

Plastic Biorefinery

Polymer

Biofuel

3.2.2 Abbreviations

ER	-	Energy recovery
HHV	-	Higher heating value
HTL	-	Hydrothermal liquefaction

3.3.3 Highlights

- HTL was used to co-process 4 common plastics with pistachio hulls.
- Over 35% bio-crude yields were obtained.
- PET is mainly broken down into aqueous phase products.
- Nylon-6 breakdown almost entirely to source monomer
- PE and PP remain largely throughout the process

3.2.3 Abstract

Mixed, wet, plastic streams containing food waste residues are being increasingly collected at point of use, but are extremely challenging to recycle and are therefore largely sent to landfill. While a challenging waste problem, this also represents an underutilised feedstock, which could be co-processed with biomass, increasing the scope of products, easing out seasonal variation in biomass production and increasing the production capacity of a traditional biorefinery. One promising method of biomass

conversion is hydrothermal liquefaction (HTL), where lignocellulosic residues are broken down in water at high temperatures and pressures to produce a bio-crude oil, a solid residue and an aqueous fertiliser. In this study, the co-processing of common plastic waste with pistachio hulls was assessed to investigate the suitability of the HTL approach. The HTL of pistachio hulls was undertaken at 350 °C over 15 and 60 minutes, with four commonly used plastics: polyethylene, polypropylene, PET and nylon-6, in blends of up to 20 wt.% plastic to biomass. A novel FT-IR method was developed to estimate the conversion of plastics in the system, and the product phases were fully analysed. High yields of up to 35% bio-crude were achieved, and under optimal conditions, nylon-6 and PET were found to break down almost completely in the system. PET generated numerous products that distributed predominantly into the aqueous phase; the major decomposition product of nylon-6 was found to be the monomer ϵ-caprolactam, also largely partitioning into the aqueous phase. The polyolefins were less reactive; a limited degree of decomposition formed oxidised products, which distributed into the bio-crude phase. This result represents a highly promising method for waste plastic valorisation.

3.2.4 Introduction

Agricultural residues can be thermally processed through a variety of methods to produce bio-oils or bio-crudes that can be upgraded to chemicals and drop-in biofuels, or even combined in a traditional refinery (Elliott et al., 2015). For wet biomass, hydrothermal liquefaction (HTL) has been reported to be an economically viable route, which gives high biomass conversion yields and produce bio-crudes with favourable higher heating values (30–39 MJ kg^{-1}), lower oxygen contents (10–20 wt%), and a controllable water content (0–5 wt%) (Peterson et al., 2008). HTL avoids the need for drying the biomass, and instead uses pressurised vessels to keep water in the liquid phase; the pressure (10–25 MPa) is generated at moderate temperatures (290–350 °C) (Akhtar and Amin, 2011; Arturi et al., 2016; Bi et al., 2017; Demirbaş, 2001; Nazari et al., 2015; Tekin et al., 2014). At subcritical conditions, water behaves simultaneously as a solvent, reactant and catalyst for a number of biomass decomposition and repolymerization reactions. This results in a liquid bio-crude product, as an aqueous phase, a solid residue fraction, and a gaseous fraction.

Although the bulk of the early research on HTL has focused on microalgae (Biller et al., 2015), HTL of lignocellulosic materials is a promising alternative, especially if waste

agricultural resources are used. To date, a number of studies have focused on HTL of lignocellulosic biomass. Typical bio-crude products from the HTL of lignocellulose includes aliphatic compounds, aromatics and phenolic derivatives, carboxylic acids, esters, and some nitrogenous compounds depending on the original protein level of the feedstock (Costanzo et al., 2016; Pedersen et al., 2016; Xiu et al., 2010). Hydrothermal liquefaction of lignocellulosic biomass is a well-known process and in depth modelling demonstrates significant energy and GHG savings in biofuel production when compared with fast pyrolysis routes (Tews et al., 2014).

Pistachio processing waste is a lignocellulosic material with considerable potential for use as a biofuel feedstock (Taghizadeh-Alisaraei et al., 2017). A number of studies investigating the pyrolysis of pistachio waste have been published to date. Yields of between 20–33% bio-oil have been reported (Demiral et al., 2008) (Apaydin-Varol et al., 2007) (Pütün et al., 2007). Açıkalın et al. achieved a yield of over 50%, in a well-swept fixed bed reactor, though the bio-oil did have a comparatively low energy content of 19.5 MJ kg^{-1} (Açıkalın et al., 2012). To date, there have been no examples of liquefaction of this feedstock.

Processing of lignocellulosic wastes to biofuels is a promising step towards decreasing the environmental impacts of fuel production, but process sustainability can be further enhanced through the integration of bio-crude production with waste management, such as the co-liquefaction of biomass with plastic waste streams. The increasing volumes of plastic waste produced globally pose a significant threat to the environment and human health. In 2016, global plastic production reached 335 million tonnes (Association of Plastic Manufacturers Europe, 2017): a dramatic increase compared to 230 million tonnes produced in 2005 (Association of Plastic Manufacturers Europe, 2016). According to the World Bank, plastic waste accounts for 8–12% of total global municipal solid waste (MSW), estimated to increase to 9–13% of the MSW by 2025 (Bhada-Tata, March 2012). Although plastic waste in the UK is partially managed through recycling, vast quantities of plastics continue to accumulate in landfill (Wong et al., 2015) due to their extremely slow degradation rates (Bezergianni et al., 2017) (Demirbas et al., 2016). The most abundant elements in plastic wastes are carbon and hydrogen, and plastics typically have high H/C ratios (Karaca and Bolat, 2000) (Shui et al., 2011) (Shui et al., 2013) (Jongwon Kim, 1999), and correspondingly high energy

contents. Therefore, the conversion of waste plastics to fuel could be an elegant solution to both the issue of plastic waste and sustainable energy production.

In recent years, a number of studies on co-pyrolysis and co-liquefaction of biomass and plastics have been published (Uzoejinwa et al., 2018) (Wu et al., 2017). Thermochemical co-processing is possible, because there is an overlap between the temperature ranges of thermal decomposition for biomass and plastics (Jakab et al., 2000). It has been suggested that plastics, such as polyethylene (PE) or polypropylene (PP) can act as a source of hydrogen for biomass liquefaction to increase bio-crude yields and improve its fuel properties (Bhattacharya et al., 2009) (Cao et al., 2019; Fekhar et al., 2018) (Cao et al., 2019) However, to date, few reports have elaborated on the mechanisms of the interaction. Wu et al. reported the co-hydrothermal liquefaction of the microalga *Dunaliella tertiolecta* with polypropylene (Wu et al., 2017). Synergistic effects were observed for oil production, and the addition of PP led to improvements in the bio-oil quality, decreasing bio-crude acid content. Another study by Sørum et al. also demonstrated synergistic effects between PVC and pine wood sawdust during co-pyrolysis (Sørum et al., 2001). Seemingly, HCl released from the PVC under pyrolytic conditions behaved as an acid catalyst to promote dehydration of the biomass. However, under the same conditions, PE and PP did not have a substantial impact on pine wood sawdust pyrolysis. Wang et al. observed that co-liquefaction of Jingou lignite, wheat straw and plastic waste in sub-critical water gave optimal oil yields at a ratio of 5:4:1 (respectively), (Wang et al., 2014). Interestingly, they also found that the addition of tourmaline gave better oil yields and higher oil quality than when using conventional catalysts.

In this study, the co-liquefaction of pistachio hulls was undertaken for the first time and co-processed with several common plastics. Furthermore, the study aimed to elucidate the effect of plastic co-liquefaction of pistachio hulls on product distribution, yields, and product chemical compositions. PE, PET, PP, and nylon-6, and mixtures of the above, were used in this study.

3.2.5 Materials and methods

3.2.5.1 Materials

Pistachio hull was selected as a biomass feedstock representative of mixed food waste, and blended in varying ratios with polyethylene (PE), polyethylene terephthalate (PET), polypropylene (PP) and nylon-6 (hereafter referred to as “nylon”). Pistachio hull biomass (2–5 mm particle size) was obtained as a waste material after pistachio processing from the Wonderful Company (USA). PE, PET, PP and nylon were obtained from Sigma-Aldrich and ground using a commercial food blender to a particle size of <350 μm prior to use. Ultimate analysis was conducted following ASTM D5291 to determine carbon, hydrogen and oxygen. The high heating value of dry pistachio hull was 17.46 (MJ kg^{-1}) which was measured following ASTM E711. The biomass composition is given in the supporting information.

3.2.5.2 Hydrothermal liquefaction of co-liquefaction of pistachio hull

Co-hydrothermal liquefaction of pistachio hulls with plastics was carried out in a 50 mL stainless steel batch reactor. The reactor was equipped with a pressure gauge and pressure relief valve, and a needle valve to release gaseous products. The temperature was monitored using a thermocouple connected to data logging software. In a typical experiment, the reactor was loaded with a total of 3 g material (pistachio hull blended with PE, PP, PET, nylon, or a mix of the four plastics). Biomass: plastic weight ratios examined were 100:0, 90:10 and 80:20. The 90:10 ratio experiments contained 2.7 g of biomass and 0.3 g of either PE, PP, PET or nylon. For the 80:20 weight ratio, the experiments contained 2.4 g of biomass and 0.6 g of either PE, PP, PET, or nylon. The feedstock was mixed with 15 g of distilled water to form a slurry. The reactor was sealed and loaded into a preheated furnace to either 500°C or 700°C. The reactor was held in the furnace until the temperature reached 350 °C, 60 and 15 min, respectively. Upon reaching the desired temperature, the reactor was removed from the furnace and allowed to cool to room temperature. Each experiment was repeated three times to determine experimental error.

3.2.5.3 Separation of liquefied product

After cooling, gaseous products were released via the needle valve into an inverted, water-filled measuring cylinder to measure total gas volume. Gas phase yield was calculated from volume using the ideal gas law. The reactor contents were filtered

through a filter paper to separate the aqueous phase from the water-insoluble fraction (consisting of the bio-crude and bio-char). The solid-liquid mixture remaining on the filter paper was washed repeatedly with chloroform until the solvent ran clear. The chloroform was removed using a rotary evaporator at 35 °C for 2 hours to isolate the bio-crude. The solids were oven-dried overnight at 60°C to determine the solid phase product yield. An aliquot of the aqueous phase products was dried overnight at 60°C to determine the yield of non-volatile organics and inorganics in the aqueous phase, designated as “aqueous phase residue”.

3.2.5.4 Yield of product

The yields of each product phase were calculated as mass percentage on a dry basis. Bio-crude was calculated from mass left after remove residual solvent via rotary evaporation. Bio-crude yield was determined using the following equation:

$$yield_{bio-crude} = \frac{mass\ bio-crude\ (g)}{mass\ dry\ biomass\ (g) + mass\ plastic(g)} \times 100 \quad (1)$$

The char yield was calculated from the collected char mass on the filter paper after letting it dry in an oven at 60℃. Solid yield was determined using the following equation:

$$yields_{solid} = \frac{mass\ solid\ phase\ (g)}{mass\ dry\ biomass\ (g) + mass\ plastic\ (g)} \times 100 \quad (2)$$

Gas volume was calculated according to literature precedent, by using the ideal gas law and assuming that the gas was completely CO_2 (Raikova et al., 2016).

$$yield_{gas} = \frac{(gas\ volume \times 1.789 \times 10^{-3})}{mass\ dry\ biomass\ (g) + mass\ plastic\ (g)} \times 100 \quad (3)$$

The solid yield in the aqueous phase was calculated by taking a 2.0 g aliquot of the phase and drying at 60 ℃. Aqueous phase residue yield was determined using the following equation:

$$yield_{aqueous\ residue} = \frac{mass\ of\ aqueous\ residue(g)}{mass\ dry\ biomass\ (g) + mass\ plastic\ (g)} \times 100 \quad (4)$$

The overall mass balance of the reaction was calculated as follows:

$$mass\ balance\ (\%) = solid\ (\%) + bio\text{-}crude\ (\%) + aqueous\ residue\ (\%) + gas\ (\%) \quad (5)$$

3.2.5.5 Characterisation of HTL products

The chemical composition of the volatile fraction of the bio-crude was investigated using an Agilent Technologies 7890A GC system fitted with a 30 m × 250 µm × 0.25 µm HP5-MS column, coupled to a 5975C inert MSD. Samples were dissolved in THF, and helium (1.2 mL min^{-1}) was used as the carrier gas. Initial oven temperature was set to 50°C, increasing to 250 °C at 10 °C min^{-1}. Initial identification of compounds was performed using the NIST mass spectral database.

Solid phase products were analysed using FTIR. Spectra were recorded on a Thermo Scientific Nicolet iS5 FTIR spectrometer in the wavenumber range between 4000–600 cm^{-1}. FTIR was used to assess the level of unreacted plastic remaining in the solid phase products as a proxy for the extent of plastic conversion. Calibration curves were developed by mixing known amounts of bio-char from the HTL of pure pistachio biomass with known amounts of plastics and grinding finely in a mortar and pestle to ensure a homogeneous blend. The blended samples were analysed by FTIR, and two characteristic absorbance's were selected for each plastic/biomass combination, one unique to the plastic, and another unique to the biomass component. The ratio of the two absorbance's was calculated as described in the study of Lao and Li (Lao and li, 2014), and used to create a calibration curve, against which the samples of bio-char produced experimentally were assessed. Each bio-char sample was analysed in triplicate; average values of absorbance ratio were used to calculate conversion. Further information is given in the supporting information.

3.2.5.6 Elemental analysis, carbon and energy recoveries

Elemental analysis (carbon, hydrogen and nitrogen content) of the biomass feedstock and products was carried out externally at London Metropolitan University on a Carlo Erba Flash 2000 Elemental Analyser. Oxygen content was determined by difference, assuming negligible sulphur in the products.

$$O\ (wt\%) = 100 - C - H - N\ (wt\%) \quad (6)$$

The higher heating values (HHV) of the biomass, bio-char and bio-crude were calculated using the Dulong formula, where C, H, and N are the weight percentages of each element:

$$HHV\ (MJ\ kg^{-1}) = 0.3383C + 1.422\left(H - \left(\frac{O}{8}\right)\right) \quad (7)$$

Energy recovery in each product phase was calculated as follows:

$$Enery\ recovery\ (\%) = \frac{HHV\ product\ (\%) \times Mass\ of\ product\ (\%)}{HHV\ of\ feedstock\ (\%)} \quad (8)$$

3.2.6 Results and Discussion

3.2.6.1 Effect of waste plastic contents on bio-crude yields and mass balance

Initially, the influence of the ratio between pistachio hull waste and plastic in the HTL feedstock on the distribution of product phases was investigated. HTL was carried out at 350 °C for 15 minutes, based on previously reported optimal conditions (Raikova et al., 2019). Mass balances are shown in Figure 3.2-1a where product yields were calculated on the basis of total feedstock (biomass and plastic) input.

In general, co-liquefaction with plastics resulted in an increase in overall bio-char yields relative to the HTL of pistachio hulls alone. The most significant impact was observed for co-liquefaction with PE, with a substantial increase in bio-char production from 22.1% to 35.6 % at a 10 wt.% blend, and from 22.1% to 40.7 % at a 20 wt.% blend. On the addition of PE, the yield of gas phase product increased slightly from 15.9 % for pure pistachio to 17.8 % for a 10 wt.% PE blend, but decreased slightly for a 20 wt.% PE blend to 15.1 %. Blending feedstocks with polyethylene was found to deplete bio-crude yields substantially, with yields decreasing from 34.1 % to 20.4 % for a 10 wt.% PE blend, but increasing somewhat to 26.8 % for 20 wt.% PE. The aqueous phase residue yield was not significantly impacted by co-liquefaction with PE and only a slight yield increase of 1.0–1.5 % was observed for 10 wt.% and 20 wt.% PE blends respectively.

For PP, higher yields of bio-crude were obtained for the 10 wt.% PP blend, whereas slight decreases were seen for the 20 wt.% PP blend (bio-crude yields of 36.3 % and 30.7 % respectively). The addition of PP also had a significant effect on bio-char production – bio-char yield increased from 22.1% to 30.1 % for the 10 wt.% PP blend, and rose further to 40.3 % for the 20 wt.% PP blend. The gas phase product yields obtained from both the 10 wt.% and 20 wt.% PP blends were similar to those obtained for HTL of pure pistachio. Co-liquefaction with PP contributed to a modest increase in aqueous phase residue production – (from 8.3% to 10 % for 10 wt.% PP loading and up to 9.6 % for the 20 wt.% PP loading). The majority of the PE and PP were recovered in the solid phase products.

For PET, the gas phase products were not strongly impacted by co-liquefaction, with 16.2 % gas phase produced at 10 wt.% PET, although this dropped to 13.2 % for the 20 wt.% PET blend. Bio-crude yields obtained on PET co-liquefaction showed a slight increase compared to HTL of pure pistachio (bio-crude increased by 0.6 % for the 10 wt.% PET blend to 34.6%, and remained almost unchanged for the 20 wt.% blend). In addition, PET was found to increase bio-char production to 24.2 % and 37.8 % for the 10 wt.% and 20 wt.% PET blend. As for PE and PP, aqueous phase residue obtained from PET blend was again not strongly affected, with a slight increase of 1.7 % and 1 % observed for the 10 wt.% and 20 wt.% PET blend.

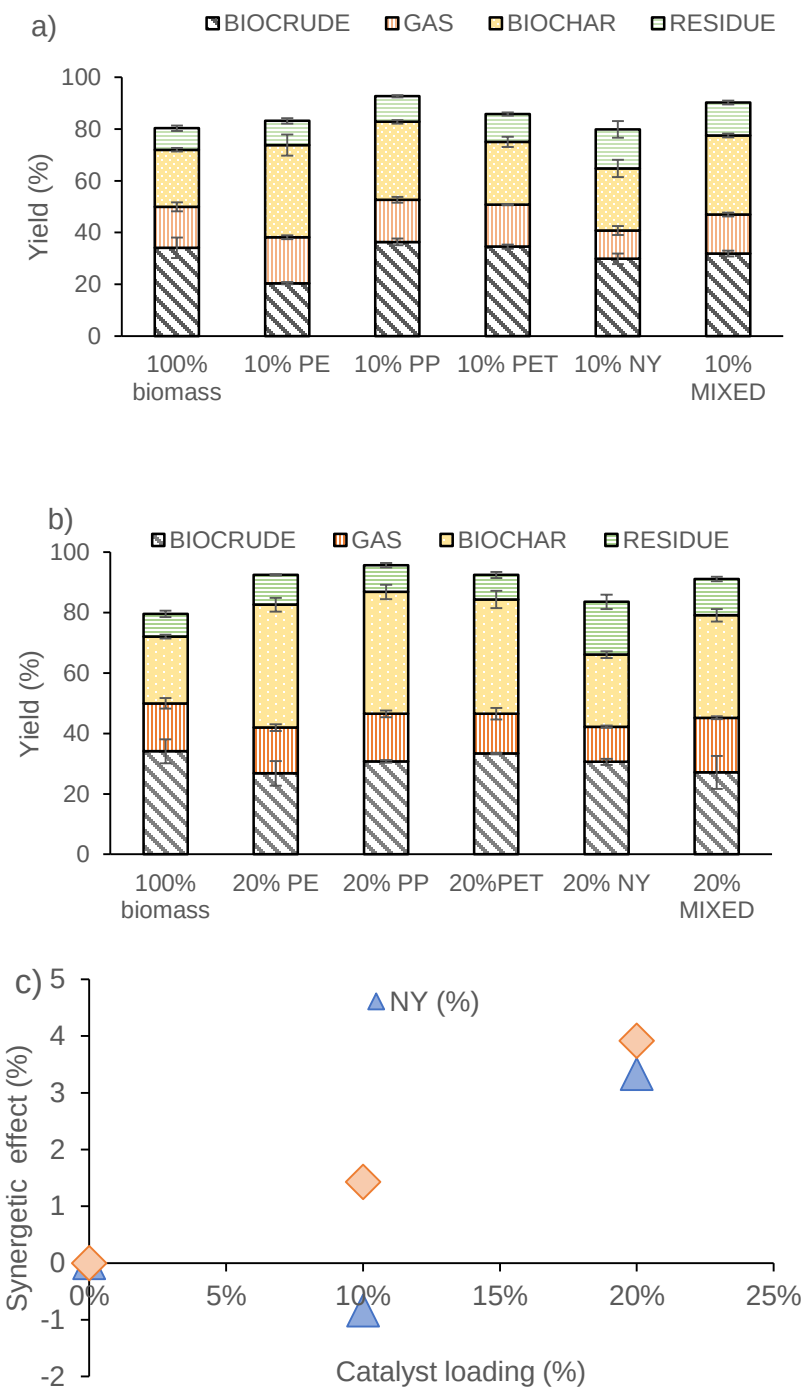

Figure 3.2- 1– a) Mass balance of HTL product from liquefaction of pistachio hull with PE, PP, PET, NY, and plastic mixture at (a) 10 wt.%, and (b) 20 wt.% of plastic blend loading. b) Synergistic effect on bio-crude yields from co-liquefaction of pistachio hull/PET and pistachio/Nylon blends (PET = polyethylene terephthalate, NY = Nylon)

In contrast with the other plastics, the increase in bio-char production was much smaller for the co-liquefaction of pistachio hull with nylon (24.1 % and 23.8 % bio-char for 10 wt.% and 20 wt.% NY, compared to 22.1 % for the liquefaction of pure pistachio hull). Bio-crude yields obtained for the nylon blends were 30.0 % for the 10 wt.% NY blend, whilst the 20 wt.% NY blend gave a similar yield of 30.1 %. Gas phase product yields decreased from 15.9 % for pure pistachio hull to 11.0 % at the 10 wt.% NY blend level and 11.6 % for the 20 wt.% NY blend. Residue from the aqueous phase increased substantially from 8.3 % for pure pistachio hull HTL to 15.1 % and 17.5 % for 10 wt.% and 20 wt.% nylon blends, respectively.

Co-liquefaction of pistachio hull with a mix of the plastics in equal proportions increased bio-char production substantially to 30.6 % and 33.9 %, respectively, for 10 wt.% and 20 wt.% blends, whilst bio-crude yields decreased to 31.9 % for the 10wt% plastic loading, and subsequently to 27.1 % for the 20wt% loading. Gas yields were not strongly affected. Aqueous phase residue yields obtained from HTL of pistachio hulls with the plastic mix showed a slight increase compared to pure pistachio hulls, rising from 8.3 % to 12.6 % and 13.3 % for 10 wt.% and 20 wt.% blends, respectively.

Co-processing with plastics does not appear to have a significant benefit in terms of bio-crude oil production from pistachio hull. Bio-crude oil yields obtained from co-liquefaction at 10 wt.% and 20 wt.% plastic blends were similar to those produced from pistachio hull waste alone for PP, PET and nylon, and depleted significantly for PE. With PET and NY there is a potential interaction between the biomass and the plastics where the biomass could synergistically aid the breakdown of plastic. The synergistic effect of the interaction between biomass and plastics can be determined by the equation 9 below:

$$Synergistic\ effect = Ybiocrude - (Xpistachio\ \times Ypistachio + (1 - Xplastic) \times Yplastic) \quad (9)$$

where, $Y_{biocrude}$ is the yield of bio-crude obtained in experiment, $X_{pistachio}$ and $X_{plastic}$ are the mass fraction of pistachio and plastics in the total reaction mixture, $Y_{pistachio}$ is the bio-crude yield of pure pistachio, and $Y_{plastic}$ is the bio-crude yield of pure plastic.

As PE and PP do not react under these conditions without biomass present, the synergistic effect was only calculated for the co-liquefaction of PET/biomass and nylon/biomass blends. Overall the presence of biomass enhances the conversion of the plastic in the liquefaction process, and a positive correlation was observed for the

total bio-crude yield, with the exception of the 10%wt nylon blend (Figure 3.2-1b). The positive effect of a synergy between biomass and PET, increasing the bio-oil yield was also observed by Çepelioğullar and Pütün, during co-pyrolysis of hazelnut shells with PET (Çepelioğullar and Pütün, 2013).

3.2.6.2 –Bio-char composition and properties

To determine the fate of the plastics, the bio-char was analysed by elemental analysis and FT-IR. The elemental composition of the bio-char produced through the co-liquefaction is presented in Figure 3.2-2. Overall, there was substantial variation in the elemental composition of the bio-chars. For example, the carbon content ranged from 50.5–75.5 %, nitrogen content ranged between 1.3–3.9 %, hydrogen contents between 3.6–9.3 % and oxygen contents of 17.1–44.0 % were observed. Co-liquefaction with PET caused the most substantial decrease in C and increase in O content in bio-chars (from 61.2 % C and 30.1 % O for pure pistachio bio-char, to 50.5 % C and 44 % O obtained for bio-char from co-liquefaction of pistachio with 20 wt.% PET). Co-liquefaction with PP contributed to an increase in C content (71.9 % and 72.3 % C for 10 wt.% and 20 wt.% PP blends, respectively). The additional PE bio-char had the highest carbon content and the lowest nitrogen (75.5 % and 1.3 %, respectively). This is suggestive that the PE and PP is not breaking down and rather distributing into the char.

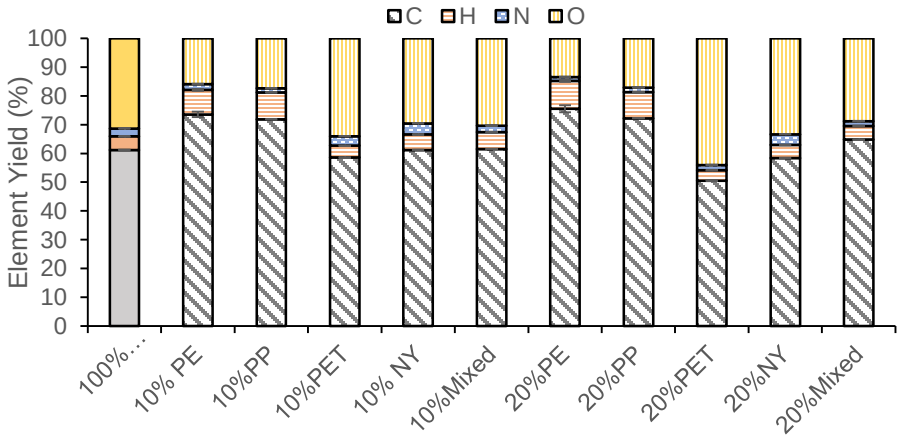

Figure 3.2- 2–Elemental composition (determined by elemental analysis) of the bio-char of different plastic contents 10 wt.% and 20 wt.% of PE, PP, PET, NY and plastic mixture.

The heating value (HHV) is commonly used to describe the energy content of any fuel (Qian et al., 2013). The bio-char produced in the HTL reaction is also suitable for combustion and as such the HHV of the bio-chars produced were calculated (Figure 3.2-3a). While the bio-char from pistachio hull had a very similar energy content to those produced from the nylon and PET reactions, the bio-char produced from the PE and PP liquefactions was extremely high with up to 37 MJ kg^{-1} observed. This suggests that the majority of the polyolefins are not reacting, and rather remaining in the bio-char increasing the HHV.

One method of assessing the suitability of bio-chars as a solid fuel is to determine and compare the elemental ratios of H/C and O/C through a Van Krevelen diagram (Van Krevelen, 1950). The H/C and O/C ratios also give an indication of the structural transformation (Wang et al., 2015) and surface hydrophilicity of bio-char (Tan et al., 2015). In this study, similar to the HHV, an increase of H/C ratios was found for the presence of PE and PP blends compared to pure pistachio, and a slight increase in the H/C ratios from 0.92 to 1.09 and 1.08 for the presence of 20 wt.% PP and PE blends, respectively. In the contrast, the H/C ratio was much smaller for pistachio with PET. The H/C ratio obtained for the bio-char from nylon blends were 0.74 and 0.66 for 10 wt.% and 20 wt.% nylon blends.

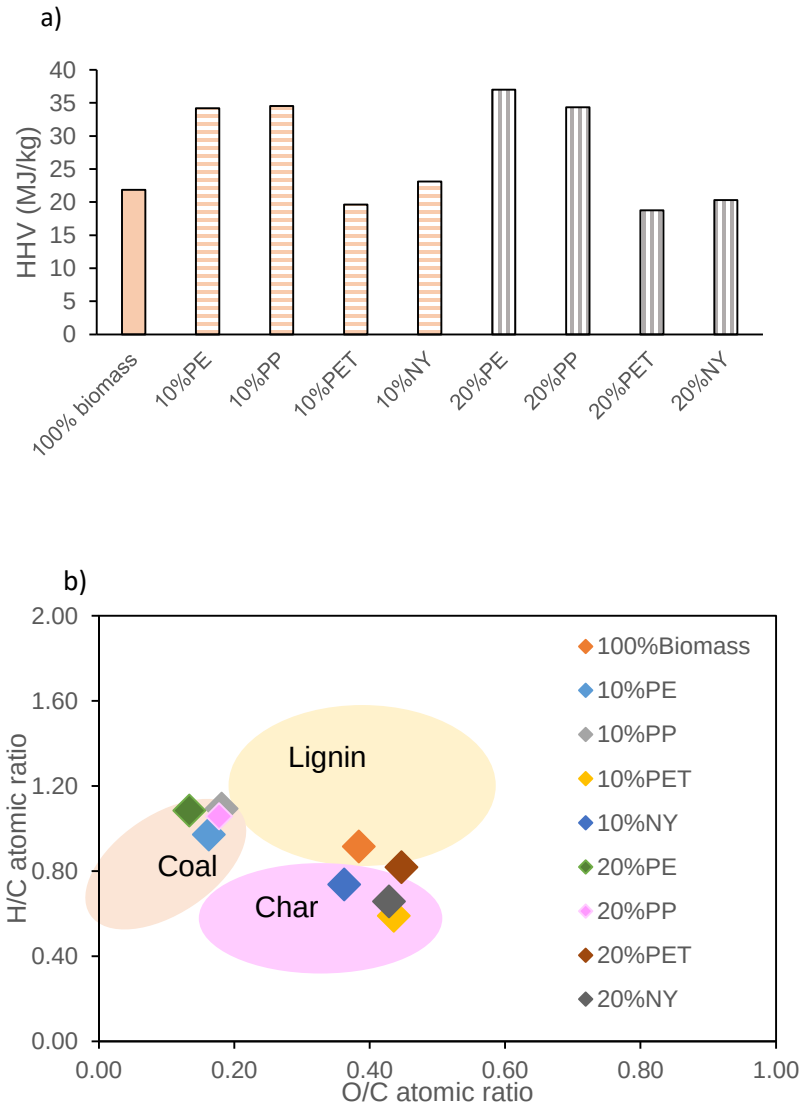

Figure 3.2- 3–a) Bio-char heating value of the bio-char of different plastic contents 10 wt.% and 20 wt.% of PE, PP, PET, and NY. b) Van Krevelen diagram with H:C and O: molar ratio for co-liquefaction of biomass with plastics char, coal, and lignin (Kookana et al., 2011)

For the O/C ratio (the degree of polarity), the additional PET has the highest O/C ratio (0.45 and 0.44 for10 wt.% and 20 wt.% PET blends). Co-liquefaction of nylon contributed to an increase 0.43 for 20 wt.% nylon but slight decrease to 0.36 for 10 wt.% nylon blend. The smallest O/C ratio was found in the additional PE (0.16 and 0.13 for 10 wt.% and 20 wt.% PE blends). Similarly, 0.18 C/O ratio was observed for

10 wt.% and 20 wt.% PP blends. The H/C and O/C ratios for the bio-chars in this study were plotted and compared to typical solid heating fuels (Figure 3.2-3b).

A lower H/C and O/H ratio have been assumed to be due to a greater the degree of aromaticity and stability (Kookana et al., 2011). The positions of the bio-char from PE and PP were similar to coal, and were presumably increased by a large level of unreacted plastic in the solid residue. For the bio-char from biomass/PET and biomass/nylon were found ranging in between lignin and nature char, this indicates a higher level of conversion in these reactions.

3.2.6.3 Identification of major functional groups in bio-char

Hydrothermal conversion of biomass produces bio-char as one of the major products, although HTL bio-char is structurally different to bio-char derived from high-temperature pyrolysis (Hu et al., 2018). For example, HTL bio-char tends to have a higher abundance of oxygen-containing functional groups (Liu et al., 2010). In order to achieve a better understanding of the effect of plastics on pistachio hull HTL, bio-chars were analysed using FT-IR to identify the key functional groups present.

The FT-IR spectra of bio-char from HTL of pure pistachio contained strong absorption bands at 2800–3300 cm^{-1}, attributable to C–H stretching vibrations from methyl and methylene-containing organic compounds. An absorbance attributed to alkane bending is seen at 1066–1145 cm^{-1}. The presence of esters and acids in the spectra is evidenced by the strong C=O absorbance at 1800–2000 cm^{-1}. The absorption peak observed around 1612 cm^{-1} can be assigned to aromatic rings in lignin and thus verified to the presence of lignin in bio-char (Konsolakis et al., 2015). A vibration at 1570 cm^{-1} and 898 cm^{-1} can be attributed to the presence of aromatic rings, likely arising from asphaltenic materials in the bio-char (Wang and Griffiths, 1985) (Lua and Yang, 2004). A similar observation was also reported for the pyrolysis of pistachio shell (Açıkalın et al., 2012; Apaydin-Varol et al., 2007) and green fabrication of Cu/pistachio shell nanocomposite (Taghizadeh and Rad-Moghadam, 2018).

For bio-char from co-liquefaction of pistachio hull with PE, peaks of moderate intensity were observed at 2936, 1593, 1267 cm^{-1}, similar to those obtained for bio-char from HTL of pure pistachio hull. However, sharp peaks at 2850 and 2920 cm^{-1} are also present, which are not observed for pure pistachio hull bio-char, attributable to C–H bonds (Figure 3.2-4a). In addition, peaks were observed at 1451 and 1376 cm^{-1}, which

were also seen in the FT-IR specta of pure PE, but not in the spectra of the bio-char from pistachio hull liquefaction. These findings suggest the presence of unreacted polyethylene in the HTL char.

On comparing the spectra of the bio-char from the HTL of pistachio hull, the bio-char from pistachio hull co-liquefaction with PP, and pure unreacted PP, absorbance attributable to C–H bond stretching vibrations at 2920 cm^{-1} and 2849 cm^{-1} are present in the co-processed samples and the pure PP, which are not seen for bio-char from pure pistachio hulls (Figure 3.2-4b). Additionally, with increasing PP loading in the blended samples, peaks at 1365 and 1420 cm^{-1} attributable to alkane C–H bending sharpen, suggesting the presence of increasing amounts of unreacted PP.

For bio-char produced from blended pistachio hull and PET, a number of peaks at similar wavenumbers to pure PET were observed (2920 cm^{-1}, 1017 cm^{-1}, 872 cm^{-1}), suggesting the presence of some unreacted plastic. However, a number of additional peaks unique to the blended pistachio/PET bio-char, and not present in either pure PET or bio-char from pure pistachio, were also observed at 820, 1400 and 1575 cm^{-1}: these are attributed to C–H, O–H and C=C bonds. The appearance of new absorbance peaks can be taken as evidence of reactions occurring between the biomass and PET under HTL conditions, and the formation of new compounds (Figure 3.2-4c).

In contrast, the FT-IR spectra of bio-char from the HTL of pistachio hulls blended with nylon were almost identical to the spectrum of pure pistachio hull bio-char (weak absorbance at 1570 cm^{-1}, 1249 cm^{-1}, 1068 cm^{-1} and 720 cm^{-1}, corresponding to O–H stretching vibrations and aromatic C=C bonds (Figure 3.2-4d). The presence of nylon co-feedstock in HTL reactions did not appear to change to composition of the bio-char, suggesting that nylon reacted more completely, forming more soluble products than the other three plastics examined.

The FTIR spectra of the char are high similar however, those produced from the co-liquefaction with PE and PP blends show a far stronger absorbance at ~2800-3000 cm^{-1} suggestive of an aliphatic functional group (Chen et al., 2008). These intensive peaks, coupled to the enhanced C and H contents, as well as HHV of the char strongly suggest unreacted polymer. In contrast, the intensity of these peaks decreased substantially in the char produced from the PET and nylon co-liquefaction studies. So much so, that the FTIR spectra of the bio-char produced from the nylon blends closely

resembles the char produced from pure pistachio hull. These results suggest that during co-liquefaction of pistachio and nylon, there is synergetic interaction between the two components improving decomposition. The complete decomposition of nylon is in agreement with another previous study of the co-liquefaction with macroalgae (Raikova et al., 2019). The most resistant polymer to decomposition was PE and this is presumably due to the to the high activation energy needed to decompose the polymer, the instability of the potential secondary products and to diffusion limitation caused by PE melted during the HTL process (Burra and Gupta, 2018).

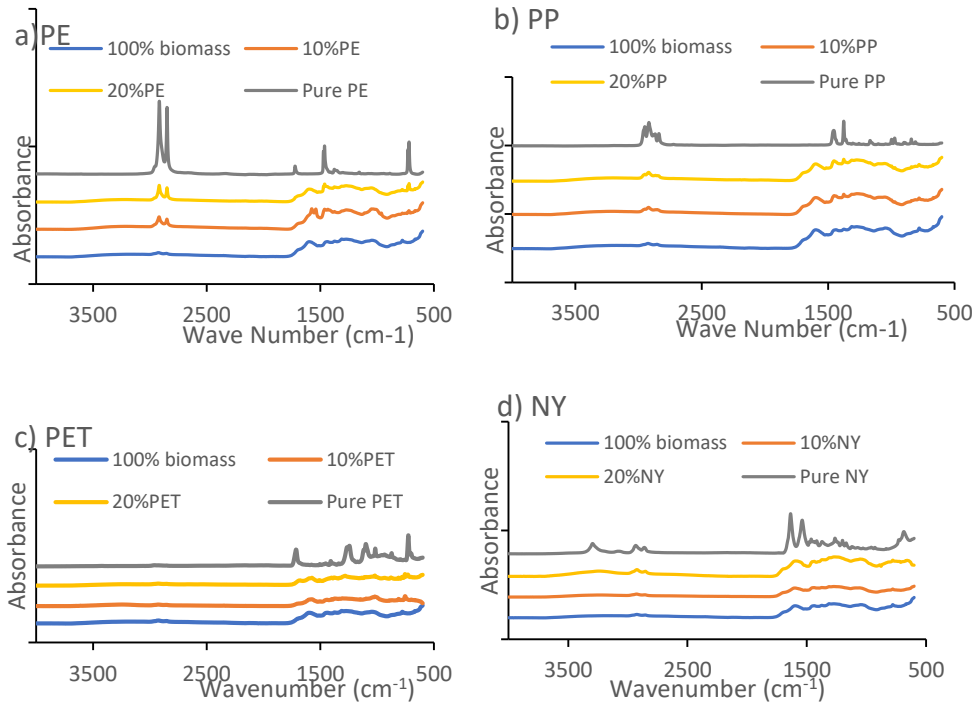

Figure 3.2- 4–FTIR of pure plastics and solid phase from hydrothermal co-liquefaction of pistachio hull with (a) polyethylene, (b) polypropylene, (c) polyethylene terephthalate, and (d) nylon.

3.2.6.5 Quantification of unreacted plastic in bio-char

The presence of plastics alongside pistachio hull biomass had an effect on the yields and composition of the four product phases. It is important to be able to quantitatively understand what proportion of the plastic remained unconverted in the HTL reaction, and how plastic degradation products are distributed between the four product phases. Co-liquefaction of pistachio hulls with all four plastics enhanced the partitioning of

material to the bio-char phase. This may be attributable to a number of factors: the presence of unreacted plastics, plastics partially or entirely converted to new solid-phase product molecules, biomass-derived solids converted to bio-char in higher quantities in the presence of plastic or a combination of the above. By identifying the proportion of unreacted plastics in the bio-char phase, it is possible to assess the degree of plastic conversion. Fourier transform infrared (FTIR) spectroscopy has played an important role in quantitative analysis of mixed solid materials in a number of studies, and can be a simple and inexpensive technique for determining plastic content in biogenic samples.

Chen et al. demonstrated quantitative determination of clay minerals, quartz and carbonates, as well as organic matter in shale, using KBr-FTIR spectroscopy (Chen et al., 2014). Pandey and Pitman used FTIR to investigate the lignin content in wood and wood decayed by the brown- rot fungus *Coniophora puteana,* by identifying characteristic FTIR absorbance peaks for lignin and wood, and using the ratio of peak intensities to determine lignin content (Pandey and Pitman, 2004). Lao et al. demonstrated that FTIR could be used to quantify biomass in wood-plastic composites. FTIR was used to analyse the wood samples and plastics independently, and peaks which were unique to the biomass and plastic components were identified (Lao and li, 2014). Taking a number of composites with different biomass contents, the peak ratios of the signature biomass and plastic peaks were calculated, and univariate regression was used to generate equations to predict biomass content in composites. Another study of wood-plastic composites by Stark and Matuana (Stark and Matuana, 2007) used Attenuated Total Reflectance Fourier Transform Infrared (ATR-FTIR) spectroscopy combined with principal component analysis to classify wood-plastic composites species.

In this study, the conversions of plastics were estimated by plotting calibration curves of known amounts of the plastics with bio-char generated from the reaction which contained only pistachio hull. Calibration curves were created for each plastic/biomass combination (polyethylene/pistachio hull, polypropylene/pistachio hull, polyethylene terephthalate/pistachio hull, nylon/pistachio hull) by mixing bio-char from HTL of pure pistachio hull with plastics at a range of known concentrations. Calibration curves and further information are provided in the Supplementary Information (Table 3.3-3–3.3-6, and Figure 3.3-1–3.3-4).

The content of unreacted plastics in the bio-char phase can be used to determine the overall conversion, which includes plastics converted to water-soluble material in the aqueous phase, as well as bio-crude, volatile gas-phase products and plastic-derived materials in the solid bio-char phase that have undergone reactions to form new molecules (although it excludes polymer chains that may have undergone reactions and lost several repeat units, but remained otherwise unchanged in the bulk of the chain).

$$Conversion\ (\%) = \frac{unconverted\ plastic\ in\ bio{-}char\ (\%) \times\ bio{-}char\ yield\ (g)}{plastic\ in\ feedstock\ (g)} \quad (10)$$

Conversions of the bulk plastic are presented in Figure 3.2-5. Nylon demonstrated the highest overall conversion through HTL (84 %); PET conversion was also high (53 %). In contrast, polyethylene and polypropylene were highly resistant to degradation. For polyethylene, only 17 % was converted into HTL products at a 10 wt.% blend, but no conversion was observed for the 20 wt.% blend. For polypropylene, approximately 9 % was converted at 20 wt.% blend level, although the 10 wt.% blend showed little reactivity. Out of all the plastics examined, PE blends were remarkably resistant to degradation. Co-liquefaction of PE blends is may attributed to diffusion limitation caused by PE melted during HTL process and increase in the stability of its decomposed (Burra and Gupta, 2018).

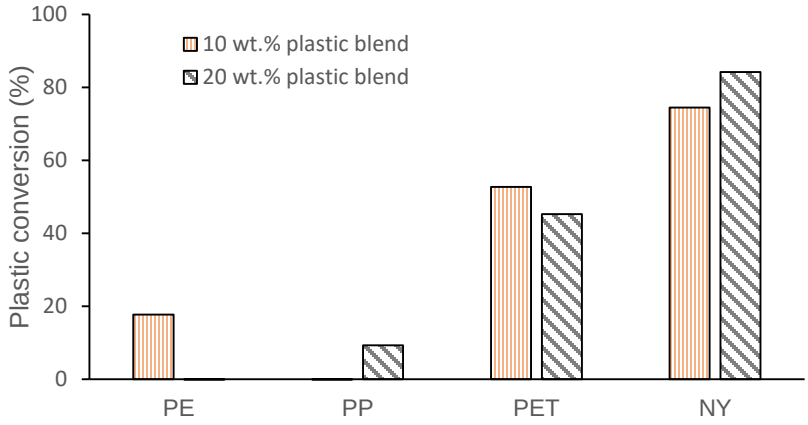

Figure 3.2- 5–Extent of plastic conversion under HTL conditions

3.2.6.6 Bio-crude elemental composition

The main product produced from the HTL conversion was the bio-crude that can be converted into an array of platform chemicals and biofuels (Biller et al., 2015). Elemental composition of the bio-crude produced from co-liquefaction of pistachio hulls with plastics did not change substantially relative to bio-crude from pure pistachio hulls (Figure 3.2-6a). Carbon content increased slightly for co-liquefaction with PE and PET, although small reductions were seen for co-liquefaction with PP and NY. Nitrogen content slightly increased with the addition of PE and nylon, which gave rise to increases in bio-crude N from 1.73 % for pure pistachio hull bio-crude to 2.18 % and 2.43 % for 10 wt.% and 20 wt.% PE blend loading and increased to a maximum of 3.47 % for a 20 wt.% nylon blend level. Oxygen levels were relatively high (ca. 18 %), and were not strongly affected by co-liquefaction with plastics, with the exception of PE, which decreased bio-crude O content to 10–13 %.

The HHV of bio-crude from co-liquefaction of pistachio hull with plastics was found to be in the range of 32–38 MJ kg^{-1} (Figure 3.2-6b). In the presence of PE, the HHV increased from 33.6 MJ kg^{-1} for pure pistachio hull bio-crude to 38.0 and 36.8 Mj/kg for 10 wt.% and 20 wt.% PE blends. However, HHV decreased slightly by 0.6–1.4 % for 20 wt.% blends of PP, PET and nylon. This value was higher than the HHV obtained from pyrolysis pistachio (19.45 MJ kg^{-1}) (Açıkalın et al., 2012). The presence of plastics in biomass hydrothermal liquefaction contribute mostly more increasing in the heating value of bio-crude obtained by reducing the high oxygen content of bio-crude from pure biomass, this resulted can be confirmed by various studies on co-pyrolysis with plastics and biomass (Jung et al., 2010) (Zhou and Yang, 2015) (Aydinli and Caglar, 2010).

According to the measure energy consumption, hydrothermal liquefaction as employed in this study is a relatively low-energy technique because it makes use of the high pressure of the saturation water. Due to specific heat capacity and the low compressibility of water, the energy consumption required to achieve the critical conditions is not excessive, with the completed reaction taking place within 15 minutes. The energy required for hydrothermal liquefaction is less in terms of biomass drying and dewatering processing due to the avoidance of the evaporation step. Therefore, hydrothermal liquefaction processing can lead to high net energy values. This investigation can be confirmed by various studies(Chan et al., 2016) (Yang et al.,

2017) (Watson et al., 2019) (Zhu et al., 2014) (Elliott et al., 2015). In order to determine the effective outcome, the energy in the feedstock is converted into the bio-crude phase product which is a key target of hydrothermal liquefaction products. The energy recovery was calculated based on the bio-crude yield, elemental composition and heating value obtained. Considering the energy recovery (Figure 3.2-6c), the highest overall energy recovery was found for 20 wt.% blend PET (70%), this was observed to be similar to bio-crude produced from straw types via pyrolysis (Tröger et al., 2013). Energy recovery was also enhanced compared to the HTL from pure pistachio (60%). In contrast, 10 wt.% blend PE showed the lowest energy conversion (38%), this result is relative to lower bio-crude oil productive of co-liquefaction pistachio with PE.

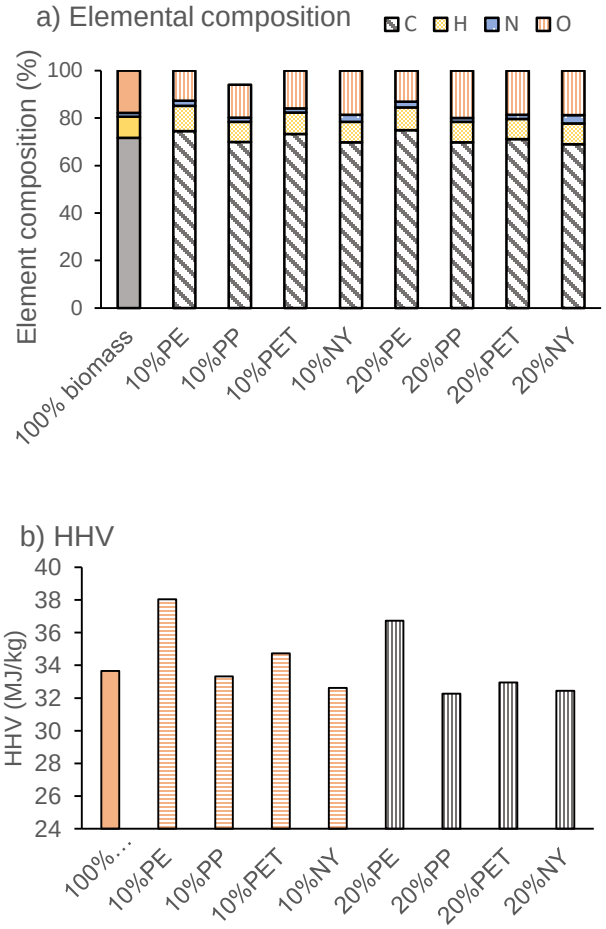

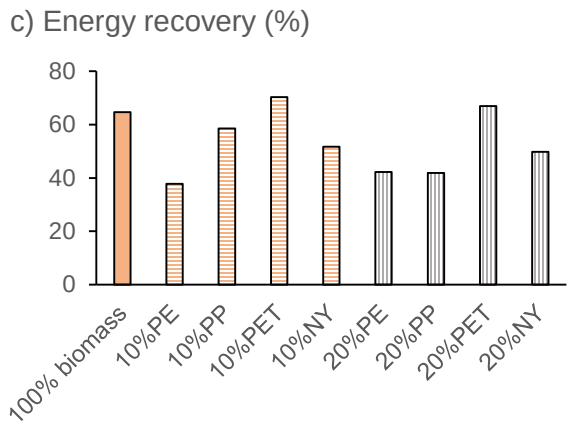

Figure 3.2- 6– (a) Bio-crude composition from the co-liquefaction of pistachio hulls with 10 wt.% and 20 wt.% PE, PP, PET and NY blend loading, b) bio-crude heating value, and (c) the energy recovery in the bio-crude products from the co-liquefaction of pistachio hulls with PE,PP, PET and NY at 10 wt.% and 20 wt.% blend levels.

3.2.6.7 Bio-crude chemical composition

In order to investigate the effect of plastics on the bio-crude composition, GC-MS was used to characterise the bio-crudes produced from co-liquefaction of pistachio hull with PP, PE, PE, NY and mixtures of the above. The compounds identified were classified into three categories based on the functional groups: (1) monoaromatics such as benzene, phenol and their derivatives, (2) aliphatic compounds such as cyclopentene and cyclohexene, and (3) oxygenated compounds such as acetic acid-4-methylphenyl ester for example. The majority of compounds identified in each bio-crude were composed predominantly of phenolic compounds – these presumably originate from lignin, which is one of the major components of the pistachio hulls.

GC-MS analysis of the bio-crude from pure pistachio hull showed the presence of phenolic compounds, substituted cyclopentenones, and low levels of 4-methyl,1,2-benzenediol. PET, PP and nylon are more susceptible to degradation than PE – kinetic studies on the decomposition of polyolefins have found that the minimum amount of energy required to activate PP and PE was equal to 243 and 301 kJ mol^{-1}, respectively (Wall et al., 1954). For co-liquefaction with PE, degradation of the polymer chains through a random scission mechanism was expected to form aliphatic hydrocarbons (Pei et al., 2012).

A slight increase in ketone formation was observed in the presence of PE, however, no increase in the abundance of medium- or long-chain aliphatic hydrocarbons was detected as evidence of PE fragmentation (although it is possible that fragmentation products were present, but too large to be soluble).

An unexpected increase in the relative abundance of pyridinol and its derivatives was also observed in the presence of PET, suggesting that PET activates protein decomposition in the pistachio hull biomass. Additionally, the presence of variously substituted benzenediols and phenols may originate from PET decomposition, although terephthalic acid monomer was not observed. Co-liquefaction of biomass with nylon 6 resulted in the appearance of a large peak attributable to monomeric caprolactam in the bio-crude. Caprolactam has previously been shown to depolymerise in aqueous conditions at temperatures as low as 120°C (Brydson, 1999). Caprolactam is soluble in both chloroform and water, so is likely to be distributed between the bio-crude and aqueous phases. A summary of the most abundant compounds in the bio-crudes produced, identified using GC-MS, is presented in the Supporting Information (Table 3.3-7).

3.2.6.8 Aqueous phase

Co-liquefaction of pistachio hulls with PE, PP and PET in the aqueous phase showed a decreased carbon and nitrogen content (Table 3.2-1). The total organic carbon and total nitrogen in the aqueous product phases is distributed very similarly with 16.7 %, 17.5 % and 18.4 % for carbon concentration and 0.87, 0.86 and 0.72 % for nitrogen at a 10 wt.% blend of PE, PP, and PET, respectively. Aqueous phase carbon and nitrogen contents decreased slightly for both 10 wt.% and 20 wt.% blends of PE and PP. In contrast, co-liquefaction with nylon shows increases in both carbon and nitrogen content in the aqueous phase at 20.8 and 31.7 % for 10 wt.% and 20 wt.% nylon blend loading. This observation is predominantly due to the formation of water-soluble caprolactam with the depolymerisation of nylon.

Table 3.2- 1–Elemental composition of aqueous phases produced from liquefaction of pistachio hulls with plastics

Sample	TOC (g L^{-1})	TN (g L^{-1})
100% biomass	17.9	0.94
10% PE	16.7	0.87
10% PP	17.5	0.86
10% PET	18.4	0.72
10% NY	20.9	1.87
10% Mix	19.7	1.26
20% PE	15.0	0.81
20% PP	15.8	0.78
20% PET	18.6	0.64
20% NY	31.7	3.54
20% Mix	22.2	1.91

3.2.6.9 Optimisation of reaction time and heating rate

Although it has previously been shown that bio-crude yields are increased at faster heating rates and shorter reaction times (Hietala et al., 2016; Valdez et al., 2012) (Faeth et al., 2013) (Eboibi et al., 2014), longer reaction times and slower heating may enhance the decomposition of unreactive plastics such as PE and PP under HTL conditions. HTL reactions were therefore carried out using slower heating rates (5.5 °C min^{-1}) to achieve longer reaction times, giving an overall reaction time of 60 min. Longer reaction times did not appear to increase bio-crude production, instead contributing to increasing bio-char and gaseous products (fig. 3.3-7), in line with previous studies on biomass liquefaction (Bezergianni et al., 2017; Duan and Savage, 2011). At longer reaction times, bio-crude products can polymerise to give heavier oil fractions and solid phase materials, but long reaction times can also result in hydrocracking of organic compounds into gases, further reducing the bio-crude yields. In terms of bio-crude production, there is no benefit to using reaction times longer than 15 min.

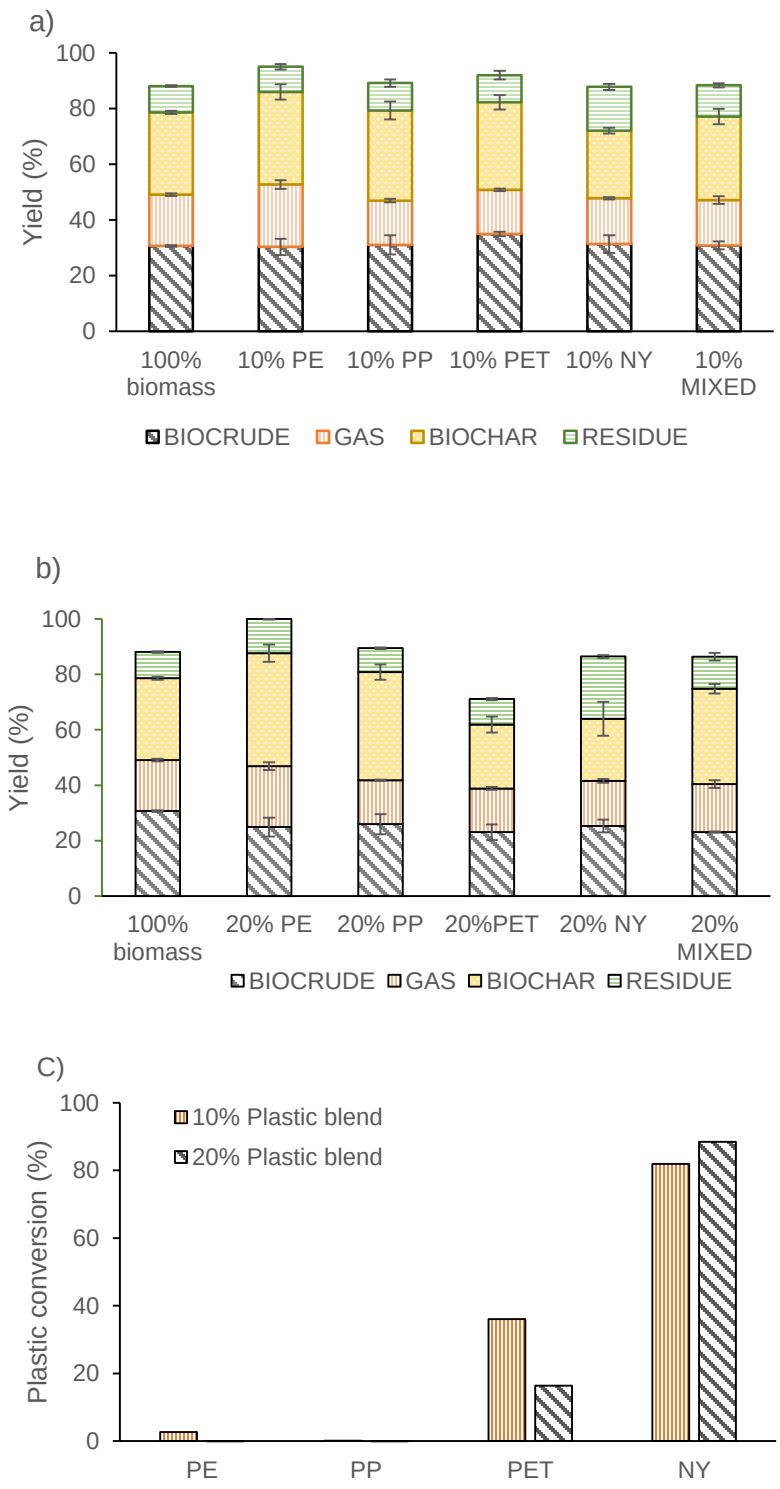

Figure 3.2- 7–Effect of longer reaction time on products yield where (a) is a plastic loading (PP, PE, PET, NY or mixture) of 10 wt.% (b) is a plastic loading of 20 wt.% (PP, PE, PET, NY or mixture) and c) is the total plastic conversion in the reaction for PE, PP, PET and NY.

Similarly, FT-IR spectroscopy of the bio-char produced from co-liquefaction at slower heating rates suggested that slower heating rates and increasing the reaction time did not facilitate the conversion of plastics. The majority of the peaks observed occurred at identical wavenumbers to those seen in bio-char produced under more severe reaction conditions, with more intense absorbance's suggesting the presence of higher levels of plastics in the bio-char. Notably, C–H adsorption bands were observed at 2924 $cm^{-1}$and 2850 cm^{-1} the PET blends, and at 2935 cm^{-1} and 2868 cm^{-1} for nylon, which were not observed for the bio-chars produced at faster heating rates (see Figure 3.3-7 in Supporting Information for all spectra).

The conversion of plastic was calculated using Eqn. 10, as previously. Compared to faster heating rates, HTL carried out at slow heating rates (5.5 °C min^{-1}) gave rise to lower overall conversions of plastics in all cases with the exception of the 10 wt.% NY blend (a slight increase from 74 to 82 % conversion for slow heating rates) and the 20 wt.% NY (a modest increase from 84 to 88 % conversion). This indicates that faster heating rates are preferred for optimising both overall bio-crude yield and plastic conversion.

3.2.5 Conclusions

Hydrothermal liquefaction is a highly promising conversion technology for lignocellulosic biomass. In this study the addition of PE, PP, PET and Nylon to the liquefaction of pistachio hulls was investigated, to determine the suitability of co-processing the waste feedstocks together. Promisingly, both PET and nylon-6 were depolymerised under HTL conditions, and in the case of nylon-6, the monomer ϵ-caprolactam was recovered predominantly in the aqueous phase. The polyolefins were much less resistant to decomposition, though what was broken down partitioned into the bio-crude phase and increased the HHV of the bio-crudes substantially. Although co-liquefaction of lignocellulosic residues and contaminated plastic wastes is a potentially elegant means to utilising waste streams for value creation, taking steps to further enhance the conversion of the recalcitrant polyolefins is necessary before plastic waste can become an integral part of a biorefinery.

3.2.8 Acknowledgements

The authors would like to acknowledge the Royal Thai Scholarship for funding this study.

3.2.9 References

Açıkalın, K., Karaca, F., Bolat, E., 2012. Pyrolysis of pistachio shell: Effects of pyrolysis conditions and analysis of products. Fuel 95, 169-177.
Akhtar, J., Amin, N.A.S., 2011. A review on process conditions for optimum bio-oil yield in hydrothermal liquefaction of biomass. Renewable and Sustainable Energy Reviews 15, 1615-1624.
Apaydin-Varol, E., Pütün, E., Pütün, A.E., 2007. Slow pyrolysis of pistachio shell. Fuel 86, 1892-1899.
Arturi, K.R., Kucheryavskiy, S., Søgaard, E.G., 2016. Performance of hydrothermal liquefaction (HTL) of biomass by multivariate data analysis. Fuel Processing Technology 150, 94-103.
Association of Plastic Manufacturers Europe, P.t.F., 2016. An analysis of the European plastics production, demand and waste data. European Association of Plastics Recycling and Recovery Organisations (2016), 1-38.
Association of Plastic Manufacturers Europe, P.t.F., 2017. An analysis of European plastics production, demand and waste data, demand and waste data, European Association of Plastics Recycling and Recovery Organisations pp. 1-44.
Aydinli, B., Caglar, A., 2010. The comparison of hazelnut shell co-pyrolysis with polyethylene oxide and previous ultra-high molecular weight polyethylene. Journal of Analytical and Applied Pyrolysis 87, 263-268.
Bezergianni, S., Dimitriadis, A., Faussone, G.-C., Karonis, D., 2017. Alternative Diesel from Waste Plastics. Energies 10, 1750.
Bhada-Tata, D.H.a.P., March 2012 WHAT A WASTE A Global Review of Solid Waste Management, World Bank Urban Development Series.
Bhattacharya, P., Steele, P.H., Hassan, E.B.M., Mitchell, B., Ingram, L., Pittman, C.U., 2009. Wood/plastic copyrolysis in an auger reactor: Chemical and physical analysis of the products. Fuel 88, 1251-1260.
Bi, Z., Zhang, J., Peterson, E., Zhu, Z., Xia, C., Liang, Y., Wiltowski, T., 2017. Biocrude from pretreated sorghum bagasse through catalytic hydrothermal liquefaction. Fuel 188, 112-120.
Biller, P., Sharma, B.K., Kunwar, B., Ross, A.B., 2015. Hydroprocessing of bio-crude from continuous hydrothermal liquefaction of microalgae. Fuel 159, 197-205.

Brydson, J.A., 1999. 18 - Polyamides and Polyimides, in: Brydson, J.A. (Ed.), Plastics Materials (Seventh Edition). Butterworth-Heinemann, Oxford, pp. 478-530.

Burra, K.G., Gupta, A.K., 2018. Kinetics of synergistic effects in co-pyrolysis of biomass with plastic wastes. Applied Energy 220, 408-418.
Cao, B., Sun, Y., Guo, J., Wang, S., Yuan, J., Esakkimuthu, S., Bernard Uzoejinwa, B., Yuan, C., Abomohra, A.E.-F., Qian, L., Liu, L., Li, B., He, Z., Wang, Q., 2019. Synergistic effects of co-pyrolysis of macroalgae and polyvinyl chloride on bio-oil/bio-char properties and transferring regularity of chlorine. Fuel 246, 319-329.
Çepelioğullar, Ö., Pütün, A.E., 2013. Thermal and kinetic behaviors of biomass and plastic wastes in co-pyrolysis. Energy Conversion and Management 75, 263-270.

Chan, Y., Tan, R., Suzana, Y., Lam, H., Quitain, A., 2016. Comparative life cycle assessment (LCA) of bio-oil production from fast pyrolysis and hydrothermal liquefaction of oil palm empty fruit bunch (EFB). Clean Technologies and Environmental Policy 18.
Chen, B., Zhou, D., Zhu, L., 2008. Transitional Adsorption and Partition of Nonpolar and Polar Aromatic Contaminants by Biochars of Pine Needles with Different Pyrolytic Temperatures. Environmental Science & Technology 42, 5137-5143.
Chen, Y., Furmann, A., Mastalerz, M., Schimmelmann, A., 2014. Quantitative analysis of shales by KBr-FTIR and micro-FTIR. Fuel 116, 538-549.
Costanzo, W., Hilten, R., Jena, U., Das, K.C., Kastner, J.R., 2016. Effect of low temperature hydrothermal liquefaction on catalytic hydrodenitrogenation of algae biocrude and model macromolecules. Algal Research 13, 53-68.
Demiral, İ., Atilgan, N.G., Şensöz, S., 2008. PRODUCTION OF BIOFUEL FROM SOFT SHELL OF PISTACHIO (PISTACIA VERA L.). Chemical Engineering Communications 196, 104-115.
Demirbaş, A., 2001. Biomass resource facilities and biomass conversion processing for fuels and chemicals. Energy Conversion and Management 42, 1357-1378.
Demirbas, A., Al-Sasi, B.O., Nizami, A.-S., 2016. Conversion of waste tires to liquid products via sodium carbonate catalytic pyrolysis. Energy Sources, Part A: Recovery, Utilization, and Environmental Effects 38, 2487-2493.
Duan, P., Savage, P.E., 2011. Hydrothermal Liquefaction of a Microalga with Heterogeneous Catalysts. Industrial & Engineering Chemistry Research 50, 52-61.
Eboibi, B.E., Lewis, D.M., Ashman, P.J., Chinnasamy, S., 2014. Effect of operating conditions on yield and quality of biocrude during hydrothermal liquefaction of halophytic microalga Tetraselmis sp. Bioresource Technology 170, 20-29.
Elliott, D.C., Biller, P., Ross, A.B., Schmidt, A.J., Jones, S.B., 2015. Hydrothermal liquefaction of biomass: Developments from batch to continuous process. Bioresource Technology 178, 147-156.
Faeth, J.L., Valdez, P.J., Savage, P.E., 2013. Fast Hydrothermal Liquefaction of Nannochloropsis sp. To Produce Biocrude. Energy & Fuels 27, 1391-1398.
Fekhar, B., Miskolczi, N., Bhaskar, T., Kumar, J., Dhyani, V., 2018. Co-pyrolysis of biomass and plastic wastes: investigation of apparent kinetic parameters and stability of pyrolysis oils. IOP Conference Series: Earth and Environmental Science 154, 012022.
Hietala, D.C., Faeth, J.L., Savage, P.E., 2016. A quantitative kinetic model for the fast and isothermal hydrothermal liquefaction of Nannochloropsis sp. Bioresource Technology 214, 102-111.
Hu, Y., Wang, S., Li, J., Wang, Q., He, Z., Feng, Y., Abomohra, A.E.-F., Afonaa-Mensah, S., Hui, C., 2018. Co-pyrolysis and co-hydrothermal liquefaction of seaweeds and rice husk: Comparative study towards enhanced biofuel production. Journal of Analytical and Applied Pyrolysis 129, 162-170.
Jakab, E., Várhegyi, G., Faix, O., 2000. Thermal decomposition of polypropylene in the presence of wood-derived materials. Journal of Analytical and Applied Pyrolysis 56, 273-285.
Jongwon Kim, S.B.L.C.B.M.B.A.A., 1999. Coliquefaction of Coal and Black Liquor to Environmentally Acceptable Liquid Fuels. Energy Sources 21, 839-847.
Jung, S.-H., Cho, M.-H., Kang, B.-S., Kim, J.-S., 2010. Pyrolysis of a fraction of waste polypropylene and polyethylene for the recovery of BTX aromatics using a fluidized bed reactor. Fuel Processing Technology 91, 277-284.

Karaca, F., Bolat, E., 2000. Coprocessing of a Turkish lignite with a cellulosic waste material: 1. The effect of coprocessing on liquefaction yields at different reaction temperatures. Fuel Processing Technology 64, 47-55.
Konsolakis, M., Kaklidis, N., Marnellos, G.E., Zaharaki, D., Komnitsas, K., 2015. Assessment of biochar as feedstock in a direct carbon solid oxide fuel cell. RSC Advances 5, 73399-73409.
Kookana, R., K. Sarmah, A., Van Zwieten, L., Van Krull, E., Singh, B., 2011. Biochar Application to Soil: Agronomic and Environmental Benefits and Unintended Consequences. Advances in Agronomy 112, 103-143.
Lao, W., li, G., 2014. Quantitative Analysis of Biomass in Three Types of Wood-Plastic Composites by FTIR Spectroscopy. Bioresources 9(4), 6073-6086.
Liu, Z., Zhang, F.-S., Wu, J., 2010. Characterization and application of chars produced from pinewood pyrolysis and hydrothermal treatment. Fuel 89, 510-514.
Lua, A.C., Yang, T., 2004. Effect of activation temperature on the textural and chemical properties of potassium hydroxide activated carbon prepared from pistachio-nut shell. Journal of Colloid and Interface Science 274, 594-601.
Nazari, L., Yuan, Z., Souzanchi, S., Ray, M.B., Xu, C., 2015. Hydrothermal liquefaction of woody biomass in hot-compressed water: Catalyst screening and comprehensive characterization of bio-crude oils. Fuel 162, 74-83.
Pandey, K.K., Pitman, A.J., 2004. Examination of the lignin content in a softwood and a hardwood decayed by a brown-rot fungus with the acetyl bromide method and Fourier transform infrared spectroscopy. Journal of Polymer Science Part A: Polymer Chemistry 42, 2340-2346.
Pedersen, T.H., Grigoras, I.F., Hoffmann, J., Toor, S.S., Daraban, I.M., Jensen, C.U., Iversen, S.B., Madsen, R.B., Glasius, M., Arturi, K.R., Nielsen, R.P., Søgaard, E.G., Rosendahl, L.A., 2016. Continuous hydrothermal co-liquefaction of aspen wood and glycerol with water phase recirculation. Applied Energy 162, 1034-1041.
Pei, X., Yuan, X., Zeng, G., Huang, H., Wang, J., Li, H., Zhu, H., 2012. Co-liquefaction of microalgae and synthetic polymer mixture in sub- and supercritical ethanol. Fuel Processing Technology 93, 35-44.
Peterson, A.A., Vogel, F., Lachance, R.P., Fröling, M., Antal, J.M.J., Tester, J.W., 2008. Thermochemical biofuel production in hydrothermal media: A review of sub- and supercritical water technologies. Energy & Environmental Science 1.
Pütün, A.E., Özbay, N., Apaydın Varol, E., Uzun, B.B., Ateş, F., 2007. Rapid and slow pyrolysis of pistachio shell: effect of pyrolysis conditions on the product yields and characterization of the liquid product. International Journal of Energy Research 31, 506-514.
Qian, K., Ajay, K., Patil, K., Bellmer, D., Wang, D., Yuan, W., Huhnke, R., 2013. Effects of Biomass Feedstocks and Gasification Conditions on the Physiochemical Properties of Char. Energies 6, 3972-3986.
Raikova, S., Knowles, T.D.J., Allen, M.J., Chuck, C.J., 2019. Co-liquefaction of Macroalgae with Common Marine Plastic Pollutants. ACS Sustainable Chemistry & Engineering 7, 6769-6781.
Raikova, S., Smith-Baedorf, H., Bransgrove, R., Barlow, O., Santomauro, F., Wagner, J.L., Allen, M.J., Bryan, C.G., Sapsford, D., Chuck, C.J., 2016. Assessing hydrothermal liquefaction for the production of bio-oil and enhanced metal recovery from microalgae cultivated on acid mine drainage. Fuel Processing Technology 142, 219-227.
Shui, H., Jiang, Q., Cai, Z., Wang, Z., Lei, Z., Ren, S., Pan, C., Li, H., 2013. Co-liquefaction of rice straw and coal using different catalysts. Fuel 109, 9-13.

Shui, H., Shan, C., Cai, Z., Wang, Z., Lei, Z., Ren, S., Pan, C., Li, H., 2011. Co-liquefaction behavior of a sub-bituminous coal and sawdust. Energy 36, 6645-6650.
Sørum, L., Grønli, M.G., Hustad, J.E., 2001. Pyrolysis characteristics and kinetics of municipal solid wastes. Fuel 80, 1217-1227.
Stark, N.M., Matuana, L.M., 2007. Characterization of weathered wood–plastic composite surfaces using FTIR spectroscopy, contact angle, and XPS. Polymer Degradation and Stability 92, 1883-1890.
Taghizadeh-Alisaraei, A., Assar, H.A., Ghobadian, B., Motevali, A., 2017. Potential of biofuel production from pistachio waste in Iran. Renewable and Sustainable Energy Reviews 72, 510-522.
Taghizadeh, A., Rad-Moghadam, K., 2018. Green fabrication of Cu/pistachio shell nanocomposite using Pistacia Vera L. hull: An efficient catalyst for expedient reduction of 4-nitrophenol and organic dyes. Journal of Cleaner Production 198, 1105-1119.
Tan, X., Liu, Y., Zeng, G., Wang, X., Hu, X., Gu, Y., Yang, Z., 2015. Application of biochar for the removal of pollutants from aqueous solutions. Chemosphere 125, 70-85.
Tekin, K., Karagöz, S., Bektaş, S., 2014. A review of hydrothermal biomass processing. Renewable and Sustainable Energy Reviews 40, 673-687.
Tews, I.J., Zhu, Y., Drennan, C., Elliott, D.C., Snowden-Swan, L.J., Onarheim, K., Solantausta, Y., Beckman, D., 2014. Biomass Direct Liquefaction Options. TechnoEconomic and Life Cycle Assessment. ; Pacific Northwest National Lab. (PNNL), Richland, WA (United States), p. Medium: ED; Size: PDFN.
Tröger, N., Richter, D., Stahl, R., 2013. Effect of feedstock composition on product yields and energy recovery rates of fast pyrolysis products from different straw types. Journal of Analytical and Applied Pyrolysis 100, 158-165.
Uzoejinwa, B.B., He, X., Wang, S., El-Fatah Abomohra, A., Hu, Y., Wang, Q., 2018. Co-pyrolysis of biomass and waste plastics as a thermochemical conversion technology for high-grade biofuel production: Recent progress and future directions elsewhere worldwide. Energy Conversion and Management 163, 468-492.
Valdez, P.J., Nelson, M.C., Wang, H.Y., Lin, X.N., Savage, P.E., 2012. Hydrothermal liquefaction of Nannochloropsis sp.: Systematic study of process variables and analysis of the product fractions. Biomass and Bioenergy 46, 317-331.
Van Krevelen, D.W., 1950. Graphical-statistical method for the study of structure and reaction processes of coal. Fuel 29, 269-284.
Wall, L.A., Madorsky, S.L., Brown, D.W., Straus, S., Simha, R., 1954. The Depolymerization of Polymethylene and Polyethylene. Journal of the American Chemical Society 76, 3430-3437.
Wang, B., Huang, Y., Zhang, J., 2014. Hydrothermal liquefaction of lignite, wheat straw and plastic waste in sub-critical water for oil: Product distribution. Journal of Analytical and Applied Pyrolysis 110, 382-389.
Wang, S.-H., Griffiths, P.R., 1985. Resolution enhancement of diffuse reflectance i.r. spectra of coals by Fourier self-deconvolution: 1. C-H stretching and bending modes. Fuel 64, 229-236.
Wang, X., Zhou, W., Liang, G., Song, D., Zhang, X., 2015. Characteristics of maize biochar with different pyrolysis temperatures and its effects on organic carbon, nitrogen and enzymatic activities after addition to fluvo-aquic soil. Science of The Total Environment 538, 137-144.
Watson, J., Lu, J., de Souza, R., Si, B., Zhang, Y., Liu, Z., 2019. Effects of the extraction solvents in hydrothermal liquefaction processes: Biocrude oil quality and energy conversion efficiency. Energy 167, 189-197.

Wong, S.L., Ngadi, N., Abdullah, T.A.T., Inuwa, I.M., 2015. Current state and future prospects of plastic waste as source of fuel: A review. Renewable and Sustainable Energy Reviews 50, 1167-1180.
Wu, X., Liang, J., Wu, Y., Hu, H., Huang, S., Wu, K., 2017. Co-liquefaction of microalgae and polypropylene in sub-/super-critical water. RSC Advances 7, 13768-13776.
Xiu, S., Shahbazi, A., Shirley, V., Cheng, D., 2010. Hydrothermal pyrolysis of swine manure to bio-oil: Effects of operating parameters on products yield and characterization of bio-oil. Journal of Analytical and Applied Pyrolysis 88, 73-79.
Yang, C., Wu, J., Deng, Z., Zhang, B., Cui, C., Ding, Y., 2017. A Comparison of Energy Consumption in Hydrothermal Liquefaction and Pyrolysis of Microalgae. Trends in Renewable Energy 3, 76-85.
Zhou, C., Yang, W., 2015. Effect of heat transfer model on the prediction of refuse-derived fuel pyrolysis process. Fuel 142, 46-57.
Zhu, Y., Biddy, M.J., Jones, S.B., Elliott, D.C., Schmidt, A.J., 2014. Techno-Economic Analysis of Liquid Fuel Production from Woody Biomass via Hydrothermal Liquefaction (HTL) and Upgrading. Applied Energy, 129:384-394, Medium: X.

3.3 Supporting Information

3.3.1 Properties of pistachio hull feedstock

Table 3.3- 1–Properties of pistachio hull feedstock

Properties	Result	Method
Moisture	14.31 wt.%	ASTM E1755
Ash	4.24 wt. %	ASTM E1755
Volatile Matter	70.09 wt. %	ASTM E1755
Fixed Carbon	11.35 wt. %	ASTME1755
Carbon	41.22 wt. %	ASTM D5291
Sulfur	0.13 wt. %	ASTM E3177
Hydrogen	6.98 wt. %	ASTM D5291
Nitrogen	1.34 wt. %	ASTM D5291
Oxygen by Difference	46.08 wt. %	ASTM D5291
Lower Heating Value	17.45 MJ kg^{-1}	ASTM E711
Higher Heating Value	18.97 MJ kg^{-1}	ASTM E711

3.3.2 Feedstock elemental compositions

The elemental compositions of the plastic feedstocks is presented in Table 3.3-2. PE and PP had the highest energy content (measured as HHV) of all five feedstocks due to their high carbon and hydrogen content. PET possessed the lowest energy content as a result of its high oxygen content; the HHV of pistachio hull biomass was somewhat higher. Nylon contained high levels of nitrogen, and had an HHV of 28.6 MJ kg^{-1}. The initial energy contents and elemental compositions of the feedstocks will have an impact on the yields and compositions of bio-crudes produced by HTL, and high feedstock oxygen and nitrogen content can pose a significant challenge – O- and N-rich bio-crudes would require significant further upgrading to create usable fuels.

Table 3.3- 2– Elemental composition and HHV of plastics

Element Analysis (%)	C	H	O	N	HHV (MJ kg^{-1})
Pistachio hull	49.3	6.8	46.1	1.78	17.5
PE	84.9	12.2	2.9	<0.1	45.6
PP	85.1	13.3	1.5	<0.1	47.4
PET	43.7	4.0	52.0	0.41	11.2
NY	60.8	8.1	19.1	12.0	28.6

3.3.3 Calibration curves for quantification of unreacted plastics in bio-char using FTIR

The FTIR and resulting calibration curves for quantification of unreacted plastics in bio-char using FTIR are presented below. The quantity of unreacted plastic in bio-char samples was used to calculate, by extension, the percentage of plastic feed undergoing conversion to other products (bio-crude, aqueous or gaseous). This method makes a number of assumptions; in particular, that the bio-char formed from pistachio hull in the presence of plastics does not undergo any changes in composition, apart from containing unreacted plastics, and that any plastics in the bio-char are entirely unchanged. These assumptions mean that the method must be treated cautiously as a semi-quantitative approximation. In some cases, conversions <0% were observed; these have been approximated as 0% after accounting for error.

3.3.3.1 Polyethylene in bio-char

Figure 3.3-1a shows infrared spectra of eight samples of pure pistachio hull bio-char blended with unreacted PE at concentrations within the range 0–100 wt.%. The strong absorption band at 898 cm^{-1} was taken as a representative peak for pistachio hull bio-char. The band at 2917 cm^{-1} was chosen as a reference for PE. The relative intensities of the characteristic bands were used as indicators of PE content in bio-chars. Peak intensity ratios (PIR) were calculated for each blend, and used to create a calibration curve, shown in **Figure 3.3-1b**. A high coefficient of determination (R^2) was obtained for the calibration curve (0.9538). PIRs were then calculated from the FTIR spectra of the bio-char resulting from HTL of pistachio hull/polyethylene at 10 wt.% and 20 wt.% blends to quantify unreacted PE.

The calculated values for unreacted PE in co-liquefaction chars are summarised in **Table 3.3-2**. For the reactions carried out at a fast heating rate, the content of unreacted PE in the bio-char was calculated as 26 % and 60 % for 10 wt.% and 20 wt.% PE blend levels, respectively; 31 % and 63 % unreacted PE were detected in the bio-char for slow heating rates for 10 wt.% and 20 wt.% PE blends**.**

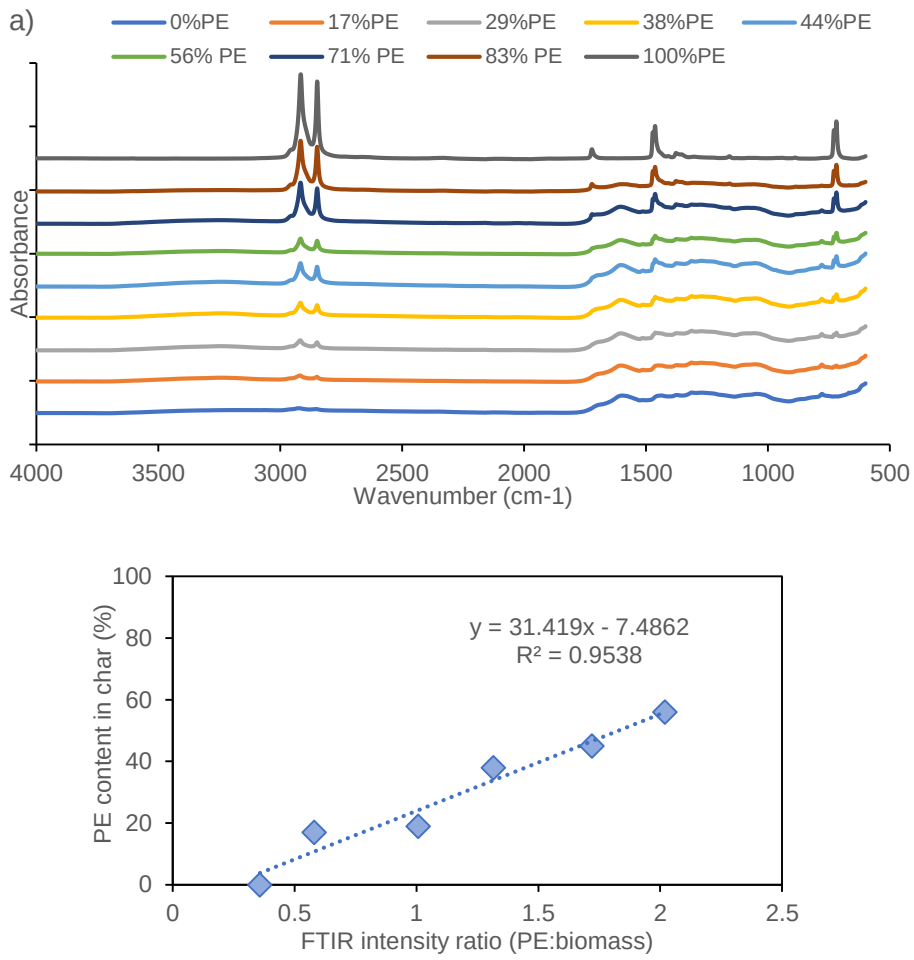

Figure 3.3- 1– (a) FTIR spectra of pistachio hulls bio-char with different polyethylene contents, and (b) peak intensity ratio calibration curve for polyethylene content in pistachio hull bio-char.

Table 3.3-3– Calculated percentage concentrations of unreacted polyethylene in bio-char from co-liquefaction of pistachio hull with PE.

	PE	Pistachio hull bio-char	PIR	Predictive equation	R^2	Unreacted PE in char (%)
	2917 cm^{-1}	**898 cm^{-1}**	**2917:898**	y = 31.419 + 7.4862	0.9538	
Fast heating rate						
10%PE	0.0434	0.0408	1.0640			26
20%PE	0.0582	0.0270	2.1578			60
Slow heating rate						
10%PE	0.037521	0.030315	1.237711			31
20%PE	0.097836	0.042746	2.288778			64

3.3.3.2 Polypropylene in bio-char

As previously, the absorbance band at 898 cm^{-1} was used as the indicative band for pistachio hull bio-char, whilst the strong peak at 2914 cm^{-1} was used to represent PP (**Figure 3.3-2a**). However, two calibration curves were created in this case for the blend level ranges 0–38 % PP in bio-char, and 38–100 % PP. Coefficients of determination of <0.85 were obtained in both cases. Unreacted polypropylene in bio-char was calculated to make up 37 % and 50 % of the total bio-char for the faster heating rate, and 55 % and 56 % for the slower heating rate for co-liquefaction of 10 wt.% and 20 wt.% PP blends in biomass, respectively (**Figure 3.3-2b**).

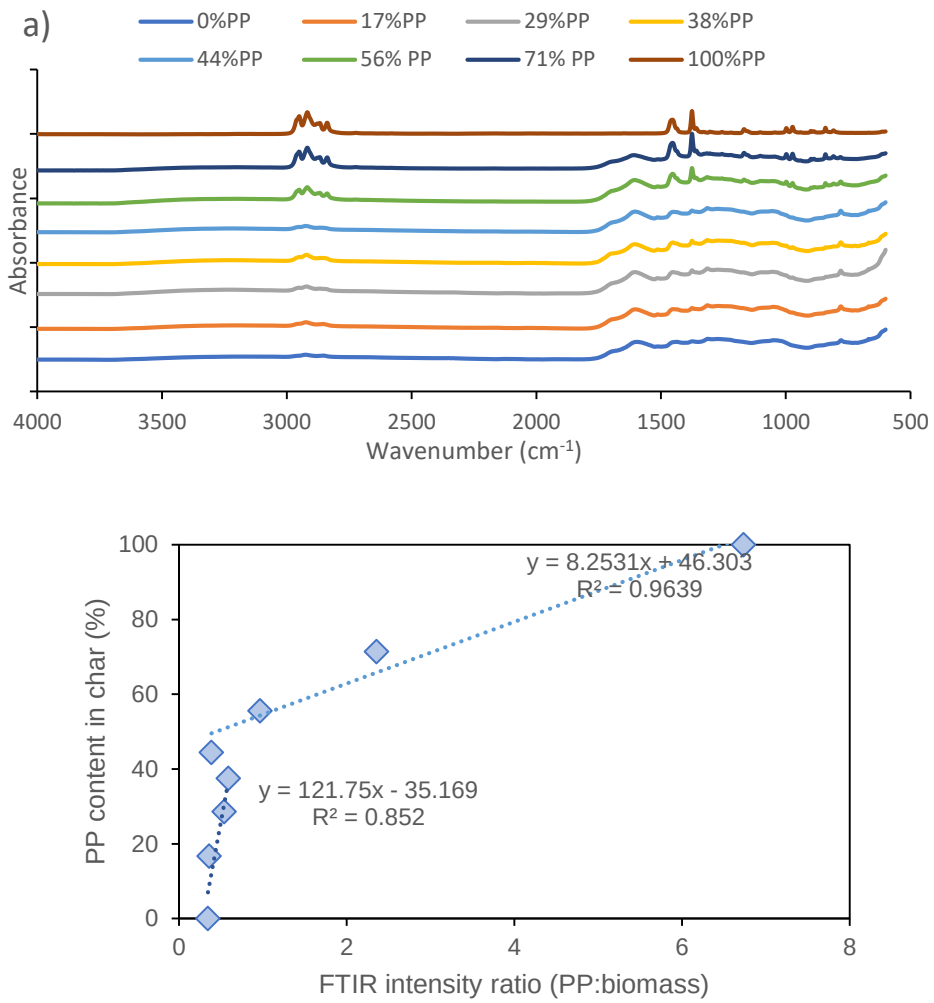

Figure 3.3- 2–(a) FTIR spectra of pistachio hull bio-char with different polypropylene contents and (b) peak ratio calibration curve for polypropylene in pistachio bio-char.

Table 3.3- 4–Calculated percentage concentrations of unreacted polypropylene in bio-char from co-liquefaction of pistachio hull with PP.

	PP	Pistachio hull bio-char	FTIR	Predictive equation	R2	Unreacted PP in char (%)
	2914 cm^{-1}	**898 cm^{-1}**	**2914:898**	0–37 % PP: y = 121.75x – 35.169 37–100 % PP: y = 8.2531 + 46.303	0.852 0.9636	
Fast heating rate						
10%PP	0.017744	0.029852	0.594401			37
20%PP	0.019885	0.028489	0.698003			50
Slow heating rate						
10%PP	0.040715	0.038076	1.06929472			55
20%PP	0.06919	0.057573	1.20177729			56

3.3.3.3 Polyethylene terephthalate in bio-char

For co-liquefaction of PET/biomass, difficulties in homogenising the calibration samples meant that a somewhat lower coefficient of determination was obtained for the calibration curve (R^2 = 0.81). A number of absorbances were examined, and the calibration curve for PET/biomass bio-char was established using the peak in the region 898 cm^{-1} as the reference for pistachio bio-char. The strongest absorption band observed for PET occurred at 726 cm^{-1} (assigned to the aromatic ring) (**Figure 3.3-3a**).

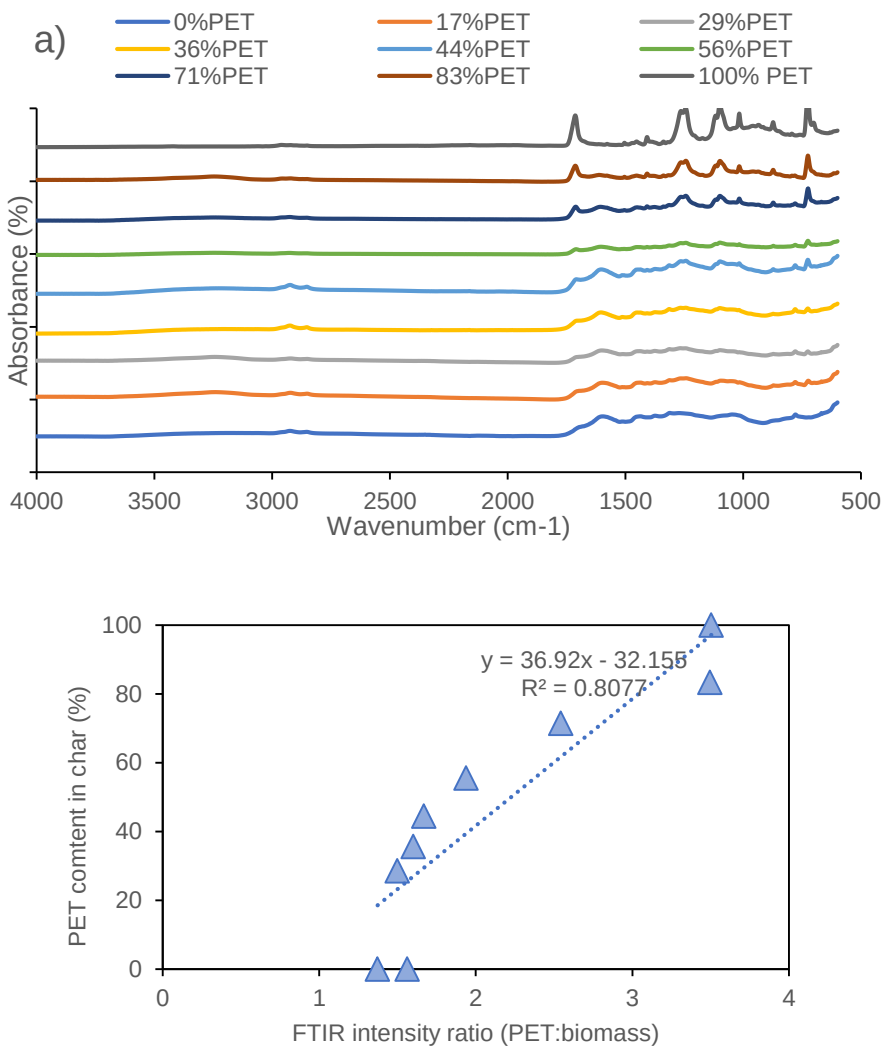

Figure 3.3- 3–(a) FTIR spectra of pistachio hulls bio-char with different polypropylene contents, and (b) peak ratio calibration curve for polyethylene terephthalate in pistachio bio-char.

Table 3.3-5– Calculated percentage concentrations of unreacted polyethylene terephthalate in bio-char from co-liquefaction of pistachio hull with PET.

	PET	Pistachio hull bio-char	FTIR	Predictive equation	R^2	Unreacted PET in char (%)
	726 cm^{-1}	**898 cm^{-1}**	**726:898**	y = 36.92x – 32.155	0.8077	
Fast heating rate						
10%PET	0.020853	0.016007	1.302738			22
20%PET	0.030037	0.048166	1.603535			32
Slow heating rate						
10%PET	0.070744	0.053181	1.330259			23
20%PET	0.08616	0.042746	2.01563			46

3.3.3.4 Nylon in bio-char

For nylon, the representative absorbance band was selected as 1534 cm^{-1}, whilst 898 cm^{-1} was used for pistachio hull bio-char. For all the calibration curves, the coefficient of determination (R^2) exceeded 0.98. The results showed that the content of unreacted nylon in co-liquefaction bio-char was around 11 % and 9 % for fast heating rates, and 7 % and 11 % for slow heating rate, for 10 wt.% and 20 wt.% nylon/pistachio blends respectively. This signifies a substantially higher overall conversion of nylon under HTL conditions relative to the other plastic feedstocks examined.

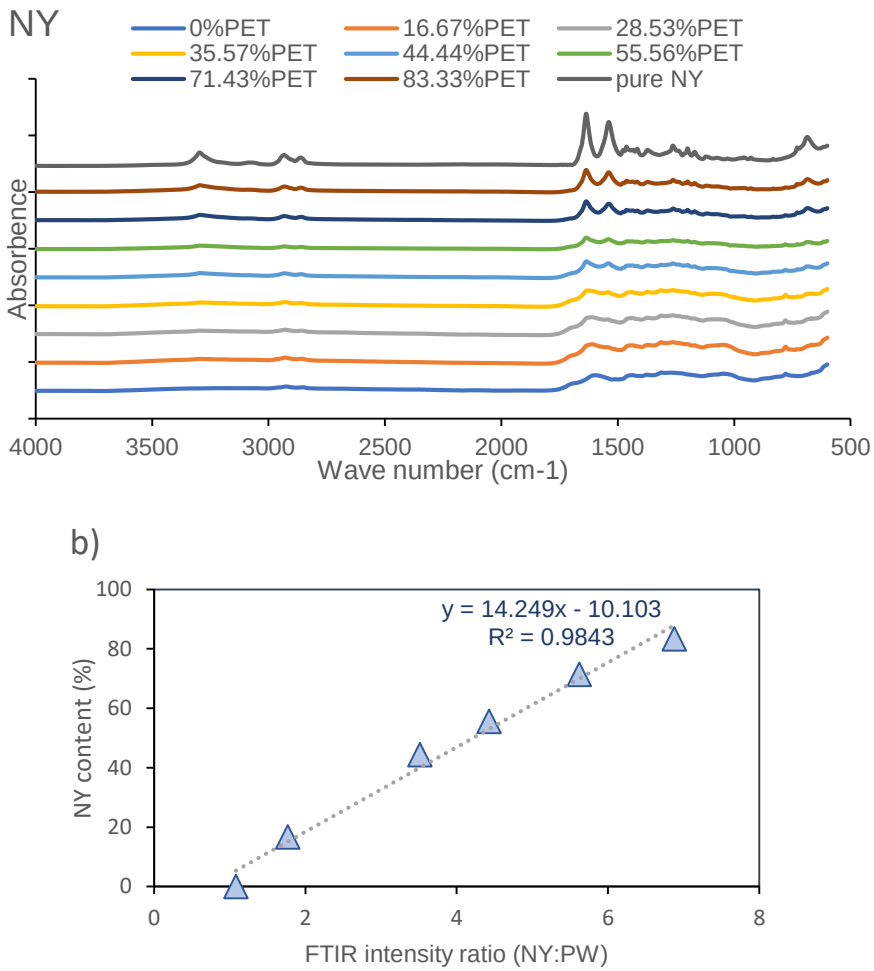

Figure 3.3- 4–(a) FTIR spectra of pistachio hulls with different nylon contents, and (b) Peak ratio calibration curve for nylon in pistachio bio-char.

Table 3.3-6–Calculated percentage concentrations of unreacted nylon in bio-char from co-liquefaction of pistachio hull with NY.

	NY	**Pistachio hull bio-char**	**PIR**	**Predictive equation**	**R^2**	**Unreacted NY in char (%)**
	1534 cm^{-1}	**898 cm^{-1}**	**1534:898**	y = 14.249x – 10.103	0.9843	
Fast heating rate						
10%NY	0.026013	0.017696	1.469988			11
20%NY	0.021795	0.015897	1.371049			9
Slow heating rate						
10%NY	0.045761	0.038718	1.181887			7
20%NY	0.087956	0.058233	1.510419			11

3.3.4 GC/MS analysis of bio-crudes

The identities of notable compounds in bio-crudes from co-liquefaction of biomass with plastics, identified using GC/MS, are presented in Table 3.3-7 below. Compounds were not quantified; shaded cells indicate the absence of a compound.

Table 3.3-7–Identities of notable compounds in bio-crude products from co-liquefaction of pistachio hull with 20 wt.% plastics (fast heating rate).

Compound identified	100 % biomass	20 wt.% PE	20 wt.% PP	20 wt.% PET	20 wt.% NY	20 wt.% mix
	Relative abundance					
Styrene			320745			370738
Butanoic acid, 4-hydroxy-	555800	524772	463658			487172
Cyclohexene, 4-ethenyl-					117169	
2-Cyclohexen-1-one, 4,4,6-trimethyl-			327277			
Phenol	1748957	1764367	1639160	2905453	2069189	1419738
.alpha.-Methylstyrene	334795	184735	305891	183980	330672	304528
Benzaldehyde			233307		264411	254020
Butyrolactone			388487			491578
Hexylene glycol			448884			684768
2-Cyclopenten-1-one, 2-methyl		258402	398410	154595	89514	384487
2-Cyclopenten-1-one, 3-methyl	386653	431833	327277	325882	340141	245221
2-Cyclopenten-1-one, 3-ethyl	180489	297973	231749	239845	210307	187640
2-Cyclopenten-1-one, 2,3-dimethyl	618682	660493	421747	408508	275334	542303
Phenol, 2-methyl	209783		181936			135424
Phenol, 2-methoxy-	1506464	1414807	1519534	1367993	1385734	1189135
Benzyl alcohol			159569		157003	145497
Phenol, 3-methyl		1239350	173031	219530		
Phenol, 4-ethyl	3980328	4634501	3166427	6533153	3220049	2737315
Acetophenone					282086	195127
p-Cresol	960836	235095	651421	923189	1056847	589546
Mequinol	776023				1314107	
3-Pyridinol	1639160	2665148	1857657	2889085	1162499	1307163
4-Pyridinemethanol		413203				

Compound identified	100 % biomass	20 wt.% PE	20 wt.% PP	20 wt.% PET	20 wt.% NY	20 wt.% mix
	Relative abundance					
2(1H)-Pyridinone, 3-methyl-				479071		
3-Pyridinol, 6-methyl-		482456		581366		
1-Cyclohexene-1-carboxylic acid		317478		347132		
1,2-Cyclooctadiene				339719		
Hydroquinone				669883		
Benzoic acid		161156				
Cyclooctane, 1,2-dimethyl-					705208	425765
Phenol, 4-ethyl-	3980328	4634501	275787	6533153	3220049	2737315
Tetradecane						313850
4-Tetradecene, (E)-						564945
Decane, 6-ethyl-2-methyl-						208372
Cresol	147932	468572	213148	731227		212187
Catechol	147932	1644297	567404	1811004	695666	576335
Caprolactam					42365211	7359304
1,2-Benzenediol, 4-methyl-	174119	634680		591879		
Phenol, 2,6-dimethoxy-	669943	2616128	1032654	3203293	1125849	975146
Phenol, 4-ethyl-2-methoxy-	283017	585694	351921	821260	401040	442576
Diphenyl sulfone						436289
Benzene, (ethylthio)-				378465		
1,2-Benzenediol, 3-methyl				241300		
1,2-Benzenediol, 3-methoxy				1138188	515636	353141
1,4-Benzenediol, 2-methyl-				536597		
Benzene, 1,2,4-trimethyl-5-(1-methylethyl)-						
Phenol, 2,6-dimethoxy-		2616128		3203293	1125849	975146
Phenol, 2-methoxy-4-propyl-		228483		383352		
Phenol, 4-methyl-2-nitro-				535130	401040	442576
4-Ethylthiophenol				729522		
Ethanone, 1-(2-hydroxyphenyl)-		249812				

Compound identified	100 % biomass	20 wt.% PE	20 wt.% PP	20 wt.% PET	20 wt.% NY	20 wt.% mix
	Relative abundance					
Phenol, 3-pentadecyl-1-Hexadecyne	3493575			7550140 375031	1267726	

3.3.5 FTIR of bio-chars obtained at from slow HTL (60 min)

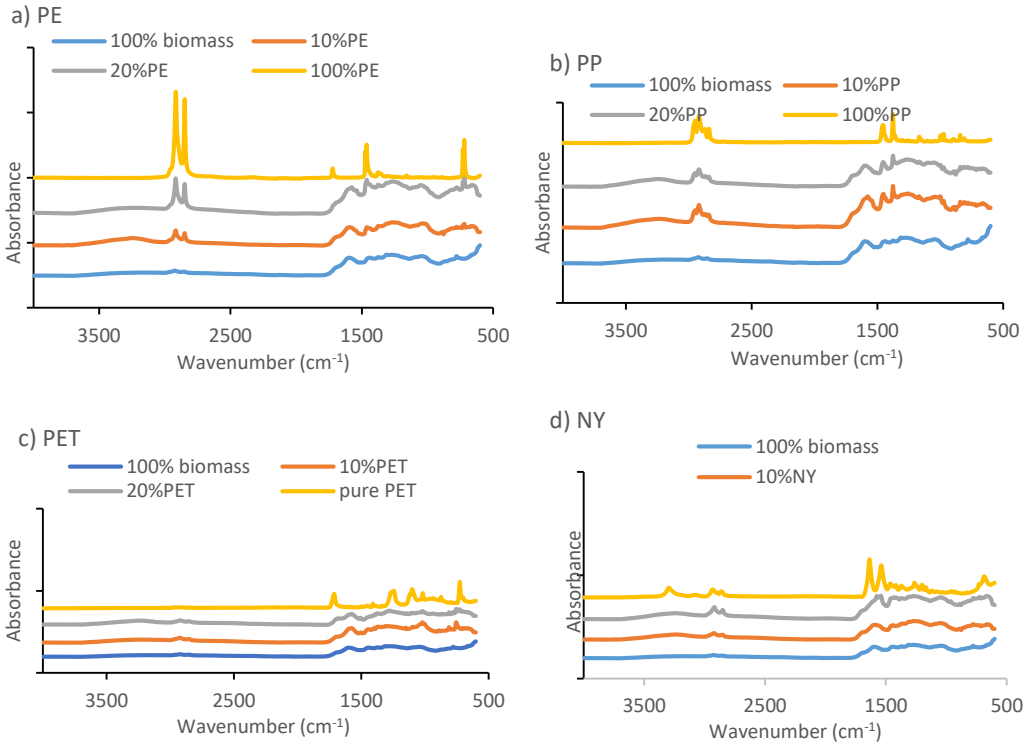

Figure 3.3-5 FTIR of pure plastics and bio-char from slow (60 min) HTL of pistachio hull with (a) polyethylene, (b) polypropylene, (c) polyethylene terephthalate, and (d) nylon 6.

3.3.6 Biomass proximate analysis

Table 3.3-8–Analysis of pistachio hull feedstock

Analyses	***Pistachio hull***
Proximate (wt.%)	
Total ash	9.4
Water Extractable Others	15.6
Biomass composition (wt.%)	
Lignin	26.6
Glucan	13.6
Xylan	5.0
Galactan	2.8
Arabinan	4.8
Fructan	0.0
Acetyl	1.4
Elemental (wt.%)	
C	41.22
H	6.98
N	1.34
O	46.08

Chapter 4

Valorising plastic contaminated waste streams through the catalytic hydrothermal processing of polypropylene with lignocellulose

4.1 Context

In the previous chapter HTL was shown to be successful in the co-liquefaction of plastics and pistachio hulls into a bio-crude, aqueous phase and solid residue product. Co-processing of pistachio hulls and plastic have potential to improve the properties of the bio-crude products compared to individual feedstocks. However, it was also shown that the polyolefin was not activated under the HTL conditions with only a limited degree of decomposition observed.

While co-processing of plastic with waste agriculture residues can help process waste plastic unsuitable for recycling, even out seasonal supply in a biorefinery and enhance future energy security, the major plastic waste stream are polyolefins. Therefore, it is important that these more recalcitrant polymers can also be converted in a bio-refinery.

Catalytic HTL is a potential technique to enhance plastic conversion and improve the yield and quality of biofuels. Homogeneous alkali catalysts, such as Na_2CO_3, offer several advantages that make them particularly suitable for lignin oxidation, improve biomass conversion and produce a crude with less oxygen and a higher hydrogen content. Metal catalysts have also gained attention as alternative catalyst support materials due to their high surface area and high chemical stability. Alternatively, zeolite catalysts have been recognized as the highest efficiency catalyst in cracking and have a significant shape-selective effect on the production of aromatics.

Additionally, synergistic effects on the use of formic acid as catalyst have been reported. The formic acid acts as an acid catalyst, promoting hydrolysis of the biopolymers at lower temperatures, leading to an increase of the interaction of soluble products. The formic acid is a source of H_2 as the acid can degrade over heterogeneous catalysts to produce hydrogen.

The aim of this chapter therefore was to assess these typical HTL catalysts, generally used to increase bio-crude yields in either HTL or pyrolysis reactions, and whether they could be further utilised to aid the breakdown of polypropylene in the co-liquefaction of biomass and polypropylene. The effect of adding a range of organic and inorganic catalysts was to evaluate the conversion from co-processing of pistachio hulls with polypropylene. The mechanism was also explored with the addition of the radical scavenger butylated hydroxytoluene.

This work was published in ACS Omega 2020. **Sukanya Hongthong**, Hannah Leese, Christopher J. Chuck*. Valorising plastic contaminated waste streams through the catalytic hydrothermal processing of polypropylene with lignocellulose, ACS Omega 2020

This chapter is submitted in an alternative format in line with Appendix 6A of the "Specifications for Higher Degree Theses and Portfolios" as required by the University of Bath

The work completed in this paper was conducted by the author with the exception of the following:

Elemental analysis was carried out by analytical department personnel at London Metropolitan University.

4.2 ACS Omega Paper

Valorising Plastic-Contaminated Waste Streams through the Catalytic Hydrothermal Processing of Polypropylene with Lignocellulose

4.2.1 Abstract

Food waste is a promising resource for the production of fuels and chemicals. However, increasing plastic contamination affects the efficiency of conversion for the more established biological routes such as anaerobic digestion or fermentation. Here, we assessed a novel route through the hydrothermal liquefaction (HTL) of a model waste (pistachio hulls) and polypropylene (PP). Pure pistachio hulls gave a bio-crude yield of 34% (w/w), though this reduced to 16% (w/w) on the addition of 50% PP in the mixture. The crude composition was a complex blend of phenolics, alkanes, carboxylic acids and other oxygenates, which did not change substantially on the addition of PP. Pure PP does not breakdown at all under HTL conditions (350 °C, 15% solids loading), and even with biomass there is only a small synergistic effect resulting in a conversion of 19% PP. This conversion was enhanced through using typical HTL catalysts including Fe, $FeSO_4$, $MgSO_4$, $ZnSO_4$, ZSM-5, aluminosilicate, Y-zeolite, and Na_2CO_3; the conversion of PP reached a maximum of 38% with the aluminosilicate for example. However, the PP almost exclusively broke down into a solid phase product, with no

enhancement of the bio-crude fraction. The mechanism was explored, and with the addition of the radical scavenger butylated hydroxytoluene (BHT) the conversion of plastic reduced substantially, demonstrating that radical formation is necessary. As a result, the plastic conversion was enhanced to over 50% through the addition of the co-solvent and hydrogen donor; formic acid, and the radical donor, hydrogen peroxide. The addition of formic acid also changed the crude composition, including more carboxylic acids and oxygenated species than the conversion of the biomass alone, however, the majority of the carbon distributed to the volatile organic gas fraction producing an array of short chain volatile hydrocarbons, which potentially could be repolymerised as a polyolefin or combined with the bio-crude for further processing. Catalytic HTL was therefore shown to be a promising method for the valorisation of polyolefins with biomass under typical HTL conditions.

4.2.2 Introduction

Declining fossil fuel reserves and an increasing awareness of their environmental impact has led to an increased interest in developing alternative resources for energy production. Organic solid waste, such as municipal and agricultural food wastes have huge potential as a renewable energy feedstock, and are now starting to be collected and converted into energy such as methane through anaerobic digestion. However, increasing levels of plastic in these waste streams interfere with the biological processing [1]. These plastics are typically polyolefins derived from plastic films, and as such have a relatively high energy content, therefore the valorisation of both streams simultaneously is a promising alternative for waste management.

Using pyrolysis, typically at 500 °C, to co-process lignocellulosic and plastics has gained much attention in the last few decades [2]. Under these conditions, polyolefins break down into a range of volatile components which make it an effective co-material for improving the quality of biomass during co-processing [3]. Polyolefin polymers such as polyethylene and polypropylene are composed of approximately 14 wt.% hydrogen which make them a good source of liquid hydrocarbons in the process [4], and therefore when decomposed with biomass through rapid heat processing, the quantity and quality of bio-oil produced can be improved. There have been several studies on co-pyrolysis of plastic and biomass which showed the beneficial synergistic effects in terms of increased liquid oil conversion.[5]

While pyrolysis offers an effective route to convert the plastic, the waste stream must be dried prior to conversion often reducing the energy balance substantially [6]. This is particularly true of wet feedstock's such as food wastes. A more effective route for processing wet food wastes is through hydrothermal liquefaction, where the slurry is processed at between 270-350 °C, keeping the water in the liquid phase under pressure, resulting in a bio-crude, aqueous phase and solid residue. The high pressure maintains the solvent in the liquid state and the combination of high pressure and temperature leads to a reduction of the dielectric constant and density, which allows solubility of more non-polar hydrocarbons [7]. Additionally, the key to HTL is the reduction in oxygen content, which is removed as carbon dioxide and water [8], leading to lower oxygen content and higher energy liquid crude oil. This makes it more comparable to the heating value for conventional petroleum fuels[9-10] and reduces the operative costs of handling equipment and storage [11].

While polyolefin/biomass co-liquefaction has been demonstrated under supercritical conditions with temperatures up to 440 °C, above the decomposition temperature of these polymers, this is far beyond the HTL region.[12] There have been far fewer studies into the co-liquefaction of plastic waste blended with biomass in the HTL range, though this could make the reaction conditions milder, allow an improved energy balance through not drying the feedstock and improve the decomposition of plastic at lower temperatures [13-15].

The majority of these studies to date have demonstrated the co-liquefaction of plastics with marine algae. The investigation into the co-liquefaction of microalgae and macroalgae with plastic blends for example, suggested the presence of plastics can alter the composition of the bio-crude fraction and presented some evidence of the minor deposition of the polyolefins in the crude fraction [16-18]. Recently Hongthong *et al* demonstrated that a range of plastics could be co-processed with pistachio hulls through hydrothermal liquefaction, with nylon and PET breaking down substantially. However, the polyolefins only demonstrated a minor synergistic effect with less than 7% of the polypropylene and polyethylene being converted under HTL conditions when 20% polymer was added [19]. A similar result was seen for the co-liquefaction with macroalgae [17].

In the hydrothermal liquefaction process, the presence of catalysts can restrain the side reactions, reduce the operational conditions, increase the chemical reactivity,

reduce the formation of solid residues, and enhance the yield and quality of bio-crude [20]. Homogeneous alkali catalysts have been used widely to this end in several investigations. For example, it was reported that alkali catalysts can improve biomass conversion giving a crude with less oxygen and a higher hydrogen content [21-22]. Na_2CO_3 is the most frequently used as a homogeneous catalyst in this regard [23]. Microporous and mesoporous catalysts for the conversion of plastic waste into liquid oil and char have also been reported in several studies recently. Metal catalysts have also gained attention as alternative catalyst support materials due to their high surface area and high chemical stability. Though it should be noted that the HTL conditions of high temperature in an aqueous environment severely limit the use of more unstable organometallic species. For example, a number of groups have demonstrated that the addition of iron (Fe) enhanced the hydrocarbon content and overall yield and quality of the bio-crude [24-25].

The most widely used cracking catalysts are acidic materials such as aluminosilicates and zeolites. Zeolite catalysts are one of the most effective catalysts because they can remove a significant number of oxygenated compounds and have a significant shape-selective effect on the production of aromatics [26-27]. At high temperatures, above 450 °C, during hydrocarbon cracking, the primary vapors diffuse into internal pores of the catalysts which are absorbed on the acid sites and converted to hydrocarbons [28]. Indeed in the HTL reaction, a zeolite catalyst was demonstrated to increase bio-crude yields in the liquefaction of *Nannochloropsis*.[29].

Formic acid is also a widely used catalyst in liquefaction. Formic acid is one of the main products from biomass decomposition and is attractive as both an organic catalyst and as a sustainable source of hydrogen as it can break down into H_2 and CO_2.[30] When used under HTL conditions, the formic acid is thought to act as an acid catalyst, promoting hydrolysis of the biopolymers at lower temperatures, increasing the interaction of soluble products and is a source of H_2 as the acid can degrade over heterogeneous catalysts to produce hydrogen. Interestingly, formic acid has been demonstrated to give higher bio-oils yields, in the liquefaction of lignin, than with hydrogen. The authors reasoned that the hydrogen was being released in the liquid phase, as such formic acid was able to deliver hydrogen far more effectively than hydrogen gas which has very low solubility in any of the phases present.[31] The hydrogen production prevents undesirable side reactions that lead to coke and

therefore leads to lower solid residue, and elevated gas production (including volatile organics).[32]

No studies have demonstrated the effective catalytic conversion of PP under HTL conditions, though for the conversion of polypropylene under higher temperatures, a number of studies have demonstrated the effective use of aluminosilicate to reduce the reaction time, lower the optimal temperature of chain scission and support the production of a narrow range of shorter chain hydrocarbons typical of the radical and catalytic cracking reactions.[33] In addition to the catalytic cracking of PP, aluminosilicates have also been demonstrated to be suitable for enhancing the degradation of biomass and polyolefins under pyrolytic conditions (375 °C).[34] In this process the cellulose derived from lignocellulosic biomass was thought to go through a sequence of dehydration, decarbonylation, and decarboxylation reactions to form furan type compounds. These could react with olefins in the presence of zeolite through Diel-Alder reactions followed by dehydration reaction to form aromatics.[35] In addition, olefin and alkanes can act as hydrogen donors for cellulose derived-oxygenated species in the presence of a zeolite catalyst [36]. The presence of hydrogen donor solvents also aids in stabilizing the lignin radicals and saturate reactive compounds to enhance bio-crude production[37].

However, while all of these studies were conducted under pyrolysis conditions, no studies have demonstrated the effective depolymerisation of polypropylene with biomass under HTL conditions, below the supercritical point of water. Therefore, the aim of this research was to determine whether a typical thermochemical catalyst, generally used to increase bio-crude yields in either HTL or pyrolysis reactions, could be further utilised to aid the breakdown of polypropylene in the co-liquefaction of biomass and PP and aid the production of further valuable products from this stream. To this end co-processing of pistachio hull and PP was undertaken with the addition of a range of organic and inorganic catalysts and the mechanism of conversion extrapolated.

4.2.3 Result & Discussion

4.2.3.1 Effect of catalyst on the HTL product distribution

While our previous work has demonstrated that HTL is a suitable process for the depolymerization of various oxygenated plastics with biomass, polyolefins are not activated by the biomass at these low temperatures, they largely do not react and rather distribute into the solid residue intact [17, 19]. In an attempt to design a system that can be used to co-process these materials, a range of commonly reported HTL catalysts were used in the co-liquefaction of 50 wt.% PP blends with pistachio hulls. This loading was selected as the highest potential level of PP that would be included in a biorefinery, and was demonstrated in previous studies as the optimal loading to still allow the analysis of the break down products even under low conversions of the initial polymer.[17-19] During hydrothermal liquefaction, the feedstock decomposed quickly to generate; bio-crude, aqueous residue, solid residue and a gas phase. Mass balances are shown in Fig. 1 where product yields were calculated on the basis of total feedstock input and the mass balance is the sum of the bio-crude, solid, gas and aqueous residue combined,

The bio-crude production for the liquefaction of pistachio hull under these conditions was found to be 34 wt%. On the addition of 50% PP this was reduced to 16 wt% suggesting that the polymer is not being converted under these conditions. The biocrude yield, with additional catalysts in the co-liquefaction resulted in a similar yield of bio-crude to the control without additional catalyst. The yield of the bio-crude product remained approximately the same (16.0% vs 16.2%) for aluminosilicate and 16.4% for Fe catalyst loading. Similarly, the yields for $FeSO_4.7H_2O$, Y-zeolite, and ZSM-5, were 15.6, 15.1, and 14.9%, respectively. The addition of Na_2CO_3 was found to deplete the bio-crude substantially, with yields decreasing from 16.0% to 6.0%.

Similarly, the gas phase product obtained from the presence of catalysts was comparable to those obtained for 50 wt.% PP blends with pistachio hulls without catalyst. The yield of gas phase products increased from 8.9% for non-catalytic to 12.4%, 10.9%, 10.2%, and 10.0% for $FeSO_4.7H_2O$, $ZnSO_4.7H_2O$, Fe, and $MgSO_4.H_2O$, respectively, but a small reduction was observed for the aluminosilicate and zeolite type catalysts. This strongly suggests that the PP is not being cracked into volatile organics species under these conditions.

For the aqueous phase residue yield, a modest increase was found with the addition of $MgSO_4.H_2O$ (23.5%) as well as with Na_2CO_3 (17.3%), $FeSO_4.7H_2O$ (16.2%), $ZnSO_4.7H_2O$ (14.5%), and ZSM-5 (14.5%) from 2.9% for the non-catalysed reaction. In contrast, the aqueous phase residue yield was not significantly impacted by the addition of aluminosilicate, Y-zeolite, and Fe.

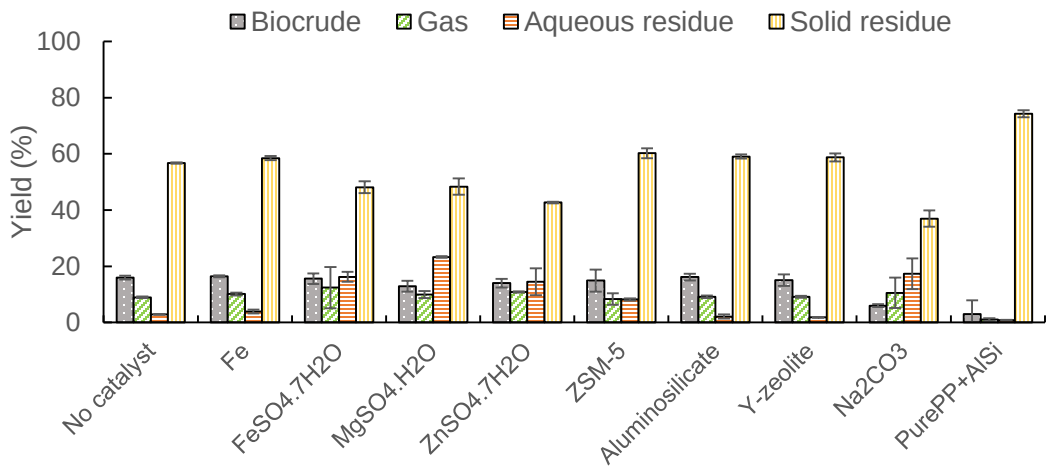

Figure 4.2- 1–Mass balance of HTL product from the co-liquefaction of pistachio hull with 50% PP blends in the absence of catalyst and with 20 w/w% of different catalysts (Fe, $FeSO_4.7H_2O$, $MgSO_4.H_2O$, $ZnSO_4.7H_2O$, ZSM-5, aluminosilicate, Y-zeolite, and Na_2CO_3).

The co-liquefaction of PP with pistachio hull mainly contributed to an increase in the solid residue with both the presence and absence of catalyst. The most significant impact was observed for co-liquefaction of 50% PP blends with pistachio hull and ZSM-5, with an increase in solid residue yield from 56.7% to 60.2%. The high solid recovery was observed following the addition of aluminosilicate, Y-zeolite, and Fe (solid residue yield of 59.1%, 58.7%, 58.5 %, respectively), which were similar to those obtained for 50% PP blends in pistachio hull without catalyst loading. In contrast, the solid residue phase yield decreased with the addition of $MgSO_4.H_2O$ $FeSO_4.7H_2O$, $ZnSO_4.7H_2O$, from 56.7% to 48.3%, 48.1%, 42.7%, respectively, and substantially decreased to 37% for Na_2CO_3 loading.

Irrespective of catalyst, the polypropylene did not break down and distribute into the crude phase and rather distributed into the solid residue phase. The reason is either the polymer is not reacting, as previous studies have demonstrated [19], or that it is

breaking down into a solid such as elemental carbon. To check the synergistic effect of co-liquefaction of biomass and plastic with and without catalyst, pure PP was also reacted under these conditions. The synergistic effect of the interaction between biomass and plastics can be determined through the equation:

Synergistic effect = $Y_{BC} – (X_{PWPP} \times Y_{PWPP} + (1–X_{PP}) \times Y_{PP})$,

where Y_{BC} is yield of bio-crude obtained in experiment, X_{PWPP} is the mass fraction of pistachio hull and PP in the total reaction mixture, X_{PP} is the mass fraction of pure PP, Y_{PWPP} is the bio-crude yield of pistachio hull with 50% blend PP without catalyst and Y_{PP} is the bio-crude yield of pure PP.

Some synergistic effect for the co-liquefaction of biomass with PP was observed for all the catalysts except Na_2CO_3 (Fig. 2a). The positive correlation was observed for the total bio-crude yield, with the highest positive correlation of 3.6% for the presence of Fe. A lower synergistic effect was observed with aluminosilicate (3.4%). The presence of $FeSO_4.7H_2O$, $ZnSO_4.7H_2O$, ZSM-5 and y-zeolite all had a lower effect on the conversion of 2.8%, 1.2%, 2.1% and 2.3%, respectively). The smallest positive correction was found for the presence of $MgSO_4.H_2O$ (0.1%).

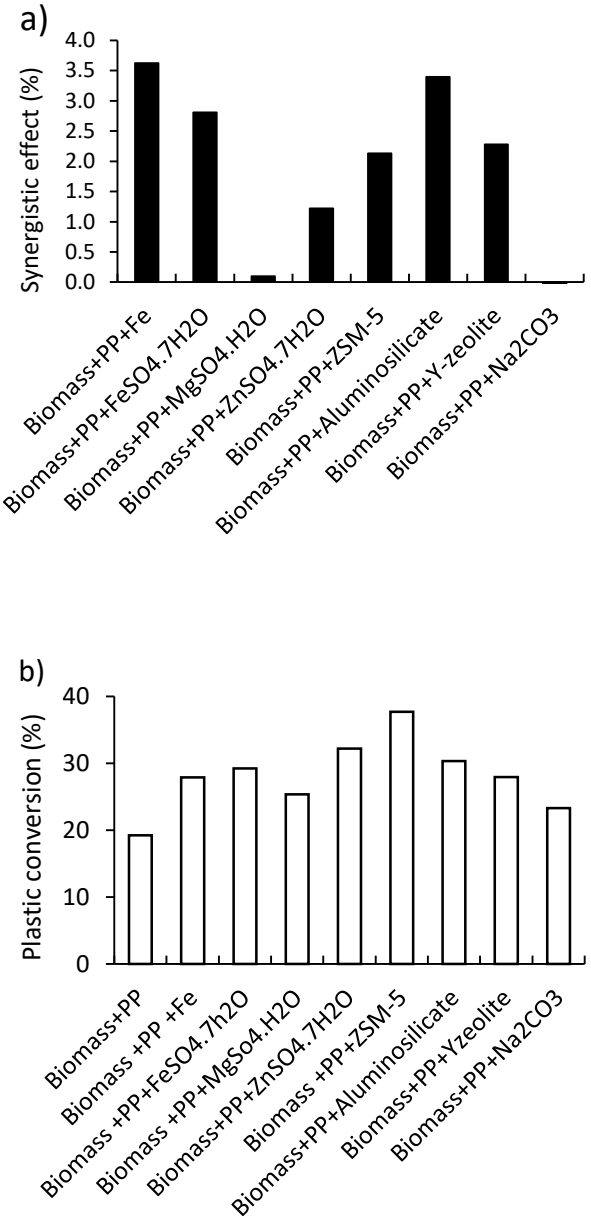

Figure 4.2-2 a) Synergistic effect of bio-crude obtained from pure PP with aluminosilicate and co-liquefaction of PP/biomass with different catalyst b) Extent of plastic conversion at 350°C, calculated using FT-IR (see supporting information for further details)

4.2.3.2 Product characterization

4.2.3.2.1 Bio-crude composition

The initial mass balance suggests that if the polypropylene is breaking down, then it is not distributing substantially into the bio-crude. Further analysis of the bio-crude supports this conclusion, with the elemental composition not changing substantially relative to bio-crude produced without a catalyst (Fig. 3a). All the bio-crudes were characterized by high carbon content, similar hydrogen levels, and reasonably low alternative elements, this suggests the bio-crude was largely unchanged by the addition of the catalysts in this system, and that the catalysts all distributed largely into other phases. As such, the energy content distributing into the crude remains relatively low.

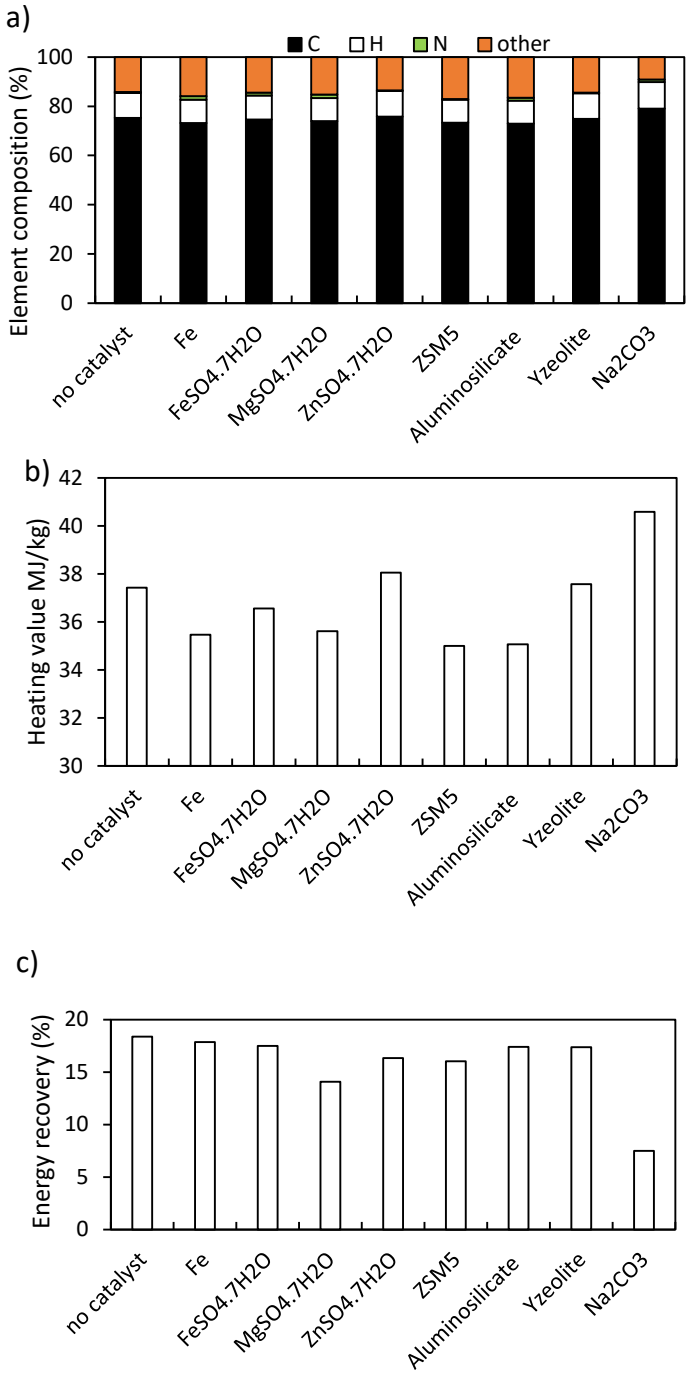

Figure 4.2-3–a) Elemental composition (determined by elemental analysis), b) heating value of the bio-crude, and c) energy recovery of bio-crude of 20 wt.% catalyst loading

To examine the effect of the additional catalyst on bio-crude composition, the bio-crudes produced from the co-liquefaction of pure pistachio hull, biomass/PP blends, and 20 wt.% aluminosilicate in biomass/PP blends were characterized by GC-MS. The major compounds (quality >80%) of the bio-crude oils are summarized in the Supporting Information (Table 3.3-5). From the GC-MS analyses, more than 50 compounds were observed in each bio-crude sample. The chemical composition of the bio-crude product fraction is connected mainly with the origin of the biomass. Some alkanes were observed in high amounts in the presence of PP blends and seem to be formed by specific interactions with the addition of catalyst. Each bio-crude contained several phenolic compounds, these presumably originate from lignin, which is one of the major components of the pistachio hulls. Additionally, the major chemical compositions were detected in the level of carboxylic acid compounds such as 3-cyclohexene-1-carboxylic acid, and alkane compounds such as decane 4-ethyl, decane 2,4-dimethyl. Similar changes were found in previous work by the co-pyrolysis of biomass with PP [38], which suggests that there is some, albeit very limited, breakdown of the PP into hydrocarbons.

For the presence of PP, a small increase in ketone and ester formation was also observed. Additionally, increased levels of ethanone, benzo-furan, carboxylic acids, ester, and methyl ester were present. These compounds were not found from the bio-crude derived from pure pistachio hull, suggesting that the co-liquefaction with PP blends can affect the chemical composition of bio-crude oil. In a previous study Coma et al demonstrated that ketones and esters were formed in the breakdown of polyethylene with microalgae, [18] suggesting that these are formed by the limited breakdown of PP catalytically.

For the presence of catalyst (aluminosilicate), an increase in carboxylic acids and fatty acids was observed. These results indicate the interaction and synergistic effect of aluminosilicate catalytic HTL during co-processing of biomass with PP blends. However, 2,4-dimethylhept-1-ene, a typical breakdown species for polypropylene formed during pyrolysis [39-40], was not observed, suggesting that the mutual influence of co-liquefaction of biomass and PP during the thermal decomposition was not completed. These findings were also confirmed in the study of functional groups in solid residue through FT-IR with the presence of unreacted PP.

The bio-crude ^{1}H NMR spectrum are given in the supporting information (Fig. S3). While exceptionally complex, specific regions, relating to functional groups, were integrated and divided into five ppm ranges (Fig. 4). The ^{1}H NMR results showed that the resulting bio-crude was of a similar bulk composition when obtained from co-liquefaction in both the presence of catalyst and without catalyst. ^{1}H NMR showed a high percentage of alkane functional groups for bio-crude oil, this suggests that the contribution of the alkane compounds was derived from the decomposition of triglycerides of pistachio hull during HTL processing. The addition of Y-zeolite demonstrated the highest alkanes (48.2%) and alcohol functionality (30%) but the lowest percentage of α-to-heteroatom functionality (22%), this suggests that there is low nitrogen content in these samples. The presence of aluminosilicate had the highest percentage of α-to-heteroatom functionality (23.6%), which was approximately the same as with ZSM-5 (23.2%). All bio-crudes presented a low percentage of the aromatic and the methoxy functionality (0.0-0.2%), which are consistent with carbohydrates converting into bio-crude, and the catalyst not cracking polypropylene and reforming is as aromatic species.

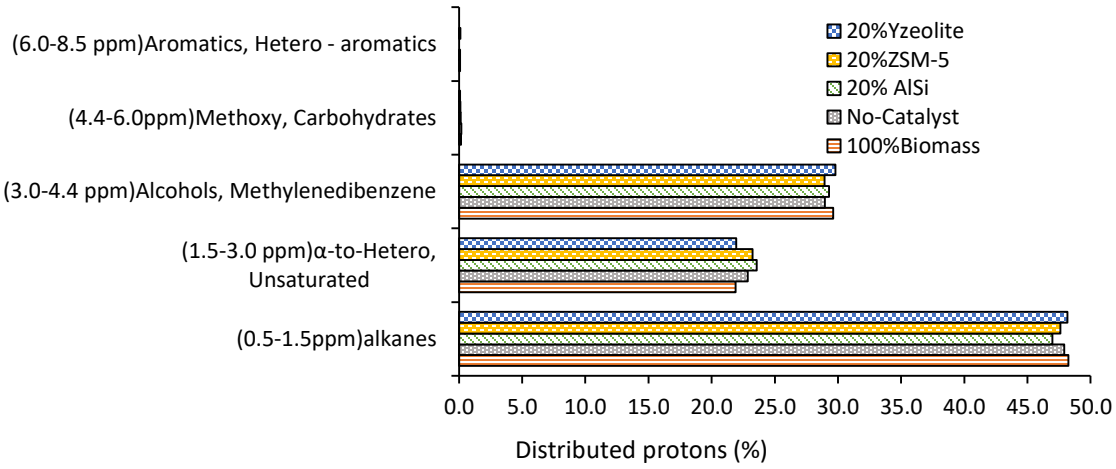

Figure 4.2- 4– ^{1}H NMR spectroscopy results of the percentage of integrated peak area regions for each range of ppm with respect to the total integral.

4.5.2.2.2 Aqueous residue characterisation

The co-liquefaction with additional catalysts, reduced the carbon and nitrogen content in the resulting aqueous phase (Table 4.2-1). The total organic carbon and total

nitrogen in the aqueous product phase is distributed very similarly, with the range of 5.2-9.7 gL^{-1} for carbon concentration and 0.3-0.7 gL^{-1} for nitrogen. This suggests that the breakdown of PP is not producing water-soluble species that are distributing into the aqueous phase.

The only significant difference is the aqueous phase produced by the co-liquefaction with Na_2CO_3, which shows a substantially increased carbon content, and slightly increased nitrogen content in the aqueous phase at 30.0 gL^{-1} and 1.0 gL^{-1}, respectively. This is presumably due to the formation of carbonic acid and sodium hydroxide with the decomposition of Na_2CO_3 in water.

Table 4.2- 1–Elemental composition of aqueous phase produced from co-liquefaction of polypropylene

Sample	TOC (g L-1)	TN (g L-1)
50%PP and Biomass	9.7	0.7
20%Aluminosilicate	7.0	0.5
20%ZSM5	6.3	0.3
20%Yzeolite	6.2	0.5
20%Na_2CO_3	30.4	1.0
20%Fe	6.5	0.6
20%$FeSO_4.7H_2O$	5.2	0.5
20%$ZnSO_4.7H_2O$	6.7	0.6
20%$MgSO_4.H_2O$	7.1	0.5

4.5.2.3 Solid-residue composition

The FT-IR spectra of the solid residue demonstrates that a large proportion of the PP is breaking down, however, hardly any typical breakdown products are observed in the bio-crude or the aqueous phase, the gas phase also remains constant. It is therefore likely that the breakdown products are distributing into the solid residue itself.

All FT-IR spectra of solid residue produced are present in Supporting Information (Fig. S1a-S1h). Generally, the spectra all show a similar intensity of peaks corresponding to stable compounds formed during the HTL process. Those produced show an intensive absorbance at ~2800-3000 cm^{-1} and ~1300-1500 cm^{-1} suggestive of an aliphatic functional group and aromatic group, respectively. However, the intensity of these peaks decreased slightly in the solid residue produced from the addition of Fe, ZSM-5, aluminosilicate, and Y-zeolite. These results suggest that there is a synergistic interaction between those catalysts thus improving decomposition. However, the addition of those catalysts did not significantly breakdown polymer blends/biomass into bio-crude, they were mostly broken down into the solid residue with the most likely compounds being aromatic species and elemental carbon.

Overall, the elemental composition changed during thermal HTL processing. All solid residue products had a higher C content and lower O/H ratio than the raw material used (Fig. 5a), which suggests that dehydration and polymerization occurred during the HTL process. Compared to the co-liquefaction of biomass with PP without a catalyst, the C content slightly decreased from 84.7% to 83.8%, 78.9%, 78.8%, and 78.6% for Na_2CO_3, $FeSO_4.7H_2O$, $ZnSO_4.7H_2O$, and $MgSO_4.H_2O$, respectively. In contrast, the C content decreased substantially from 84.7% to 66.6%, 63.1%, 62.0% and 54.3% for aluminosilicate, Fe, ZSM-5, and Y-zeolite, respectively. This result can be confirmed by the appearance of the peaks at ~2920 and 2850 cm^{-1}, and ~1400 cm^{-1} during liquefaction as proposed in the FT-IR spectra. These intensive peaks enhanced the C content of the solid residue, which strongly suggests the presence of unreacted polymer. The N content was not significantly impacted by any of the additional catalyst loadings, with a similar N content of 0.1-0.5% for each experiment. The addition of Y-zeolite caused the H content to decrease substantially from 14.3% to 8.5%, while the addition of aluminosilicate, ZSM-5, and Fe caused the H content to decrease from 14.3 % to 11%, 10.5%, and 10% respectively. The O content again was

not strongly affected, with a slight increase of 2.2-4.0% with the exception of Na_2CO_3 (a decrease from 2.2% to 1.2%).

The HHVs of solid residue produced were calculated as shown in Fig. 5b. As low oxygen was obtained, the solid residue produced from co-liquefaction of 50% PP blends/biomass without catalyst showed the highest HHVs observed at 48.7 MJ kg^{-1}. Reduced HHVs were observed at 48.1 MJ kg^{-1}, 43.7 MJ kg^{-1}, 43.5 MJ kg^{-1}, 43.2 MJ kg^{-1} for Na_2CO_3, $FeSO_4.7H_2O$, $MgSO_4.H_2O$, and $ZnSO_4.7H_2O$, respectively. A substantial reduction in the HHV was observed for the other solid residues produced with Fe (34.4 MJ kg^{-1}), aluminosilicate (37.1 MJ kg^{-1}), ZSM-5 (35.3 MJ kg^{-1}) and Y-zeolite (29.8 MJ kg^{-1}). This is highly suggestive that the polypropylene is breaking down somewhat into a less energy-dense material with the alternative catalysts as opposed to the non-catalytic residue, which has an HHV very similar to PP. Because of its high heating value, solid residue obtained from the co-liquefaction of pistachio hull and PP in the addition of catalyst could potentially be used as a solid fuel.

Van Krevelen diagrams of solid residues are used to determine the degree of aromaticity and maturation during thermochemical degradation. During the HTL process, some of the oxygen in the biomass is removed in the form of H_2O (dehydration) or CO_2 (decarboxylation). A reduction of H and O content in the substance can be defined by the H/C and O/C ratio. The diagram shows the comparison of biomass with peat and lignite, brown coal, coal and anthracite. The H/C ratio is related to the degree of carbonization, where the O/C is also a useful measure of the surface hydrophilicity due to O relating to polar-group content [41-43]. While the amount of PP in the samples obviously makes these solids difficult to compare with alternative biomass samples in the literature, the comparison across the dataset is illuminating. Overall, H and O were exhausted in the bio-residues examined and it became carbon-rich during hydrothermal liquefaction. The O/C ratios of solid residue produced were substantially increased compared to the raw feedstock (Fig. 6). The O/C ratio of solid residue produced was very low, presumably in part due to the unreacted PP in the solid, with O/C ratios of 0.01-0.1 observed. The lower O/C ratio showed more aromatic and less hydrophilic content of the solid residue produced due to a higher degree of carbonization and extinction of polar functional groups during hydrothermal processing. For H/C ratio, the co-liquefaction of 50% blends PP/biomass

without catalyst and the addition of catalysts provided a similar level of H/C ratio (0.16-0.17).

So, while, the solid residue could be combusted akin to a coal product, the presence of PP in the sample would still be problematic from a regulatory point of view [44]. However, potentially a higher value route might be to use the solid remediator as a soil remediation fertiliser. The high carbon content of solid residue can provide beneficial properties for maximizing the amount of carbon storage [45], and in effect takes fossil carbon from the PP and converts it into a bio-available, long-term carbon storage option when coupled with reforestation [46].

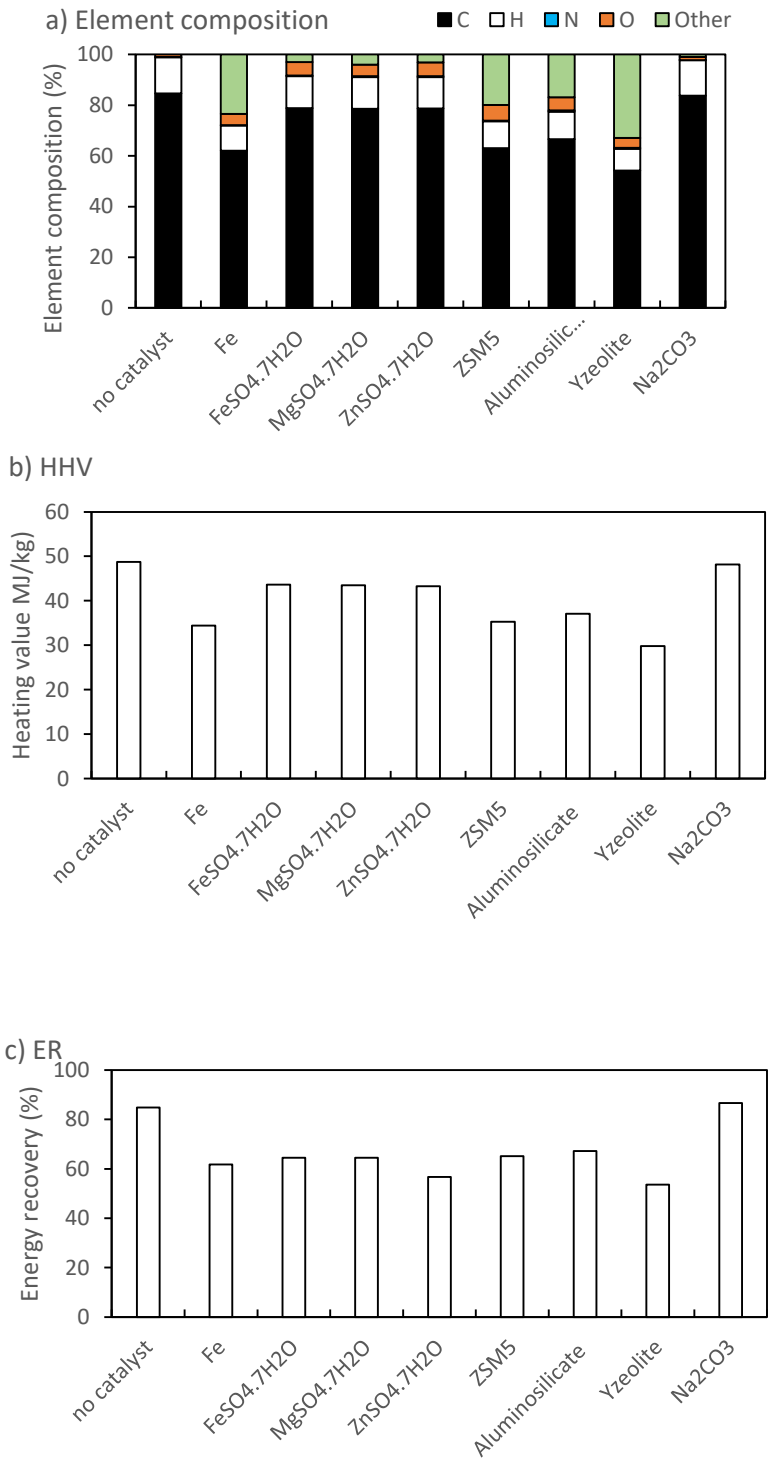

Figure 4.2- 5 a) Elemental composition of the solid residue of 20 wt.% different catalyst loading, b) heating value, and c) energy recovery (%)

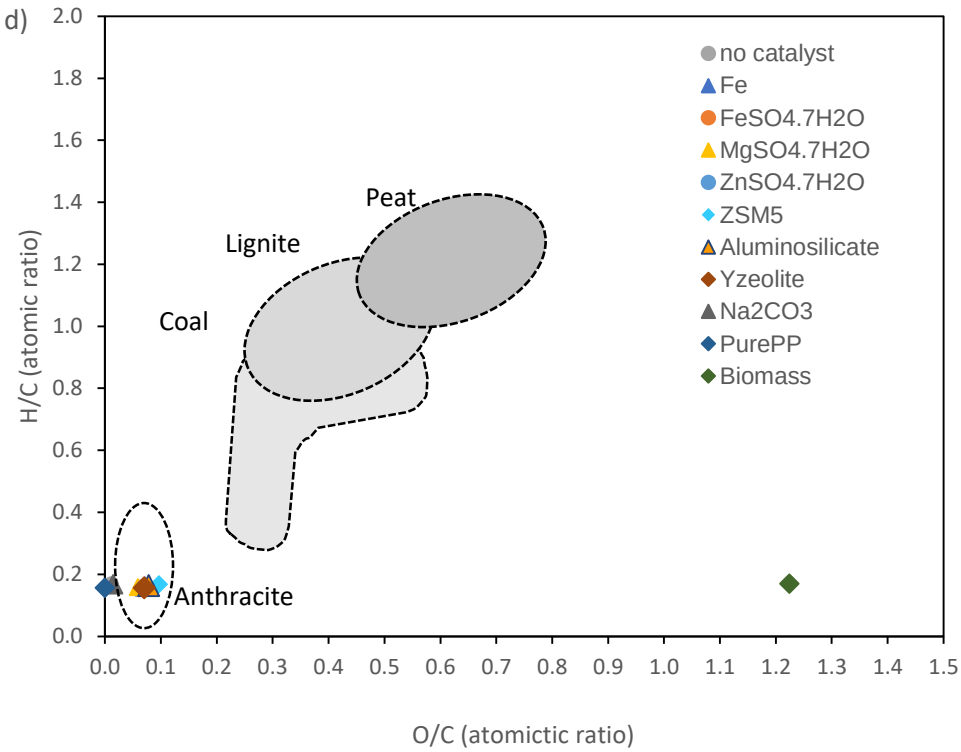

Figure 4.2- 6. Van Krevelen diagram with H: C and O: C molar ratio of various catalysts and without catalyst for co-liquefaction of polypropylene and pistachio hull

4.2.5.4 Enhancing the liquefaction of PP and biomass

Due to the lower HHV of the solid residue, higher conversion rates and low cost, aluminosilicate was taken forward as a suitable catalyst for further development. Significant research into HTL has been achieved with a very fast heating rate and short reaction time [47], however the exact mechanisms of the HTL still remain unclear mainly due to the complexity of the feedstock and HTL product [48]. While high heating rates favour higher crude production, a slower heating rate may possibly affect the decomposition of plastic and increase bio-crude yields [49]. The experiments were therefore conducted using slower heating rates of 7.7 °C min^{-1} with the total time of 45 minutes for the co-liquefaction of PP/Biomass with the presence of aluminosilicate. As the reaction time increased, the bio-crude oil yield did not increase significantly (Fig. 7a), solid residue and gaseous products from all long reaction times also produced similar results. This finding indicates that a long reaction time was not an essential factor in the depolymerisation of PP in this study.

HTL was also carried out at this lower heating rate and rapid heating rates (33 °C min^{-1}) over different temperatures (250 °C, 300 °C, and 350 °C), and gave rise to lower overall conversions of plastics in all cases with the exception of reaction temperature at 350 °C (increase from 17 to 26 % conversion for slow heating rates). This indicates that faster heating rates are preferred for balancing both overall bio-crude yield and plastic conversion. This demonstrates the synergistic effect of processing the PP with biomass and using a catalyst, as there is no appreciable conversion of PP at this temperature range when PP is added to water alone.

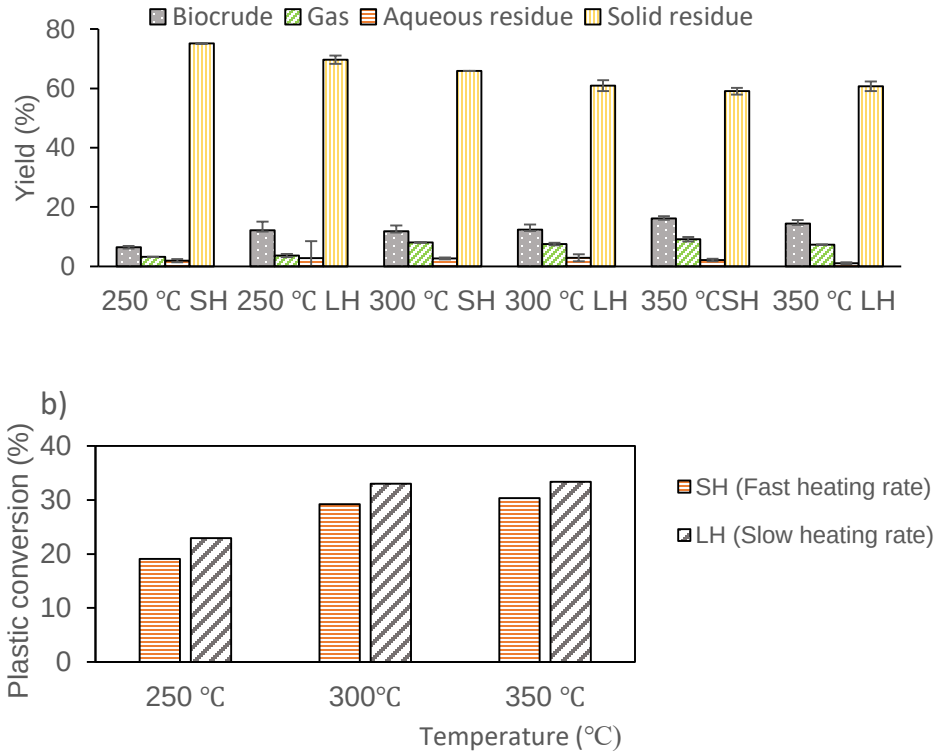

Figure 4.2- 7. a) Effect of faster heating rate on product yield and mass balance on different temperature and reaction rate of faster heating rate (SH), and slow heating rate (LH) for the aluminosilicate catalysed HTL conversion of PP and pistachio hulls, b) the estimated plastic conversion for the same system calculated through FT-IR.

Despite the catalysts improving the conversion yield substantially compared to the non-catalytic route the mechanism of conversion remains unclear. To assess the major pathway for the liquefaction, three further organic additives were used in the aluminosilicate catalysed reaction of PP and pistachio hull. Firstly, the co-liquefaction of biomass/PP blends with the aluminosilicate catalyst was undertaken in the presence

of formic acid. Formic acid has been demonstrated to give higher crude yields in the HTL of microalgae [30], and breaks down into H_2 and CO_2 under high temperatures as well as acting as an acid catalyst which increases the interaction of soluble HTL products during hydrothermal liquefaction and prevents undesirable side reactions which has been shown to lead to lower solid residues and an increase in gas production [32]. As such, in the liquefaction of lignin, formic acid has been demonstrated to increase bio-oil yields, decreasing the amount of carbon that goes into the solid residue.[31]

Another possible mechanism is the free radical decomposition, to investigate this a stable radical donor (hydrogen peroxide, H_2O_2) was added, and this was compared to the radical scavenger antioxidant: butylated hydroxytoluene (BHT). Hydrogen peroxide has been applied for enhancement of liquid yield from liquefaction to many types of biomass, aiding in the generation of radicals [50-52]. During liquefaction, the hydrogen peroxide can oxidize unsaturated side chains and crack aromatic rings as part of lignin leading to improvement of the polymerization and enhancement of the degradation in solvent effectively [51, 53-54]. Besides, hydrogen peroxide gives a source of radicals that may aid the radical scission of the PP chain.

The product distribution and PP conversion is given in Fig. 8a. The addition of FA showed bio-crude obtained increased from 12% to 20%, whilst slightly increased from 12% to 14.1% with the presence of hydrogen peroxide, but bio-crudes remained unchanged in the presence of BHT. Gas yield were significantly impacted on the addition of formic acid, and increased from 7.2% to 33.0%. Gas yields also increased in the presence of H_2O_2, from 7.2% to 12.2%, but remained unchanged in the presence of BHT. These findings suggest that formic acid is breaking down into CO_2 and H_2 which has led to the increase in gas fraction, as previously observed [20]. However, this would give a theoretical increase of gas phase produce yields to approximately 29.4%, assuming no hydrogen reacts with the products, much lower than observed, suggesting an increased breakdown of biomass and PP into the gas phase. This was confirmed with a range of over 150 volatile organic compounds observed by gas phase GC-MS (see supporting information), this effect was also observed in the liquefaction of lignin with formic acid in ethanol [55].

The amount of solid residue substantially decreased from 67.8% for the catalysed process to 30.3% with the addition of formic acid and to 38.2% in the addition of H_2O_2. The presence of FA and H_2O_2 in HTL reactions decreased the solid residue formation substantially, suggesting that both the addition of hydrogen and the generation of free radicals aided the decomposition of the PP chain, through either a cracking or free radical scission reaction, that produced elevated levels of VOC in the gas stream. The role of the free radical mechanism was further demonstrated by reducing the polymer scission on the addition of BHT.

To optimise the system further formic acid was added to the aluminosilicate catalysed reaction at both 250, 300 and 350 °C (Fig. 8c). At a reaction temperature of 250°C, the bio-crude yields tended to decrease concomitantly with solid residue formation decreasing. A substantial increase in bio-crude yield was observed when the reaction was performed at 300°C, with the solid residue product reduced. However, the reaction at 350 °C did not result in higher bio-crude yields obtained compared to 300°C but a slight increase was found in terms of gas-phase formation.

On analysis, the condensable gas phase was found to contain over 164 C3-C10 compounds. Over 60% of these were hydrocarbons, with 33% of the total compounds being branched or linear alkanes and alkenes, this contained significant proportions of branched C7-C10 fragments, including high levels of 2,4-dimethylhept-1-ene, other substituted C9 alkenes and propylene. (full analysis is given in the Table T4.3-6 and Fig. 4.3-4 in the Supporting Information). The amount of unsaturated species in the volatile phase supports a free radical, or catalytic cracking mechanism.

The presence of aluminosilicate facilitates the cracking of polypropylene due to the high surface area and acidity, with the pore size providing some shape selectivity for small species. The addition of the hydrogen donor further enhances the cracking and hydrogenation reactions. Therefore, the incorporation of the formic acid seems to aid the fluid catalytic cracking reaction leading to a range of low MW alkenes as the final product. Since polypropylene degradation takes place initially on the external surface of catalyst and disperses into small internal cavities of catalyst, they further degraded to the small size of gaseous hydrocarbons, particularly iso-alkanes and alkenes. This is supported by the product profile which is consistent with other similar pyrolysis studies, where a high content of volatile hydrocarbons were achieved from cracking

over the acidic alumiosilicate catalyst.[28, 33] These results suggest that PP can be thermally depolymerised under these conditions forming a range of alkene fragments suitable for further valorisation either to recombine in to an upcycled polyolefin polymer or combined with the crude for further hydroprocessing into a fuel.

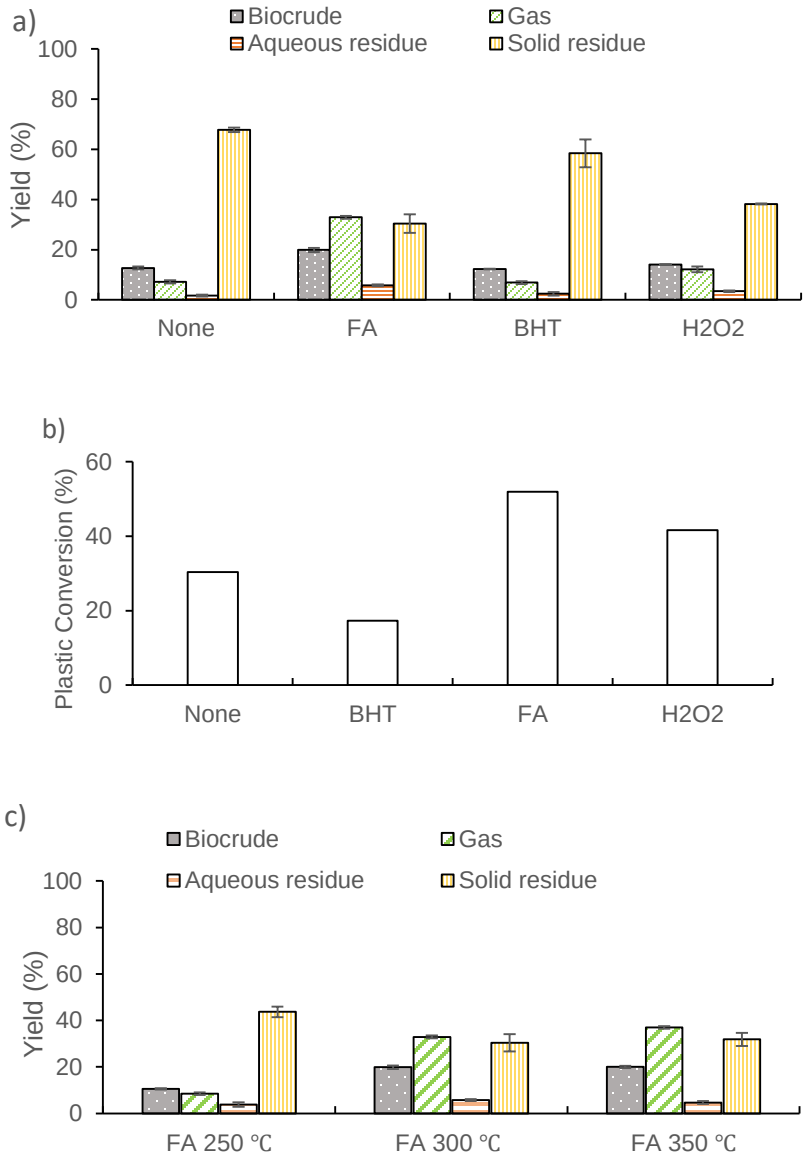

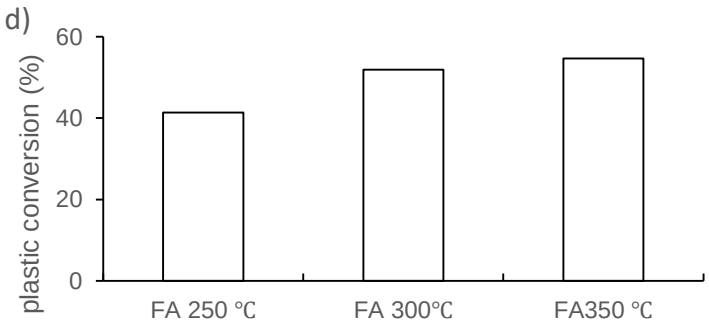

Figure 4.2- 8. a) Effect of the addition of FA, H_2O_2, and BHT on the product yield distribution on co-liquefaction biomass with 50 wt.% PP blends with 20% aluminosilicate loading at 300 °C and 10 min reaction time, b) plastic conversion (%), c) Effect of the addition of formic acid (FA) on the product yield distribution with different temperature, and d) plastic conversion (%) of the addition of FA

4.2.4 Conclusions

Increasing plastic contamination in biomass waste streams is a significant issue which interferes with traditional fuel processing routes. Here we report a possible solution through the catalytic co-liquefaction of biomass and polypropylene. Previous work demonstrated that in water alone below 370 °C there is no appreciable conversion of PP, with the addition of biomass, a synergistic effect does occur but leads to very low conversions (<10%). In this study, the effect of using an additional catalyst in the hydrothermal liquefaction of biomass with polypropylene was investigated for the first time. The bio-crude was largely unchanged by the addition of the catalysts in terms of elemental composition, however using aluminosilicate species, a large proportion of the polymer could be converted into a solid residue suitable for use as a possible solid fertiliser or further energy product. The activity could be further enhanced by adding either a radical promotor or the organic hydrogen donor formic acid. This reduced the amount of fossil carbon going to the solid fraction and rather volatile organic species were predominantly produced, with the majority of the components being C3-C10 branched hydrocarbon fragments. The ability to stop the reaction through the addition of BHT demonstrated the importance of a radical mechanism for the depolymerisation. This work demonstrates that it is possible to combine polyolefins in a HTL biorefinery, though catalysis and additional radical producers are needed to produce a suitable range of products. This volatile organic carbon stream could be used to produce further polyolefins in a circular economy methodology or be combined with the crude product

and hydrotreated to add to the total liquid energy product produced from this system. Future studies should therefore aim to assess the viability of adding hydrogen and radical donors to the HTL system.

4.2.3 Material and methods

4.2.3.1 Feedstock sources and characterization

Pistachio hull was selected as a representative of agriculture waste based on our previous work in this area, and the relatively high lipid and protein content of the feedstock.[19] Pistachio hull biomass (3 mm particle size) was sourced as a waste material after pistachio processing from the Wonderful Company, CA, USA. The full characterisation is given in the supporting information. Polypropylene (PP) was selected as the fossil based plastic, with an average molecular weight number M_W=12,000 g mol^{-1}, was sourced from Sigma-Aldrich and ground to a particle size of <350 µm. Iron (Fe), $FeSO_4.7H_2O$, $MgSO_4.H_2O$, $ZnSO_4.7H_2O$, aluminosilicate, Y-zeolite, Na_2CO_3, hydrogen peroxide, and butylated hydroxytoluene were all purchased from Sigma Aldrich and used without further purification. ZSM-5 (Zeolyst CBV 3024E) was purchased from Zeolyst International and used without further treatment or purification. Formic acid was purchased from Fisher chemicals and used without further purification. Further material analysis is given in the supporting information (Table 4.3-1).

4.2.3.2 Co-processing hydrothermal liquefaction

Co-hydrothermal liquefaction of multiple solid wastes was carried out using a stainless-steel batch reactor of 50 ml. According to a previous relevant study [17], the reactor was equipped with a pressure gauge and pressure relief valve, and a needle valve to release gaseous products. The temperature was monitored using a thermocouple inside the reactor, placed half way down the length and was connected to data logging software and used to control the temperature of the reaction. The experiments contained either 1.5g of PP and 1.5g of pistachio hull for the control experiments, or 1.2g of PP, 1.2g of pistachio hull and 0.6g of catalyst (either Fe, $FeSO_4.7HO_2$, $MgSO_4.7HO_2$, $ZnSO_4.7H_2O$, ZSM5, aluminosilicate, Y-zeolite, or Na_2CO_3). This gave a total catalyst loading of 20 w/w% of the overall mixture in the reactor. For the further additive experiments, 0.65 g of formic acid (FA), 0.5 g of

Hydrogen peroxide (H_2O_2), or 0.02 g of Butylated hydroxytoluene (BHT) was mixed with 15 g of distilled water to form a slurry feedstock, this was then added to the 3g of total solids. A total of 18 g of slurry feedstock was therefore loaded into the reactor for each reaction and the reactor was sealed and loaded into a preheated furnace to 800 °C (rapid heating rate) or 600 °C (lower heating rate).

As reaction time is also considered to play an important role in the product fraction and HTL pathway, the reactor was held in the furnace until the temperature reached 350 °C for either 10 min (furnace temperature of 800 °C, heating rate of 33 °C min^{-1}) and 45 min (furnace temperature of 600 °C, heating rate of 7.7 °C min^{-1}). Upon reaching the desired temperature, the reactor was removed from the furnace rapidly and allowed to cool to room temperature. Each experiment was repeated at least three times to determine the average values and the standard deviation. Both the reactor set-up and examples of the temperature profile for the reactions are given in the supporting information. The pressure is generated predominantly by the water being heated, and reached approximately 165 bar under the conditions tested at 350 °C, 100 bar at 300 °C and below 45 bar at 250 °C.

4.2.3.3 Separation of liquefied product

After cooling, gaseous products were released via the needle valve into an inverted, water-filled measuring cylinder to determine the total gas volume. Gas-phase yield was determined according to literature precedent, by using the ideal gas law and assuming that the gas was completely CO_2 [25]. The liquid-solid mixtures were filtered through a filter paper to separate the aqueous phase from the water-insoluble fraction (consisting of the bio-crude and solid residue). The solid-liquid mixture remaining on the filter paper was washed repeatedly with chloroform until the solvent was clear. The chloroform was removed using a rotary evaporator at 40 °C for 1.5 hours to isolate the bio-crude. The solids were oven-dried overnight at 60°C to determine the solid phase product yield as “solid residue”. An aliquot of the aqueous phase products was dried overnight at 60°C to determine the yield of non-volatile organics and inorganics in the aqueous phase, designated as “aqueous residue”.

4.2.3.4 HTL product characterization

FT-IR and ^{1}H NMR

Functional group information in the solid-phase and bio-crude products was derived through FT-IR and NMR spectroscopic data. FT-IR spectra were recorded using a Thermo Scientific Nicolet iS5 FTIR spectrometer in the wavenumber range from 4000 to 600 cm^{-1}. FTIR was also used to assess the level of unreacted plastic remaining in the solid phase products as a proxy for the extent of plastic conversion (the same method reported in our previous works [19]).

^{1}H NMR spectra were collected using a Bruker Avance III NMR spectrometer operating at 500.13 MHz, using Topspin 3.5. Samples were prepared by dissolving bio-crude oil in deuterated chloroform. Samples were then filtered to remove any suspended particulates before loading into NMR tubes. Spectra were obtained using the zg30 pulse sequence, with td = 65536 and ns = 16 and a relaxation delay of 1 s.

Element composition and energy recovery

Elemental analysis of the biomass feedstock and products was conducted at London Metropolitan University. Samples were processed for carbon, hydrogen, and nitrogen on a Carlo Erba Flash 2000 Elemental Analyser. Oxygen analysis of solid residue was analyzed at Elemental Microanalysis in Devon UK. The higher heating values (HHV; MJ kg^{-1}) of the biomass, solid residue, and bio-crude were calculated using the Dulong formula [29, 56-57] based on the elemental composition; $HHV = 0.3383C + 1.422 \times (H-O/8)$. The energy recovery in each product phase was calculated as the bio-crude divided by that combined feedstock; Energy recovery = HHV product (%) × Mass of product (%)/ HHV of feedstock (%).

Bio-crude composition by gas chromatography–mass spectroscopy (GC-MS)

The chemical composition of the volatile fraction of the bio-crude was identified by comparing the mass spectra with those in the NIST mass spectral database using an Agilent Technologies 8890 GC system fitted with a 30 m × 250 µm × 0.25 µm HP5-MS column, coupled to a 5977B inert MSD. Samples were dissolved in THF, and helium (1.2 mL min^{-1}) was used as the carrier gas. The initial oven temperature was set to 50 °C, increasing to 250 °C at 10 °C min^{-1}.

Gas analysis by gas chromatography–mass spectroscopy (GC-MS)

Approximately 50 ml of each gas sample was collected to Texax tube (TA 200 mg 35/60 Mesh Inert coated conditioned stainless-steel TD tube) and analyzed using a TD100-XR GC system coupled to an 8890 gas chromatograph (Agilent) with 5977B MSD (Agilent). The column was Agilent HP-5MS (30 m, 0.25mm, 0.25µm). Pre-trap fire purging was performed for 1 min, after which the trap was fired at 300 °C for 3 min. Split flow during trap desorption was 50 ml min^{-1} resulting in a split ratio of 42:1. Helium was applied as carrier gas at 1.2 mL min^{-1}. The column program was started at 40 °C which was held for 7 min, and increased at a rate of 10 °C min^{-1} to 150°C and then 40 °C min^{-1} to 325°C which was held for 7 min, giving a total run time of 27.3 min.

4.2.4 Acknowledgments

The authors would like to acknowledge the Royal Thai Scholarship for funding the PhD studentship (Sukanya Hongthong) and Dr. Tim Woodman for his help with the NMR analysis through the Materials and Chemical Characterisation facility at the University of Bath (MC^2).

4.2.5 References

1. Thompson, R.; Moore, C.; vom Saal, F.; Swan, S., Plastics, the environment and human health: Current consensus and future trends. *Philos. Trans. R. Soc., B* **2009,** *364*, 2153-66.

2. Marin, N.; Collura, S.; Sharypov, V. I.; Beregovtsova, N. G.; Baryshnikov, S. V.; Kutnetzov, B. N.; Cebolla, V.; Weber, J. V., Copyrolysis of wood biomass and synthetic polymers mixtures. Part II: characterisation of the liquid phases. *J. Anal. Appl. Pyrolysis* **2002,** *65* (1), 41-55.

3. Block, C.; Ephraim, A.; Weiss-Hortala, E.; Minh, D. P.; Nzihou, A.; Vandecasteele, C., Co-pyrogasification of Plastics and Biomass, a Review. *Waste Biomass Valorization* **2019,** *10* (3), 483-509.

4. Sharypov, V. I.; Marin, N.; Beregovtsova, N. G.; Baryshnikov, S. V.; Kuznetsov, B. N.; Cebolla, V. L.; Weber, J. V., Co-pyrolysis of wood biomass and synthetic polymer mixtures. Part I: influence of experimental conditions on the evolution of solids, liquids and gases. *J. Anal. Appl. Pyrolysis* **2002,** *64* (1), 15-28.

5. Paradela, F.; Pinto, F.; Gulyurtlu, I.; Cabrita, I.; Lapa, N., Study of the co-pyrolysis of biomass and plastic wastes. *Clean Technol. Environ. Policy* **2009,** *11* (1), 115-122.

6. Jesus, M. S.; Napoli, A.; Trugilho, P. F.; Abreu Júnior, Á. A.; Martinez, C. L. M.; Freitas, T. P., Energy and mass balance in the pyrolysis process of Eucalyptus wood. *Revista Cerne* **2018,** *24*, 288-294.

7. Peterson, A. A.; Vogel, F.; Lachance, R. P.; Fröling, M.; Antal, J. M. J.; Tester, J. W., Thermochemical biofuel production in hydrothermal media: A review of sub- and supercritical water technologies. *Energy Environ. Sci.* **2008,** *1* (1), 32-65.

8. Goudnaan, F.; Beld, B.; Boerefijn, F. R.; Bos, G. M.; Naber, J. E.; Wal, S.; Zeevalkink, J., Thermal Efficiency of the HTU® Process for Biomass Liquefaction. *Prog. Thermochem. Biomass Convers., [Conf.], 5th* 2008; Vol. 18–21, pp 1312-1325.

9. Xu, C.; Lad, N., Production of heavy oils with high caloric values by direct liquefaction of woody biomass in sub/near-critical water. *Energy Fuels* **2008,** *22* (1), 635-642.

10. Demirbas, A., Competitive liquid biofuels from biomass. *Appl. Energy* **2011,** *88* (1), 17-28.

11. Bensaid, S.; Conti, R.; Fino, D., Direct liquefaction of ligno-cellulosic residues for liquid fuel production. *Fuel* **2012,** *94*, 324-332.

12. Arun, J.; Gopinath, K. P.; SundarRajan, P.; JoselynMonica, M.; Felix, V., Co-liquefaction of Prosopis juliflora with polyolefin waste for production of high grade liquid hydrocarbons. *Bioresour. Technol.* **2019,** *274*, 296-301.

13. Wang, B.; Huang, Y.; Zhang, J., Hydrothermal liquefaction of lignite, wheat straw and plastic waste in sub-critical water for oil: Product distribution. *J. Anal. Appl. Pyrolysis* **2014,** *110*, 382-389.

14. Yuan, X.; Cao, H.; Li, H.; Zeng, G.; Tong, J.; Wang, L., Quantitative and qualitative analysis of products formed during co-liquefaction of biomass and synthetic polymer mixtures in sub- and supercritical water. *Fuel Process. Technol.* **2009,** *90* (3), 428-434.

15. Sugano, M.; Komatsu, A.; Yamamoto, M.; Kumagai, M.; Shimizu, T.; Hirano, K.; Mashimo, K., Liquefaction process for a hydrothermally treated waste mixture containing plastics. *J. Mater. Cycles Waste Manage.* **2009,** *11* (1), 27-31.

16. Wu, X.; Liang, J.; wu, Y.; Hu, H.; Shaobin, H.; Wu, K., Co-liquefaction of microalgae and polypropylene in sub-/super-critical water. *RSC Adv.* **2017,** *7*, 13768-13776.

17. Raikova, S.; Knowles, T. D. J.; Allen, M. J.; Chuck, C. J., Co-liquefaction of Macroalgae with Common Marine Plastic Pollutants. *ACS Sustainable Chem. Eng.* **2019,** *7* (7), 6769-6781.

18. Coma, M.; Martinez-Hernandez, E.; Abeln, F.; Raikova, S.; Donnelly, J.; Arnot, T.; Allen, M.; Hong, D. D.; Chuck, C. J., Organic waste as a sustainable feedstock for platform chemicals. *Faraday Discuss.* **2017,** *202*, 175-195.

19. Hongthong, S.; Raikova, S.; Leese, H. S.; Chuck, C. J., Co-processing of common plastics with pistachio hulls via hydrothermal liquefaction. *Waste Manage.* **2020,** *102*, 351-361.

20. Biller, P.; Ross, A. B., Potential yields and properties of oil from the hydrothermal liquefaction of microalgae with different biochemical content. *Bioresour. Technol.* **2011,** *102* (1), 215-225.

21. Akhtar, J.; Kuang, S. K.; Amin, N. S., Liquefaction of empty palm fruit bunch (EPFB) in alkaline hot compressed water. *Renewable Energy* **2010,** *35* (6), 1220-1227.

22. Karagöz, S.; Bhaskar, T.; Muto, A.; Sakata, Y.; Oshiki, T.; Kishimoto, T., Low-temperature catalytic hydrothermal treatment of wood biomass: analysis of liquid products. *Chem. Eng. J.* **2005,** *108* (1), 127-137.

23. Xu, D.; Lin, G.; Guo, S.; Wang, S.; Guo, Y.; Jing, Z., Catalytic hydrothermal liquefaction of algae and upgrading of biocrude: A critical review. *Renewable Sustainable Energy Rev.* **2018,** *97*, 103-118.

24. Hirano, Y.; Miyata, Y.; Taniguchi, M.; Funakoshi, N.; Yamazaki, Y.; Ogino, C.; Kita, Y., Fe-assisted hydrothermal liquefaction of cellulose: Effects of hydrogenation catalyst addition on properties of water-soluble fraction. *J. Anal. Appl. Pyrolysis* **2020,** *145*, 104719.

25. Raikova, S.; Smith-Baedorf, H.; Bransgrove, R.; Barlow, O.; Santomauro, F.; Wagner, J. L.; Allen, M. J.; Bryan, C. G.; Sapsford, D.; Chuck, C. J., Assessing hydrothermal liquefaction for the production of bio-oil and enhanced metal recovery from microalgae cultivated on acid mine drainage *Fuel Process. Technol.* **2016,** *142*, 219-227.

26. Stefanidis, S. D.; Kalogiannis, K. G.; Iliopoulou, E. F.; Lappas, A. A.; Pilavachi, P. A., In-situ upgrading of biomass pyrolysis vapors: Catalyst screening on a fixed bed reactor. *Bioresour. Technol.* **2011,** *102* (17), 8261-8267.

27. Cheng, S.; Wei, L.; Zhao, X.; Julson, J., Application, Deactivation, and Regeneration of Heterogeneous Catalysts in Bio-Oil Upgrading. *Catalysts* **2016,** *6* (12), 195.

28. Panda, A.; Singh, R. K., Catalytic performances of kaoline and silica alumina in the thermal degradation of polypropylene. *J. Fuel Chem. Technol.* **2011,** *39*, 198-202.

29. Duan, P.; Savage, P. E., Hydrothermal Liquefaction of a Microalga with Heterogeneous Catalysts. *Ind. Eng. Chem. Res.* **2011,** *50* (1), 52-61.

30. Valentini, F.; Kozell, V.; Petrucci, C.; Marrocchi, A.; Gu, Y.; Gelman, D.; Vaccaro, L., Formic acid, a biomass-derived source of energy and hydrogen for biomass upgrading. *Energy Environ. Sci.* **2019,** *12* (9), 2646-2664.

31. Matsagar, B. M.; Wang, Z.-Y.; Sakdaronnarong, C.; Chen, S. S.; Tsang, D. C. W.; Wu, K. C.-W., Effect of Solvent, Role of Formic Acid and Rh/C Catalyst for the Efficient Liquefaction of Lignin. *ChemCatChem* **2019,** *11* (18), 4604-4616.

32. Biller, P.; Riley, R.; Ross, A. B., Catalytic hydrothermal processing of microalgae: Decomposition and upgrading of lipids. *Bioresour. Technol.* **2011,** *102* (7), 4841-4848.

33. Panda, A.; Singh, R. K.; Mishra, D., Thermolysis of waste plastics to liquid fuel: A suitable method for plastic waste management and manufacture of value added products--A world prospective. *Renewable Sustainable Energy Rev.* **2010,** *14*, 233-248.

34. Wang, K.; Kim, K. H.; Brown, R. C., Catalytic pyrolysis of individual components of lignocellulosic biomass. *Green Chem.* **2014,** *16* (2), 727-735.

35. Zhang, X.; Lei, H.; Zhu, L.; Qian, M.; Zhu, X.; Wu, J.; Chen, S., Enhancement of jet fuel range alkanes from co-feeding of lignocellulosic biomass with plastics via tandem catalytic conversions. *Appl. Energy* **2016,** *173*, 418-430.

36. Zhang, H.; Zheng, J.; Xiao, R.; Shen, D.; Jin, B.; Xiao, G.; Chen, R., Co-catalytic pyrolysis of biomass and waste triglyceride seed oil in a novel fluidized bed reactor to produce olefins and aromatics integrated with self-heating and catalyst regeneration processes. *RSC Adv.* **2013,** *3* (17), 5769-5774.

37. Jacobson, K.; Maheria, K. C.; Kumar Dalai, A., Bio-oil valorization: A review. *Renewable Sustainable Energy Rev.* **2013,** *23*, 91-106.

38. Ye, J.; Cao, Q.; Zhao, Y., Co-pyrolysis of Polypropylene and Biomass. *Energy Sources* **2008,** *Part A*, 1689-1697.

39. Ladislav, S.; Kubinec, R.; Jurdáková, H.; Hájeková, E.; Martin, B., GC-MS of polyethylene and polypropylene thermal cracking products. *Pet. Coal* **2006,** *48*.

40. Hájeková, E.; Špodová, L.; Bajus, M.; Mlynková, B., Separation and characterization of products from thermal cracking of individual and mixed polyalkenes. *Chem. Pap.* **2007,** *61*, 262-270.

41. Chun, Y.; Sheng, G.; Chiou, C. T.; Xing, B., Compositions and Sorptive Properties of Crop Residue-Derived Chars. *Environ. Sci. Technol.* **2004,** *38* (17), 4649-4655.

42. Chen, X.; Chen, G.; Chen, L.; Chen, Y.; Lehmann, J.; McBride, M. B.; Hay, A. G., Adsorption of copper and zinc by biochars produced from pyrolysis of hardwood and corn straw in aqueous solution. *Bioresour. Technol.* **2011,** *102* (19), 8877-8884.

43. Tan, X.; Liu, Y.; Zeng, G.; Wang, X.; Hu, X.; Gu, Y.; Yang, Z., Application of biochar for the removal of pollutants from aqueous solutions. *Chemosphere* **2015,** *125*, 70-85.

44. European Commission Publications Office, *General Union Environment Action Programme to 2020: Living well, within the limits of our planet*. Publications Office of the European Union: Luxembourg, 2014; p 92.

45. Lee, Y.; Eum, P.-R.-B.; Ryu, C.; Park, Y.-K.; Jung, J.-H.; Hyun, S., Characteristics of biochar produced from slow pyrolysis of Geodae-Uksae 1. *Bioresour. Technol.* **2013,** *130*, 345-350.

46. Devasahayam, S.; Bhaskar Raju, G.; Mustansar Hussain, C., Utilization and recycling of end of life plastics for sustainable and clean industrial processes including the iron and steel industry. *Mater. Sci. Energy Technol.* **2019,** *2* (3), 634-646.

47. Hietala, D. C.; Faeth, J. L.; Savage, P. E., A quantitative kinetic model for the fast and isothermal hydrothermal liquefaction of Nannochloropsis sp. *Bioresour. Technol.* **2016,** *214*, 102-111.

48. Gollakota, A. R. K.; Kishore, N.; Gu, S., A review on hydrothermal liquefaction of biomass. *Renewable Sustainable Energy Rev.* **2018,** *81*, 1378-1392.

49. Cai, J.; Wang, Y.; Zhou, L.; Huang, Q., Thermogravimetric analysis and kinetics of coal/plastic blends during co-pyrolysis in nitrogen atmosphere. *Fuel Process. Technol.* **2008,** *89* (1), 21-27.

50. Ayeni, A. O.; Hymore, F. K.; Mudliar, S. N.; Deshmukh, S. C.; Satpute, D. B.; Omoleye, J. A.; Pandey, R. A., Hydrogen peroxide and lime based oxidative pretreatment of wood waste to enhance enzymatic hydrolysis for a biorefinery: Process parameters optimization using response surface methodology. *Fuel* **2013,** *106*, 187-194.

51. Cheng, Y.; Zhao, P.-X.; Alma, M. H.; Sun, D.-F.; Li, R.; Jiang, J.-X., Improvement of direct liquefaction of technical alkaline lignin pretreated by alkaline hydrogen peroxide. *J. Anal. Appl. Pyrolysis* **2016,** *122*, 277-281.

52. Karagoz, P.; Rocha, I.; Ozkan, M.; Angelidaki, I., Alkaline peroxide pretreatment of rapeseed straw for enhancing bioethanol production by Same Vessel Saccharification and Co-Fermentation. *Bioresour. Technol.***2011,** *104*, 349-57.

53. Huang, H.-j.; Yuan, X.-z.; Zeng, G.-m.; Liu, Y.; Li, H.; Yin, J.; Wang, X.-l., Thermochemical liquefaction of rice husk for bio-oil production with sub- and supercritical ethanol as solvent. *J. Anal. Appl. Pyrolysis* **2013,** *102*, 60-67.

54. Long, J.; Xu, Y.; Wang, T.; Yuan, Z.; Shu, R.; Zhang, Q.; Ma, L., Efficient base-catalyzed decomposition and in situ hydrogenolysis process for lignin depolymerization and char elimination. *Appl. Energy* **2015,** *141*, 70-79.

55. Ouyang, X.; Huang, X.; Zhu, Y.; Qiu, X., Ethanol-Enhanced Liquefaction of Lignin with Formic Acid as an in Situ Hydrogen Donor. *Energy Fuels* **2015,** *29* (9), 5835-5840.

56. Brown, T. M.; Duan, P.; Savage, P. E., Hydrothermal Liquefaction and Gasification of Nannochloropsis sp. *Energy Fuels* **2010,** *24* (6), 3639-3646.

57. Zhou, D.; Zhang, L.; Zhang, S.; Fu, H.; Chen, J., Hydrothermal Liquefaction of Macroalgae Enteromorpha prolifera to Bio-oil. *Energy Fuels* **2010,** *24* (7), 4054-4061.

4.3 Supporting information

4.3.1. Properties of pistachio hull feedstock

Table 4.3- 1 – Properties of pistachio hull feedstock

Analyses	Pistachio hull
Proximate (wt.%)	
Total ash	9.4
Water Extractable Others	15.6
Biomass composition (wt.%)	
Lignin	26.6
Glucan	13.6
Xylan	5.0
Galactan	2.8
Arabinan	4.8
Fructan	0.0
Acetyl	1.4
Elemental (wt.%)	
C	49.3
H	6.8
O	46.1
Energy (MJ kg^{-1})	
LHV	17.45
HHV	18.97

4.3.2 Feedstock elemental compositions

Table 4.3- 2 – Elemental composition and HHV of pistachio hull and polypropylene

Element Analysis (%)	C	H	Other	N	HHV (MJ kg^{-1})
Pistachio hull	49.3	6.8	46.1	1.78	17.5
PP	85.1	13.3	1.5	<0.1	47.4

4.3.3 Identification of major functional group in solid residue

The FT-IR spectra of solid residue from HTL of co-liquefaction pistachio hull and PP without catalyst displayed strong absorbance bands at 2927, 2857, 1445, and 1370 cm^{-1}, attributable mainly to CH2 in biopolymer. This observation was like spectra obtained from pure PP. The band at 1621 cm^{-1} can be assigned to the C=C and C=O of the aromatic ring, while 890 cm^{-1} can be assigned to aromatic rings in lignin and thus verified to the presence of lignin derived from pistachio hull in bio-char.

Considering the product of the additional Fe (Fig. S1a), the large molecule solid residue was observed at around 845, 978, 1365, 1420 cm^{-1}, similar to those obtained for solid residue from HTL of pure pistachio hull, which mainly contribute to aromatic rings and CH2 in biopolymer. However, sharp peaks at 2800-3000 cm^{-1} and 676 cm^{-1} are also present, which are not observed for pure pistachio hull solid residue, attributable to aliphatic C–H vibrations and halogen compound. These peaks were similar wavenumbers to the spectra of pure PP and pure Fe, respectively. These findings suggest the presence of unreacted polyethylene and Fe in the HTL char.

For the solid residue produced from the additional $FeSO_4.7H_2O$, $MgSO_4.H_2O$, and $ZnSO_4.H_2O$, several peaks showed a slightly decrease intensity of the absorption compared to the additional Fe, indicating that a decrease of nonpolar content (Fig. S1b-S1d). The deformation stretching vibrations for CH2 deformation, C-H deformation, and aromatic rings at 2920 cm^{-1}, 1476-1376 cm^{-1}, and 870 cm^{-1}. The appearance of peak at 1032 cm^{-1} can be assigned to carboxylate groups. However, the FT-IR spectra observed (2920 cm^{-1}, 1476-1376 cm^{-1}) from $ZnSO_4.H_2O$ also showed decrease intensive peak compare to $FeSO_4.7H_2O$ and $MgSO_4.H_2O$, possible due to the reaction reacted more completely, forming more soluble products than the other catalyst mentioned above.

Besides, the weak FT-IR spectra of solid residue produced from the additional of ZSM-5, aluminosilicate, and Y-zeolite were observed at 2900-2800 cm^{-1}, 1445 cm^{-1}, and 1370 cm^{-1}, corresponding to an aliphatic C-H stretch (Fig. S1e-S1g). This observation may indicate that the oxygen-containing functional groups like carboxylic and phenolic groups experienced some chemical changes during liquefaction due to the cracking reactions catalysed by the acid sites on the zeolite surface. However, the main vibration at 980 cm^{-1}, 1086 cm^{-1}, and 1066 cm^{-1} (ZSM-5, aluminosilicate, and Y-zeolite, respectively) were designated as Si–O (Ahmad et al., 2019), which was sharp in pure silica and zeolite samples during the liquefaction process.

In contrast, an increase intensive peaks (2900-2800 cm^{-1}, 1445 cm^{-1}, and 1370 cm^{-1}) were seen with the additional Na_2CO_3 (Fig. S1h). However, the intensive peak at 880 from the raw Na_2CO_3 was not observed. This suggest that Na_2CO_3 may completely soluble during hydrothermal liquefaction but cannot change the interaction between plastic and biomass during the process.

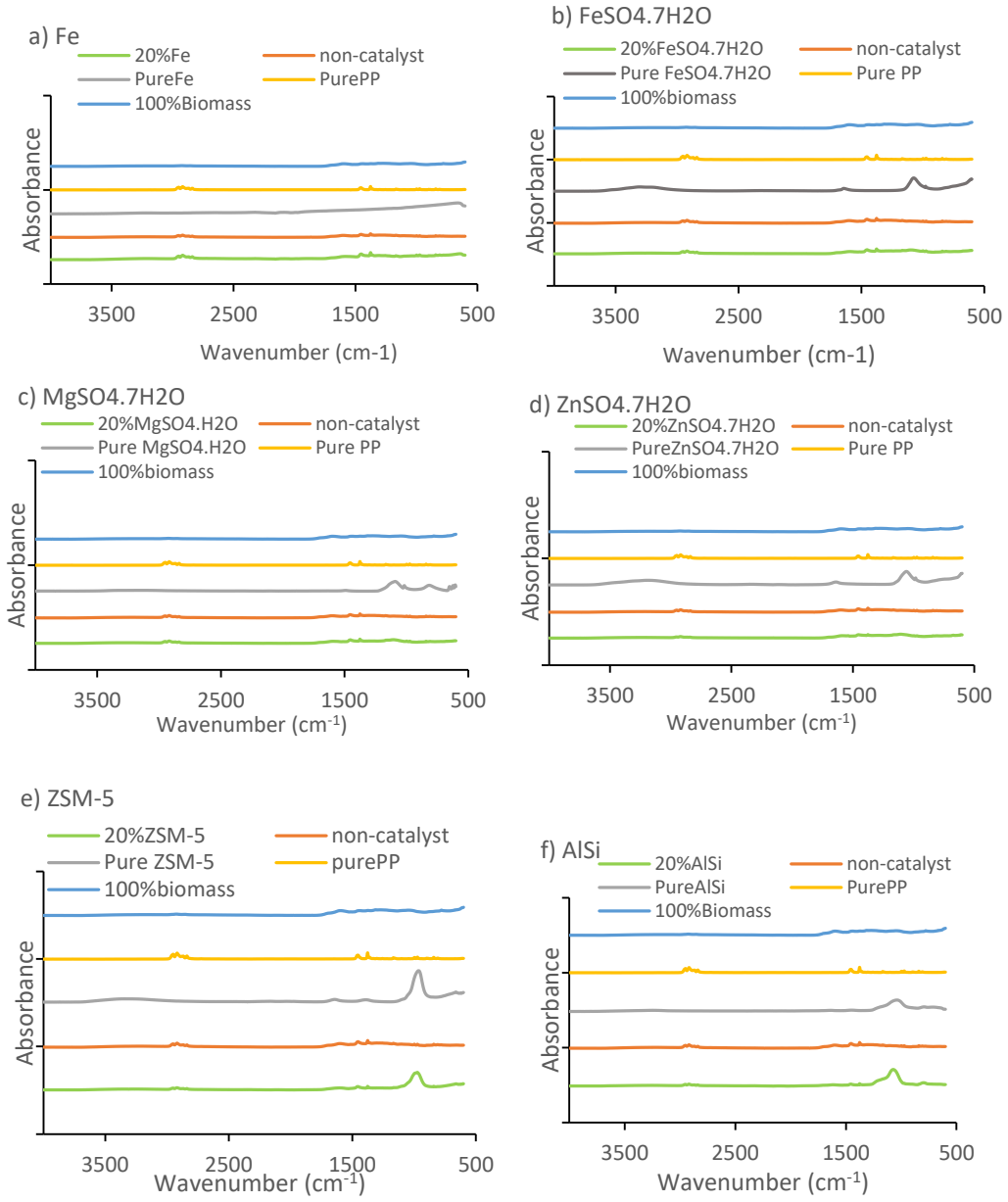
a) Fe
20%Fe
non-catalyst
PureFe
PurePP
100%Biomass
Absorbance
3500
2500
1500
500
Wavenumber (cm-1)
b) FeSO4.7H2O
20%FeSO4.7H2O
non-catalyst
Pure FeSO4.7H2O
Pure PP
100%biomass
Absorbance
3500
2500
1500
500
Wavenumber (cm-1)
c) MgSO4.7H2O
20%MgSO4.H2O
non-catalyst
Pure MgSO4.H2O
Pure PP
100%biomass
Absorbance
3500
2500
1500
500
Wavenumber (cm-1)
d) ZnSO4.7H2O
20%ZnSO4.7H2O
non-catalyst
PureZnSO4.7H2O
Pure PP
100%biomass
Absorbance
3500
2500
1500
500
Wavenumber (cm-1)
e) ZSM-5
20%ZSM-5
non-catalyst
Pure ZSM-5
purePP
100%biomass
Absorbance
3500
2500
1500
500
Wavenumber (cm-1)
f) AlSi
20%AlSi
non-catalyst
PureAlSi
PurePP
100%Biomass
Absorbance
3500
2500
1500
500
Wavenumber (cm-1)

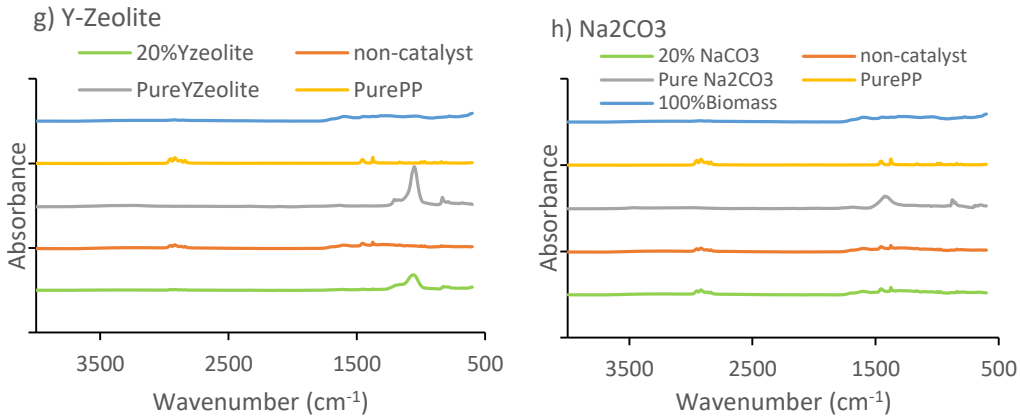

Figure 4.3- 1FTIR of pure PP, pure catalyst and solid phase from hydrothermal of pistachio with PP with 20% different catalyst loading

4.3.4 Calibration curves for quantification of unreacted plastics in solid residue using FTIR

Fig. S2a shows infrared spectra of eight samples of pure pistachio hull solid residue blended with unreacted PP at concentrations within the range 0–100 wt.%. The strong absorption band at 898 cm^{-1} was taken as a representative peak for pistachio hull bio-char. The band at 1376 cm^{-1}, 1455 cm^{-1}, and 2912 cm^{-1} were chosen as a reference for PP. The relative intensities of the characteristic bands were used as indicators of PP content in bio-chars. Peak intensity ratios (PIR) were calculated for each blend, and used to create a calibration curve, shown in Fig. S2b. However, three calibration curves were created. Coefficients of determination of >0.95 were obtained. PIRs were then calculated from the FTIR spectra of the solid residue resulting from HTL of pistachio hull/polypropylene at different catalyst loadings to quantify unreacted PP.

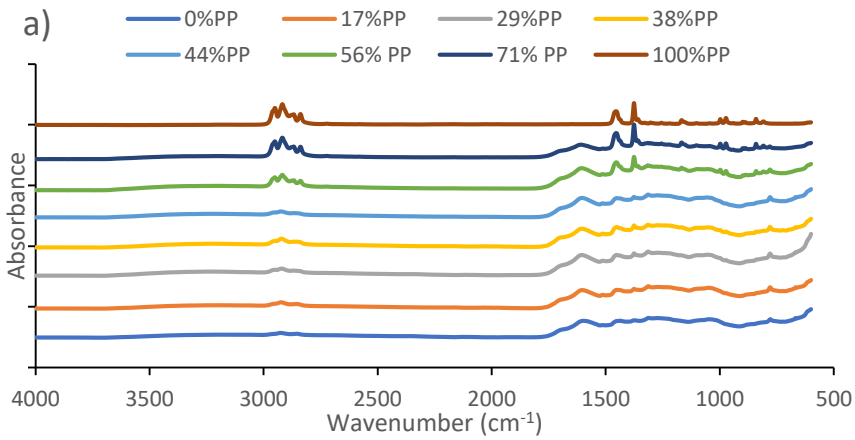

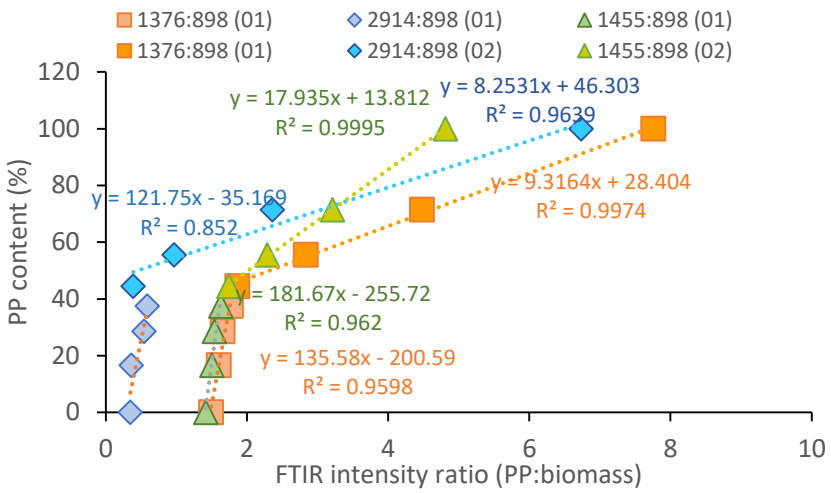

Figure 4.3- 2 (a) FTIR spectra of pistachio hull bio-char with different polypropylene contents and (b) peak ratio calibration curve for polypropylene in pistachio bio-char.

Table 4.2- 2– Calculated percentage concentrations of unreacted polypropylene in bio-char from co-liquefaction of pistachio hull with PP.

	PP	***Pistachio hull bio-char***	***PIR***	***Predictive equation***	***R2***	***Estimated PP content of char (%)***
	2912 cm^{-1} 1376 cm-1 1455 cm-1	**898 cm^{-1} 898 cm^{-1} 898 cm^{-1}**	**2912:898 1376:898 1455:898**	y = 8.2531+46.303 y = 9.3164+28.404 y = 17.935+13.812	0.9636 0.9974 0.9995	
No-catalyst	0.051939	0.014697	3.533814			72 %
Fe	0.137342	0.102288	1.342698			46 %
$FeSO_4.7H_2O$	0.065164	0.035997	1.810248			51 %
$MgSO_4.H_2O$	0.068378	0.032808	2.084178			55 %
$ZnSO_4.7H_2O$	0.058160	0.038908	1.494818			48 %
ZSM-5	0.037764	0.050429	0.748860			39 %
Aluminosilicate	0.050429	0.012520	1.192777			49 %
Y-zeolite	0.018539	0.013200	1.404411			46 %
Na_2CO_3	0.065411	0.021984	2.975296			65 %
BHT	0.029556	0.015027	1.966786			52 %
FA	0.020348	0.015636	1.301385			45 %
H_2O_2	0.025541	0.015987	1.597574			48 %

4.3.5 Quantification of plastic conversion

$$Plastic\ in\ solid\ residue\ (g) = \frac{unconverted\ plastic\ in\ char\ (\%) \times\ char\ yield\ (g)}{100}$$

$$Plastic\ convert\ (g) = plastic\ in\ feedstock - plastic\ in\ solid\ residue$$

$$Conversion\ (\%) = \frac{plastic\ convert\ (g) \times\ 100}{plastic\ in\ feedstock\ (g)}$$

Table 4.2- 3 Summary of plastics conversion

Plastic components	Initial PP in feedstock (g)	Total solid residue from reaction (g)	Estimated PP content of char (%)	Amount of PP in solid residue (g)	PP conversion (%)
No-catalyst	1.50 g	1.68 g	72 %	1.21 g	19
Fe	1.20 g	1.90 g	46 %	0.87 g	28
$FeSO_4.7H_2O$	1.20 g	1.65 g	51 %	0.96 g	29
$MgSO_4.H_2O$	1.20 g	1.64 g	55 %	0.85 g	25
$ZnSO_4.7H_2O$	1.20 g	1.69 g	48 %	0.81 g	32
ZSM-5	1.20 g	1.93 g	39 %	0.75 g	38
Aluminosilicate	1.20 g	1.91 g	49 %	0.84 g	30
Y-zeolite	1.20 g	1.90 g	46 %	0.86 g	28
Na_2CO_3	1.20 g	1.42 g	65 %	0.92 g	23
BTH	1.20 g	1.89 g	52 %	0.99 g	17
FA	1.20 g	1.27 g	45 %	0.58 g	52
H_2O_2	1.20 g	1.45 g	48 %	0.70 g	42

4.3.6 GC/MS analysis of bio-crudes

Table 4.2- 4 Bio-crude element composition

Valuable Chemical	Area					
	Alumina-silicate	(PP/ biomass)	100% biomass	BHT	FA	H_2O_2
Phenol						
Phenol	1618974	1975631	-	-	1417659	1058270
Phenol, 2-(1,1-dimethylethyl)-4-methyl-	-	-	-	4514422	-	73660
p-Cresol	1070657	1283830	493760	547149	923498	498792.
3-Tridecylphenol	15098750	13908114	14709587	39262311	18054157	14761802
Phenol, 4-ethyl-	8023788	6308547	3466544	1012049	7845488	2483446
Phenol, 2-methoxy-	154884	753487	328761	272635	489325	
Phenol, 3-pentadecyl-	8013164	6477394	6295010	12712370	10430108	7096446
Phenol, 2-methyl-	154884	174943	85054	146480	-	468521
Phenol, 2,4-dimethyl-	-	-	-	523171	-	-
Phenol, 2,6-dimethoxy-	2590201	1584263	440226		1163368	942998
Phenol, 4-ethyl-2-methoxy-	936716	885637	288186	390510.	1663841	-

Valuable Chemical	Area					
	Alumina-silicate	(PP/ biomass)	100% biomass	BHT	FA	H_2O_2
Phenol, 2-(1-methylethyl)-	-	-	93180	-	-	-
Phenol, 2-methoxy-4-propyl-	885637	885637	152960	-	-	-
2-Methoxy-5-methylphenol	-	193236	113756	81365	-	-
Phenol, 3,4,5-trimethyl-	-	-	-	81991	-	149048
(Z)-3-(Heptadec-10-en-1-yl)phenol	1891365	-	-	109288	2391302	1575769
2,5-Dihydroxy-4-methoxyacetophenone	310844	132279	174895	-	-	-
2,3-Dimethoxyphenol	-	-	-	1096692	-	-
Ketone						
2-Cyclopenten-1-one, 2-methyl-	112444	286663	-	62581	137429	102295
2-Cyclopenten-1-one, 2,3-dimethyl-	523171	232176	201923	844587	-	-
2-Cyclopenten-1-one, 3-methyl-	243121	228133	73612	-	110340	127511
2-Cyclopenten-1-one, 3-ethyl-	83037	97522	69811	-	-	-
2-Cyclopenten-1-one, 2,3-dimethyl-	42035	232176	146480	-	-	-
1,2-Cyclopentanedione, 3-methyl-	-	260510	-	796713	-	495498
2-Cyclopenten-1-one, 3-ethyl-2-hydroxy-	-	97522	-	160386	-	-
2-Cyclopenten-1-one, 2-hydroxy-3-methyl-	1041900	-	-	1891365	842554	-
Cyclooctane, butyl-	-	-	-	-	410032	-
3-Pyridinol	2592838	5728456	1017152	8404151	8309730	3759956
2-Pyrrolidinone	-	-	-	382127	-	-
Pyridine, 2,3-dimethyl-						33149
Pyridine, 2,5-dimethyl-	109289	54028	-	59926		39264
2,6-Lutidine	81991	35761	-			
Ethanone, 1-(2-methyl-1-cyclopenten-1-yl)-	-	-	23210			
Ethanone, 1-(1-methyl-1H-pyrrol-2-yl)-	63257	107883	-	85452		
Ethanone, 1-(2-furanyl)-	-	38263	-		73580	
Ethanone, 1-(2-hydroxy-4-methoxyphenyl)-	130274	-	-			
2,5-Hexanedione					199964	
Furan						
Benzofuran, 2,3-dihydro-	158440	393695	-	45925	229981	
Carboxylic acids						
3-Cyclohexene-1-carboxylic acid	215405	113294	44067	138446	334121	47794
2-Hexene, 4,4,5-trimethyl-				496089	551437	
Hexane, 2,2,5-trimethyl-				84518	601757	
Octane, 2-methyl-	243738	-	-			
Octane, 2,7-dimethyl-				183771		

Valuable Chemical	Area					
	Alumina-silicate	(PP/ biomass)	100% biomass	BHT	FA	H_2O_2
Octane, 5-ethyl-2-methyl-				274150		
Acetic anhydride	35948	-	-			
Benzenemethanol, .alpha.-methyl-	-	75488	-			
Benzene, 1-methyl-3-(1-methylethyl)-					177999	156262
Benzene, 4-ethenyl-1,2-dimethyl-					101857	
Benzene, 1,3-dimethyl-						58993
Benzene, 1-ethyl-2,3,4,5,6-pentafluoro-					95201	58702
Propanoic acid	22157	-	-			
Octane, 2,3,3-trimethyl-	94354	-	-			
Acetyl iodide	113410	73784	-			
3-Ethyl-3-methylheptane	94354	-	-			
5-Methyl-2-pyrrolidinone					1380126	
Pentanoic acid, 4-methyl-	55858	-	-		364680	
Propanoic acid, 2-methyl-, 2-propenyl ester						103289
Acetic anhydride	35948	-	-			
Pyrazine, methyl-(1-Ethyl-2-methylpropyl) methylamine	65857	-	-		243733	
Heptane, 2,6-dimethyl-					495376	
Nonane, 5-methyl-5-propyl-				700299		
Ester						
Sulfurous acid, 2-ethylhexyl hexyl ester	61611	-	-		404131	516174
Hexanedioic acid, dioctyl ester					3901932	
Oxalic acid, cyclohexyl tetradecyl ester	421217	-	-		590894	
Octyl tetradecyl ether				277683		
Hexadecyl octyl ether	-	77178	-			
Alkane						
Decane, 3-ethyl-3-methyl-	-	54476	-	54898		
Dodecane, 4,6-dimethyl-	107900	-	-	765002	1485007	262308
1-Dodecanol, 2-hexyl-				243975		
Decane, 4-ethyl-	-	148674	-			139703
Decane, 2,4-dimethyl-	-	-	125089			
Decane, 3,6-dimethyl-				262998		
Benzocyclodecene, tetradecahydro-	-	-	205154			
Alcohols						
Catechol	-	843509	233032	279563.		87256
Phenylethyl Alcohol					394537	36629
Ethanone, 1-(1H-pyrrol-2-yl)-				114614.		
Hexadecyl octyl ether	-	77178	-			

Valuable Chemical	Area					
	Alumina-silicate	(PP/ biomass)	100% biomass	BHT	FA	H_2O_2
1-Hexadecanol				465419		134059
11-Methyldodecanol	278535	-	-		410032	
1-Decanol, 2-hexyl-				36885	200888	
2-Tridecanol	139524	-	-	134628	240888	
Syringylacetone	149943	-	-	-	-	-
11-Methyldodecanol	-	-	-	783778	-	-
1-Octanol, 2-butyl-	-	-	-	317487	-	-
2-Furanol, tetrahydro-	-	-	-	-	401352	
Amines						
Succinimide	-	27102	-	-	-	-
Isomaltol	-	34989	-	-	-	-
p-Aminotoluene	25529					-
Acetamide, N				24595		
Fatty acid						
13-Octadecenoic acid, methyl ester	-	87512	-	-	-	-
Oxalic acid, cyclohexyl tetradecyl ester	421217	-	-	553678	590894	301578
8-Octadecenoic acid, methyl ester	132536	-	-			
9-Octadecenoic acid, methyl ester					290273	
11-Octadecenoic acid, methyl ester, (Z)-	132536	-	-	675722	290273	351180
Pentanoic acid, 4-oxo-				105653		
Propanoic acid, anhydride				1015233		

4.3.7 NMR analysis of bio-crude

a) 100% Biomass

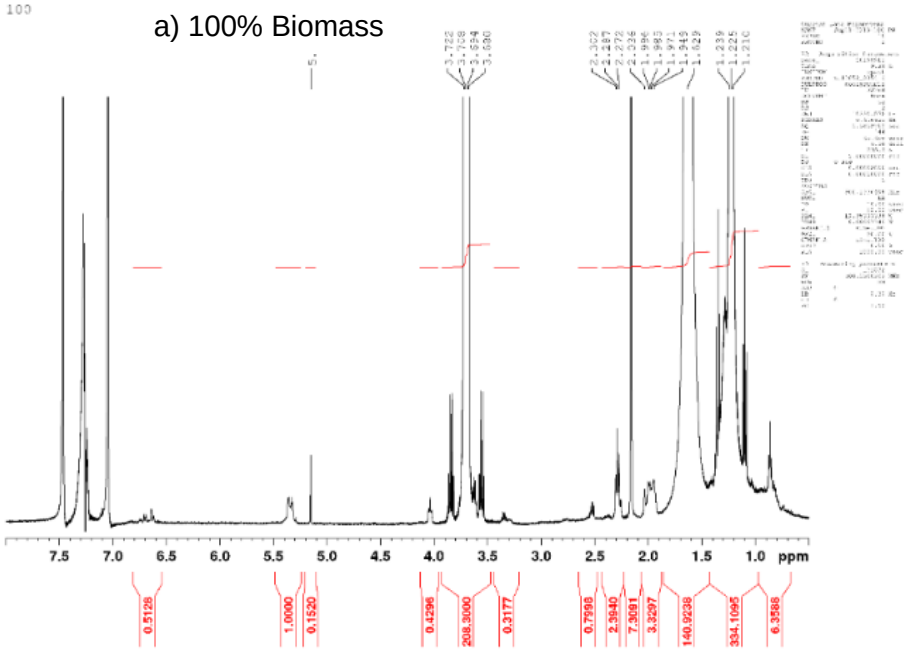

b) 50%biomass and PP (non-

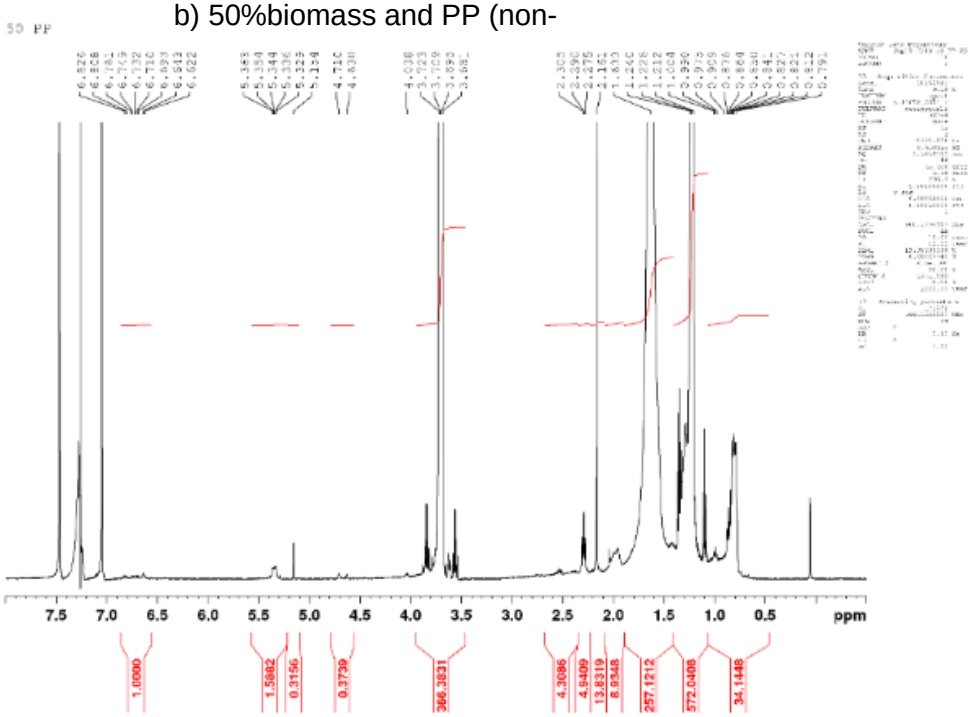

c) 20% Al Si loading in 50%PP blend with biomass

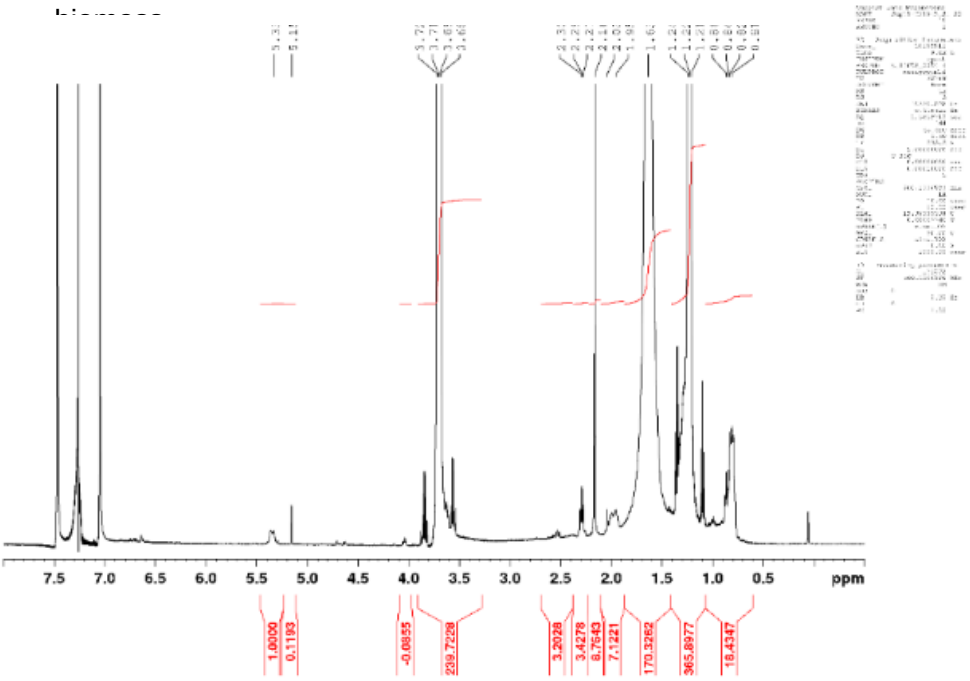

d) 20% ZSM-5 loading in 50%PP blend with

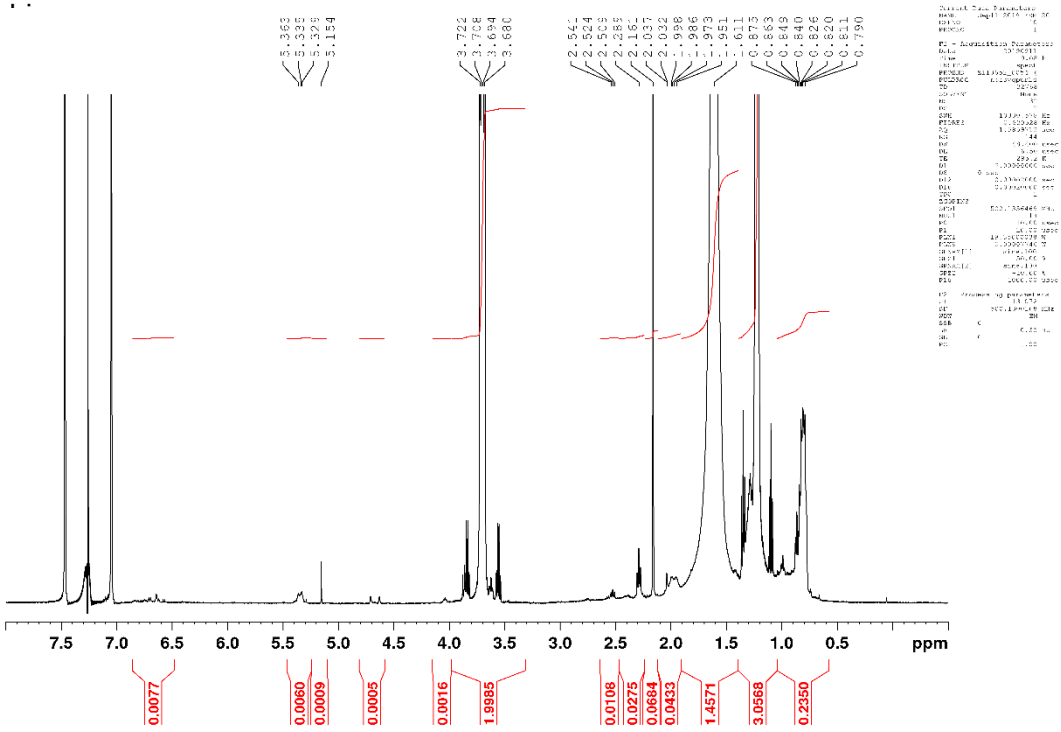

YZeo e) 20% Y-zeolite loading in 50%PP with

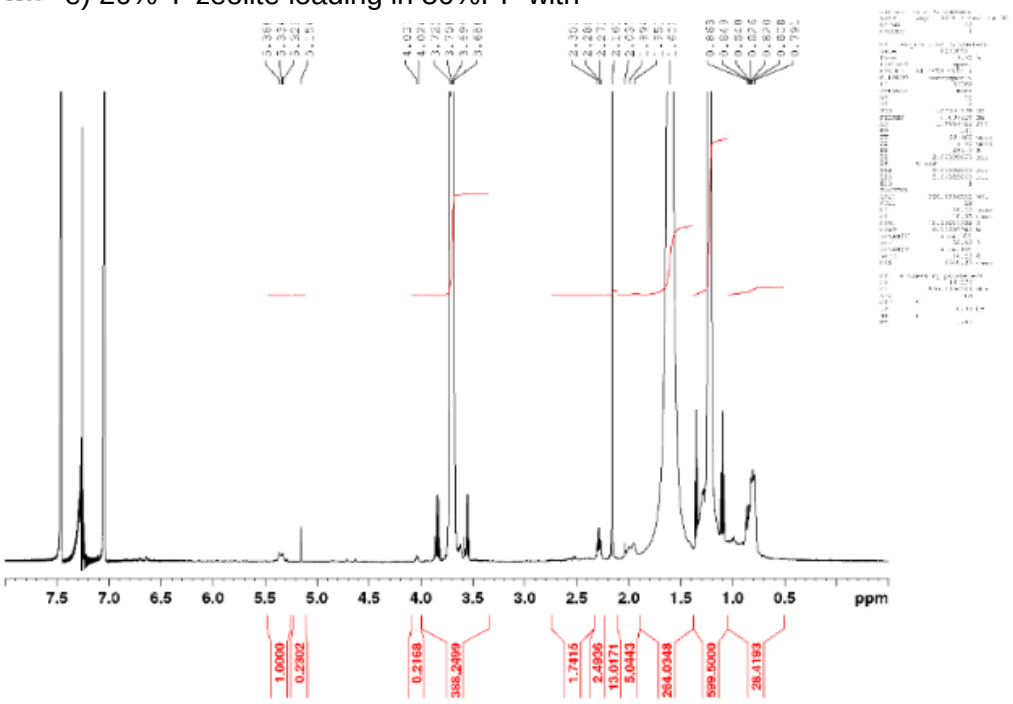

Figure 4.3- 3 – (a) 1HNMR spectra of pure pistachio hull bio-char (b) 50%PP blend with pistachio hull without catalyst loading (c) 50%PP blend with pistachio hull with 20% aluminosilicate loading (d) 50%PP blend with pistachio hull with 20% ZSM-5 (d) 50%PP blend with pistachio hull with 20% Y-zeolite loading.

4.3.8 Gas analysis

Table 4.2- 5–Gas composition by GC-MS analysis of co-liquefaction of biomass with 50% PP blends with aluminosilicate as catalyst and formic acid.

Component RT	Compound Name	Formula	Base Peak Area
2.882	(2-Aziridinylethyl)amine	C4H10N2	10011510.39
2.950	Propene	C3H6	1853600.473
3.144	1-Propene, 2-methyl-	C4H8	1102015.507
3.187	Sulfur dioxide	O2S	327885.9138
3.523	1H-Tetrazole, 5-vinyl-	C3H4N4	479236.1949
3.523	Furan	C4H4O	449055.0971
3.616	2-Butanone	C4H8O	652048.4229
4.334	3-Methylglutaric anhydride	C6H8O3	771740.9536
4.513	Furan, 3-methyl-	C5H6O	1312387.247
4.705	Trichloromethane	CHCl3	853268.2331

Component RT	Compound Name	Formula	Base Peak Area
4.918	1-Butene, 2,3-dimethyl-	C6H12	987566.046
4.923	1-Butene, 3,3-dimethyl-	C6H12	983818.508
5.012	(Z),(Z)-2,4-Hexadiene	C6H10	30380832.45
5.088	3-Hexyne	C6H10	31647756.54
5.179	1-Pentene, 2,4-dimethyl-	C7H14	2513051.052
5.268	1-Hexene, 3-methyl-	C7H14	7989087.731
5.360	Cyclopentene, 1-methyl-	C6H10	35983735.45
5.401	Nonane, 5-methylene-	C10H20	5723409.193
5.565	Methane, isocyanato-	C2H3NO	3294282.939
5.572	3-Penten-2-one, 4-(acetyloxy)-, (Z)-	C7H10O3	2459849.355
5.586	2-Methyl-1-hexanol	C7H16O	8837071.493
5.636	2,4-Hexadiene	C6H10	21140834.65
5.787	Hexane, 3-methyl-	C7H16	5343430.939
5.885	1,5-Hexadiene, 2-methyl-	C7H12	23465054.8
6.125	1-Hexene, 2-methyl-	C7H14	27454969.68
6.407	Cyclobutane, (1-methylethylidene)-	C7H12	14009802.32
6.452	Heptane	C7H16	29601132.41
6.742	Ethanone, 1-(methylenecyclopropyl)-	C6H8O	39299406.18
6.848	4-Methyl-2-hexene,c&t	C7H14	5162063.373
6.848	2-Hexene, 3-methyl-, (Z)-	C7H14	5160276.662
6.949	2,3-dimethylfuran	C6H8O	10065601.92
6.957	3,4-dimethylfuran	C6H8O	8204330.632
6.986	(R)-(+)-3-Methylcyclopentanone	C6H10O	6326795.125
6.988	Diethylcyanamide	C5H10N2	6326795.125
7.065	2,3-dimethylfuran	C6H8O	5042165.336
7.298	Cyclohexene, 4-methyl-	C7H12	4487273.659
7.322	2-Vinylfuran	C6H6O	2695418.552
7.467	3,5-Dimethylcyclopentene	C7H12	3871659.19
7.506	Cyclopentene, 1,2,3-trimethyl-	C8H14	8922743.125
7.506	Cyclopentene, 1,2,3-trimethyl-	C8H14	5341864.173
7.595	Valeric anhydride	C10H18O3	196868.079
7.612	1,3-Pentadiene, 2,3-dimethyl-	C7H12	18028140.72
7.612	Cyclobutane, (1-methylethylidene)-	C7H12	17831497.64
7.855	Cyclopentane, 1,2,4-trimethyl-	C8H16	8552828.781
7.867	Cycloheptanol, trifluoroacetate	C9H13F3O2	15031260.39
7.867	Cyclohexane, methylene-	C7H12	14160633.32
7.905	Methyl Isobutyl Ketone	C6H12O	2403192.103
7.927	1,3-Cyclopentadiene, 5,5-dimethyl-	C7H10	15264834.68
8.002	Bicyclo[4.1.0]hept-2-ene	C7H10	13784879.79
8.002	1,3-Cyclopentadiene, 5,5-dimethyl-	C7H10	13784879.79
8.089	2-Hexene, 2,3-dimethyl-	C8H16	10148398.33

Component RT	Compound Name	Formula	Base Peak Area
8.177	Bicyclo[4.1.0]hept-2-ene	C7H10	7080871.324
8.185	Cyclopentene, 1,2,3-trimethyl-	C8H14	17132131.87
8.250	Bicyclo[4.1.0]hept-2-ene	C7H10	12218803
8.289	2,4-Dimethyl-1-hexene	C8H16	16890275.2
8.745	Dimethylphosphinic fluoride	C2H6FOP	2958193.302
8.745	Dimethylphosphinic fluoride	C2H6FOP	2958193.302
8.920	Cyclohexene, 1-methyl-	C7H12	31435503.72
8.977	Thiophene, 3-methyl-	C5H6S	1382958.506
9.027	cis-1-Butyl-2-methylcyclopropane	C8H16	5422515.199
9.134	1-Pentanone, 1-(2-furanyl)-	C9H12O2	3634837.47
9.251	Bicyclo[4.1.0]hept-2-ene	C7H10	13466030.77
9.329	1,7-Octadiene	C8H14	4450348.391
9.390	Furan, 2-(2-propenyl)-	C7H8O	1260052.334
9.444	3-Heptanone, 2,4-dimethyl-	C9H18O	1528126.872
9.444	1-Heptene, 2-methyl-	C8H16	9234747.097
9.465	1-Heptene, 2-methyl-	C8H16	9234747.097
9.468	1-Heptene, 2-methyl-	C8H16	9234747.097
9.686	2-Methyl-1,5-heptadiene (c,t)	C8H14	5148600.502
9.790	Cyclohexan-1-ethanol, 1-hydroxymethyl-	C9H18O2	21880173.17
9.830	Hydroxymethyl 2-hydroxy-2-methylpropionate	C6H12O4	652349.1081
9.880	Octane	C8H18	17658300.61
9.959	Cyclohexene, 1,2-dimethyl-	C8H14	35459008.99
9.961	1,3-Dimethyl-1-cyclohexene	C8H14	35399306.89
10.094	1-Hexene, 2,5,5-trimethyl-	C9H18	8497408.61
10.101	1H-1,3-Diazepine, 4,5,6,7-tetrahydro-2-methyl-	C6H12N2	4262868.314
10.168	Cyclopentane, 1,1,3,4-tetramethyl-, cis-	C9H18	25480199.02
10.197	Cyclopentene, 1,2,3-trimethyl-	C8H14	26317282.71
10.247	Propanoic acid, anhydride	C6H10O3	18135969.45
10.277	2,3-Dimethyl-3-heptene, (Z)-	C9H18	48218572.11
10.277	Heptane, 2-methyl-3-methylene-	C9H18	48005455.35
10.313	2-Acetyl-2-methyltetrahydrofuran	C7H12O2	14658754.95
10.392	Furan, 2,3,5-trimethyl-	C7H10O	15386982.09
10.552	Ethylamine, 2-((p-bromo-.alpha.-methyl-.alpha.-phenylbenzyl)oxy)-N,N-dimethyl-	C18H22BrNO	1863103.832
10.583	Heptane, 2,4-dimethyl-	C9H20	27307351.7
10.634	Cyclotrisiloxane, hexamethyl-	C6H18O3Si3	5163046.852
10.679	Cyclopentene, 1,2,3-trimethyl-	C8H14	25428288.87
10.753	Cyclohexene, 1,4-dimethyl-	C8H14	22421264.98
10.861	Cyclohexane, 1,3,5-trimethyl-	C9H18	42641565.32
11.152	Sulphuric acid dibutyl ester	C8H18O4S	82459564.73

Component RT	Compound Name	Formula	Base Peak Area
11.325	2,3-Dimethyl-3-heptene, (Z)-	C9H18	4261052.431
11.337	1,3-Cyclohexadiene, 5,6-dimethyl-	C8H12	5424548.825
11.455	1,1-Dimethyl-4-methylenecyclohexane	C9H16	20484502.05
11.704	1,2,4,4-Tetramethylcyclopentene	C9H16	12291269.65
11.704	2,4-Heptadiene, 2,6-dimethyl-	C9H16	12283666.6
11.748	Ethylbenzene	C8H10	28579101.45
11.791	Decane, 5,6-dimethyl-	C12H26	5135586.72
11.791	Undecane, 5,6-dimethyl-	C13H28	5135586.72
11.816	1-(3-Methyl-2H-pyrazol-4-yl)ethanone	C6H8N2O	2386254.051
11.891	N,N-Dimethylacetamide	C4H9NO	16852426.76
11.976	Benzene, 1,3-dimethyl-	C8H10	22608312.95
11.992	Cyclopropane, 1,1-dimethyl-2-(2-methyl-1-propenyl)-	C9H16	28792126.63
12.065	4,4-Dimethyl octane	C10H22	2068784.224
12.137	cis-1,2-Cyclohexanedimethanol	C8H16O2	5047919.532
12.162	3,3-Diethoxy-1-propyne	C7H12O2	3181488.587
12.235	Cyclohexene, 3,3,5-trimethyl-	C9H16	25084307.61
12.525	1-Nonene	C9H18	22371152.51
12.730	1,7-Octadiene, 2,3,3-trimethyl-	C11H20	20224790.98
12.815	Cyclopentene, 1,3-dimethyl-2-(1-methylethyl)-	C10H18	20157272.13
12.879	1,5-Heptadien-4-one, 3,3,6-trimethyl-	C10H16O	10302863.03
12.994	Cyclohexane, bromo-	C6H11Br	3545940.399
12.994	Oxalic acid, dicyclohexyl ester	C14H22O4	3385106.961
13.028	1,4-Cyclohexadiene, 3,3,6,6-tetramethyl-	C10H16	2022543.211
13.100	3,7-Decadiene, 2,9-dimethyl-	C12H22	21589429.68
13.173	Cyclopentene, 1,4-dimethyl-5-(1-methylethyl)-	C10H18	12999638.97
13.304	Heptane, 3-ethyl-2-methyl-	C10H22	2114885.996
13.304	Octane, 2,6-dimethyl-	C10H22	2114885.996
13.320	.alpha.-Phellandrene	C10H16	5544144.744
13.373	Benzene, (1-methylethyl)-	C9H12	12022905.19
13.401	Citronellyl tiglate	C15H26O2	3577085.244
13.639	Cyclopentane, 1,2,3,4,5-pentamethyl-	C10H20	2444303.61
13.678	2-Heptanone, 4-methyl-	C8H16O	2496494.503
13.702	3-Cyclohexene-1-methanol, .alpha.,4-dimethyl-	C9H16O	3538158.451
13.956	Camphene	C10H16	10384209.25
14.051	Benzene, propyl-	C9H12	4270750.575
14.059	Pentane, 3-ethyl-	C7H16	2017557.482
14.371	Benzene, 1,2,3-trimethyl-	C9H12	4521706.137
14.371	Mesitylene	C9H12	4517650.015
14.560	Phenol	C6H6O	16095983.95
14.702	Benzene, 1-ethyl-4-methoxy-	C9H12O	607555.7324

Component RT	Compound Name	Formula	Base Peak Area
14.730	Cyclohexane, 1-methyl-4-(1-methylethenyl)-, cis-	C10H18	1650196.511
14.730	3,7-Dimethyloct-6-enyl ethyl carbonate	C13H24O3	1650196.511
14.805	Cyclodecane	C10H20	2604986.517
14.811	1-Decene	C10H20	2591129.902
14.884	2-Decene, 4-methyl-, (Z)-	C11H22	13248444.77
14.902	Cyclotetrasiloxane, octamethyl-	C8H24O4Si4	1324255.417
14.937	2-Decene, 4-methyl-, (Z)-	C11H22	8646117.187
14.988	2-Decene, 4-methyl-, (Z)-	C11H22	6287318.313
15.034	Heptane, 3,3,5-trimethyl-	C10H22	2168587.383
15.093	1-Decene, 3,4-dimethyl-	C12H24	1680040.736
15.093	Decane, 4-methyl-	C11H24	1686116.34
15.172	Decane, 4-methyl-	C11H24	13941115.16
15.254	Nonane, 2,6-dimethyl-	C11H24	12951001.83
15.383	1,3-Cyclohexadiene, 1-methyl-4-(1-methylethyl)-	C10H16	2247872.847
15.537	o-Cymene	C10H14	15897076.32
15.623	D-Limonene	C10H16	1612096.7
15.795	Indane	C9H10	346401.9434
15.947	l-Isoleucine, n-propargyloxycarbonyl-, heptyl ester	C17H29NO4	77325.50411
16.103	Dodecane	C12H26	1644020.587
16.168	2-Decene, 2,4-dimethyl-	C12H24	11035671.24
16.241	2-Decene, 2,4-dimethyl-	C12H24	9046521.155
16.509	1-Decene, 2,4-dimethyl-	C12H24	8313460.017
16.583	1-Decene, 2,4-dimethyl-	C12H24	5544978.579
16.751	Benzene, 1-methyl-3-(1-methylethenyl)-	C10H12	320760.416
17.206	Thymol	C10H14O	227611.398
17.678	2-[(Trimethylsilyl)oxy]-2-{4-[(trimethylsilyl)oxy]phenyl}ethanamine	C14H27NO2Si2	223241.5474
17.799	Benzoic acid	C7H6O2	352321.2836
17.824	Benzoic acid	C7H6O2	341281.1308
18.500	Ethanone, 1-(2,3,4-trimethylphenyl)-	C11H14O	127243.2691
19.114	4-t-Butylbenzeneamine	C10H15N	189571.2468
20.975	2,6-Dihydroxyacetophenone, 2TMS derivative	C14H24O3Si2	333668.7839
21.561	Diethyl Phthalate	C12H14O4	5201041.688
22.421	Benzene, 1,1'-[1,2-ethanediylbis(oxy)]bis-	C14H14O2	264202.1861

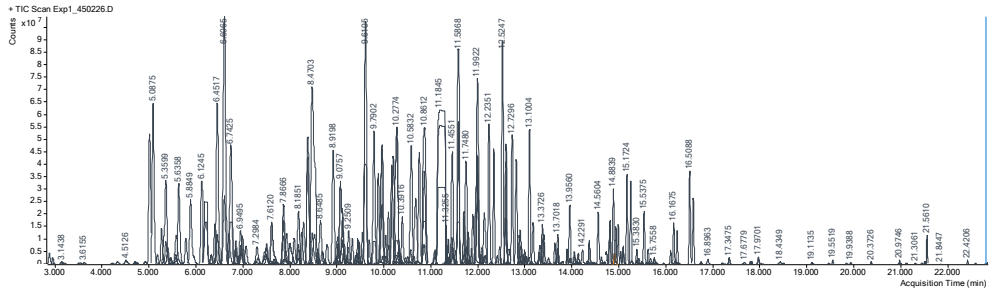

Figure 4.3- 4 GC-MS diagram of gas compound analysis of co-liquefaction of biomass with 50% PP blends and the addition of aluminosilicate and formic acid.

Chapter 5

Assessment of the impact of nylon contamination on the optimised macroalgal hydrothermal liquefaction process

5.1 Context

The preceding chapters focused on the conversion of plastic waste with waste lignocellulose into biofuel production through liquid phase pyrolysis and hydrothermal liquefaction. The main aims were to reduce the resulting environmental pollution from these sources. However, another key source of plastic contamination is in the marine environment. In the oceans, there is an increasing awareness of the impact of microplastic and macroplastic debris on marine ecosystems. There is an estimated 640,000 tonnes of nylon fishing gear floating on the ocean surface, which is thought to make up approximately 10% of the total amount of marine debris(Good, June et al. 2010). It has been reported that these discarded fishing items, including monofilament lines and nylon netting used in fishing activity, have contributed to the considerable growth in marine plastic contamination that has a global impact on the entanglement of marine life(Other and Lozano 2009).

In the previous chapters there is clear evidence that monomers of nylon 6 could be produced under HTL conditions, and that this could significantly add to the value of a marine biorefinery by being able to effectively chemically recycle the waste nylon alongside producing bio-crude and fertiliser products.

Thus, the conversion of macroalgal biomass with marine plastic pollutants (nylon ranges) was explored in this chapter. The aim was to build on the promising results for nylon 6 (Chapter 3), and systematically assess the co-hydrothermal liquefaction of macroalgae biomass with a range of nylons commonly found in maritime plastic litter including nylon 6, nylon 6/6, nylon 6/12, and nylon 12. The technique was then applied to an actual sample of marine macroalgae collected at sea, entangled with nylon fishing line.

This chapter is draft manuscript on the process and submitted in an alternative format in line with Appendix 6A of the “Specifications for Higher Degree Theses and Portfolios” as required by the University of Bath.

5.2 Abstract

Marine macroalgae offers a promising third generation feedstock for the production of fuels and chemicals, avoiding competition with conventional agriculture and potentially helping to improve eutrophication in sea and oceans. However, an increasing amount of plastic is being distributed into the oceans, and as such is contaminating macroalgal

beds. One of the major plastic contaminants is nylon 6 derived from discarded fishing gear, though an increasing amount of alternative nylon polymers, derived from fabrics, are also observed. This study aimed to assess the effect of these nylon contaminants on the hydrothermal liquefaction of *Fucas serratus*. The HTL of macroalgae was undertaken at 350 °C for 10 mins, with a range of nylon polymers (nylon 6, nylon6/6, nylon 12 and nylon 6/12), in the blend of 5, 20 and 50 wt% nylon to biomass. 17 wt.% bio-crude was achieved from *F. serratus* and co-liquefaction with nylon 6 increased this yield. In addition, nylon 6 completely broke down in the system producing the monomer caprolactam. The suitability of converting fishing gear was further demonstrated by conversion of actual fishing line (nylon 6) with the macroalgae, producing an array of products. The alternative nylon polymer blends were less reactive, with nylon 6/6 only being broken down 54% under the HTL conditions, forming cyclopentanone which distributed into the biocrude phase. Nylon 6/12 and nylon 12 were even less reactive, and only traces of the monomer cyclododecanone were observed in the bio-crude phase. This study demonstrates that while nylon 6 derived from fishing gear can be effectively integrated into a macroalgal biorefinery, alternative nylon polymers from other sectors are too stable to be converted under these conditions and present a real challenge to a macroalgal biorefinery.

5.3. Introduction

Marine biorefineries, based around the valorisation of salt water macroalgae, have been suggested as a promising alternative to terrestrial alternatives (Jung, Lim et al. 2013, Raikova, Le et al. 2017). Macroalgae are very photosynthetically efficient, do not compete with agricultural land, do not contain lignin and offer a largely untapped promising bioresource. To this end, a large body of research has been invested in the valorisation of macroalgae, including pre-treatments, fermentation and thermochemical conversion routes (Schultz-Jensen, Thygesen et al. 2013, Abeln, Fan et al. 2019, Raikova, Allen et al. 2019). A considerable number of challenges remain however, including having the ability to convert multiple species with highly variable composition (Raikova, Olsson et al. 2018, Beacham, Cole et al. 2019), to handle salt water as part of the process (Jones, Raikova et al.) and to be able to cope with either heavy metal (Piccini, Raikova et al. 2019) or plastic contamination (Galgani, Hanke et al. 2015). As such, it seems likely that feedstock agnostic processes, that can handle

a wide variability and produce an array of products, will be key to the further development of this field.

One such processing methodology is hydrothermal liquefaction (HTL), a promising thermochemical pathway identified as a cost-competitive process for converting high-moisture biomass. HTL avoids energy losses associated with drying which is needed for other thermochemical processes (Anastasakis, Biller et al. 2018). HTL delivers a high-energy bio-crude (30–40 MJ kg^{-1}) (Anastasakis, Biller et al. 2018) and produces a more stable crude product than pyrolysis (Peterson, Vogel et al. 2008, Bridgwater 2012, Palomino, Godoy-Silva et al. 2020). HTL generally uses temperatures between 280-370°C and pressures between 10 and 25 MPa to maintain water in the liquid state (Behrendt, Neubauer et al. 2008). Water acts as an important reactant and the addition of catalyst leads to several opportunities for separations and further chemical reactions(Biller and Ross 2011, Jindal and Jha 2016) The reactions that take place during HTL are decomposition and repolymerisation to form bio-crudes with high heating values, a solid residue containing the inorganic fraction and a water-soluble fraction which can be used as a fertiliser (Raikova, Smith-Baedorf et al. 2016). Research on hydrothermal liquefaction of marine macroalgae has gained significant traction in recent years (Yang, Feng et al. 2004, Aresta, Dibenedetto et al. 2005, Zhou, Zhang et al. 2010, Díaz-Vázquez, Rojas-Pérez et al. 2015, Neveux, Magnusson et al. 2015).

Contamination of oceans by microplastic and macroplastic debris has become one of the biggest marine environmental issues of recent years, affecting all the world's oceans. Plastics have been accumulating in substantial densities in the marine environment, from the sea surface down to deep-sea sediments (Van Cauwenberghe, Vanreusel et al. 2013, Woodall, Sanchez-Vidal et al. 2014). In a marine biorefinery, macroalgae could possibly be washed in clean water to remove microplastics, but residual microplastics can be absorbed onto the surface marine macroalgae (Gutow, Eckerlebe et al. 2016). Macroplastic on the other hand would need to be manually removed. Marine plastics originate mainly from many types of plastic debris, such as fishing nets, ropes, and plastic bags. While the majority of focus has been on terrestrial PET and polyolefin litter, over 20% of marine plastic debris found in the ocean is estimated to come from commercial fishing activity (Li, Tse et al. 2016). For example, an estimated 640,000 tonnes of nylon fishing gear enters the oceans every year which

amounts to approximately 10% of the total marine debris (Good, June et al. 2010). These discarded fishing items, including monofilament lines and nylon netting used in fishing activity, have contributed to the considerable growth in marine plastic contamination that is having global impact on the entanglement of marine life (Li, Tse et al. 2016). Due to the nature of the fibres, nylon fishing lines are one of the main contaminants found in macroalgal beds and seaweed farms (Galgani, Hanke et al. 2015).

Nylon refers to simple polyamides (Figure 5.3-1). For example, nylon 6 is synthesized by the ring opening polymerisation of caprolactam (Zhang, Zhang et al. 2019). While the vast majority of maritime fishing lines are produced from Nylon 6 there is increasing concern that alternative nylon polymers such as Nylon 6/6, Nylon 12 and Nylon 6/12 are increasingly distributing into the oceans from synthetic textile fibres that have been worn down during washing.

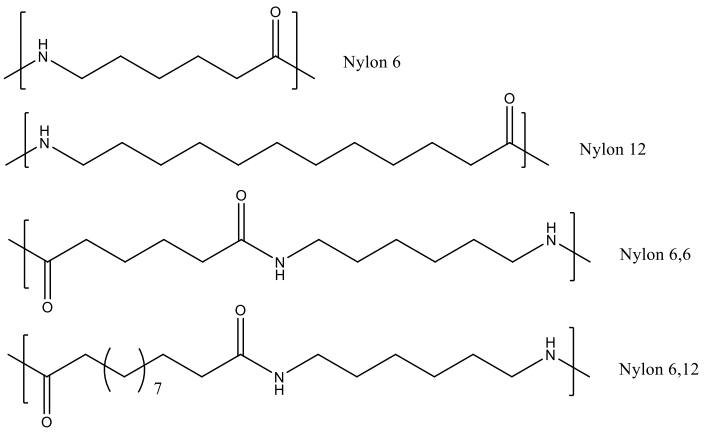

Figure 5.3- 1–Structure of common polyamide polymers used in the fishing industry

A number of publications have investigated the co-liquefaction of marine biomass with plastics. Wu et al. reported the co-liquefaction of microalgae with polypropylene and found that the composition of the bio-crude products was improved with reducing acid content (Wu, Liang et al. 2017). A similar observation was made by Coma et al. (Coma, Martinez-Hernandez et al. 2017), for the co-liquefaction of Spirulina and *Ulva sp.* with polyolefins distributing partially into the crude phase. In a more in depth study, Hongthong et al. demonstrated that a range of plastics could be co-processed with pistachio hulls through hydrothermal liquefaction, including nylon 6, that broke down almost completely (>80%) under the HTL conditions when combined with biomass (Hongthong, Raikova et al. 2019). Similarly, Raikova et al, screened multiple plastics,

including nylon 6 in the co-liquefaction of macroalgae. In this study they demonstrated that the nylon 6 did break down under the HTL conditions and one of the monomers, ϵ-caprolactam was observed, predominantly in the aqueous phase (Raikova, Knowles et al. 2019).

Plastics are one of the most promising resources for fuel production, with an average high heating value of 25 MJ/kg (Fekhar, Miskolczi et al. 2018), compared to 14-16 MJ/kg for macroalgae biomass (Neveux, Magnusson et al. 2015). Moreover, the high content of metal in the ash of macroalgae biomass can play an important role as catalysts in thermochemical processes (Ross, Jones et al. 2008, Yanik, Stahl et al. 2013), as a result, co-processing may lead to synergistic effects that promote the decomposition of biomass as well as plastic waste (Jin, Wang et al. 2019). Therefore, the conversion of macroalgal biomass and marine plastic, could not only reduce costs through no longer needing to separate the two components, but could lead to a significant enhancement in the efficiency and economics of a process as well as environmental protection. Moreover, with some evidence that monomers of nylon 6 could be selectively produced(Raikova, Knowles et al. 2019), this could significantly add to the value of a marine biorefinery by being able to effectively chemically recycle waste nylon alongside producing bio-crude and fertiliser products.

The aim of this research was to build on these promising results for nylon 6, and systematically assess the co-hydrothermal liquefaction of macroalgae biomass with a range of nylons commonly found in maritime plastic waste including nylon 6, nylon 6/6, nylon 6/12, and nylon 12. The technique was then applied to an actual sample of marine macroalgae collected at sea, entangled with nylon fishing line to demonstrate the concept.

5.4. Materials and methods

5.4.1 Materials

Fresh *F. serratus* samples were collected from Saltern Cove, Paignton, Devon. Prior to analysis, all samples were freeze-dried and milled to 10 μm diameter. Nylon 6, nylon 6/6, nylon 6/12, and nylon 12 were obtained from Sigma-Aldrich and used without further purification. All samples were stored at ambient conditions. The original composition (C, H, and N) of the raw material was measured by elemental analysis

and carried out externally at London Metropolitan University on a Carlo Erba Flash 2000 Elemental Analyser. The analysis is shown in supporting information (Table 5.9-1).

5.4.2 Hydrothermal of co-liquefaction of nylon and microalgae

Co-hydrothermal liquefaction of nylon and *F. serratus* was performed in a stainless-steel batch reactor according to previous report (Raikova, Knowles et al. 2019). The reactor had an approximate internal volume of 50 mL, and was connected with a pressure gauge, thermocouple, needle valve, and relief valve. The temperature was monitored using a thermocouple connected to data logging software. The reactor was loaded with a total of 3 g biomass (*F. serratus* mixed with nylon: 100:0, 95:5, 80:20, and 50:50) and 15 g of distilled water and heated within a tubular furnace until the temperature reached 350 °C, then removed from the furnace and allowed to cool to room temperature. Total heating time was approximately 10 min with a heating rate of average 35 °C min^{-1}. The experiments were repeated three times under the same conditions.

5.4.3 Calculation of HTL products

After cooling, gaseous products were released via the needle valve into an inverted, water-filled measuring cylinder to measure gaseous fraction volume. The yields of each product phase were calculated as mass percentage on ash-free basis. Gas phase yields were calculated using the ideal gas law, approximating the gas phase as 100 % CO_2, assuming an approximate molecular weight of 44 g mol^{-1} and a volume of 22.465 dm^3 mol^{-1} gas phase at 25 °C. The yield of gaseous product was determined using the following equation:

$$Gas\ yield\ (B,\%) = \frac{Gas\ volume\ \times 1.789\ \times 10^{-8}}{Mass\ macroalgae\ (g) + Mass\ nylon\ (g)} \times 100 \qquad (1)$$

The aqueous phase was separated to eliminate undissolved materials, the reactor contents were filtered by 1 μm pore size filter paper pre-dried overnight at 60 °C. Product yield in the water phase was determined by leaving a 2.0 g aliquot and drying in a 60 °C oven overnight and scaling the aqueous residue yield to the total aqueous phase mass. Aqueous phase residue yield was determined using the following equation:

$$Aqueous\ residue\ yield\ (A,\%) = \frac{Mass\ aqueous\ residue\ (g)}{Mass\ macroalgae\ (g) + Mass\ nylon\ (g)} \times 100 \quad (2)$$

To separate the remaining bio-oil and solid residue phase, the reactor was washed repeatedly with chloroform until the solvent was clear, the solution was filtered, and any residual bio-oil washed off the filter paper. The chloroform was removed using a rotary evaporator at 40 °C for 1.5 hours to give a dark oil (bio-crude). Bio-crude yield was determined using the following equation:

$$Biocrude\ yield\ (B,\%) = \frac{Mass\ biocrude\ (g)}{Mass\ macroalgae\ (g) + Mass\ nylon\ (g)} \times 100 \quad (3)$$

The solid residue on the filter paper was oven-dried overnight at 60°C to determine the solid residue product yield. Solid residue bio-char yield was determined using the following equation:

$$Solid\ residue\ (S,\%) = \frac{Mass\ solid\ phase\ (g)}{Mass\ macroalgae\ (g) + Mass\ nylon\ (g)} \times 100 \quad (4)$$

Mass losses occurred during the separation process, mainly through the loss of volatile organic compounds during the evaporation of solvent during removal of the bio-crude phases through filtration. The overall mass balance of the reaction was calculated according to the following equation:

$$Mass\ balance(\%) = G(\%) + A(\%) + B(\%) + S\ (\%) \quad (5)$$

5.4.4 Characterisation

The moisture content (%) was determined by drying 2 g of *F. serratus* . The sample was put into an oven at 105 °C and heated overnight. The dried sample was allowed to cool and reweighed. *F. serratus* ash was measured by heating a 100 mg of *F. serratus* in a Carbolite CWF 11 muffle furnace at 550 °C for 24 hours. The mass remaining at the end of the experiment was calculated as the ash content. *F. serratus* protein content was calculated from biomass elemental N concentration; mass fraction quoted dry basis using a conversion factor of 6.5. *F. serratus* total lipid content was extracted from the samples with chloroform/methanol (2:1, v/v). Approximately 200 mg of dried *F. serratus* was placed into a tube, 14 ml of the chloroform-methanol mixture

was added, and after 2 min in a vortex mixer the contents of the tube were filtered through 1 μm pore size filter paper. The filtered extract was washed with a chloroform-methanol mixture. The chloroform-mixture was removed using a rotary evaporator. The solid retained was determined as the total content of the macroalgae biomass.

Total carbohydrate was calculated, determined by difference

$$X_{carbohydrate} = 100\% - X_{protein} - X_{lipid} - X_{ash} \quad (6)$$

where $X_{component}$ is the mass fraction (%) of each biochemical component.

Elemental analysis (carbon, hydrogen and nitrogen content) of the biomass feedstock and products was carried out externally at London Metropolitan University on a Carlo Erba Flash 2000 Elemental Analyser. The oxygen content was determined by the difference from the sum of carbon, nitrogen, and hydrogen, assuming negligible sulphur in the products.

$$Oxygen\ (O, wt\%) = 100 - Carbon\ (C) - Hydrogen(H) - Nitrogen(N, wt\%) \quad (7)$$

The higher heating values (HHV) of the biomass, bio-char and bio-crude were calculated using data from the elemental composition in the following equation proposed by the Dulong formula (Valdez, Nelson et al. 2012), where C, H, and N are the weight percentages of each element:

$$HHV\ (MJkg^{-1}) = 0.3383C + 1.422\left(H - \left(\frac{O}{8}\right)\right) \quad (8)$$

The chemical energy recovery (ER) was calculated for the bio-crude and solid residue bio-char as follows:

$$Energy\ recovery = \frac{HHV\ Product\ (\%) \times Mass\ of\ product\ (\%)}{HHV\ of\ feedstock\ (\%)} \quad (9)$$

The extent of interactive synergistic effects between the *F. serratus* and plastics were calculated in terms of biocrude yield. Theoretical results are determined by comparing the experimental biocrude obtained during co-hydrothermal liquefaction with the individual feedstock by the equation below:

$$Synergistic\ effect = Y_B - (X_M \times Y_M + (1 - X_{NY}) \times Y_{NY} \quad (10)$$

where, Y_B is the yield of bio-crude obtained in the HTL experiment, X_M and X_{NY} are the mass fraction of *F. serratus* and nylon in the total reaction mixture, Y_M is the bio-crude yield of *F. serratus* , and Y_{NY} is the bio-crude yield of pure nylon plastic.

The chemical composition of the volatile fraction of the bio-crude was investigated using an Agilent Technologies 7890A GC system fitted with a 30 m × 250 µm × 0.25 µm HP5-MS column, coupled to a 5975C inert MSD. Samples were dissolved in THF, the carrier gas was helium, with a flow rate 1.2 mL min^{-1}. An initial oven temperature was set to 50°C, increasing to 250 °C at 10 °C min^{-1}. Initial identification of compounds was performed by means of the National Institute of Standards and technology (NIST) library of mass spectral database.

The aqueous phase from HTL was characterised through liquid chromatography using an Acquity UPLC BEH C18, 1.7 µM, 2.1 x 50 mm reverse phase column (Waters, Milford, MA, USA) with a flow rate of 0.3 mL/min at 45°C, and an injection volume of 10 µL. Mobile phases A and B consisted of 0.1% v/v formic acid in water, and 0.1% v/v formic acid in methanol, respectively. Gradient elution was carried out with 5% mobile phase B for 2 min followed by a linear gradient to 100% B for 5 min, these conditions were held at 100% B for 8 min, then returned to 5% B in 12 min.

Total metal content for solid residue and biocrude products were analysed using an Agilent 7700 Series ICP-MS. Samples were digested in aqua regia. Briefly, 50 mg solid residue was dissolved to 3 g hydrochloric acid (37%; Fisher Tracemetal grade), 1 ml concentrated nitric acid (67%; Fisher Tracemetal grade) was then added and left to digest at room temperature for 15 min. The digest was then heated to 95 °C for 60 min, then left to digest at ambient temperature overnight and made up to 25 ml with distilled water. The resulting solution was filter through a 1 µm filter membrane prior to analysis.

5.5 Results and discussion

5.5.1 Product yields and distribution

The *F. serratus* was co-processed with 5, 20 and 50 wt% weight loadings of nylon 6, nylon 6/6, nylon 6/12 and nylon 12 at 350 °C, and a residence time of 10 min. Mass balances are shown in Figure 5.5-1 where product yields were calculated on the ash-free basis (DAF%) of total feedstock input. The solid residue char formation can be

reduced for co-liquefaction of *F. serratus* with nylon 6, where the yield decreased from 52.4% for pure seaweed to 45.1%, 40.1 %, 36.2 % for 5 wt.%, 20 wt.%, and 50 wt.% nylon 6 blends respectively. Under the same conditions, without *F. serratus* 66.3 wt.% of the nylon 6 remains unreacted and distributes into the char phase.

Blending of *F. serratus* with nylon 6 was found to increase bio-crude yields, with the yield increasing from 13.2% for pure *F. serratus* to 16.5% for the 50 wt.% nylon 6 blend. On the addition of the nylon 6 blend, the yields of the gas phase product decreased slightly, and no gas was observed in the liquefaction of nylon 6 without *F. serratus*. The aqueous phase residue yield increased from 21.8 % for pure *F. serratus* to 24.7%, 30.6 %, 32.8% for 5 wt.%, 20 wt.%, and 50 wt.% nylon 6 blend respectively. This trend in yield is highly suggestive that the nylon 6 is breaking down in the reaction and distributing to both the crude and aqueous phases.

In contrast, the other nylon polymers (nylon 6/6; nylon 6/12 and nylon 12) did not behave in a similar manner under the optimal HTL conditions. For the co-liquefaction of nylon 6/6, the solid residue increased on increasing nylon blend wt% and the bio-crude production remained approximately constant irrespective of the amount of nylon in the feedstock. This result suggests that limited reactivity and thus breakdown/conversion is occurring. Similarly, little bio-crude or aqueous phase residue was recovered from the liquefaction without *F. serratus*, with the majority of mass being retained in the solid residue.

A similar reactivity was observed for both nylon 6/12, and nylon 12 where the majority of the mass is retained in the solid residue. Like nylon 6/6, both nylon 6/12 and nylon 12 did not break down significantly in the reaction without *F. serratus*.

While no nylons readily biodegrade in the natural environment, nylon 6/6 is known to be more thermally stable than nylon 6 due to kinetic studies on the thermal decomposition of nylons have found that the minimum activation energy for decomposition nylon6 and nylon 6/6 was 180 $kJmole^{-1}$ (Reardon and Barker 1974) and 223 $kJmole^{-1}$(Jellinek and Dunkle 1982), respectively. Activation energy is affected by the process of bond breaking at the C-N bonds, which rate-determining step of decomposition in nylon. Nylon 12, on the other hand, has a higher hardness and tensile strength than nylon 6 and nylon 6,6. Nylon 12 contains a lower content of the amide groups per unit area, also leading to a lower moisture absorption (Chen,

Tang et al. 2019). As the amide linkages are the most unstable parts of the nylon polymer, having a more olefin-type structure leads nylon 12 to demonstrate a higher resistance to chemical degradation, and a higher tensile strength and stiffness. This suggests that nylon 12 and nylon 6/12 are more stable compared to other nylons, and therefore more resistant to being broken down.

There appears to be interactions between the *F. serratus* and the nylon blends where the *F. serratus* synergistically aids the breakdown of nylon plastic. Results revealed that co-processing reduced solid residue bio-char formation, and bio-crude production was increased during co-liquefaction compared to individual component liquefaction.

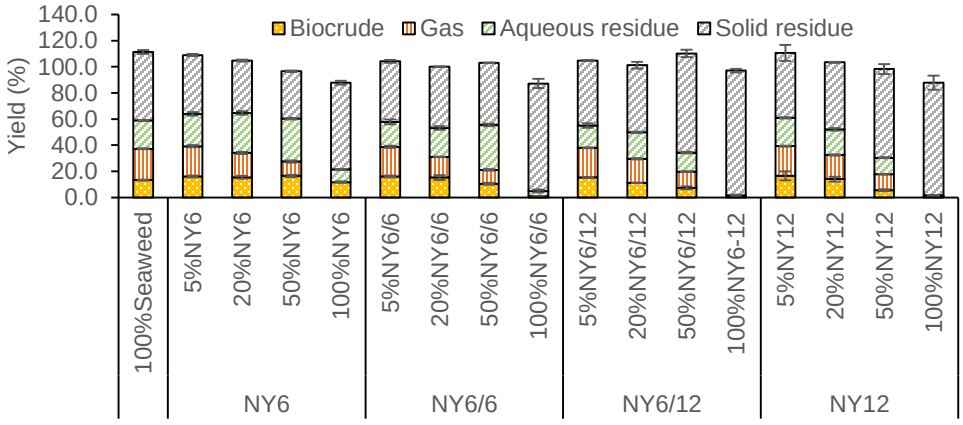

Figure 5.5- 1 –a) Mass balance of the products from the HTL reaction b) Synergistic effect of bio-crude obtained co-liquefaction of marine macroalgae with different nylon blend loadings

5.5.2 Nylon conversion

Fourier transform infrared analysis was performed to determine the amount of nylon remaining in the solid residue and therefore to estimate the overall nylon conversion (Figure 5.5-2). To do this, the FT-IR spectra were compared against a standard curve created with known increasing amounts of nylon added to the solid residue obtained from the HTL of pure *F. serratus*. For the solid residue from co-liquefaction of *F. serratus* and nylon 6, peaks of moderate-intensity were observed similar to those obtained for solid residue from HTL of pure *F. serratus* biomass (peak absorbance at 1089 cm^{-1}, 1570 cm^{-1} and 2850-2970 cm^{-1}). The presence of nylon 6 co-feedstock in HTL reactions did not appear to change the composition of the bio-char. This result

suggests that during co-liquefaction of *F. serratus* and nylon 6, there is a synergistic interaction between the two components resulting in an improved decomposition. For example, even at 50 wt.% blends there are only trace amounts of nylon left in the solid fraction (**Figure 5.5-3**).

However, on comparing the spectra of the bio-char from co-liquefaction of *F. serratus* with nylon 6/6, the spectra blend closely resembles the solid residue from pure *F. serratus* in the addition of 5 wt.% nylon 6/6 blend, while the intensity peak at 1089 cm^{-1} decreased with increasing the addition of 20 wt.% nylon 6/6, this suggests that the derived solid residue from the addition of 20 wt.% nylon 6/6 had lower ash content than the addition of 5 wt.% nylon 6/6. Peak intensities from HTL of pure *F. serratus* bands decreased in almost all the solid residue obtained with the addition of 50 wt.% nylon 6/6 blend, strong peaks were observed at 1535 cm^{-1} corresponding to stretching vibration of N-B-N and N=Q=N where –B– and =Q= stand for benzenoid and quinoid moieties in the polymer(Fazullin, Mavrin et al. 2015). In addition, a peak was observed at 1631 $cm^{-1,}$ corresponding to carbonyl groups of nylon 6/6(Fazullin, Mavrin et al. 2015). Another relevant band observed at 2949 cm^{-1} and 2823 $cm^{-1}$is attributed to CH_2 stretching, and peaks were observed at 3298 cm^{-1} corresponding to N-H stretch. These peaks were also seen in the FT-IR spectra of pure nylon 6/6, but not seen in the spectra of the bio-char from *F. serratus*. These findings indicate the presence of a large unreacted portion nylon 6/6 in the HTL solid residue.

Similar patterns in IR absorbance of the solid residue were observed for nylon 6/12 and nylon 12, where increasing blend levels gave rise to similar increases in the peaks associated with nylon 6/12 and nylon 12. Demonstrating that under this system only nylon 6 undergoes conversion and the alternative nylon species are too stable for conversion under optimal HTL conditions.

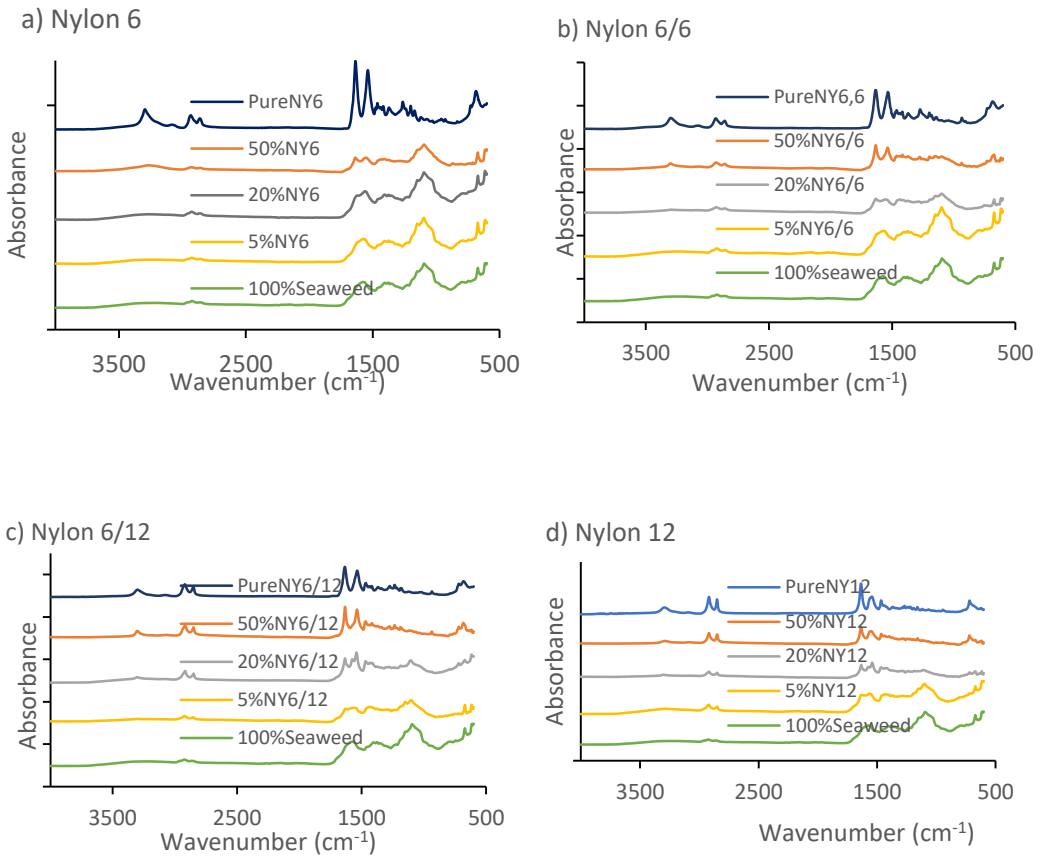

Figure 5.5-2–FTIR of pure nylon and the solid phase from hydrothermal co-liquefaction of *F. serratus* with (a) nylon *6*, (b) nylon 6/6, (c) nylon 6/12, and (d) nylon12.

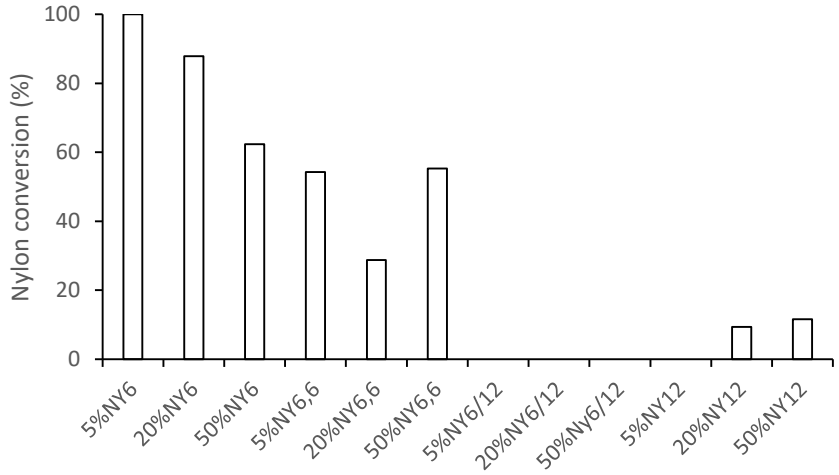

Figure 5.5- 3–Estimated nylon conversion in the co-liquefaction of *F. serratus* as calculated by FT-IR (see supporting information for the full method)

5.5.3 Bio-crude composition

The bio-crude samples were analysed by GC-MS to determine the chemical components of the bio-crude. A change in the chemical compounds found in the bio-crude was observed when adding a range of different nylon blends. The *F. serratus* alone produced a bio-crude product that contained mainly phenolic compounds potentially derived from the reaction of organic acids and carbohydrates in the system. Under HTL conditions, co-liquefaction with nylon 6, produced pure oil that contained ϵ-caprolactam, the monomer used in the polymerisation of nylon 6. When increasing the nylon 6 at 5 wt.%, 20 wt.%, 50 wt.%, and 100 wt.% blend levels, the level of ϵ-caprolactam observed increased substantially. This observation suggests that nylon 6 is successfully decomposed by hydrolysis at subcritical conditions to form high yields of ϵ-caprolactam via an ϵ-aminocaproic acid intermediate in bio-crude production(Iwaya, Sasaki et al. 2006). In addition, low levels of ϵ-caprolactam were also present in biocrude from pure *F. serratus*, possibly from protein decomposition in the marine macroalgae forming ϵ-caprolactam.

During HTL processing, the presence of nylon 6/6 led to an increased formation of cyclopentanone which is formed by a cyclic degradation mechanism in adipic acid(Gijsman, Steenbakkers et al. 2002). Concentrations of cyclopentanone are detected highest in the presence of 50 wt.% nylon 6/6 blend. In addition, for co-liquefaction of nylon 6/6 blend levels, low levels of ϵ-caprolactam were observed. Though these are presumably produced from the original *F. serratus*.

For liquefaction with nylon 6/12 and *F. serratus,* cyclododecanone was observed with the addition of 20 wt.% nylon 6/12. Cyclododecanone a cyclic ketone, is an important precursor involved in the synthesis of nylon 6/12 and nylon 12 (Feng, Yuan et al. 2011). Both cyclopentanone and cyclododecanone were not observed in the bio-crude derived from *F. serratus* alone. This is possibly the breakdown product produced from the degradation of the polymer.

Nylon 12 is more stable than nylon 6, partly as the polymer contains a lower concentration of amide groups (Levchik, Weil et al. 1999). A small amount of cyclododecanone was obtained from the conversion, which originates from nylon 12. However, the main chemical components are similar to bio-crude observed from pure macroalgae, containing mainly phenol and 2-Cyclopenten-1-one, 2-methyl.

The elemental composition of the bio-crude products obtained from co-liquefaction of *F. serratus* and nylon blends are presented in Figure 5.5-4. Hydrothermal liquefaction of pure *F. serratus* alone had a significant change from the pure *F. serratus* feedstock resulting in a substantial carbon increase and oxygen decrease (C increasing from 35.2% to 71.3% and O decreasing from 57.5% to 15.9%). With the increasing of nylon blend levels, the overall impact on bio-crude element composition was similar to those observed for *F. serratus* alone, however different trends were found in the presence of the nylon 6 blends. Carbon content decreased slightly with the increase of nylon 6/6, nylon 6/12, and nylon 12 blend levels, but decreased substantially for the increase of nylon 6 blend (which gave a decrease from 71.3% for pure macroalgae to 60.4% for 50 wt.% nylon 6 blend). There are no significant differences in elemental hydrogen and nitrogen composition in the bio-crude samples obtained from the presence of nylon blends (ranged from 8.4 to 9.5 for hydrogen content and ranged between 4.3 and 7.9 for nitrogen content). A slight increase in both hydrogen and nitrogen were observed for the increasing of all nylon blends. This suggests that *F. serratus* biomass and nylon radicals contribute through a biomolecular termination reaction, where a hydrogen radical is transferred from a nylon chain to biomass radicals(Ojha and Vinu 2018). It is also possible that hydrogen is donated from the water and transferred into the bio-crude during the degradation process (Masaru, Toshinari et al. 1997, Moriya and Enomoto 1999).

The high heating value (HHV) obtained from pure *F. serratus* alone was significantly improved through hydrothermal liquefaction, with a substantial improvement from 9 $MJkg^{-1}$ to 33 $MJkg^{-1}$ for pure macroalgae feedstock and hydrothermal liquefaction of pure *F. serratus* respectively. A similar observation was reported for hydrothermal liquefaction of *Sargassum* spp. macroalgae biomass(Díaz-Vázquez, Rojas-Pérez et al. 2015). In the presence of nylon blends, the HHV was not strongly affected, HHV from co-liquefaction of *F. serratus* with nylon blends was found to be in the range of 28-35 MJ kg^{-1}. However, the largest HHV change was found in the presence of 50 wt.% blend nylon 6/12, with a substantial decrease from 33 $MJkg^{-1}$ to 28 $MJkg^{-1}$. This suggests that the bio-crude was largely changed by the addition of 50 wt.% nylon 6 blend. The highest energy recovery value (38%) was obtained for the bio-crude obtained from the addition of 5 wt.% nylon 6 blend, while the lowest energy recovery (5.4%) was obtained from the addition of 50 wt.% nylon 12.

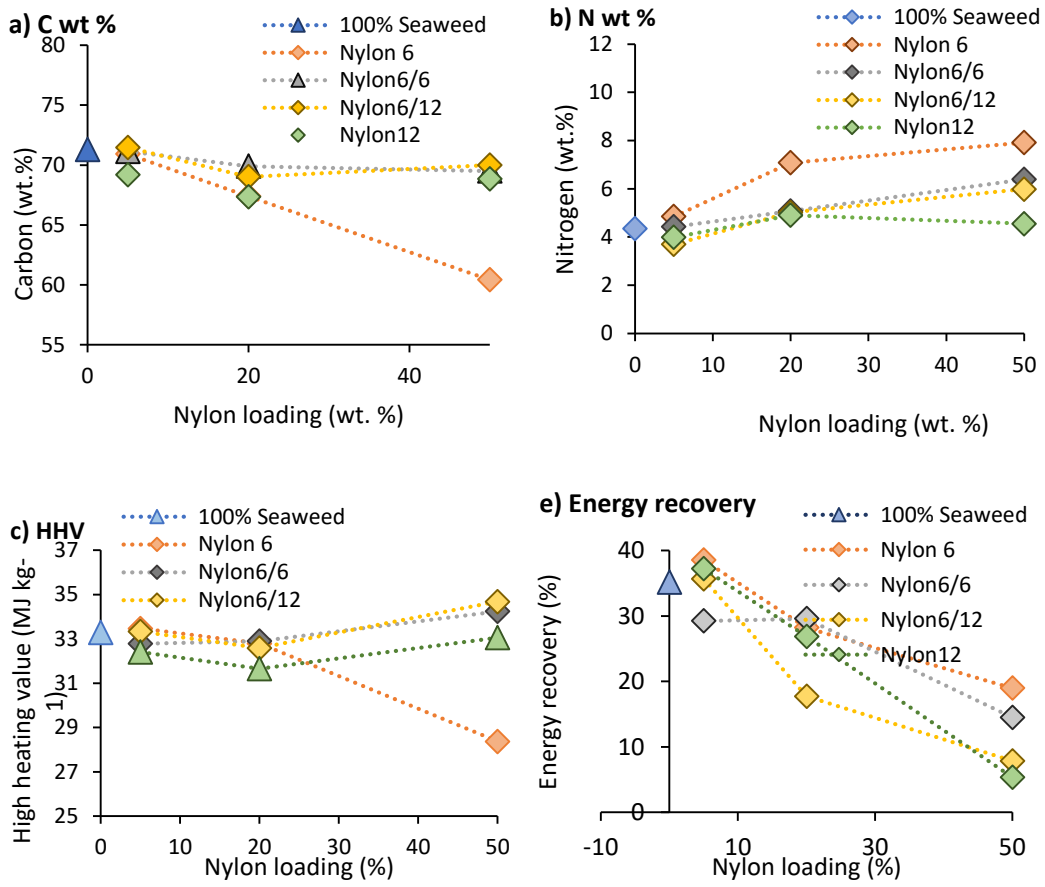

Figure 5.5-4–Bio-crude compositions produced from the co-liquefaction of macroalgae biomass with nylon 6, nylon 6/6, nylon 6/12, and nylon 12 a) is carbon wt. %, b) nitrogen wt. % c) is HHV of the bio-crudes, and d) is energy recovery (%)

5.5.4 Solid residue composition

Compared to the raw *F. serratus* biomass, the quality of the solid residues improved with increased carbon content and high heating value (from 32% to 53% for carbon content and from 9 $MJkg^{-1}$ to 17 $MJkg^{-1}$ for high heating value). The high carbon content of the solid residues resulted from the condensation and carbonization reaction through hydrothermal processing(Jung, Kim et al. 2016). The derived solid residue from co-liquefaction with nylon 6 has similar carbon, hydrogen, and nitrogen content to solid residue produced from pure macroalgae (**Figure 5.5-5**). Slight increases in elemental composition of the solid residue produced was observed with the addition of nylon 6/6 blends. Co-liquefaction of nylon 6/12 contributed to an increase in C content (55%C, 58%C, and 63%C for 5 wt.%, 20 wt.%, and 50 wt.% respectively). The

additional nylon 12 solid residue had the highest carbon content and hydrogen content (67 % C and 10 % H, respectively) suggesting that nylon 12 is the most difficult to break down and instead distributes into the solid residue.

For a better understanding of the elemental composition, the classification of solid residue fuel obtained from the HTL process can be illustrated using a Van Krevelen diagram (plot of H/C and O/C atomic ratios). A decrease in H/C and O/C atomic ratio suggests the development in aromatic structure in solid residue due to the removal of hydrogen and oxygen from the original feedstock(McKendry 2002). The effective combustion also preferably needs lower O/C and H/C ratios as they reduce thermodynamic energy losses, produce less smoke and water vapour (Rago, Surroop et al. 2018). Figure 5.5-6a-d shows the Van Krevelen diagram for all conditions used in this study and corresponding solid residue produced at different nylon blend loadings. Co-liquefaction of 5 wt.% blends of nylon 6, nylon 6/6, and 20 wt.% nylon 6 showed a very similar range of atomic ratios for solid residue from pure macroalgae, the O/C ratio ranged from 0.60 to 0.74, and H/C ratio ranged of 0.08. This suggested that 5 wt.% nylon 6, 20 wt.% nylon 6 were found to break down completely in the HTL process. A slightly higher H/C atomic ratios were observed in the additional 20 wt.% of nylon 6/6, nylon 6/12 blends and 50 wt.% nylon 6 blend (from 0.08 for pure macroalgae to 0.10, 0.12, 0.11, and 0.12 H/C atomic ratio obtained for 20 wt.% of nylon 6/6, nylon 6/12 blends and 50 wt.% nylon 6 blend, respectively). In contrast, co-liquefaction of 50 wt.% nylon 6/6, nylon 6/12, and nylon 12 blends contributed to a substantially H/C atomic ratio increase, while the O/C atomic ratio of the solid residues obtained substantially decreased. This significant difference was increased by a large level of unreacted nylons in the solid residue.

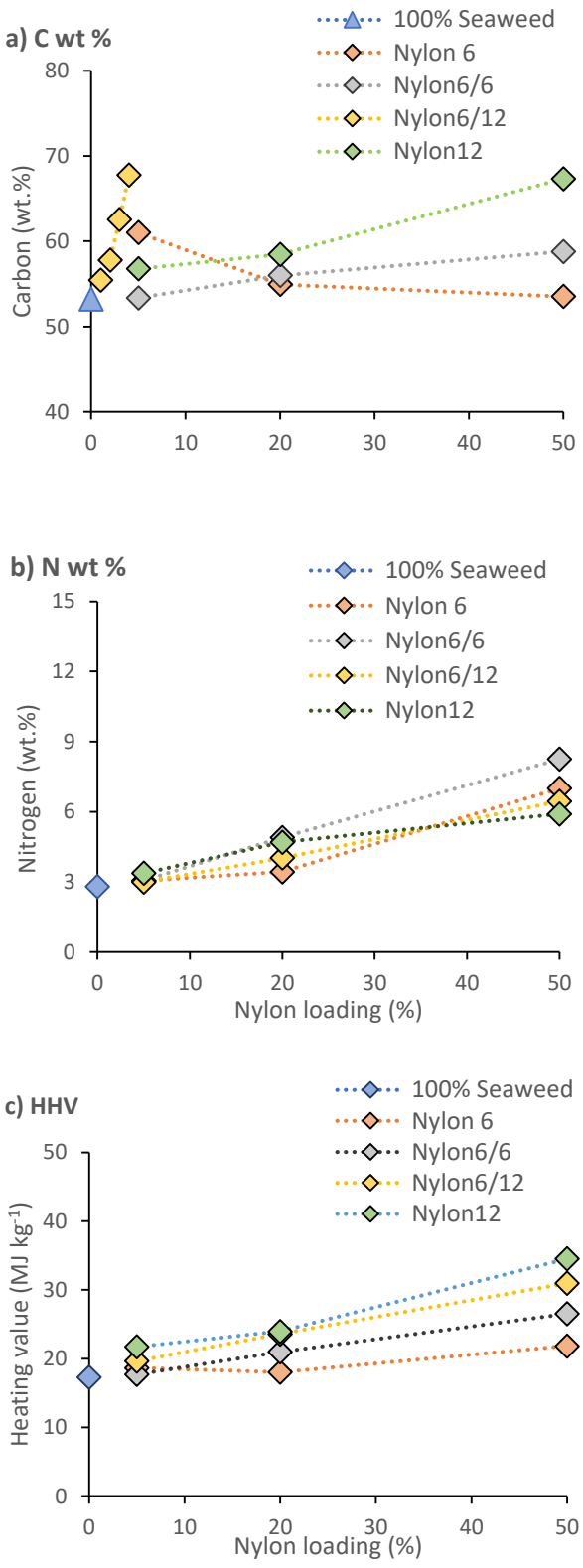

Figure 5.5- 5 Elemental composition of the bio-char of different nylon contents 5 wt.%, 20 wt.% and 50 wt.% of nylon 6, nylon 6/6, nylon 6/12, and nylon 12 a) is carbon wt. %, b) nitrogen wt. % c) is HHV of the bio-crudes

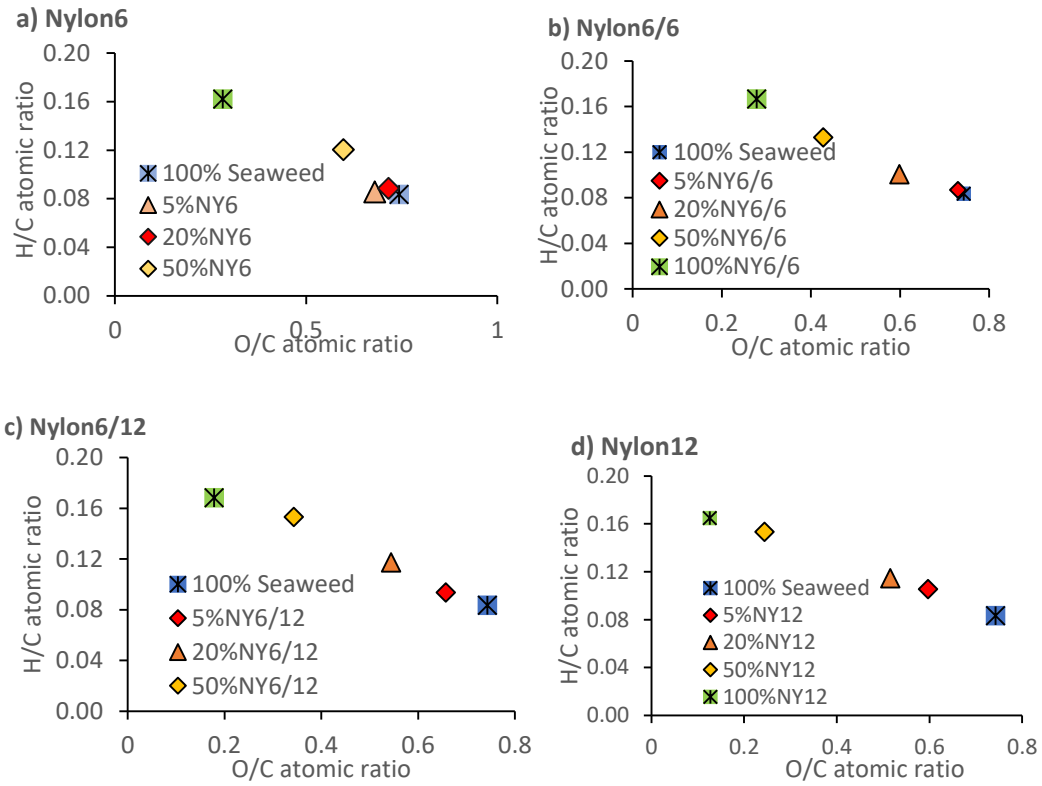

Figure 5.5- 6–Van Krevelen diagram with H: C and O: C molar ratio for co-liquefaction of macroalga with a) nylon6, b) nylon6/6, c) nylon6/12, and d) nylon 12

5.5.5 Yield of nylon products from the system

Due to the elevated conversion of nylon 6, and nylon 6/6, the aqueous phase and biocrude produced from these two polymers was also assessed for the production of chemicals produced from the breakdown of the polymers through LC-MS and GC-MS analysis. Since ε-caprolactam is the largest compound formation of nylon found in the aqueous phase and biocrude, ε-caprolactam was used to estimate the yield of nylon products from the system in both observed from aqueous and biocrude products. The quantification of the main compounds present in the aqueous phase and bio-crude are shown in Table 5.5-1. The presence of ε-caprolactam was observed in the range of 0.006-0.7 g L^{-1}, and 0.006.0-1.1 g L^{-1} for LC-MS and GC-MS respectively. The significant affects were observed for the presence of nylon 6 blends, with a substantial increase in the formation of ε-caprolactam in the aqueous phase. The presence of these compounds suggests that nylon 6 was almost completely decomposed into ε-aminocaproic acid by hydrolysis followed by cyclodehydration to ε-caprolactam

(Iwaya, Sasaki et al. 2006). Co-liquefaction of marine macroalgae with plastic therefore not only produces a suitable product suite, but with further separations could yield the nylon monomer for further valorisation. Calibration curves and future information are provided in the Supplementary Information (Figure 5.9-5-6, and Table 5.9-8).

Table 5.5-1–Quantitative result from LC MS and GC MS of selected nylon product in aqueous phase and oil phase for co-liquefaction of nylon with macroalgae

Sample	LC-MS	GC-MS
5% nylon6	0.07 g L^{-1}	0.22 g L^{-1}
20% nylon6	0.23 g L^{-1}	0.77 g L^{-1}
50% nylon6	0.70 g L^{-1}	1.11g L^{-1}
5% nylon6/6	0.06 g L^{-1}	0.06 g L^{-1}
20% nylon6/6	0.0 g L^{-1}	0.006 g L^{-1}
50% nylon6/6	0.0 g L^{-1}	0.03 g L^{-1}

5.5.6 Conversion of macroalgae with actual nylon fishing line

The results observed the identified positive correlation between nylon blend and *F. serratus* for enhancing the nylon conversion and bio-crude properties. In order to demonstrate the potential benefit a *real* waste system, nylon fishing line was co-processed with *F. serratus.*

The pure nylon fishing line was analysed using FT-IR to identify the key functional groups present. Peaks of intensity were observed at 3300 cm^{-1}, 2940 cm^{-1}, 1638 cm^{-1}, and 1538 cm^{-1}, which were similar to those observed from pure nylon 6 and nylon 6/6 (Figure 5.5-7). However, the intensity peak at 1638 cm^{-1}, and 1538 cm^{-1} were more similar to those observed from nylon 6/6. This suggests that the nylon fishing line was made from nylon 6/6.

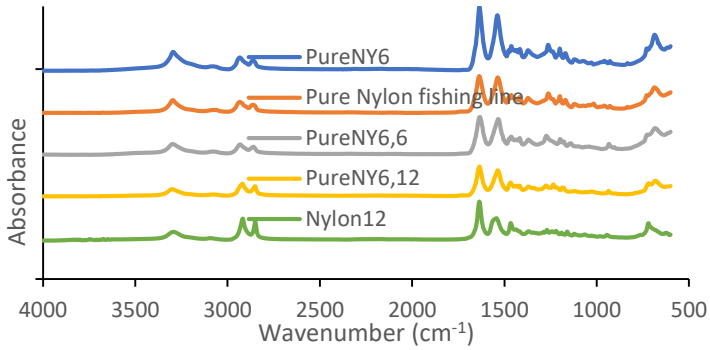

Figure 5.5- 7–FTIR of pure nylon fishing line compared to pure nylon 6, nylon6/6, nylon 6/12, and nylon 12

Similarly to the model compounds, the HTL of nylon fishing line with *F. serratus* was found to increase the bio-crude yields compared to pure *F. serratus***.** A modest increase in bio-crude yield was observed for 20 % blend of nylon fishing line blends (18.1 wt.%), whilst decreases in overall bio-crude production were seen for 5% and 50% blends (bio-crude yields of bio-crude products of 15.8 wt% and 10.8 wt%, respectively). Residue aqueous phase product recovery increased steadily (18 wt.% for 5% nylon fishing blend, increased to 28.7 wt% at a 50% nylon fishing blend), whilst increasing nylon fishing blend levels also caused a modest decrease in the yield of gas product at 50 wt.% blend level. These results were similar to those observed for HTL of nylon 6/6 blend. However, some of the polymer remained unconverted in the HTL reaction demonstrating a slightly lower overall conversion compared to co-liquefaction of the model nylon 6/6 blends.

The FTIR spectra of solid residue from HTL of nylon fishing line at 5% and 20% blends and *F. serratus* were almost identical to the spectrum of pure macroalgae solid bio-char (Figure 5.5-8b, 5.5-8c). The presence of nylon fishing line did not appear to change to composition of the solid residue, suggesting that nylon fishing line at 5% and 20% blends decomposed almost completely and forming soluble products. In contrast, a number of peaks are similar to pure nylon fishing line were observed at the biochar produced from 50% blended nylon fishing line, suggesting the presence of some unreacted nylon fishing line. The effect between the *F. serratus* and the nylon fishing line suggests the presence of *F. serratus* reactive fragments affects the thermal stability of nylon fishing line. The presence of metals in *F. serratus* ash can enhance the plastic decomposition, which becomes a hydrogen donor(Singh and Sharma

2008), preventing undesirable side reactions, leading to lower solid residue and higher biocrude formation (Biller, Riley et al. 2011).

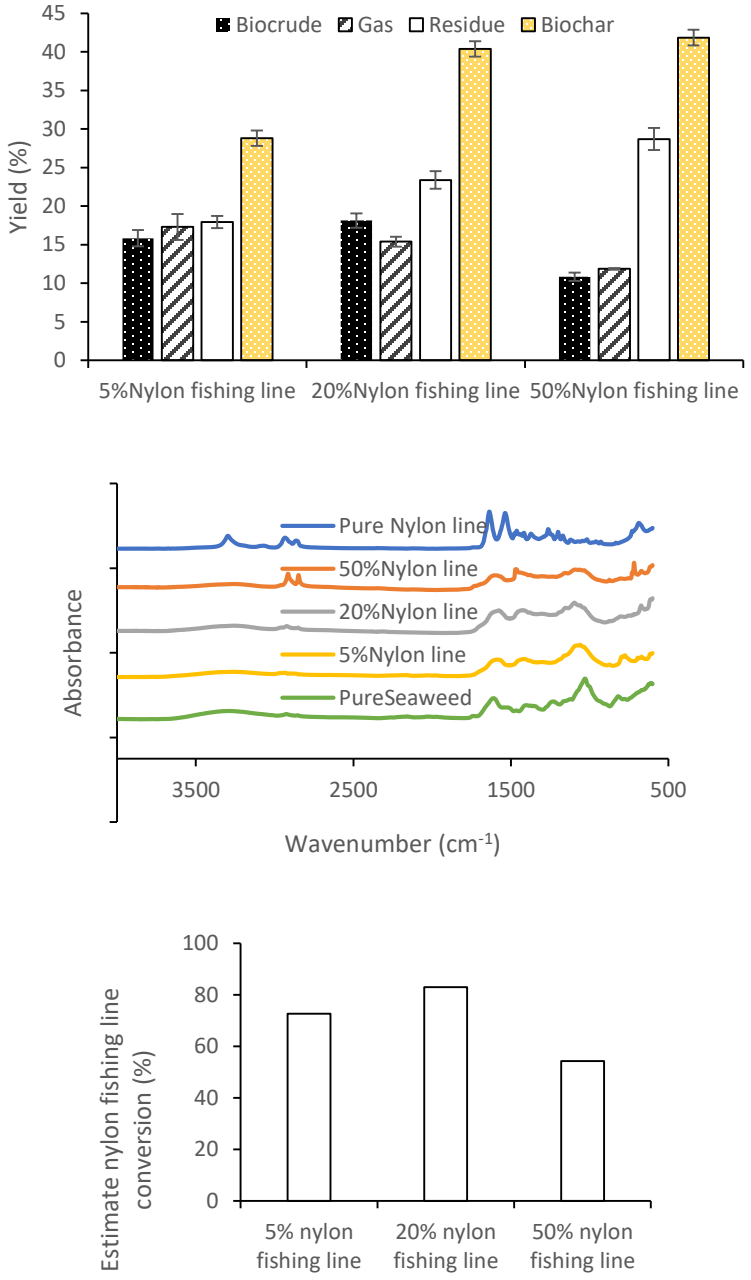

Figure 5.5- 8– a) Mass balance of co-liquefaction of fishing line and *F. serratus* b) FT-IR spectra of pure nylon fishing line and the solid phase from hydrothermal co-liquefaction of *F. serratus* with 5%, 20%, and 50% nylon fishing line blends. c) Estimated nylon fishing line conversion in the co-liquefaction of *F. serratus* as calculated by FT-IR (see supporting information for the full method)

5.6. Conclusion

Plastic is continuously accumulating in the world's oceans and has led to negative impacts across successive levels of the marine ecosystem. The main plastic contaminant found in macroalgae beds is nylon derived from fishing gear (predominantly nylon 6, though increasingly nylon 6,6), and increasingly from fabrics (alternative nylon compositions). This plastic waste presents a major challenge for a macroalgal biorefinery and would need to be able to be integrated into the conversion technology. In this study, we investigated a possible solution through including the nylon in an optimised HTL process. The co-liquefaction of nylon 6 and *F. serratus* was promising as the nylon was found to almost completely break down producing the monomer ϵ-caprolactam. Nylon 6/6 demonstrated some activity albeit reduced compared to nylon 6. In contrast, nylon 6/12 and nylon 12 did not break down at all and were retained in the solid residue. To demonstrate the suitability of this approach actual fishing line was converted with the macroalgal species recovered from a marine site, and when converted showed overall enhancement of the bio-crude products. This work demonstrates that while nylon derived fishing 'ghost gear' can be converted alongside the macroalgae producing an array of high value products, alternative nylon polymers, derived from fabrics and other nylon blends, would still cause an issue in a macroalgal HTL biorefinery and contaminate the solid residue.

5.7 Acknowledgments

The authors would like to acknowledge the Royal Thai Scholarship for financial support.

5.8 References

[1] K.A. Jung, S.-R. Lim, Y. Kim, J.M. Park, Potentials of macroalgae as feedstocks for biorefinery, Bioresource technology, 135 (2013) 182-190.
[2] S. Raikova, C. Le, T. Beacham, R. Jenkins, M. Allen, C. Chuck, Towards a marine biorefinery through the hydrothermal liquefaction of macroalgae native to the United Kingdom, Biomass and Bioenergy, 107 (2017) 244-253.
[3] N. Schultz-Jensen, A. Thygesen, F. Leipold, S.T. Thomsen, C. Roslander, H. Lilholt, A.B. Bjerre, Pretreatment of the macroalgae Chaetomorpha linum for the production of bioethanol–Comparison of five pretreatment technologies, Bioresource technology, 140 (2013) 36-42.
[4] F. Abeln, J. Fan, V.L. Budarin, H. Briers, S. Parsons, M.J. Allen, D.A. Henk, J. Clark, C.J. Chuck, Lipid production through the single-step microwave hydrolysis of macroalgae using the oleaginous yeast Metschnikowia pulcherrima, Algal research, 38 (2019) 101411.
[5] S. Raikova, M.J. Allen, C.J. Chuck, Hydrothermal liquefaction of macroalgae for the production of renewable biofuels, Biofuels, Bioproducts and Biorefining, 13 (2019) 1483-1504.
[6] S. Raikova, J. Olsson, J.J. Mayers, G.r.M. Nylund, E. Albers, C.J. Chuck, Effect of geographical location on the variation in products formed from the hydrothermal liquefaction of Ulva intestinalis, Energy & Fuels, (2018).
[7] T.A. Beacham, I.S. Cole, L.S. DeDross, S. Raikova, C.J. Chuck, J. Macdonald, L. Herrera, T. Ali, R.L. Airs, A. Landels, Analysis of Seaweeds from South West England as a Biorefinery Feedstock, Applied Sciences, 9 (2019) 4456.
[8] E. Jones, S. Raikova, S. Ebrahim, S. Parsons, M.J. Allen, C.J. Chuck, Saltwater based fractionation and valorisation of macroalgae, Journal of Chemical Technology & Biotechnology.
[9] M. Piccini, S. Raikova, M.J. Allen, C.J. Chuck, A synergistic use of microalgae and macroalgae for heavy metal bioremediation and bioenergy production through hydrothermal liquefaction, Sustainable energy & fuels, 3 (2019) 292-301.
[10] F. Galgani, G. Hanke, T. Maes, Global distribution, composition and abundance of marine litter, Marine anthropogenic litter, Springer, Cham2015, pp. 29-56.
[11] K. Anastasakis, P. Biller, R.B. Madsen, M. Glasius, I. Johannsen, Continuous Hydrothermal Liquefaction of Biomass in a Novel Pilot Plant with Heat Recovery and Hydraulic Oscillation, Energies, 11 (2018) 2695.
[12] A.A. Peterson, F. Vogel, R.P. Lachance, M. Fröling, J.M.J. Antal, J.W. Tester, Thermochemical biofuel production in hydrothermal media: A review of sub- and supercritical water technologies, Energy & Environmental Science, 1 (2008) 32-65.
[13] A.V. Bridgwater, Review of fast pyrolysis of biomass and product upgrading, Biomass and Bioenergy, 38 (2012) 68-94.
[14] A. Palomino, R.D. Godoy-Silva, S. Raikova, C.J. Chuck, The storage stability of biocrude obtained by the hydrothermal liquefaction of microalgae, Renewable Energy, 145 (2020) 1720-1729.
[15] F. Behrendt, Y. Neubauer, M. Oevermann, B. Wilmes, N. Zobel, Direct Liquefaction of Biomass, Chemical Engineering & Technology, 31 (2008) 667-677.
[16] P. Biller, A.B. Ross, Potential yields and properties of oil from the hydrothermal liquefaction of microalgae with different biochemical content, Bioresource Technology, 102 (2011) 215-225.
[17] M. Jindal, M. Jha, Effect of process parameters on hydrothermal liquefaction of waste furniture sawdust for bio-oil production, RSC Adv., 6 (2016).
[18] S. Raikova, H. Smith-Baedorf, R. Bransgrove, O. Barlow, F. Santomauro, J.L. Wagner, M.J. Allen, C.G. Bryan, D. Sapsford, C.J. Chuck, Assessing hydrothermal

liquefaction for the production of bio-oil and enhanced metal recovery from microalgae cultivated on acid mine drainage, Fuel Processing Technology, 142 (2016) 219-227.
[19] D. Zhou, L. Zhang, S. Zhang, H. Fu, J. Chen, Hydrothermal Liquefaction of Macroalgae Enteromorpha prolifera to Bio-oil, Energy & Fuels, 24 (2010) 4054-4061.
[20] M. Aresta, A. Dibenedetto, M. Carone, T. Colonna, C. Fragale, Production of biodiesel from macroalgae by supercritical CO2 extraction and thermochemical liquefaction, Environmental Chemistry Letters, 3 (2005) 136-139.
[21] Y.F. Yang, C.P. Feng, Y. Inamori, T. Maekawa, Analysis of energy conversion characteristics in liquefaction of algae, Resources, Conservation and Recycling, 43 (2004) 21-33.
[22] N. Neveux, M. Magnusson, T. Maschmeyer, R. de Nys, N.A. Paul, Comparing the potential production and value of high-energy liquid fuels and protein from marine and freshwater macroalgae, GCB Bioenergy, 7 (2015) 673-689.
[23] L.M. Díaz-Vázquez, A. Rojas-Pérez, M. Fuentes-Caraballo, I.V. Robles, U. Jena, K.C. Das, Demineralization of Sargassum spp. Macroalgae Biomass: Selective Hydrothermal Liquefaction Process for Bio-Oil Production, Frontiers in Energy Research, 3 (2015).
[24] L. Van Cauwenberghe, A. Vanreusel, J. Mees, C.R. Janssen, Microplastic pollution in deep-sea sediments, Environmental Pollution, 182 (2013) 495-499.
[25] L.C. Woodall, A. Sanchez-Vidal, M. Canals, G.L.J. Paterson, R. Coppock, V. Sleight, A. Calafat, A.D. Rogers, B.E. Narayanaswamy, R.C. Thompson, The deep sea is a major sink for microplastic debris, Royal Society Open Science, 1 (2014) 140317.
[26] L. Gutow, A. Eckerlebe, L. Giménez, R. Saborowski, Experimental Evaluation of Seaweeds as a Vector for Microplastics into Marine Food Webs, Environmental Science & Technology, 50 (2016) 915-923.
[27] W.C. Li, H.F. Tse, L. Fok, Plastic waste in the marine environment: A review of sources, occurrence and effects, Science of The Total Environment, 566-567 (2016) 333-349.
[28] T.P. Good, J.A. June, M.A. Etnier, G. Broadhurst, Derelict fishing nets in Puget Sound and the Northwest Straits: Patterns and threats to marine fauna, Marine Pollution Bulletin, 60 (2010) 39-50.
[29] S. Zhang, J. Zhang, L. Tang, J. Huang, Y. Fang, P. Ji, C. Wang, H. Wang, A Novel Synthetic Strategy for Preparing Polyamide 6 (PA6)-Based Polymer with Transesterification, Polymers, 11 (2019) 978.
[30] X. Wu, J. Liang, Y. Wu, H. Hu, S. Huang, K. Wu, Co-liquefaction of microalgae and polypropylene in sub-/super-critical water, RSC Advances, 7 (2017) 13768-13776.
[31] M. Coma, E. Martinez-Hernandez, F. Abeln, S. Raikova, J. Donnelly, T. Arnot, M. Allen, D.D. Hong, C.J. Chuck, Organic waste as a sustainable feedstock for platform chemicals, Faraday discussions, 202 (2017) 175-195.
[32] S. Hongthong, S. Raikova, H. Leese, C. Chuck, Co-processing of common plastics with pistachio hulls via hydrothermal liquefaction, Waste management (New York, N.Y.), 102 (2019) 351-361.
[33] S. Raikova, T.D.J. Knowles, M.J. Allen, C.J. Chuck, Co-liquefaction of Macroalgae with Common Marine Plastic Pollutants, ACS Sustainable Chemistry & Engineering, 7 (2019) 6769-6781.
[34] B. Fekhar, N. Miskolczi, T. Bhaskar, J. Kumar, V. Dhyani, Co-pyrolysis of biomass and plastic wastes: investigation of apparent kinetic parameters and stability of pyrolysis oils, IOP Conference Series: Earth and Environmental Science, 154 (2018) 012022.

[35] A.B. Ross, J.M. Jones, M.L. Kubacki, T. Bridgeman, Classification of macroalgae as fuel and its thermochemical behaviour, Bioresource Technology, 99 (2008) 6494-6504.
[36] J. Yanik, R. Stahl, N. Troeger, A. Sinag, Pyrolysis of algal biomass, Journal of Analytical and Applied Pyrolysis, 103 (2013) 134-141.
[37] Q. Jin, X. Wang, S. Li, H. Mikulčić, T. Bešenić, S. Deng, M. Vujanović, H. Tan, B.M. Kumfer, Synergistic effects during co-pyrolysis of biomass and plastic: Gas, tar, soot, char products and thermogravimetric study, Journal of the Energy Institute, 92 (2019) 108-117.
[38] B.L. Deopura, 2 - Polyamide fibers, in: B.L. Deopura, R. Alagirusamy, M. Joshi, B. Gupta (Eds.) Polyesters and Polyamides, Woodhead Publishing2008, pp. 41-61.
[39] G. Chen, K. Tang, G. Niu, K. Pan, X. Feng, L. Zhang, Synthesis and characterization of the novel nylon 12 6 based on 1,12-diaminododecane, Polymer Engineering & Science, 59 (2019) 192-197.
[40] D. Fazullin, G. Mavrin, M. Sokolov, I.G. Shaikhiev, Infrared Spectroscopic Studies of the PTFE and Nylon Membranes Modified Polyaniline, Modern Applied Science, 9 (2015) 242-249.
[41] T. Iwaya, M. Sasaki, M. Goto, Kinetic analysis for hydrothermal depolymerization of nylon 6, Polymer Degradation and Stability, 91 (2006) 1989-1995.
[42] P. Gijsman, R. Steenbakkers, C. Fürst, J. Kersjes, Differences in the flame retardant mechanism of melamine cyanurate in polyamide 6 and polyamide 66, Polymer Degradation and Stability, 78 (2002) 219-224.
[43] Q. Feng, D.-K. Yuan, D.-Q. Wang, X.-M. Liang, J.-J. Zhang, J.-P. Wu, F.-H. Chen, Eco-friendly Synthesis of Cyclododecanone from Cyclododecatriene, Green and Sustainable Chemistry, Vol.01No.03 (2011) 7.
[44] S.V. Levchik, E.D. Weil, M. Lewin, Thermal decomposition of aliphatic nylons, Polymer International, 48 (1999) 532-557.
[45] D.K. Ojha, R. Vinu, Chapter 12 - Copyrolysis of Lignocellulosic Biomass With Waste Plastics for Resource Recovery, in: T. Bhaskar, A. Pandey, S.V. Mohan, D.-J. Lee, S.K. Khanal (Eds.) Waste Biorefinery, Elsevier2018, pp. 349-391.
[46] T. Moriya, H. Enomoto, Characteristics of polyethylene cracking in supercritical water compared to thermal cracking, Polymer Degradation and Stability, 65 (1999) 373-386.
[47] N. Masaru, T. Toshinari, W. Chihiro, F. Emi, E. Heiji, 13C-NMR Evidence for Hydrogen Supply by Water for Polymer Cracking in Supercritical Water, Chemistry Letters, 26 (1997) 163-164.
[48] K.-W. Jung, K. Kim, T.-U. Jeong, K.-H. Ahn, Influence of pyrolysis temperature on characteristics and phosphate adsorption capability of biochar derived from waste-marine macroalgae (Undaria pinnatifida roots), Bioresource Technology, 200 (2016) 1024-1028.
[49] P. McKendry, Energy production from biomass (part 1): overview of biomass, Bioresource Technology, 83 (2002) 37-46.
[50] Y.P. Rago, D. Surroop, R. Mohee, Torrefaction of textile waste for production of energy-dense biochar using mass loss as a synthetic indicator, Journal of Environmental Chemical Engineering, 6 (2018) 811-822.
[51] B. Singh, N. Sharma, Mechanistic implications of plastic degradation, Polymer Degradation and Stability, 93 (2008) 561-584.
[52] P. Biller, R. Riley, A.B. Ross, Catalytic hydrothermal processing of microalgae: Decomposition and upgrading of lipids, Bioresource Technology, 102 (2011) 4841-4848.

5.9 Supporting information

5.9.1 Feedstock elemental compositions

Table 5.9-1–Feedstock elemental compositions

Analysis	Seaweed	Nylon6	Nylon6/6	Nylon6/12	Nylon12
Moisture	4.9	-	-	-	-
Ash	25%	-	-	-	-
Element Analysis (%)					
C	35.3	63.3	62.7	68.9	72.6
H	5.1	10.1	10.2	11.6	12.0
N	7.1	12.3	12.4	9.0	7.0
other	57.5	14.25	14.6	10.4	8.3
HHV	8.9	33.2	33.2	38.0	40.2
Component analysis (wt.%)					
Carbohydrate	53.6				
Protein	13.8				
lipid	7.5				

5.9.2 Calibration curves for quantification of unreacted plastics in bio-char using FTIR

The conversion of nylons6 was estimated by plotting calibration curves of known amounts of the nylons with solid residue generated from the HTL reaction which contained only macroalgae biomass. Calibration curves were created for each nylon/biomass combination (nylon6/macroalgae, nylon66/macroalgae, nylon6,12/macroalgae, nylon 12/ macroalgae) by mixing bio-char from HTL of pure marine macroalgae with nylons at a range of known concentrations.

5.9.2.1 Nylon 6 in solid bio-char

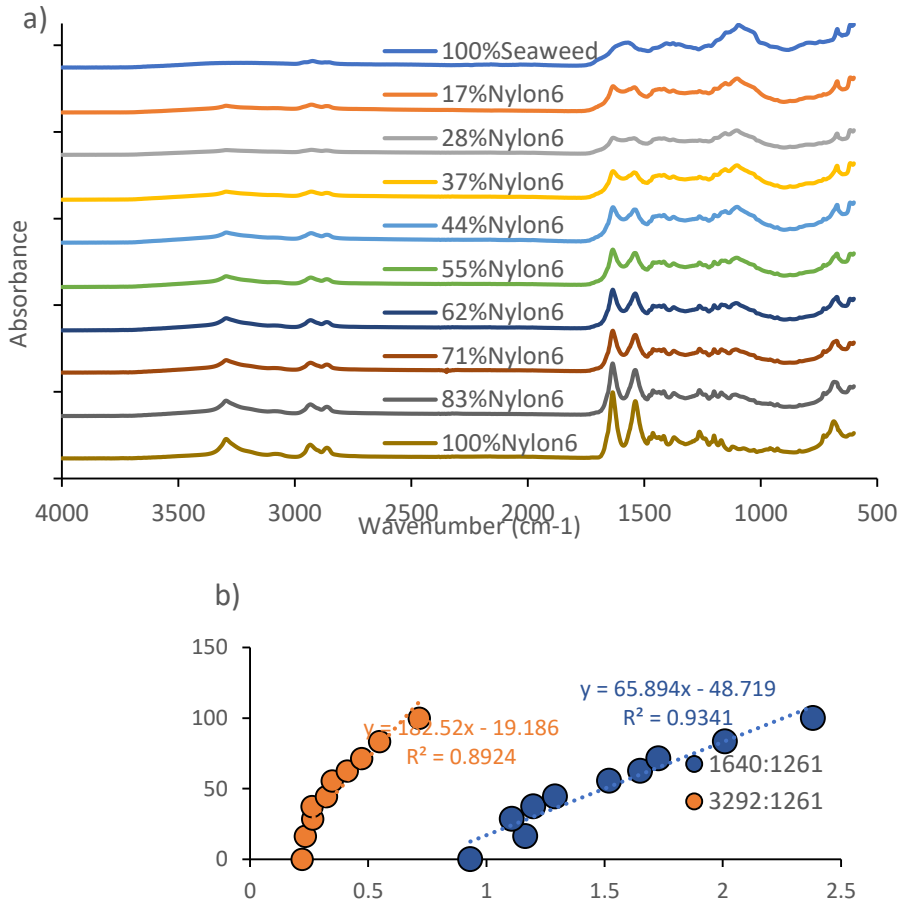

Figure 5.9- 1–(a) FTIR spectra of macroalgae bio-char with different nylon6 contents, and (b) peak intensity ratio calibration curve for nylon6/6 content in macroalgae bio-char.

Table 5.9- 2 –Calculated percentage concentrations of unreacted nylon6 in bio-char from co-liquefaction of macroalgae with nylon6.

	Nylon 6	**Macroalgae solid residue**	**PIR**	**Predictive equation**	**R2**	**Estimated Nylon 6 content of char (%)**
	1640 cm^{-1}	**1261 cm^{-1}**	**1640:1261**	Y = 65.859x-48.934	0.94	
5% Nylon 6	0.01962	0.02332	0.84126			6.5 %
20% Nylon 6	0.03596	0.04031	0.8921			9.8%
50% Nylon 6	0.02047	0.01571	1.3031			36.8%
	3292 cm^{-1}	**1261 cm^{-1}**	**3292:1261**	Y= 199.82x – 17.088		

5 % Nylon 6	0.00114	0.02332	0.04895	0.0%
20 % Nylon 6	0.00561	0.04031	0.13906	6.0%
50 % Nylon 6	0.00894	0.01571	0.56932	84.4%

5.9.2.2 **Nylon 6/6 in solid char**

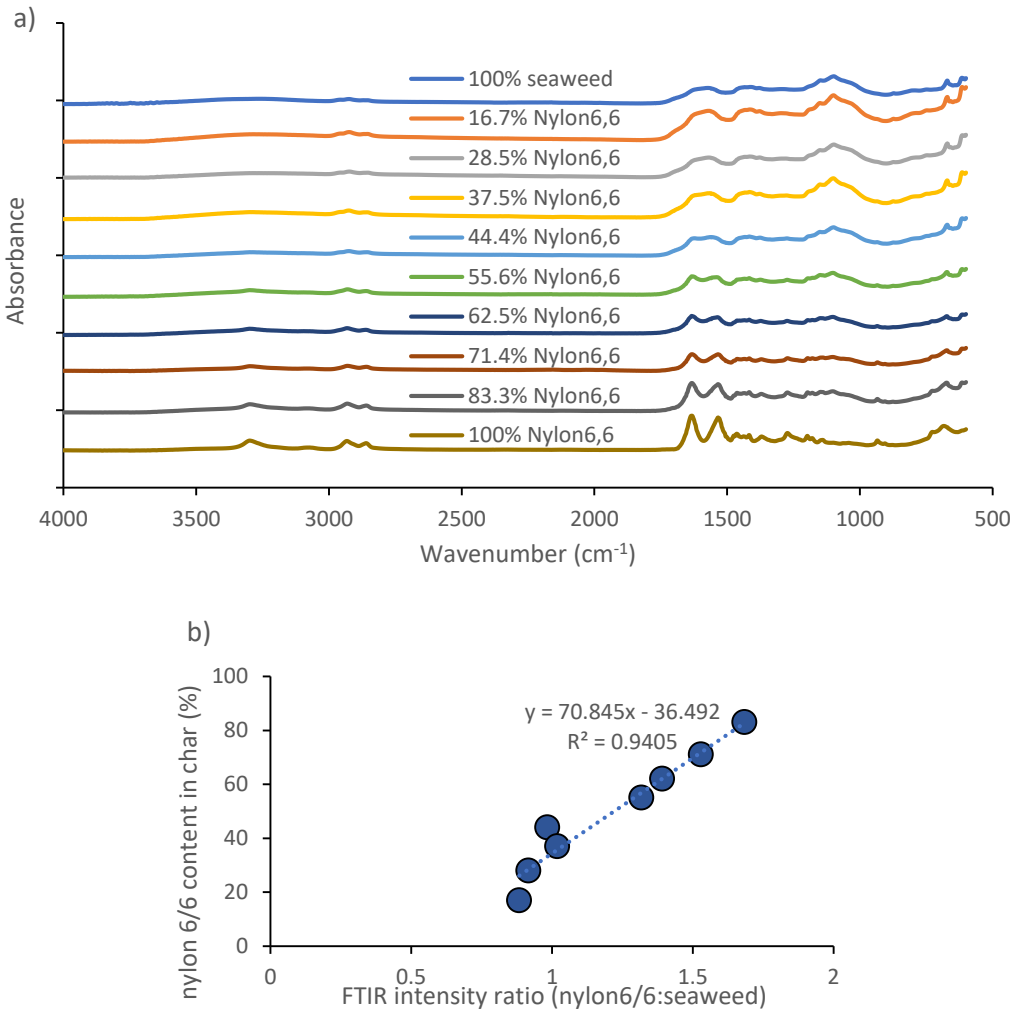

Figure 5.9-2–(a) FTIR spectra of macroalgae bio-char with different nylon6/6 contents, and (b) peak intensity ratio calibration curve for nylon6/6 content in macroalgae bio-char.

Table 5.9- 3–Calculated percentage concentrations of unreacted nylon6/6 in bio-char from co-liquefaction of macroalgae with nylon6/6.

	Nylon 6/6	seaweed solid residue	PIR	Predictive equation	R2	Estimated Nylon 6 content of char (%)
	1640 cm^{-1}	**1261 cm^{-1}**	**1640:1261**	Y = 70.845x-36.492	0.94	
5% Nylon 6/6	0.02251	0.037211	0.604955			6.4 %
20% Nylon 6/6	0.03188	0.027787	1.147120			44.8%
50% Nylon 6/6	0.04821	0.03052	1.588451			76.0%

5.9.2.3 Nylon 6/12 in solid bio-char

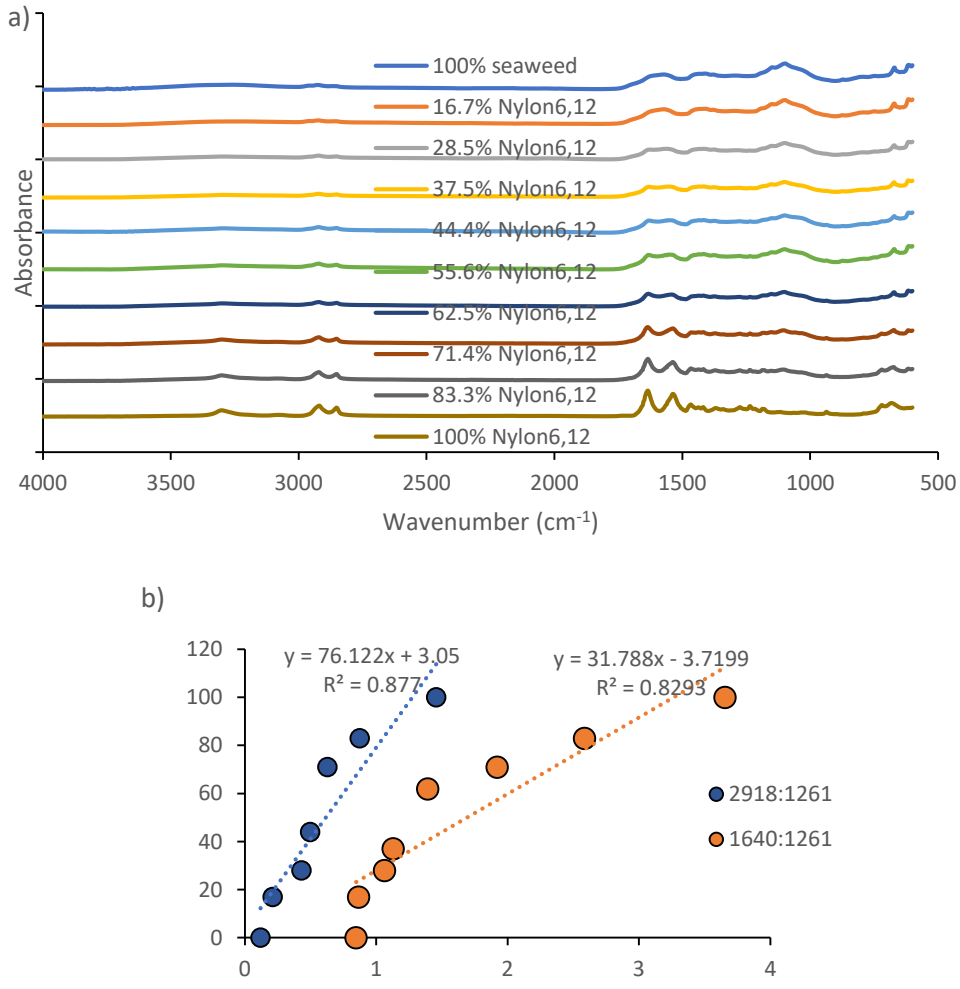

Figure 5.9-3– (a) FTIR spectra of macroalgae bio-char with different nylon6/12 contents, and (b) peak intensity ratio calibration curve for nylon6/12 content in macroalgae bio-char.

Table 5.9- 4 – Calculated percentage concentrations of unreacted nylon6/12 in bio-char from co-liquefaction of macroalgae with nylon6/12.

	Nylon 6/12	seaweed solid residue	PIR	Predictive equation	R2	Estimated Nylon 6 content of char (%)
	1640 cm^{-1}	1261 cm^{-1}	1640:1261	Y = 31.788-3.7199	0.83	
5%Nylon6/12	0.033626	0.036728	0.9155473			25.4 %
20%Nylon6/12	0.03394	0.022046	1.5396717			45.2%
50%Nylon6/12	0.05401	0.021718	2.4885014			75.4%
	2981 cm^{-1}	1261 cm^{-1}	2981:1261	Y= 76.122x + 3.05	0.88	
5 % Nylon 6/12	0.01232	0.036728	0.33532			28.6%
20 %Nylon 6/12	0.01865	0.022046	0.84611			67.5%
50 %Nylon 6/12	0.03917	0.02171	1.80478			140.4%

5.9.2.4 Nylon 6/12 in solid bio-char

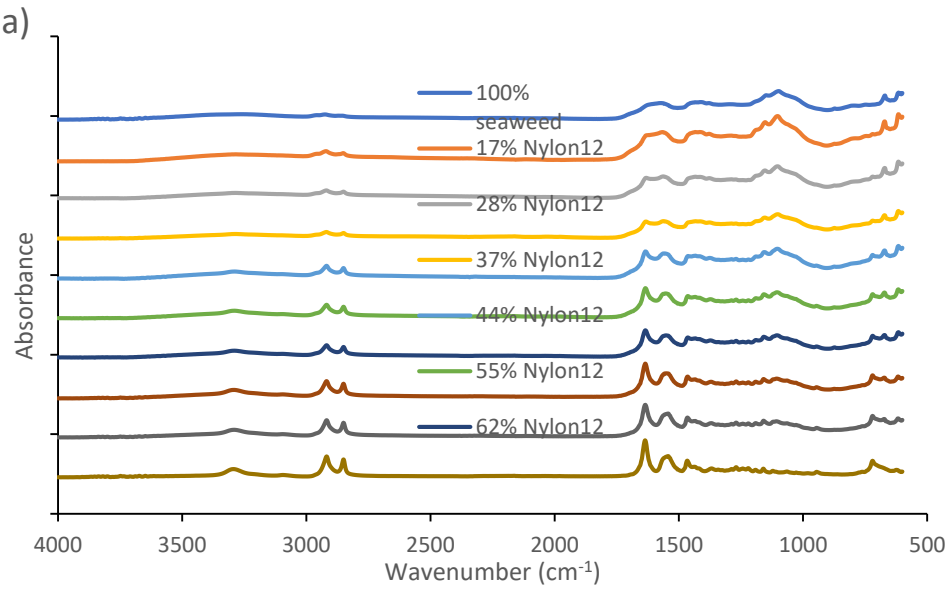

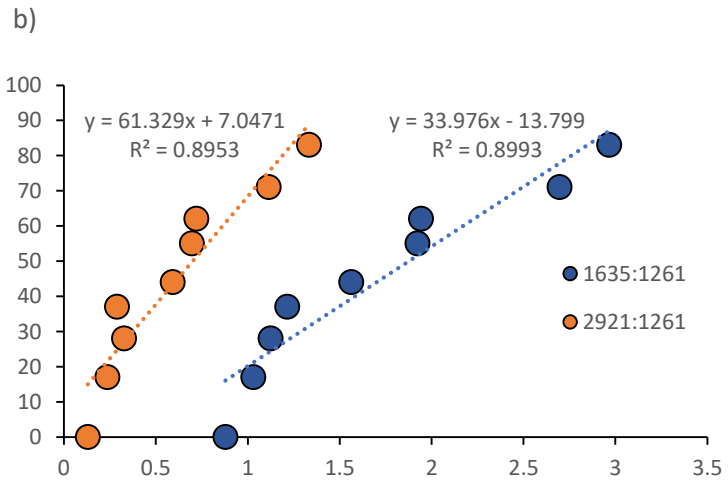

Figure 5.9-4–(a) FTIR spectra of macroalgae bio-char with different nylon12 contents, and (b) peak intensity ratio calibration curve for nylon12 content in macroalgae bio-char.

Table 5.9- 5– Calculated percentage concentrations of unreacted nylon12 in bio-char from co-liquefaction of macroalgae with nylon12.

	Nylon 12	**Macroalgae solid residue**	**PIR**	**Predictive equation**	**R2**	**Estimated Nylon 6 content of char (%)**
	1635 cm^{-1}	1261 cm^{-1}	1635:1261	Y = 33.976x-13.799	0.8993	
5% Nylon 12	0.04848	0.04414	1.09848			23.0 %
20% Nylon 12	0.03356	0.01629	2.06066			56.2 %
50% Nylon 12	0.07234	0.02729	2.65072			76.3 %
	2912 cm^{-1}	1261 cm^{-1}	2912:1261	Y= 61.329x + 7.0471	0.8953	
5% Nylon 12	0.00617	0.04414	0.13984			32.9 %
20% Nylon 12	0.00297	0.01629	0.18255			40.6 %
50% Nylon 12	0.00143	0.02729	0.52393			102.6 %

5.9.3 Quantification of plastic conversion

$$Plastic\ in\ solid\ residue\ (g) = \frac{unconverted\ \ in\ solid\ residue\ (\%) \times\ solid\ residue\ yield\ (g)}{100}$$

$$Plastic\ convert\ (g) = plastic\ in\ feedstock - plastic\ in\ solid\ residue$$

$$Conversion\ (\%) = \frac{plastic\ convert\ (g) \times\ 100}{plastic\ in\ feedstock\ (g)}$$

Table 5.9- 6 Summary of plastics conversion

Plastic components	Initial nylon in feedstock (g)	Total solid residue from reaction (g)	Estimated nylon content of char (%)	Amount of nylon in solid residue (g)	nylon conversion (%)
5% Nylon 6	0.15 g	0.98 g	0%	0.15 g	100%
20% Nylon 6	0.6 g	0.93 g	7.9%	0.53 g	88%
50% Nylon 6	1.50 g	0.93 g	61 %	0.94 g	62%
5% Nylon 6/6	0.15 g	1.07 g	6.4 %	0.08 g	54%
20% Nylon 6/6	0.6 g	1.09 g	44.8%	0.11 g	19%
50% Nylon 6/6	1.50 g	1.22 g	76%	0.57 g	38%
5% Nylon 6/12	0.15 g	1.09 g	25.4%	0 g	0%
20% Nylon 6/12	0.6 g	1.07 g	56%	0 g	0%
50% Nylon 6/12	1.50 g	1.66 g	108%	0 g	0%
5% Nylon 12	0.15 g	1.22 g	28.2 %	0 g	0%
20% Nylon 12	0.6 g	1.12 g	48.3%	0.06 g	9%
50% Nylon 12	1.50 g	1.50 g	89.4%	0.17 g	12%
5% Nylon line	0.15 g	0.66	6.2	0.041	73%
20% Nylon line	0.6 g	0.97	10.5	0.10	83%
50% Nylon line	1.50 g	1.10	62.4	0.69	54%

5.9.4 GC/MS analysis of bio-crudes

The identities of notable compounds in bio-crudes from co-liquefaction of macroalgal biomass with nylon blends, identified using GC/MS, are presented in Table 5.9-7 below.

Table 5.9-7– Identities of notable compounds in bio-crude products from co-liquefaction of macroalgal biomass with 20 wt.% nylons.

Compound identified	100% SW	20 wt.% NY6	20 wt.% NY6/6	20 wt.% NY6/12	20 wt.% NY12
Ethane, 1,1-diethoxy-	-			-	-
Toluene	-	-		-	
Formic acid, TBDMS derivative	-	-			-

Compound identified	100% SW	20 wt.% NY6	20 wt.% NY6/6	20 wt.% NY6/12	20 wt.% NY12
Cyclopentanone	-			-	-
Butanoic acid					
Piperidine, 1-ethyl-					
1-Methoxy-2-propyl acetate	-			-	-
4-Piperidone	-	-		-	-
Hexamethylenimine	-	-			-
1-Butanamine, N-methyl-N-2-propenyl-	-	-	-		-
2-Cyclopenten-1-one, 2-methyl-					
Acetic acid, TBDMS derivative	-	-			-
Butyrolactone	-				
2-Cyclopenten-1-one, 3-methyl-					
Phenol					
2-Cyclopenten-1-one, 3,4-dimethyl-					
2-Cyclopenten-1-one, 2,3-dimethyl-					
Propanoic acid, TBDMS derivative	-	-			
Butyric Acid, TBDMS derivative					-
p-Cresol					
tert-Butyldimethylsilyl methacrylate	-	-			-
Furan, 2-propyl-	-		-		-
2,5-Pyrrolidinedione, 1-methyl-					
Phenol, 2-methyl-					
Ethanone, 1-(1-cyclohexen-1-yl)-					
Ethanone, 1-(2-thienyl)-					
Phenylethyl Alcohol					
3-Pyridinol					
Caprolactam				-	-
m-Aminophenylacetylene	-	-			-
Phenol, p-tert-butyl-			-		-
Indole					
Dodecanamide			-		-
Tetradecanoic acid			-		
n-Hexadecanoic acid			-		-
Pentanoic acid	-	-			
Cyclododecanone	-	-	-		
Benzenesulfonamide, N-butyl-					-

Compound identified	100% SW	20 wt.% NY6	20 wt.% NY6/6	20 wt.% NY6/12	20 wt.% NY12
9-Octadecenamide, (Z)-	-		-		-
Ethanol, 2-ethoxy-		-			-
Phthalic acid, cyclobutyl tridecyl ester	-		-	-	-
1,8-Diazacyclotetradecane-2,7-dione	-	-		-	-
Myristic acid, TBDMS derivative	-	-	-		
Heneicosane	-	-	-		
Heptadecane	-	-	-		
Oleic Acid, (E)-, TBDMS derivative	-	-	-		-
Phthalic acid, di(2-propylpentyl) ester	-	-			

5.9.5 Yield of nylon product

The yield of nylon products from the system in both observed from aqueous and biocrude product from co-liquefaction of macroalgal biomass with nylon blends were estimated using LC/MS and GC/MS.

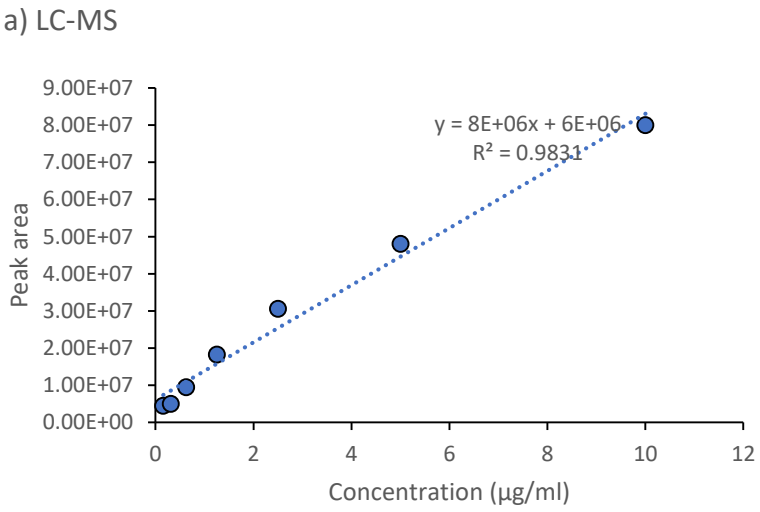

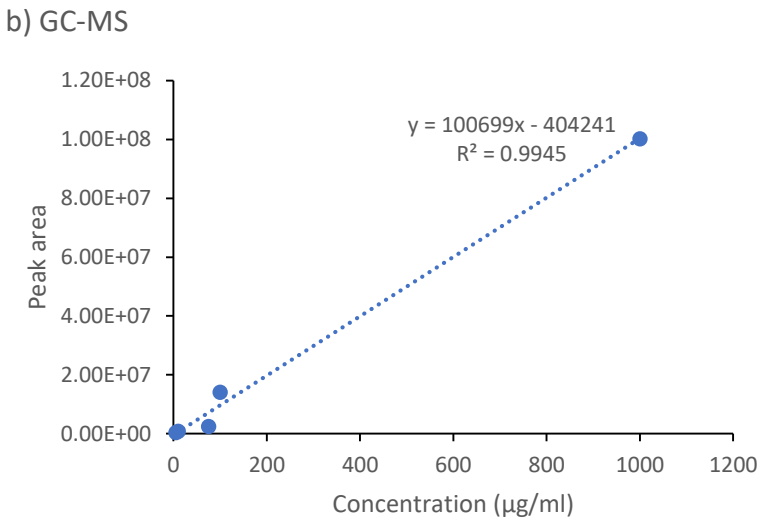

Figure 5.9- 5–Calibration curve the peak area of ε-caprolactam by a) LC-MS, and b) GC-MS using the standard additional method

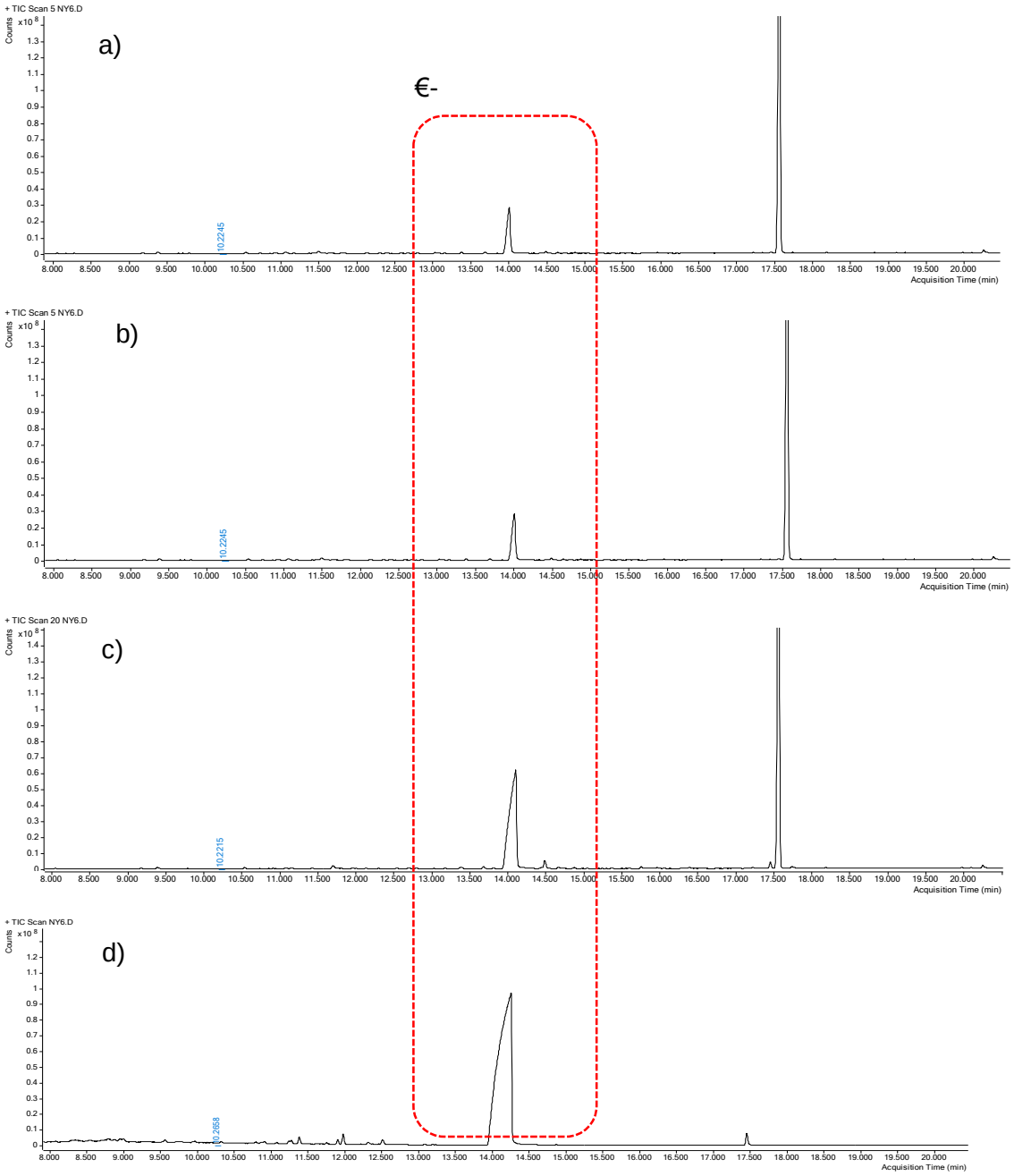

Figure 5.9-6. GC-MS chromatographs of bio-crude created from (a) 100%pure marine macroalgae, (b) 5 wt.% nylon 6 blend (c) 20 wt.% nylon 6 blend, and (d), 100 wt.% nylon 6

Chapter 6

Conclusions and future work

6.1 Conclusion

In this thesis, two promising thermochemical routes for the co-liquefaction of plastics and biomass were assessed. The first technology was the pressure-less catalyst depolymerisation (KDV) through collaboration with the Wonderful Company. The process was assessed for its suitability to produce a hydrocarbon advanced fuel from pistachio hulls. The KDV process was mimicked on the lab scale and carried out in 1L and 5L reactors, with different catalysts: 4A zeolite, ZSM-5, and aluminosilicate, and two different carrier oils, with different volatility. These results were compared to the pilot scale process underway at Ekotrend in Poland. Despite concerted efforts in the lab, very little bio-oil was produced under the conditions given in the literature, and of this product, hardly any of the distillate was from the biomass. Indeed, the catalyst-free reaction converted less biomass to distillate than conventional slow pyrolysis or LPP on both the lab and pilot scale. The maximum amount of distillate obtained when using a heavier carrier oil was relatively low, with less than half of the pistachio hull used. The liquid product contained not only pyrolysis oil but also 30-50 wt.% water. The bio-content as determined through ^{14}C analysis was found to be remarkably low for all reaction conditions, demonstrating that the majority of the product came from the carrier oil. The apparently high yields of fuels which are a key claim of the company delivering the technology seem to be predominantly due to the cracking and distillation of the fossil carrier oil. Overall, this technology is not a viable route for biomass valorisation, or for the co-processing of plastics with biomass.

Another potential alternative thermochemical process is to convert the pistachio hulls through hydrothermal liquefaction, where lignocellulosic residues were broken down in water at high temperatures and pressures to produce a bio-crude oil, a solid residue and an aqueous fertiliser. The effect of PE, PP, PET and Nylon on the liquefaction of pistachio hulls was examined, to determine the suitability of co-processing the waste feedstocks together. This technology produced a high yield of biocrude from pistachio hulls alone (up to 35 wt.%.) In the co-processing, modest synergistic effects were observed for PET and nylon-6, and in the case of nylon-6, the monomer ϵ-caprolactam was recovered predominantly in the aqueous phase. This result presents a promising revenue stream in future biorefineries. However no significant appreciable conversion of polyolefins was observed with the addition of biomass (<10%).

Based on these results, a number of challenges remain to be overcome, taking steps to further enhance the conversion of the recalcitrant polyolefins is necessary before plastic waste can become an integral part of a biorefinery. The processing of plastics with pistachio hulls through the catalytic co-liquefaction of biomass and plastic was therefore examined.

Various inorganic catalysts and organic additives were studied to enhance the conversion of polypropylene through hydrothermal liquefaction in the presence of pistachio hulls. However, with the exception of a radical promotor or the organic hydrogen donor formic acid, none of the catalysts used displayed significant enhancement in polypropylene conversion. The presence of formic acid as a co-solvent reduced the amount of fossil carbon going to the solid fraction and rather volatile organic species were predominantly produced, with the majority of the components being C3-C10 branched hydrocarbon fragments. The plastic conversion was enhanced to over 50% through the addition of the hydrogen donor formic acid. This effect was related to the activity of formic acid to act as an acid catalyst, promoting hydrolysis of the biopolymers at lower temperatures, increasing the interaction of soluble products, and is a source of H_2 as the acid can degrade over heterogeneous catalysts to produce hydrogen. In addition, the ability to stop the reaction through the addition of butylated hydroxytoluene (BHT) demonstrated the importance of a radical mechanism for the depolymerisation.

Previous studies reported that monomers of nylon 6 could significantly add to the value of an HTL marine biorefinery, as opposed to one containing lignocellulose presented in this thesis, by being able to effectively chemically recycle the waste nylon alongside producing bio-crude and fertiliser product. Hence, the effect of co-processing various other nylon types with marine macroalgae was examined using an actual sample of marine macroalgae collected at sea, entangled with nylon fishing line as well as nylon 6, nylon 6/6, nylon 6/12, and nylon 12. Synergistic effects between macroalgae and plastic on bio-crude yields were obtained, with increased hydrocarbon formation in bio-crude, and providing an overall improvement in bio-crude properties. However, while nylon 6 broke down almost entirely, and there was a modest conversion of nylon 6/6, nylon 12 and nylon 6/12 were left largely intact.

Through the work described in this thesis, HTL has been demonstrated to have a lot of potential for the co-liquefaction of plastic with biomass, that can produce monomers such as caprolactam or olefin gas stream being produced under optimal conditions. Co-liquefaction therefore has the potential to reduce the disposal of waste plastics in landfills and to help even out the seasonality issues that are inherent in biorefinery production.

6.2 Future work

The thesis presented here explored a number of avenues for converting plastics and biomass together to generate useful fuel pre-cursors.

KDV was assessed on the lab and pilot scale to determine the suitability of this approach for producing hydrocarbons from pistachio hulls. However, none of the work presented here demonstrated that the catalytic depolymerisation process is a viable biofuel production route. This work demonstrates the unsuitability of this one-step process for fuel production. Therefore, it is the opinion of the author that no further studies should be conducted on the KDV of biomass or in the future co-processing with plastic.

In contrast, the co-processing of plastic with pistachio hulls through hydrothermal liquefaction explored the effect of plastic pollutants on biofuel production. The bio-crude generated is a highly promising fuel precursor but cannot function as a fuel without future treatment. Further work should therefore investigate the upgrading of bio-crude to improve the physical and chemical properties enabling production for direct use as a fuel, or for co-refining with crude oils in conventional fossil refineries. The presence of nylon resulted in bio-crude and a high production of monomer ϵ-caprolactam in the aqueous phase. This monomer can be extracted to provide a novel route for a high value product. The fractionation of bio-crudes, separation and purification protocols for caprolactam should be further investigated.

Although the organic catalysts displayed enhanced hydrogenation activity during the conversion of plastics, they did not significantly improve the bio-crude quality. Consequently, further work should investigate a wider number of catalysts to further enhance bio-crude yield as well as its properties. Liquefaction studies should be

conducted under continuous flow conditions, to allow a better evaluation of industrial applicability of this technology. A radical promotor or the organic hydrogen donor formic acid resulted in enhancing the volatile organic compound stream. Further research would benefit from an investigation into utilising the gas stream to produce further polyolefins resulting in a circular economy methodology. Or by combining the gas stream with the crude product for future hydrotreating to add to the total energy product produced from HTL system.

A recycled and reused aqueous phase as a reaction medium for the co-liquefaction process is particularly promising as it can help to minimize the waste generated from the different processes. The aqueous phase from HTL of macroalgae may be used as a suitable growth medium fertiliser for terrestrial plants because of its high concentration of nitrogen and phosphorus. Therefore, the valorization of HTL aqueous products could be explored and assess whether the additional plastic has a negative effect on plant growth. Based on this data, the economic feasibility of the whole process could be assessed.

The synergistic effects on co-processing of plastic and macroalgal biomass were found to be stronger than those obtained for lignocellulosic biomass. This is potentially attributable to differences in the biochemical composition of macroalgae biomass; possibly the metal content in the inorganic fraction of macroalgae biomass may play a significant catalytic role in reaction conversion. Further research with a more detailed investigation of the inorganic composition of the macroalgae would be extremely beneficial. Further work should therefore investigate the isolation of individual inorganic components conducive to plastic conversion. This may ultimately lead to beneficial improvements of biofuel yields within a biorefinery.